VOLUME 119 NUMBER 2

THE ASTROPHYSICAL JOURNAL

AN INTERNATIONAL REVIEW OF SPECTROSCOPY AND ASTRONOMICAL PHYSICS

MARCH 1954

THE SPECTRUM OF THE CN^+ MOLECULE . . . *A. E. Douglas and P. M. Routly* 303
RELATIVE SOLAR ENERGY DISTRIBUTION IN THE SPECTRAL REGION 10,000–25,000 A . . . *A. Keith Pierce* 312
THE FORMATION OF ATMOSPHERIC O_3 EMISSION IN THE AIRGLOW . . . *Joseph W. Chamberlain* 328
MULTIPLE-STAR SYSTEMS IN EMISSION NEBULAE . . . *Stewart Sharpless* 334
A HEAVILY OBSCURED O-ASSOCIATION IN CYGNUS . . . *H. L. Johnson and W. W. Morgan* 344
THE RADIAL VELOCITY OF DELTA SCUTI . . . *G. F. Paddock and Otto Struve* 346
AERODYNAMIC MOTIONS OF INTERSTELLAR GAS CLOUDS . . . *G. C. McVittie* 352
TWO MODELS FOR THE INTERIOR OF THE SUN . . . *Peter Nemec* 365
RADIATIVE OPACITY OF STELLAR MATTER . . . *Harold Zirin* 371
THE GAUNT FACTOR FOR FREE-FREE TRANSITIONS IN PURE HYDROGEN . . . *Russell M. Kulsrud* 386
ON THE REFLECTION AND REFRACTION OF ALFVÉN WAVES . . . *V. C. A. Ferraro* 393
ON THE EQUILIBRIUM OF MAGNETIC STARS . . . *V. C. A. Ferraro* 407
ON THE RADIAL PULSATIONS OF AN INFINITE CYLINDER WITH A MAGNETIC FIELD PARALLEL TO ITS AXIS . . . *Ejnar Lyttkens* 413
COMPTON SCATTERING BY ELECTRON ATMOSPHERES. II. PROBLEMS WITH INCIDENT NORMAL FLUX . . . *Frank N. Edmonds, Jr.* 425
THE PHYSICAL THEORY OF METEORS. V. THE MASSES OF METEOR-FLARE FRAGMENTS . . . *Henry J. Smith* 438
A STOCHASTIC MODEL OF A FLUCTUATING DENSITY FIELD . . . *Allahi Ramakrishnan* 443

NOTES

RADIO EMISSION FROM THE ORION NEBULA AND OTHER SOURCES AT λ 9.4 CM . . . *F. T. Haddock, C. H. Mayer, and R. M. Simmonds* 456
$H\alpha$-EMISSION STARS ASSOCIATED WITH A DARK LANE IN LUPUS . . . *Karl G. Henize* 459
RECENT CHANGES IN THE SPECTRA OF FOUR Be STARS . . . *Arne Slettebak* 460
STELLAR WAVE LENGTHS OF Eu II AS AFFECTED BY HYPERFINE STRUCTURE . . . *Horace W. Babcock* 463
ON THE EFFECT OF ELECTRON SCREENING ON THERMONUCLEAR ENERGY GENERATION . . . *Erwin Schatzman* 464
THE DISPERSION IN ORIENTATION OF INTERSTELLAR POLARIZERS . . . *George Stranahan* 465

ERRATUM . . . 467

ABSTRACTS OF ASTROPHYSICAL JOURNAL: SUPPLEMENT SERIES

SPECTROSCOPIC OBSERVATIONS OF MIRA CETI, 1934–1952 . . . *Alfred H. Joy* 468
AN ANALYSIS OF W VIRGINIS . . . *Helmut A. Abt* 469

ANNOUNCEMENTS . . . 470

THE UNIVERSITY OF CHICAGO PRESS
CHICAGO, ILLINOIS, U.S.A.

March 1954 Vol. 119, No. 2

THE ASTROPHYSICAL JOURNAL

AN INTERNATIONAL REVIEW OF SPECTROSCOPY AND ASTRONOMICAL PHYSICS

Founded in 1895 by George E. Hale and James E. Keeler

Published in Collaboration with the American Astronomical Society

S. CHANDRASEKHAR
Managing Editor

GERARD P. KUIPER
Associate Editor

Yerkes Observatory of the University of Chicago

EDITORIAL BOARD

MARTIN SCHWARZSCHILD, JR. (1954-58)
Princeton University Observatory

H. W. BABCOCK (1953-57)
Mount Wilson Observatory of the Carnegie Institution of Washington

G. HERZBERG (1952-56)
National Research Council, Ottawa

FRED L. WHIPPLE (1952-56)
Harvard College Observatory

C. D. SHANE (1952-55)
Lick Observatory, University of California

The Astrophysical Journal is published bimonthly by the University of Chicago at the University of Chicago Press, 5750 Ellis Avenue, Chicago 37, Illinois, during January, March, May, July, September, and November. ¶Two volumes are published per year, one beginning with the January issue and the other beginning with the July issue. The subscription price is $6.00 per volume or $12.00 per year; the price of single copies is $3.00. (Orders for service of less than a volume will be charged at the single copy rate.) ¶Postage is prepaid by the publishers on all orders from the United States and its possessions. No extra charge is made for postage to countries in the Pan American Postal Union. ¶Postage is charged extra as follows: for Canada, 20 cents per volume, 40 cents per year (total $6.20 per volume, $12.40 per year); on single copies 5 cents (total $3.05); for all other countries in the Postal Union, 40 cents per volume, 75 cents per year (total $6.40 per volume, $12.75 per year), on single copies 10 cents (total $3.10). ¶Subscriptions are payable in advance. Please make all remittances payable to The University of Chicago Press, in United States currency or its equivalent by postal or express money orders or bank drafts.

The following is an authorised agent:

For the British Empire, except North America and Australasia: The Cambridge University Press, Bentley House, 200 Euston Road, London, N.W. 1, England. Prices of yearly subscriptions and of single copies may be had on application.

Claims for missing numbers should be made within the month following the regular month of publication. The publishers expect to supply missing numbers free only when losses have been sustained in transit, and when the reserve stock will permit.

Business correspondence should be addressed to The University of Chicago Press, Chicago 37, Illinois.

Communications for the editors and manuscripts should be addressed to: S. Chandrasekhar, Editor of THE ASTROPHYSICAL JOURNAL, Yerkes Observatory, Williams Bay, Wisconsin.

Line drawings and photographs should be made by the author, and all marginal notes such as co-ordinates, wave lengths, etc., should be included in the cuts. It will not be possible to set up such material in type.

One copy of the corrected galley proof should be returned as soon as possible to the editor, Yerkes Observatory, Williams Bay, Wisconsin. Authors should take notice that the manuscript will not be sent to them with the proof.

The cable address is "Observatory, Williamsbay, Wisconsin."

The articles in this journal are indexed in the *International Index to Periodicals*, New York, N.Y.

Applications for permission to quote from this journal should be addressed to The University of Chicago Press, and will be freely granted.

Microfilms of complete journal volumes are available to regular subscribers only and may be obtained at the end of the year. Orders and inquiries should be addressed to University Microfilms, 313 North First Street, Ann Arbor, Michigan.

Notice to subscribers: If you change your address, please notify us and your local postmaster immediately.

Entered as second-class matter, July 31, 1900, at the Post-Office at Chicago, Ill., under the Act of March 3, 1879.
Acceptance for mailing at special rate of postage provided for in United States Postal Act of October 3, 1917, Section 1103, amended February 28, 1925.
Copyright 1954 by the University of Chicago.

[printed in U.S.A.]

THE ASTROPHYSICAL JOURNAL

AN INTERNATIONAL REVIEW OF SPECTROSCOPY AND ASTRONOMICAL PHYSICS

VOLUME 119 MARCH 1954 NUMBER 2

THE SPECTRUM OF THE CN^+ MOLECULE*

A. E. DOUGLAS AND P. M. ROUTLY†

Division of Physics, National Research Council, Ottawa, Canada

Received September 21, 1953

ABSTRACT

In a discharge through *He* mixed with a trace of C_2N_2, two new band systems have been found. It has been shown that these systems are due to two $^1\Sigma - ^1\Sigma$ transitions of the CN^+ molecule. For the first system the followng constants have been determined: $\nu_{00} = 45844.6$, $B_0' = 1.8870$, $B_0'' = 1.8868$, $\omega_e' = 2670.5$, $\omega_e'' = 2033.0$ cm^{-1}. The second system, which has the same lower state as the first, cannot be completely analyzed because of perturbations and overlapping. Probable values of the constants are $\nu_{00} = 31381.6$, $\omega_e' = 1265$, and $B_0' = 1.402$ cm^{-1}. Four bands, as yet unidentified, are discussed.

I. INTRODUCTION

The ionized CN molecule is isoelectronic with C_2 and, therefore, the spectra of the two molecules should be similar. While the spectrum of C_2 is readily excited and is well known, the spectrum of CN^+ had, until recently, never been observed. Because of the spectroscopic interest in CN^+ and because CN^+ is of considerable astrophysical importance, a search for its spectrum was undertaken in these laboratories.

Preliminary results of this work have already been published in a previous note.[1] In particular, a new band system was described which is believed to arise from CN^+. The present paper gives a more complete account of this first system and, in addition, reports on a second new band system which apparently also arises from CN^+. Finally, four miscellaneous bands are discussed, whose identity is as yet uncertain but whose appearance is similar to that of the CN^+ bands.

II. EXPERIMENTAL

A hollow cathode discharge tube containing *He*, with a trace of C_2N_2, was used as a light-source. The gases were streamed rapidly through the tube by means of a mechanical pump having a pumping speed of 23 liters per second. Under these operating conditions it was found that a spectrum could be obtained which was relatively free from the intense band systems of N_2, N_2^+ and C_2.

The spectrum of the discharge was photographed from 8500 to 1900 A with a 21-foot

* Contribution No. 3218 from the National Research Council of Canada.

† National Research Laboratories Postdoctorate Fellow.

[1] A. E. Douglas and P. M. Routly, *Ap. J.*, **117**, 461, 1953.

grating spectrograph having a dispersion in the first order of 2.5 A/mm. Exposure times ranged from 15 to 30 minutes in the first order at the red limit, using sensitized Eastman I-N plates, to 9 hours in the fifth order at the ultraviolet limit, using Ilford Q-2 plates. Overlapping from lower orders of the grating was eliminated in the fourth- and fifth-order spectrograms by a quartz foreprism.

As reported earlier,[1] a large number of new bands was observed on the plates in the region from 4500 to 1900 A. The majority of these have now been measured and analyzed. It has been found that twenty-two of the new bands can be assigned to four new band systems in neutral CN, and approximately ten more to an extension of the tail bands of CN. These new data on CN will be presented in another paper.

Eleven of the new bands, however, definitely do not belong to neutral CN. They can be assigned to two new band systems with a common lower state. A detailed discussion of these two band systems is given in Sections III and IV of this paper, while arguments favoring CN^+ as the emitter of the new systems are presented in Section VI. Measurements of four additional bands, also probably due to CN^+, are included in Section VII.

III. THE FIRST BAND SYSTEM OF CN^+

The first band system to be analyzed and attributed to CN^+ lies in the vicinity of 2150 A. It consists of four headless bands, each possessing a single P and a single R branch. Reproductions of the two strongest bands at 2180.6 and 2153.5 A are given in Figure 1, *a* and *b*. Table 1 gives the wave numbers of the rotational lines in each of the four bands observed.

Perturbations in line intensity and position occur in all four bands. A perturbation, in which the $P(19)$ and $R(17)$ lines are missing and in which the lines adjacent to these two are slightly displaced, can be seen in the (1–1) band of Figure 1, *b*. Much more violent intensity perturbations occur in the (2–2) and (3–3) bands where all lines up to $J = 7$ in the (2–2) band and up to $J = 13$ in the (3–3) band are missing. All perturbations thus far observed in the first band system occur in the upper electronic state of the transition. It is probable that these perturbations are accidental predissociations, but so little is known of the energy levels of CN^+ that the exact nature of the perturbations cannot be ascertained.

As pointed out above, the bands of the first system have no Q branches. Also, in the strongest band at 2180.6 A, both the $R(0)$ and the $P(1)$ lines have been observed. It therefore appears certain that the bands of the first system arise from a $\Sigma - \Sigma$ transition. Further, no multiplet splitting of the rotational lines could be detected, even for the highly perturbed lines. Since a perturbation will almost certainly cause a splitting of a multiplet level, and hence of a line which originates or terminates on this level, it follows that the Σ state giving rise to the first band system must be singlet; i.e., the transition is ${}^1\Sigma - {}^1\Sigma$.

The results of a rotational analysis of the four bands are given in Table 2. The assignment of the bands to a $\Delta v = 0$ sequence, with the 2180.6 A band being the (0–0) transition, appears to be the only one compatible with the observed B values and the positions and intensities of the bands. Because of the perturbations present in the (2–2) and (3–3) bands, accurate band origins and B' values could not be determined for these bands.

IV. THE SECOND BAND SYSTEM OF CN^+

The second band system, thought to be due to CN^+, consists of seven bands shaded to the red and lying in the region from 3250 to 2900 A. One of the strongest bands of the system is reproduced in Figure 2, *a*. Table 3 gives the wave numbers of the rotational lines in each of the seven bands observed.

The bands of the second system, like those of the first, have single P and R branches and possess no Q branches. Moreover, as will be shown below, the first and second band

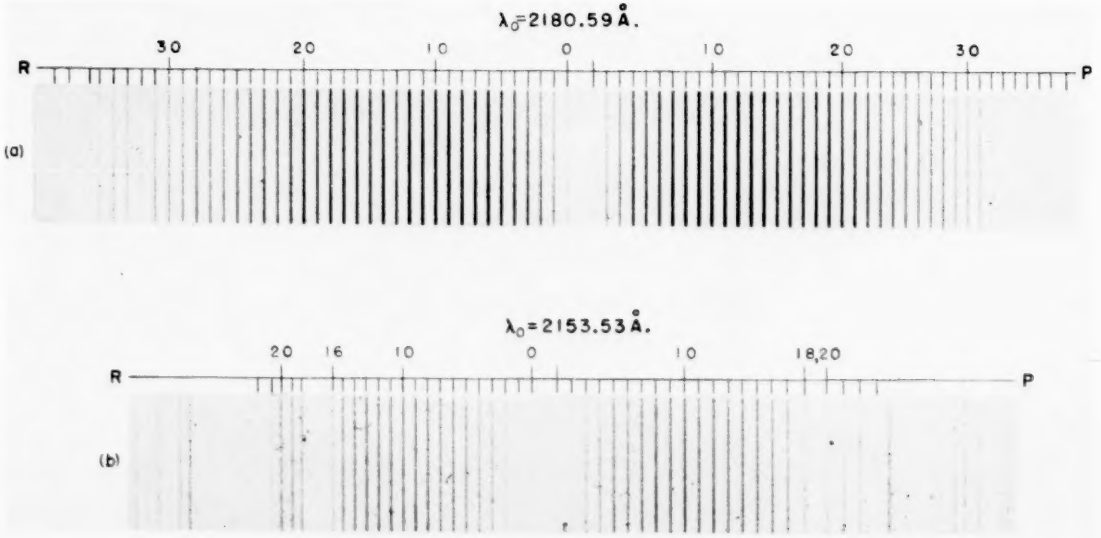

FIG. 1.—*a*, the 0–0 and *b*, the 1–1 bands of the $f^1\Sigma - a^1\Sigma$ system of CN^+

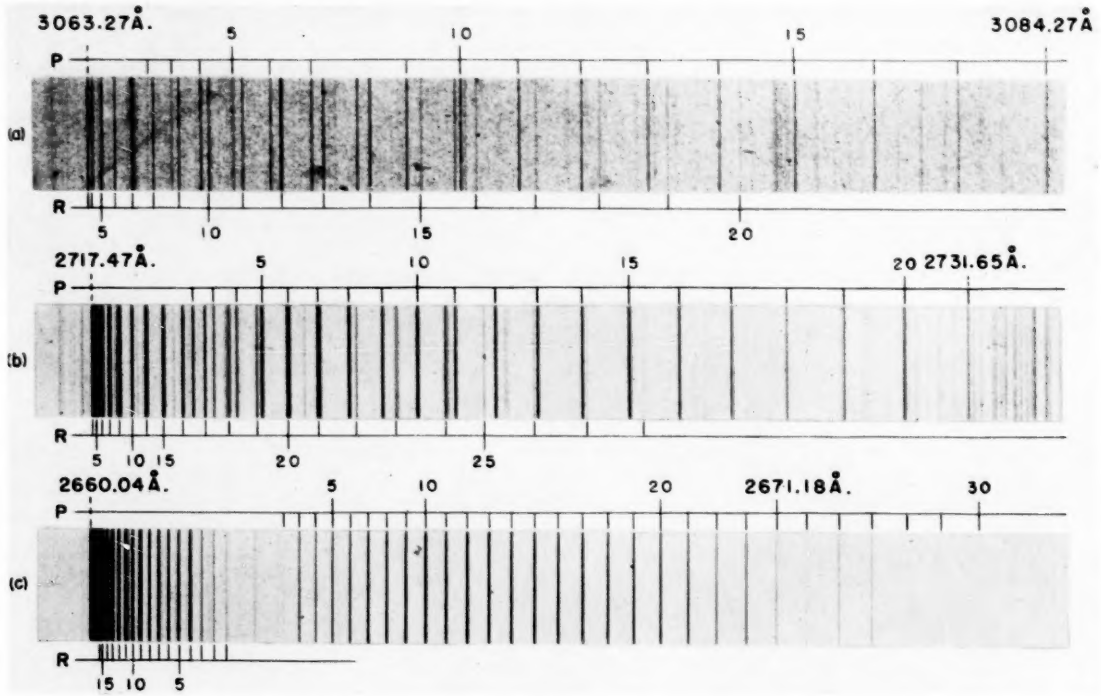

FIG. 2.—*a*, the 1–0 band of the $c^1\Sigma - a^1\Sigma$ systems of CN^+; *b*, *c*, two unidentified bands probably due to CN^+

TABLE 1

WAVE NUMBERS OF THE LINES OF BANDS OF THE FIRST ($f^1\Sigma - a^1\Sigma$) SYSTEM OF CN^+

J	(0–0) Band $\nu_0 = 45{,}844.65$ Cm^{-1}		(1–1) Band $\nu_0 = 46{,}420.68$ Cm^{-1}		(2–2) Band $\nu_0 = 46{,}935.3$ Cm^{-1}		(3–3) Band $\nu_0 = 47{,}395.0$ Cm^{-1}	
	$P(J)$	$R(J)$	$P(J)$	$R(J)$	$P(J)$	$R(J)$	$P(J)$	$R(J)$
0	.....	45,848.40	.....	.....	.....	.....	.....	.....
1	45,840.82	52.19	.....	46,428.10	.....	.....	.....	.....
2	37.08	55.93	46,413.19	31.74	.....	.....	.....	.....
3	33.36	59.74	09.40	35.37	.....	.....	.....	.....
4	29.54	63.54	05.61	38.99	.....	.....	.....	.....
5	25.84	67.31	01.75	42.61	.....	.....	.....	.....
6	22.06	71.01	397.92	46.13	.....	.....	.....	.....
7	18.30	74.84	93.98	49.62	.....	46,964.08?	.....	.....
8	14.48	78.61	90.13	53.14	.....	66.72	.....	.....
9	10.72	82.38	86.19	56.61	46,901.39	69.66	.....	.....
10	06.97	86.15	82.23	60.05	896.57	72.48	.....	.....
11	03.21	89.94	78.23	63.50	92.04	75.53	.....	.....
12	799.37	93.69	74.25	66.85	87.71	78.31	.....	.....
13	95.68	97.41	70.21	70.22	83.25	81.38	.....	47,435.72
14	91.93	901.25	66.21	73.45	78.79	84.18	.....	37.41
15	88.17	05.04	62.10	76.69	74.44	86.96	47,329.62	39.16
16	84.46	08.79	57.91	79.44	70.20	89.65	24.11	40.99
17	80.75	12.61	53.68	.....	66.20	.....	18.66	42.79
18	77.04	16.49	49.09	88.06	.....	.....	13.11	44.29
19	73.36	20.26	.....	90.78	.....	.....	07.65	45.85
20	69.65	24.08	42.83	93.77	.....	.....	02.03	47.29
21	66.00	27.87	38.17	96.34	.....	.....	296.31	48.64
22	62.28	31.71	33.69	500.25	.....	.....	90.51	.....
23	58.70	35.57	28.90	.....	.....	.....	.....	.....
24	55.07	39.46	.....	.....	.....	.....	.....	.....
25	51.45	43.32	.....	.....	.....	.....	.....	.....
26	47.91	47.23	.....	.....	.....	.....	.....	.....
27	44.34	51.13	.....	.....	.....	.....	.....	.....
28	40.78	55.02	.....	.....	.....	.....	.....	.....
29	37.31	58.99	.....	.....	.....	.....	.....	.....
30	33.81	62.94	.....	.....	.....	.....	.....	.....
31	30.36	67.01	.....	.....	.....	.....	.....	.....
32	26.95	70.99	.....	.....	.....	.....	.....	.....
33	23.61	75.09	.....	.....	.....	.....	.....	.....
34	20.20	79.13	.....	.....	.....	.....	.....	.....
35	16.90	83.18	.....	.....	.....	.....	.....	.....
36	13.66	86.04	.....	.....	.....	.....	.....	.....
37	10.32	91.92	.....	.....	.....	.....	.....	.....
38	05.80	95.94	.....	.....	.....	.....	.....	.....
39	04.53	46,000.13	.....	.....	.....	.....	.....	.....
40	01.17	.....	.....	.....	.....	.....	.....	.....
41	698.01	.....	.....	.....	.....	.....	.....	.....

TABLE 2

BAND ORIGINS AND ROTATIONAL CONSTANTS OF THE $f^1\Sigma - a^1\Sigma$ BANDS OF CN^+

Band Origins		Vib. Assign. v'–v''	B_v' (Cm^{-1})	B_v'' (Cm^{-1})
λ_{air} (A)	ν_{vac} (Cm^{-1})			
2180.595	45,844.65	0–0	1.8870	1.8868
2153.533	46,420.68	1–1	1.8553	1.8673
2129.9	46,935.3	2–2	.....	1.849
2109.3	47,395	3–3	.....	1.834

TABLE 3

WAVE NUMBERS OF THE LINES OF THE BANDS OF THE SECOND ($c^1\Sigma - a^1\Sigma$) SYSTEM OF CN^+

J	(1-1) BAND $\nu_0 = 30{,}629.23$ CM^{-1}		(0-0) BAND $\nu_0 = 31{,}381.60$ CM^{-1}		(4-2) BAND $\nu_0 = 32{,}321.85$ CM^{-1}		(1-0) BAND $\nu_0 = 32{,}630.01$ CM^{-1}		(3-1) BAND $\nu_0 = 33{,}101.89$ CM^{-1}		(2-0) BAND $\nu_0 = 33{,}854.79$ CM^{-1}		(4-1) BAND $\nu_0 = 34{,}290.36$ CM^{-1}	
	$P(J)$	$R(J)$	$P(J)$	$R(J)$	$P(J)$	$R(J)$	$P(J)$	$R(J)$	$P(J)$	$R(J)$	$P(J)$	$R(J)$	$P(J)$	$R(J)$
0	.....	30,632.07	.....	31,384.26	.....	.....	.....	.....	.....	.....	.....	.....	.....	34,293.18
1	30,625.46	33.92	31,377.62	85.93	.....	.....	.....	.....	.....	33,107.13	33,850.86	33,858.90	34,286.72	94.80
2	20.81	34.86	73.33	87.03	.....	32,327.67	.....	32,635.36	.....	07.13	45.77	60.14	82.10	95.93
3	15.18	34.86	67.36	87.03	32,308.08	27.67	32,615.83	35.36	.....	07.13	40.47	60.14	76.55	95.93
4	08.65	33.92	.....	85.93	01.77	27.09	09.09	34.25	33,081.11	.....	33.77	58.90	69.99	94.80
5	01.20	32.07	53.01	83.83	294.54	25.36	01.44	32.20	73.45	04.01	26.11	56.86	62.46	93.18
6	592.77	29.22	44.42	80.84	86.38	22.89	592.80	29.13	64.93	01.02	17.42	53.77	54.09	90.37
7	83.47	25.46	34.82	76.86	77.38	19.42	83.14	25.13	55.41	097.03	07.78	49.66	44.69	86.72
8	73.23	20.81	24.25	71.89	67.46	15.15	72.56	20.11	44.97	92.11	797.17	44.62	34.49	82.10
9	62.05	15.18	12.67	65.90	56.65	09.97	61.00	14.16	33.59	86.28	85.54	38.58	23.52	76.55
10	49.90	08.65	00.23	59.03	44.99	03.89	48.47	07.20	21.20	79.53	72.94	31.50	11.34	69.99
11	36.77	01.20	286.72	51.07	32.49	296.91	34.96	599.25	07.89	71.75	59.38	23.49	198.30	62.46
12	22.76	592.77	72.27	42.21	18.95	89.05	20.48	90.35	32,993.69	63.10	44.78	14.40	84.35	54.09
13	07.78	83.17	56.87	32.35	04.70	80.31	05.03	80.46	78.47	53.50	29.24	04.40	69.42	45.08
14	.....	72.84	.....	21.49	.....	70.72	488.60	69.58	62.29	42.98	12.67	793.40	.....	34.95
15	.....	61.63	.....	09.69	.....	60.23	71.21	57.77	45.37	31.49	695.11	81.33	.....	23.52
16	.....	49.42	.....	296.86	.....	.....	52.82	44.90	27.37	19.18	76.59	68.21	.....	11.34
17	.....	36.24	.....	83.12	.....	36.14	33.49	31.15	08.53	05.81	57.06	.....	.....	198.30
18	.....	22.16	.....	.....	.....	.....	13.18	16.33	888.79	32,991.67	.....	39.15	.....	84.78
19	.....	07.10	.....	.....	.....	.....	391.85	00.55	68.11	76.53	.....	23.04	.....	.....
20	.....	.....	.....	.....	.....	.....	69.57	483.83	.....	.....	.....	05.86	.....	.....
21	.....	.....	.....	.....	.....	.....	.....	.....	.....	.....	.....	.....	.....	.....
22	.....	.....	.....	.....	.....	.....	.....	47.33	.....	.....	.....	.....	.....	.....

systems have the same lower state. It is therefore concluded that the second band system also arises from a $^1\Sigma - {}^1\Sigma$ transition. The fact that the two band systems have a common lower state is demonstrated in Table 5, where the lower-state combination differences, $\Delta_2''F(J)$, of the (0–0) band of the first system and of the (1–0) band of the second system are listed together. It is seen from the table that the two sets of numbers agree within the experimental errors. Equally good agreement between the lower-state

TABLE 4

BAND HEADS, ORIGINS, AND ROTATIONAL CONSTANTS OF THE $c^1\Sigma - a^1\Sigma$ BANDS OF CN^+

BAND HEADS	BAND ORIGINS	VIB. ASSIGN.		
λ_{air} (A)	ν_{vac} (Cm^{-1})	$v'-v''$	B_v' (Cm^{-1})	B_v'' (Cm^{-1})
3263.317	30,629.23	1–1	1.403	1.871
3185.111	31,381.60	0–0	1.402	1.888
3092.430	32,321.85	4–2	1.403	1.850
3063.273	32,630.01	1–0	1.3995	1.8869
3019.620	33,101.89	3–1	1.387	1.870
2952.465	33,854.79	2–0	1.398	1.888
2915.681	34,290.36	4–1	1.404	1.868

TABLE 5*

COMBINATION DIFFERENCES OF THE $v'' = 0$ LEVELS IN THE LOWER STATES OF THE FIRST AND SECOND BAND SYSTEMS

J	First System $\Delta_2F''(J)$ (Cm^{-1})	Second System $\Delta_2F''(J)$ (Cm^{-1})	J	First System $\Delta_2F''(J)$ (Cm^{-1})	Second System $\Delta_2F''(J)$ (Cm^{-1})
1	11.32		9	71.64	71.64
2	18.83		10	79.17	79.20
3	26.39	26.27	11	86.78	86.72
4	33.90	33.92	12	94.26	94.22
5	41.48	41.45	13	101.76	101.75
6	49.01	49.06	14	109.24	109.25
7	56.53	56.57	15	116.79	116.76
8	64.12	64.13	16	124.29	124.28

* Combination differences listed were obtained from the (0–0) band of the first system and from the (1–0) band of the second system.

combination differences of the two band systems can be obtained for the $v'' = 1$ and $v'' = 2$ vibrational levels.

The results of a rotational analysis of the second system are given in Table 4. The vibrational numbering of the bands in this system will be discussed in the next section. It is evident from Table 4 that the B' values of the upper $^1\Sigma$ state do not decrease regularly with increasing vibrational quantum number. The B' value for the $v' = 3$ level, for example, is less than the value of B' for the $v' = 4$ level. Further, the apparent centrifugal stretching constant D' of the $v' = 3$ level (not given in Table 4) is negative. Since the lines of the P and R branches form regular series in each band, it is certain that the anomalous B' and D' values are not caused by rotational perturbations. It is more probable that these anomalous B' and D' values are caused by a vibrational (homogeneous)

perturbation in the upper $^1\Sigma$ state of the second band system. That this state is vibrationally perturbed is borne out by the vibrational analysis discussed in the next section.

V. VIBRATIONAL ANALYSIS AND ELECTRONIC STATES

For convenience the common lower state of the two band systems has been designated as the $a^1\Sigma$ state, while the upper states of the first and second systems have been designated the $f^1\Sigma$ and $c^1\Sigma$ states, respectively.

As mentioned previously, the bands of the first ($f^1\Sigma - a^1\Sigma$) system probably represent a $\Delta v = 0$ sequence, with the band at 2180.6 A being the (0–0) transition. Because of this vibrational assignment and because the two band systems have their lower states ($a^1\Sigma$) in common, the correct lower-state vibrational numbering can be given to the bands of the second system. The vibrational numbering of the upper state ($c^1\Sigma$) of the second system is, however, quite uncertain. On the long-wave-length side of the second system, no bands were observed beyond the moderately intense band at 3260 A. It is quite possible that additional CN^+ bands belonging to the second system do exist to the red of 3260 A, but their detection would be exceedingly difficult because of the intense

TABLE 6

CONSTANTS OF THE THREE $^1\Sigma$ STATES IN CN^+

State	T_e (Cm^{-1})	ω_e (Cm^{-1})	$\omega_e x_e$ (Cm^{-1})	B_0 (Cm^{-1})	D_0 (Cm^{-1})	B_e (Cm^{-1})	a_e (Cm^{-1})	r_e (10^{-8} Cm)
$a^1\Sigma$	0*	2033.05	16.14	1.8871	7.0×10^{-6}	1.8964	0.0188	1.1727
$c^1\Sigma$	31,771†	1265†	11†	1.402	13×10^{-6}	1.403†	.002†	1.363†
$f^1\Sigma$	45,533.6	2670.5	46.9	1.8870	4.7×10^{-6}	1.903	0.032	1.171

* Value of T_e for the $a^1\Sigma$ state was arbitrarily set equal to zero.

† Approximate values.

bands of neutral CN that effectively mask this region. The upper-state vibrational numbering for the second ($c^1\Sigma - a^1\Sigma$) band system given in Table 4 must, therefore, be considered only a relative numbering.

The constants of the three $^1\Sigma$ states in CN^+ are given in Table 6. For the $a^1\Sigma$ state, the values are of the order of magnitude to be expected for a molecule like CN^+. (T_e in this state has been arbitrarily set equal to zero.) The values of both ω_e and $\omega_e x_e$ in the $f^1\Sigma$ state, however, are extraordinarily high. Normally, values of ω_e as high as 2700 cm^{-1} are found only in diatomic hydrides. The determination of constants for the $c^1\Sigma$ state presented special difficulties because the vibrational levels of this state are not regularly spaced; the $v' = 3$ level, in particular, seems to be shifted upward by approximately 40 cm^{-1}. It might be questioned whether the band in Table 4, denoted the (3–1) band, does, in fact, belong to the second ($c^1\Sigma - a^1\Sigma$) band system. Even if this band is omitted from the system, however, it is found that the $v = 0$, 1, 2, and 4 vibrational levels of the $c^1\Sigma$ state do not form a regular series. It seems probable, therefore, that the vibrational levels of the $c^1\Sigma$ state are perturbed and that the perturbation of the $v = 3$ level is particularly strong. As mentioned in the previous section, such a perturbation might account for the anomalous B' values in Table 4. Because of this vibrational perturbation, the vibrational constants for the $c^1\Sigma$ state (values followed by a dagger in Table 6) could not be determined accurately. Approximate values were obtained by ignoring the highly displaced $v = 3$ level and fitting as closely as possible the remaining levels of the $c^1\Sigma$ state to the usual vibrational equation. Apart from perturbations, the constants of the $c^1\Sigma$ state (rotational and vibrational) are uncertain because the vibrational numbering of this state is only relative.

VI. IDENTITY OF THE EMITTER

Thus far it has been assumed in this paper that the emitter of the two new $^1\Sigma-{}^1\Sigma$ band systems is CN^+. The evidence supporting this assumption will be reviewed here.

As stated in Section II, the new bands were obtained from a discharge through helium and C_2N_2 in a hollow cathode discharge tube. It is well known that both the presence of *He* and the hollow cathode type of discharge are favorable for the production of ionized molecules. Hence, from experimental considerations, it is not unreasonable to suspect that the emitter of the new bands might be CN^+.

Other molecules besides CN^+ may, of course, be responsible. From the magnitude of the B values derived from the two band systems and from the singlet nature of the electronic states involved, the other possible emitters are limited to NO^+, CO, C_2, N_2, and O_2. Since the rotational lines of the bands in the two new systems show no intensity alternation (see Figs. 1 and 2) and since lines of both even and odd J are present, the homonuclear molecules are at once excluded. Further, since none of the intense band systems of NO, CO, or CO^+ were observed on the plates, it appears most unlikely that the new bands could arise from a molecule containing oxygen. The absence of oxygen in the new emitter was further confirmed by the fact that plates, taken with a minute trace of oxygen deliberately introduced into the discharge, showed very strong CO bands but no increase in the intensity of bands belonging to the new systems.

VII. UNIDENTIFIED BANDS

Besides the two $^1\Sigma-{}^1\Sigma$ band systems of CN^+ already described, four bands, as yet unidentified, were observed which appear to arise from singlet states. The bands are all shaded to the red with heads at 2717.5, 2677.9, 2660.1, and 2039.4 A. Each band consists of a single P and a single R branch and resembles in appearance the $(c^1\Sigma-a^1\Sigma)$ CN^+ bands. Figure 2, *b* and *c*, shows reproductions of the two strongest bands at 2717.5 and 2660.1 A; the 2677.9 A band appears somewhat weaker on the plates, while that at 2039.4 A is quite faint. Except for the 1717.5 and 2677.9 A bands, which have one state in common, the four bands do not appear to be related to one another or to any previously known band system, including the new systems discussed in this paper. Because of their similarity to the CN^+ bands, however, it is not unlikely that they arise from additional singlet states in CN^+.

The wave numbers of the lines of the four miscellaneous bands are given in Table 7. Since it has not been possible to determine the band origins unambiguously (except possibly for the 2660.1 A band), the J numbering in Table 7 is uncertain by one unit. The B values quoted may correspondingly be in error. The band at 2660.1 A appears to have a faint line at the band origin; it is thought quite possible that this band arises from a $^1\Pi-{}^1\Pi$ transition and that the central line is the first line of the weak Q branch to be expected from such a transition.

VIII. DISCUSSION

The two $^1\Sigma-{}^1\Sigma$ band systems described in Sections III and IV and perhaps the four bands of Section VII represent the first spectroscopic evidence of the existence of the CN^+ ion.

Too little is known at present of the electronic energy levels of CN^+ to make possible a detailed comparison with the energy levels of the isoelectronic molecule C_2. In certain respects the $f^1\Sigma-a^1\Sigma$ bands are indeed similar to the Mulliken bands of C_2. The B values of the $f^1\Sigma$ and $a^1\Sigma$ states of CN^+, for example, are similar to the B values of the upper and lower states of the Mulliken system. Moreover, the $f^1\Sigma-a^1\Sigma$ bands of CN^+ occur in the same spectral region as the Mulliken bands. The analogy is not close, however, since the ω_e value in the $f^1\Sigma$ state of CN^+ is 2700 cm^{-1}, while the ω_e value in the corresponding state of the Mulliken system is only 1829 cm^{-1}. The large value of ω_e in the $f^1\Sigma$ state leads to the unusual nature of the $f^1\Sigma-a^1\Sigma$ system. Like the Mulliken bands,

the $f^1\Sigma - a^1\Sigma$ bands are headless because the B' and B'' values in each band are nearly equal; unlike the Mulliken system, however, where all bands of the $\Delta v = 0$ sequence fall together, the corresponding bands of the $f^1\Sigma - a^1\Sigma$ system are separated by approximately 550 cm^{-1}.

There appears to be no analogy in C_2 to the $c^1\Sigma$ state of CN^+. Freymark[2] recently

TABLE 7*

WAVE NUMBERS OF THE LINES OF THE MISCELLANEOUS BANDS

J	λ_A (AIR) = 2717.473 A		λ_A (AIR) = 2677.889 A		λ_A (AIR) = 2660.044 A†		λ_A (AIR) = 2039.350 A	
	P(J)	R(J)	P(J)	R(J)	P(J)	R(J)	P(J)	R(J)
0	.....	.....	.....	.....	.....	37,550.91	.....	49,016.89
1	36,770.26	36,779.47	37,314.16	37,329.45	37,537.79	53.76	.....	18.48
2	66.08	82.16	08.84	31.11	34.20	56.57	48,998.30	19.42
3	61.52	84.42	03.20	.....	30.47	59.24	93.07	19.42
4	56.48	86.06	295.84	.....	26.59	61.78	86.81	19.42
5	50.98	87.21	88.28	31.11	22.59	64.16	79.92	18.48
6	45.10	88.01	80.13	29.45	18.47	66.42	72.51	16.89
7	38.75	88.01	71.25	27.21	14.19	68.53	64.38	14.85
8	31.92	88.01	61.75	24.38	09.79	70.51	55.70	11.94
9	24.61	87.21	51.50	20.62	05.26	72.35	46.24	08.53
10	16.83	86.06	40.62	16.27	00.59	74.05	36.30	04.47
11	08.62	84.42	29.03	11.21	495.73	75.58	25.67	48,999.77
12	699.89	82.16	16.68	05.43	90.79	76.95	14.35	94.39
13	90.65	79.47	03.65	298.92	85.70	78.16	02.41	88.41
14	80.91	76.28	189.90	91.74	80.44	79.21	889.91	81.79
15	70.66	72.57	.....	83.77	75.05	80.07	76.67	74.47
16	59.82	68.32	.....	75.11	69.46	80.75	62.86	66.54
17	48.47	63.48	.....	65.60	63.74	81.33	.....	57.95
18	36.52	58.12	.....	55.45	57.83	81.78	.....	48.94
19	24.01	52.10	.....	44.67	51.75	.....	.....	39.15
20	10.94	45.43	.....	.....	45.47	.....	.....	28.44
21	597.17	38.26	.....	.....	39.06	.....	.....	17.27
22	.....	30.35	.....	.....	32.39	.....	.....	05.69
23	.....	21.63	.....	.....	25.46	.....	.....	.....
24	.....	.....	.....	.....	.....	.....	.....	.....
25	.....	02.33	.....	.....	.....	.....	.....	.....
26	.....	691.53	.....	.....	.....	.....	.....	.....
27	.....	79.91	.....	.....	.....	.....	.....	.....
	$\nu_{0(v_{00})} = 36{,}774.0\ cm^{-1}$ $B' = 1.649\ cm^{-1}$ $B'' = 1.863\ cm^{-1}$		$\nu_{0(v_{00})} = 37{,}322.6\ cm^{-1}$ $B' = 1.648\ cm^{-1}$ $B'' = 1.994\ cm^{-1}$		$\nu_{0(v_{00})} = 37{,}544.59\ cm^{-1}$ $B' = 1.600\ cm^{-1}$ $B'' = 1.666\ cm^{-1}$		$\nu_{0(v_{00})} = 49{,}011.18\ cm^{-1}$ $B' = 1.483\ cm^{-1}$ $B'' = 1.802\ cm^{-1}$	

* The J numbering in these bands is uncertain; hence, values of ν_0, B', and B'' for these bands are also uncertain.

† A line at 37,544.40 cm^{-1} has also been observed in this band and is thought to be a $Q(1)$ line.

found a third $^1\Sigma$ state in C_2, but this state lies too high energetically to correspond to the $c^1\Sigma$ state of CN^+. The intense 2660.1 A band, mentioned in the preceding section and thought to be a $^1\Pi - {}^1\Pi$ transition of CN^+, may be the counterpart of a band of the Deslandres-d'Azambuja system of C_2, but it is not understood why only one band of the supposed $^1\Pi - {}^1\Pi$ CN^+ system should be developed.

None of the triplet bands corresponding to the Fox-Herzberg or Swan systems of C_2 have been observed in CN^+. Unfortunately, a large number of neutral CN bands, which are much stronger than the $^1\Sigma - {}^1\Sigma$ CN^+ bands, appear on the spectrograms from 3500 A

[2] *Ann. d. Phys.*, **8**, 221, 1951.

to the infrared. Thus, if bands arising from triplet transitions in CN^+ exist and are of approximately the same intensity as the CN^+ singlet bands, it is unlikely that the triplet bands would be found on our plates.

Of the singlet bands reported in this paper and known to belong to CN^+, only four—(1–1), (0–0), (4–2), and (1–0)—bands of the $c^1\Sigma - a^1\Sigma$ system at 3263.3, 3085.1, 3092.4, and 3063.3 A, respectively, fall sufficiently far to the red of the terrestrial ozone cutoff to be of astrophysical interest. Whether these bands can be expected in an astrophysical source containing CN^+ depends largely upon the $a^1\Sigma$ state being the ground state of CN^+. Similarities between the $f^1\Sigma - a^1\Sigma$ system of CN^+ and the Mulliken system of C_2, discussed earlier, suggest that the lower states of the two systems are analogous. Since the lower state of the Mulliken system is believed to be only 5000 cm^{-1} above the ground state of C_2, it follows that the $a^1\Sigma$ state of CN^+ is also very probably of low energy and is the lowest singlet state of CN^+. There is no a priori reason, however, why the situation in CN^+ cannot be slightly different from that in C_2 and why the $a^1\Sigma$ state might not, in fact, be the ground state of CN^+. If such is the case, the (1–1), (0–0), (4–2), and (1–0) bands of the $c^1\Sigma - a^1\Sigma$ system may be found in emission in the spectra of intense comets; perhaps, also, the first few lines of the (0–0) band could be detected in absorption spectra of the interstellar medium.

Further laboratory work should be done on the spectrum of CN^+ in an effort to detect additional band systems of this molecule, particularly those arising from triplet-triplet transitions, and to determine, if possible, the exact nature of the ground state.

The authors take pleasure in expressing their thanks to Dr. G. Herzberg for many helpful discussions of this problem and to Mrs. Ruth Innes, who assisted materially with the calculations.

RELATIVE SOLAR ENERGY DISTRIBUTION IN THE SPECTRAL REGION 10,000–25,000 A*

A. KEITH PIERCE
McMath-Hulbert Observatory, University of Michigan, Pontiac, Michigan
Received October 2, 1953

ABSTRACT

Tables are given of the observed relative solar energy distribution for zero air mass in the wave-length interval 10,000–25,000 A. The observations are based on measures made at Mount Wilson at the Snow telescope with high resolution—band pass 0.30 A. The calibration of the spectral response of the equipment was evaluated by observations of a black-body source and a pyrometric arc. A detailed description of the comparison sources and their use is given.

INTRODUCTION

A knowledge of the temperature, pressure, and opacity of the sun's atmosphere forms the groundwork for studies of Fraunhofer line intensities and profiles. Observations of limb darkening and energy distribution are fundamental to the solution, as these define the angular distribution of the emergent radiation and its intensity for all wave lengths—the boundary condition for the solution of the transfer problem. Previous observational work has served to give approximate solutions to the equation of transfer, but more accurate data are needed to implement and test recent exact theoretical solutions of the transfer equations and to establish more accurate model solar atmospheres. The purpose of this paper is to present new and more accurate data on the solar energy distribution of radiation from the center of the solar disk in the wave-length region 10,000–25,000 A. As a by-product, the atmospheric extinction at Mount Wilson was found for the days of observation.

The work of C. G. Abbot and of I. Wilsing has long been known to be in error for the energy distribution in the region beyond 10,000 A.[1] Recently R. Peyturaux[2] has considered the problem anew, and his observations show that the earlier results of Abbot are probably the more reliable. The energy distribution obtained by Abbot and by Wilsing refer to integrated energy from the whole solar disk. Minnaert[3] converted Abbot's measures to absolute values for the center of the sun's disk by the use of the solar constant and the curves of limb darkening. This procedure involves an additional step and can be avoided by direct observation of the sun's center.

Three principal observational problems must be solved in order to determine the relative solar energy distribution: (1) the calibration of the spectral response of the equipment, including the imaging system, if any; (2) the reduction of the observations for the effect of the absorption of the earth's atmosphere; and (3) the specification of the spectral purity of the observations and their reduction to infinite resolving power.

The first problem has been solved in two ways. Abbot[4] calibrated the transmission of his spectrographs and the reflectivity of the coelostat mirrors by building duplicate instruments. Observations obtained with each alone and in series permitted him to evaluate the transmission or reflectivity of each component separately. This procedure

* Supported in part by Contract N60nr-232-V with the Office of Naval Research.

[1] A. Unsöld, *Physik der Sternatmosphären* (Berlin: Julius Springer, 1938), p. 32.

[2] *Ann. d'ap.*, **15**, 302, 1952.

[3] *B.A.N.*, **2**, 75, 1924.

[4] *Ann. Smithsonian Inst.*, Vol. **2**, 1908.

is an expensive one, unless more than one instrument is to be built, one of which is to be used later in another installation. Wilsing[5] calibrated the response of his equipment by the use of a source of known spectral distribution, namely, a platinum-wire-wound furnace operated at 1560° K.

Calibration problems become more difficult as one attempts to use high dispersion and resolution; for, in order to duplicate as closely as possible the conditions with which the sun is observed, the intensity of the calibrating source must be increased so that the photometric step between sun and source is within receiver range. At the present time, it would seem that the highest temperature source suitable for this problem is the pyrometric arc.[6] Even with this source ($T = 3875°$ K) one must bridge an intensity ratio between sun and arc of 2.3 times at 2μ, 4.0 at 1μ, 14 at 0.5μ, and 84 at 0.3μ. In practice, these ratios should offer no great difficulty, since modern photoelectric amplifiers and cells can be made nearly linear for brightness ratios of 1000 to 1. A source of continuing difficulty, however, is the great variation in sensitivity of cells over moderate wavelength intervals.

The procedure used in determining the atmospheric extinction is well known, and a surprisingly accurate extrapolation to zero air mass can be made if one is located so that observations can be made through a sufficient range of solar altitude. The requirements for success are a transparent sky and a stable recording system.

The third problem, namely, the increase in spectral resolution, has received little attention. In general, previous observations have been made with low-dispersion spectrographs. By evaluating the effect of the Fraunhofer lines, attempts have been made to reduce the observations to a continuum. This was the method G. F. W. Mulders[7] used to correct Abbot's observations. H. H. Plaskett[8] observed the sun with moderate dispersion and selected regions free of strong absorption lines. R. Canavaggia, D. Chalonge, M. Egger-Moreau, and H. Ozoil-Peltey[9] corrected observations made in the wavelength region 3200–5000 A with a theoretical resolving power of about 1 A, by comparison of their records with the Utrecht *Atlas*.

The specification of a continuum in the violet or ultraviolet portion of the solar spectrum is very difficult or impossible, because of the great density of solar lines and their extensive wings. Here we must be satisfied with fixing the intensity scale of the observed spectrum and reducing to infinite resolving power. This procedure involves the use of the integral equation relating the instrumental profile and the observed contour of the spectrum. Within the limitation of the calibration problem, this is most accurately accomplished by direct observations with high-dispersion equipment. In the near infrared a continuum can be said to exist. There the advantage of high dispersion is the ability to work in regions of moderate atmospheric absorption, i.e., at the narrow windows between strong H_2O lines.

In May, 1949, by the kind permission of Dr. Ira S. Bowen and the staff of the Mount Wilson and Palomar Observatories, an all-reflecting infrared spectrometer of the Pfund type was installed by the McMath-Hulbert Observatory in the spectrograph room of the Snow horizontal telescope. This instrument has served to map the near infrared with high dispersion and to determine the wave lengths of about 6000 lines by the method of overlapping orders. To this instrumentation was added in April, 1950, an auxiliary optical path which served to image a small black-body source or a pyrometric arc on the first slit of the predisperser. Since the spectral energy distribution of each source was known, the spectral response of the equipment could be determined. The introduction of

[5] *Potsdam Pub.*, Vol. **23**, No. 72, 1917.

[6] H. G. MacPherson, *J. Opt. Soc. America*, **30**, 189, 1940.

[7] Diss. Utrecht, 1934.

[8] *Pub. Dom. Ap. Obs. Victoria*, **2**, 242, 1923.

[9] *Ann. d'ap.*, **13**, 355, 1950.

a new optical path to the previous system made it necessary to evaluate the relative reflectivity of the solar and the comparison paths.

OPTICAL AND RECORDING SYSTEMS

The Snow coelostat[10] follows a design suggested by C. G. Abbot. Sunlight is reflected from the coelostat, an aluminized glass flat, 76 cm in diameter, to a second plane mirror, 61 cm in aperture, mounted in a short fork at the top of a massive column. The coelostat mirror is rotated by a large sector through a gear train actuated by a weight-driven clock, while smaller sectors provide slow and fast motions for each mirror.

An $F/30$ spherical mirror, 61 cm in diameter, forms an image of the sun about 18 cm in diameter on the first slit of a 35-cm focal-length prismatic predisperser, which acts as a broad-band filter in front of the grating spectrometer. The spectrometer is an all-mirror system similar in design to the Pfund spectrometer arrangement at the McMath-Hulbert Observatory.[11] The Mount Wilson grating No. 42B, by Babcock, has a ruled area 142 × 183 mm, containing 74,000 grooves, spaced 400 grooves per millimeter. The focal length of the collimator and telescope mirrors is 4.7 meters; thus the predisperser and the spectrometer form a very unequal double monochromator. No detectable scattered light from other orders or from wave lengths more than 10 A away has been found. During the course of all observations, the entrance and exit slits were fixed at 10 × 0.066 mm. The width corresponds to a band pass of 0.30 A. At each wave length, it was necessary to "peak" the deflection of the recorder by adjusting the position of the low-dispersion spectrum on the spectrometer slit.

The receiver is a Cashman lead sulfide cell of the Dewar flask type and is cooled by a mixture of solid carbon dioxide and acetone. A Wilson[12] amplifier, with a step-gain control, amplifies the signal from the cell and feeds an input signal to a matching network with adjustable time constant. The output is recorded by a Leeds and Northrup Speedomax Recorder.

The comparison path for the black body and arc differs from the solar path, because a large collimator was not available or convenient to mount and use. The arrangement is illustrated schematically by Figure 1, *b*. Light from the comparison path was collimated by an 18° off-axis mirror having an aperture of 7 cm and a focal length of 27.5 cm. Parallel light from this mirror illuminated a small portion near the edge of a 27-cm mirror of 127-cm focal length, which formed a fivefold magnified image of the source on the first slit of the predisperser.

BLACK-BODY SOURCE

A carbon-tube furnace furnishes one of the simplest and most conveniently operated black-body sources. A. S. King[13] has published detailed suggestions for the design and operation of this type of furnace based on his years of experience. In the usual design the central resistance tube serves as a black-body chamber, and light is taken from one end of the tube. But, to accommodate a beam of large angular aperture, it is necessary to modify the arrangement so that light can be brought from a small opening in the side wall (see Fig. 2). The resistance tubes were fabricated from $\frac{1}{2}$-inch-diameter carbon-arc electrodes cut to 6-inch lengths and drilled axially with a $\frac{5}{16}$-inch hole. They were ground to close dimensions and to a circular cross-section in a center grinder. The black-body aperture was a slot $\frac{1}{2} \times 3$ mm. Two inches at each end of the tube were clamped in carbon contact blocks, which were, in turn, held by large water-cooled bronze castings. Water-cooled squirt tubes served as electrical conductors and as supports. Flared connections permitted easy assembly and removal of the various parts for repairs.

[10] G. E. Hale, *Ap. J.*, **23**, 6, 1906.

[11] R. R. McMath and O. C. Mohler, *J. Opt. Soc. America*, **39**, 903, 1949.

[12] G. P. Kuiper, W. Wilson, and R. J. Cashman, *Ap. J.*, **106**, 243, 1947.

[13] *J. Opt. Soc. America*, **12**, 503, 1926.

As it was necessary to operate in an inert atmosphere or in a vacuum, a water-cooled box, $5 \times 5\frac{1}{2} \times 8$ inches, surrounded the furnace. The radiation from the black body passed through a 2-inch diameter fused-quartz window provided with a vane shutter.

It is convenient to reduce the power consumption and cooling requirements by suitable heat baffling wherever possible. Thin sheets of stainless steel were placed inside the walls of the outer box. But the most effective shield was a carbon spool within a carbon tube, forming a double-walled inclosure surrounding the resistance tube. In order to improve the black-body conditions, the ends of the resistance tube were plugged with carbon rods, which were sawed nearly through radially at several points so as to act as heat shields.

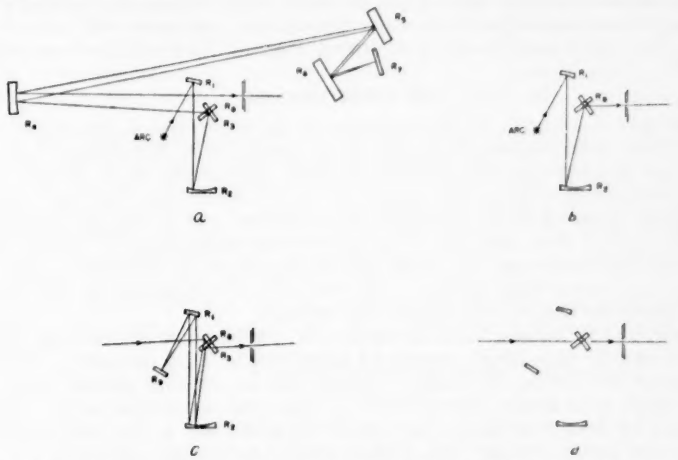

FIG. 1.—Schematic representation of the optics and optical paths used to determine the reflectivity of the imaging mirrors. Mirrors R_6 and R_8 form the coelostat system, and R_4 is a 24-inch diameter concave mirror of 60-foot focal length. The comparison optical path is shown by *b*.

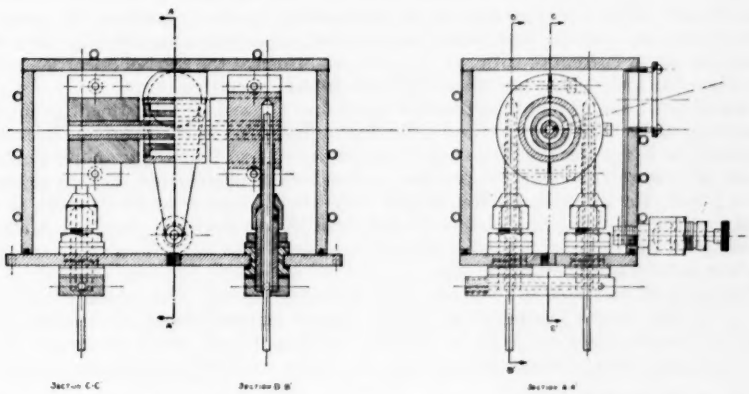

FIG. 2.—Black-body source. The scale is indicated by the central carbon resistance tube, 6 inches long.

The current was supplied from three current transformers, fed by 220 volts at about 15 amperes. Three turns of copper wire of large cross-section supplied 400 amperes to the furnace. A 220-volt Variac in the leg of one transformer permitted the temperature to be adjusted to the desired operating range.

The furnace was operated for periods of about ½ hour, the only limitation being in the heating of the recirculated cooling water. It was found that, at temperatures above 2700° K or with a new unfired tube, the quartz window became slightly dirty during operation. Under these conditions the transmission fell from its initial value of 94 per cent, which was independent of wave length, to about 92 per cent at 25,000 A and 90 per cent at 10,000 A. An improved design would place the window at a greater distance from the carbon resistance tube. Since the black body was operated without voltage regulation, it was necessary to follow its temperature variations with an optical pyrometer. The total range of variation during a set of observations amounted to less than 15°.

THE PYROMETRIC ARC

An arc light was used in the determination of the reflectivity of the mirrors and also served as a secondary standard to calibrate the spectrometer. A complete description of the arc and its operating characteristics has been published by H. G. MacPherson,[6] so that a short account of its use will suffice here. The pyrometric arc provides a convenient reproducible source of very high brightness, dependent only on the physical properties of a pure element—the constancy of the sublimation temperature of carbon. The constant maximum brightness and energy distribution make it an attractive source for a radiation standard of high intensity, with the added advantage that it can be operated in air without the necessity of a windowed inclosure.

C. Fabry and H. Buisson[14] used the carbon arc to reduce their observations of the solar spectrum in the wave-length region λλ 3200–2900 A. They adopted a distribution temperature of 3750° K. H. Plaskett[15] found that an arc with neutral cored carbons burned with a color temperature of 3080° K. This value, as we shall see, is considerably lower than for the pyrometric arc and can be explained only on the basis of the low arc currents used and by the fact that a cored positive carbon was employed.

The pyrometric arc, consisting of two movable electrodes mounted at 90° to each other, was set with the larger positive electrode vertical and the negative horizontal. The vertical electrode, ¼ inch in diameter, of spectroscopically pure graphite was matched with a horizontal cored carbon electrode. This was done to increase the stability of the arc, which, in practice, can be troublesome, as the conditions for operation require that it be operated just below its hiss point, a phenomenon which prevails with too high an arc or current or with the unstable conditions at the start of operation before the carbon has become hot and spindled to its normal operating shape.

A small synchronous motor and variale speed unit allowed for adjustment to the rate of burning, while clutches permitted individual adjustment of each carbon. In normal operation the tip of the negative carbon was positioned so that the graphite electrode burned off squarely, leaving the positive carbon free of obstruction. For an electrode gap of ¼ inch, the arc with suitable ballast drew 10–12 amperes at 60–70 volts. It was found that the operating conditions were very sensitive to electrode positions. A magnified image of the carbons, projected through a pinhole onto index lines on a card, gave sufficient control of the electrode gap.

The arc is not so stable as a voltage-controlled electric lamp. The intensity variations at a given wave length (periods 10 seconds to several minutes) amounted to about 1 per cent standard deviation at 15,000 A. Intensity changes of 5 per cent were common if the gap or voltage was suddenly changed, but the return to average brightness was within

[14] *Ap. J.*, **54**, 297, 1921.

[15] *Pub. Dom Ap. Obs. Victoria*, **2**, 213, 1923.

30 seconds. The short time variations, which might be called "noise," were of the order of 1 per cent.

The distribution temperature of the arc, a temperature based on the spectral distribution of energy measured over the wave interval λλ 2500–7500 A, was found by MacPherson to be 3860° K. This value becomes 3875° when the second radiation constant, $c_2 = 1.438$, is used.

DETERMINATION OF REFLECTIVITY OF THE MIRRORS

Sunlight was sent to the spectrometer by reflection from the coelostat, the first flat and the 24-inch concave mirror. In the comparison path, two concave mirrors and a small flat mirror imaged the black body or arc on the spectrometer slit. Although each path employed three reflections from aluminized mirrors, it is possible that the ratio of the two paths as a function of wave length was not the same. The coelostat and 24-inch mirrors had been aluminized 3 years prior to this set of observations and were somewhat white with water stain, while the mirrors of the comparison train had been recently aluminized.

The size and weight of the coelostat and 24-inch mirrors prevented easy handling in different optical arrangements. If we select the optical paths illustrated in Figure 1, *a* and *c*, by introducing auxiliary mirrors, then each mirror of the solar path and the comparison path acts to reflect the light twice. This procedure has the advantage of increasing the accuracy of the final determination. Mirrors R_8 and R_3 were mounted on parallel tracks (perpendicular to the page of Fig. 1), so that either one or the other could be used or they could be abutted to each other, as in Figure 1, *c*.

Referring to Figure 1, let $\delta_a(\lambda)$ be the observed deflection for path *a*, $\delta_b(\lambda)$ the observed deflection for path *b*, and so on; then, by performing experiments *a* and *b*, we find

$$\delta_a(\lambda) = KR_1R_2R_3R_4^2R_5^2R_6^2R_7 \tag{1}$$

and

$$\delta_b(\gamma) = KR_1R_2R_8 . \tag{2}$$

By taking the log of the ratio and rearranging terms, we have

$$\log(R_4R_5R_6) = \frac{1}{2}\left[\log\frac{\delta_a(\lambda)}{\delta_b(\lambda)} - \log R_7 - \log\frac{R_3}{R_8}\right]. \tag{3}$$

In a similar manner, by the use of the auxiliary mirror R_9, we observed the responses $\delta_c(\lambda)$ and $\delta_d(\lambda)$ of experiments *c* and *d*. The proportionalities are

$$\delta_c(\lambda) = CR_3R_2^2R_1^2R_9R_8 \tag{4}$$

and, for the direct image, we observe

$$\delta_d(\lambda) = C . \tag{5}$$

The ratio can be written

$$\frac{R_8}{R_9}\frac{\delta_c(\lambda)}{\delta_d(\lambda)} = R_3R_2^2R_1^2R_8^2 ; \tag{6}$$

and, by taking logs and rearranging terms, we obtain

$$\log(R_1R_2R_8) = \frac{1}{2}\left[\log\frac{\delta_c(\lambda)}{\delta_d(\lambda)} - \log R_9 - \log\frac{R_3}{R_8}\right]. \tag{7}$$

The logarithm of the ratio of the reflectivities of the two paths, equations (3) and (7), is

$$\log\frac{R_4R_5R_6}{R_1R_2R_8} = \frac{1}{2}\left[\log\frac{\delta_a(\lambda)}{\delta_b(\lambda)} - \log R_7(\lambda)\right] - \frac{1}{2}\left[\log\frac{\delta_c(\lambda)}{\delta_d(\lambda)} - \log R_9(\lambda)\right]. \tag{8}$$

If the reflectivities of the auxiliary mirrors R_7 and R_9 are known as a function of wave length or if they were prepared at the same time, the right-hand member of equation (8) is completely determined.

Figure 3 illustrates the mean reflecting curves resulting from observations made on many days during the same period of time for which solar runs were obtained. The solid line through the open circles refers to the reflectivity of the three mirrors R_1, R_2, and R_3 of the comparison path, while the dashed line applies to the three mirrors R_4, R_5, and R_9 of the solar path. The difference in reflectivity of the two paths was found to be

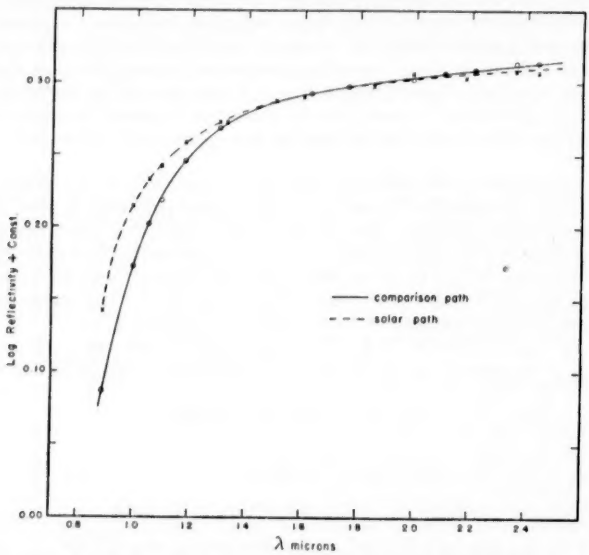

FIG. 3.—Reflectivity of three mirrors of the comparison path and three mirrors of the solar path plotted on a logarithmic scale as a function of wave length. All mirrors were coated with aluminum.

caused by a slight brown coat on mirror R_8. This was not noticed when the aluminization was performed but was readily visible when compared side by side with a properly coated mirror. The greater scatter of points for the solar path was due to two causes: the long optical path, from the coelostat to the 24-inch concave mirror and to the spectrometer, introduced considerable "seeing" (this effect was more pronounced for the arc because of its small size than for the large-diameter solar image used in the determination of the reflectivity of the comparison path); and, in addition, the brightness of the arc was not so stable as the sun.

SELECTION OF WAVE LENGTHS

The wave lengths for observation were chosen from the many available regions in the near infrared. Intervals free from absorption lines are numerous, and the selection was based, first, on the principle of uniform coverage and, second, on freedom from atmospheric and solar absorption lines. Owing to time limitations and cloudy weather, only about half the selected points were observed.

The wave lengths observed were: λλ 25074, 24388, 22443, 22115, 21028, 17587, 15950, 15575, 15274, 14301, 13381, 12986, 10478, and 9937. Of these, only λλ 25074,

14301, and 13381 are in the wings of strong atmospheric absorption lines. The latter were included to provide observations close to the large gaps in the solar spectrum caused by strong H_2O absorption and to test these points for exponential extrapolation to zero air mass.

OBSERVATIONS OF SUN AND COMPARISON SOURCE

The program of observations was started in the early morning as soon as the sun cleared distant Mount San Antonio and near-by live-oak trees on Mount Wilson. The measures began when the secant z, corrected for refraction and curvature of the earth, obtained values of 12–15 at 5:00 A.M. and were carried to secant z about 1.3 at 10:00 A.M. There is little gain in going to smaller air masses at these long wave lengths because of the small intensity change between 10:00 A.M. and noon, and the small gain in leverage of extrapolation to zero air mass. In fact, the incidence of the smog layer expanding from the valley and rolling in thick clouds over the top of Mount Wilson completely disrupted the smooth trend of the observations in the late morning. Hence the remainder of the day was confined to calibration runs with black body or arc.

Five to nine wave lengths were selected for a day's run. The grating table was set about 5 A beyond each observational point, and a 2-minute run was made over a 10 A interval toward shorter wave lengths. Thus in 15–20 minutes a set of selected wave lengths could be observed. This procedure was then repeated throughout the early morning, although it was generally interrupted at small secants for various calibration purposes requiring sunlight and stable transparency conditions.

On the same day on which secant z runs were made, the spectral sensitivity of the spectrometer and receiver was obtained from observations of the black-body source by way of the comparison path. At each wave length of observation, the Speedomax recorded the deflection, and, at the same moment, the temperature was observed by means of an optical pyrometer which had been calibrated by the National Bureau of Standards. On May 21 and on succeeding days the spectral sensitivity records were made, using the standard graphite arc.

The accuracy of the determination of the energy distribution depends directly on the linearity calibration of the recording system. Because the response of the Wilson amplifier was known to be nonlinear, it was felt that a daily determination of the response-curve was necessary. No change in the curve was detected with time or temperature.

The relation between recorder deflection and incident intensity to the spectrometer was obtained by means of series of 10 sectors of known transmission. This procedure postulates that the signal from the lead sulfide cell is not frequency-dependent; a test of this, by changing the speed of rotation of the sectors, showed no alteration in the observed deflection except at very low speeds of rotation, which were not used for calibrating purposes. Hence these experiments were taken as partial proof that, over the range of sector speed employed, the recording equipment responded to the sectors as if they were neutral screens of known transmission. An independent check was made by the method of summing the deflections of a series of apertures. By use of the calibration-curve determined with the sectors, the sums obtained equaled the predicted quantities to within $\frac{1}{4}$ per cent. Hence the response-curve was known to $\frac{1}{4}$ per cent accuracy.

Figure 4 illustrates the difference between a linear characteristic through the origin and the observed curve. The abscissa gives the observed deflection in millimeters on the original tracing. The ordinate gives the correction in millimeters to be applied to the observed deflection, to correct it to a linear intensity scale. At very low light-levels and high amplifier gain, the correction-curve is somewhat higher.

MEASUREMENTS AND REDUCTIONS OF OBSERVATIONS

The methods developed by S. P. Langley[16] for correcting observations made within our atmosphere have been employed throughout. If we assume that the absorption is uniform

[16] *Ann. Ap. Obs., Smithsonian Inst.*, Vol. 1, 1902.

in azimuth and arranged in concentric layers about the earth's surface, Bouguer's formula for exponential absorption with increasing air mass can be used. It should be noted that the proper application of the formula is limited to observations made in wave-length regions free of strong absorption lines; otherwise, the exponential absorption law is modified by saturation effects. Since the wave-length interval (0.30 A) transmitted by the spectrometer was small, it was possible to select many regions visibly free from absorption lines and in other regions to observe at the peaks or "windows" between strong lines. These peaks are part of the resonance wings of saturated lines for which the absorption coefficient is directly proportional to the number of effective absorbers. Hence, in the absence of emission, the equation of transfer reduces to Bougeur's exponential absorption law.

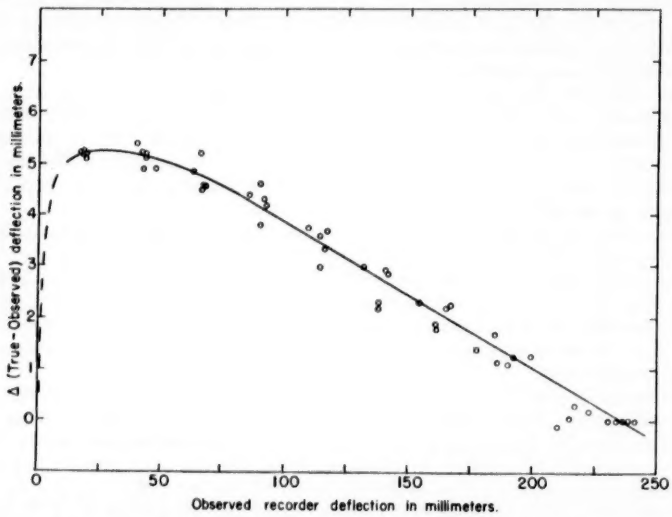

FIG. 4.—Linearity-curve of the recording equipment. The curve is the difference between the observed deflection and a linear characteristic through the origin.

The deflection on each tracing was measured by a millimeter scale at the proper wave length. The hour angle of the sun for the instant of observation was interpolated from time marks. The recording paper was run continuously at a slow rate, and time marks were placed by pencil on the paper at convenient integer minutes, as read from a clock giving the local hour angle of the sun.

The deflections were corrected for nonlinearity of the amplifier and converted to logarithms. Tables giving the cosine of the zenith distance of the sun for each 5 minutes after sunrise had been prepared for each day of the month. The mean correction, for refraction at Mount Wilson and curvature of the earth, had been entered as small corrections to the cosine values. The use of the modified cosine permitted easy and accurate interpolation, and by simple reciprocals the true air mass was quickly determined. Plots of secant z versus $\log_{10}$ deflection were prepared for examination and a weighted least-squares solution for the best straight line fitting the observations was computed. In general, points for which secant $z > 10$ were rejected because of their larger scatter; also it was felt that the correction for refraction was not too well known for these points. Figure 5 shows the plot of the observations obtained on May 8, 1953.

The black-body runs were measured and reduced, using the observed temperatures at the times of observation. Appropriate corrections to the temperature were made for the known transmission of the quartz window and for the calibration of the optical pyrometer. From the black-body runs, the logarithm of the response of the complete equipment, including the comparison optical path, is found from the difference log (deflection) − log (energy black body). The relative black-body energy output was found from tables computed with the second radiation constant $c_2 = 1.438$ and then corrected for the transmission of the quartz window. The logarithm of the sensitivity of the complete equipment is illustrated by Figure 6. The resulting curve is a combination of the effects of the reflectivity of the various mirrors in the optical train, the effect of the predisperser, the blaze of the grating, and, finally, the response-curve of the lead sulfide receiver.

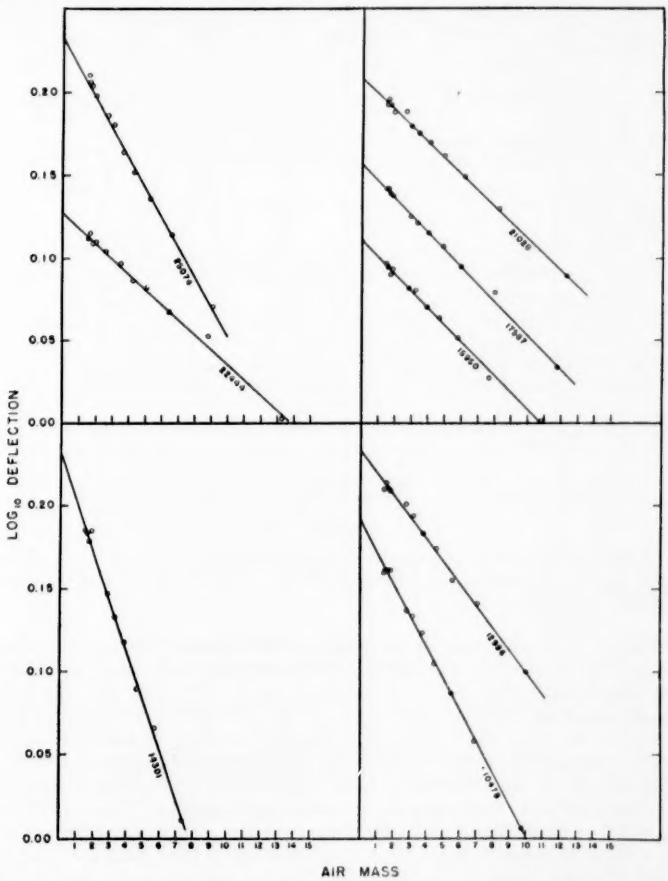

FIG. 5.—Observations of May 8, 1953, at eight different wave lengths. The lines and curves show the extrapolation of the solar intensity as observed at various air masses to the value obtained outside the atmosphere.

The log of the relative intensity as a function of wave length for the center of the sun's disk has been computed from the relation

$$\log I_\lambda(0) = \log \delta_\lambda(\text{sun})_{M=0} + \log I_\lambda(BB) - \log \delta_\lambda(BB) + \log T_\lambda + \log \frac{R_\lambda(\text{comp.})}{R_\lambda(\text{solar})} . \quad (9)$$

In equation (9), δ designates the corrected recorder deflections of the sun and black body; I the intensities; R the reflectivities; and T the transmission of the quartz window of the black body.

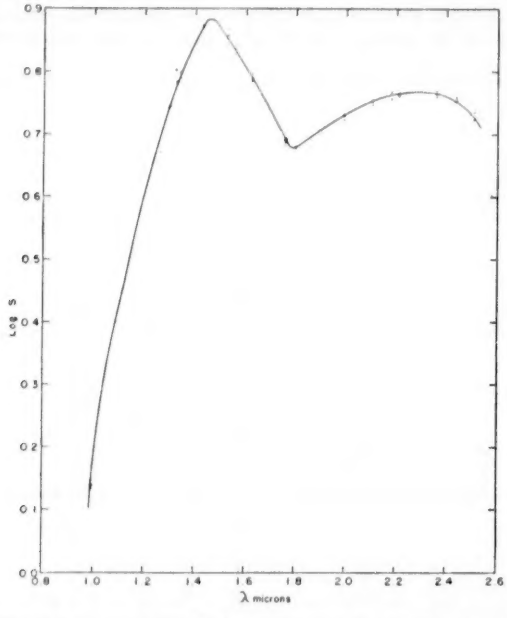

FIG. 6.—Logarithm of the spectral sensitivity versus wave length. The shape of the curve is determined by the blaze of the grating, the response of the lead sulphide cell, and the reflectivity of the spectrometer mirrors.

Table 1 gives the final results for each day's observation of the sun. The first column lists the wave length of observation, while the succeeding nine columns, headed by the dates of observation, list log $I_\lambda(0)$ for the sun's center. The root mean-square error of each observation is listed below each value of log $I_\lambda(0)$ and is discussed further in the section on error analysis. The observations obtained on May 21 are based on the pyrometric arc as a reference standard at 3875° K. The results are given in the ninth column. A much better fit to the black-body runs is obtained if we adopt a temperature of 3775° K, which leads to the values given in the tenth column. This is 100° below the corrected value of MacPherson. The temperature effect of operating the arc on Mount Wilson at a reduced pressure is not known. Application of the Clausius-Clapeyron equation for the pressure difference between 1000 feet of elevation and the top of Mount Wilson, 5700 feet, predicts a reduction of 40° C to the arc temperature.

The column headed "Smoothed Means" in Table 1 gives values obtained from the best curve drawn by eye on a large-scale plot of the separate observations. Table 2 supple-

TABLE 1*

Logarithm of Relative Energy Distribution at Center of Sun's Disk

[log $I_\lambda(0)$]

Wave Length (A)	Date of Observation									Smoothed Mean
	May 7	May 8	May 9	May 11	May 12	May 17	May 18	May 21	May 21	
25074	0.1173	0.1165	.....	.....	.....	.....	.....	.....	.....	0.1170
	0.0042	0.0053	.....	.....	.....	.....	.....	.....	.....	.....
24388	.....	.....	0.1688	0.1662	0.1678	0.1877	0.1679	.....	.....	0.1675
	.....	.....	0.0039	0.0046	0.0044	0.0047	0.0041	.....	.....	.....
23595	.....	.....	.....	.....	.....	.....	.....	0.2128	0.2249	0.2220
	.....	.....	.....	.....	.....	.....	.....	0.0041	0.0041	.....
22443	0.2938	0.3057	.....	.....	.....	.....	.....	.....	.....	0.3000
	0.0037	0.0038	.....	.....	.....	.....	.....	.....	.....	.....
22115	.....	.....	0.3188	0.3282	0.3244	0.3387	0.3280	.....	.....	0.3275
	.....	.....	0.0042	0.0039	0.0041	0.0039	0.0043	.....	.....	.....
21800	.....	.....	.....	.....	.....	.....	.....	0.3375	0.3486	0.3500
	.....	.....	.....	.....	.....	.....	.....	0.0038	0.0038	.....
21028	0.4037	0.4043	0.4022	0.4053	0.4069	0.4120	0.4115	.....	.....	0.4080
	0.0037	0.0036	0.0047	0.0041	0.0043	0.0041	0.0044	.....	.....	.....
19910	.....	.....	.....	.....	.....	.....	.....	0.4774	0.4872	0.4950
	.....	.....	.....	.....	.....	.....	.....	0.0043	0.0043	.....
17587	0.6939	0.6944	0.6959	0.6973	0.6987	0.6886	0.6953	0.6872	0.6950	0.6940
	0.0038	0.0036	0.0049	0.0039	0.0039	0.0038	0.0041	0.0038	0.0038	.....
16265	.....	.....	.....	.....	.....	.....	.....	0.8066	0.8131	0.8140
	.....	.....	.....	.....	.....	.....	.....	0.0037	0.0037	.....
15950	0.8303	0.8317	.....	0.8434	0.8410	.....	.....	.....	.....	0.8365
	0.0039	0.0038	.....	0.0035	0.0037	.....	.....	.....	.....	.....
15575	.....	.....	0.8668	.....	.....	.....	.....	.....	.....	0.8630
	.....	.....	0.0044	.....	.....	.....	.....	.....	.....	.....
15274	.....	.....	.....	.....	.....	0.8698	0.8834	0.8833	0.8885	0.8830
	.....	.....	.....	.....	.....	0.0039	0.0043	0.0037	0.0037	.....
14301	.....	0.9443	0.9580	0.9450	0.9361	.....	.....	.....	.....	0.9470
	.....	0.0041	0.0043	0.0097	0.0041	.....	.....	.....	.....	.....
13381	.....	.....	.....	.....	.....	1.0240	1.0282	1.0249	1.0273	1.0260
	.....	.....	.....	.....	.....	0.0037	0.0059	0.0039	0.0039	.....
12986	1.0665	1.0653	1.0694	1.0611	1.0585	1.0635	1.0574	.....	.....	1.0630
	0.0039	0.0039	0.0039	0.0052	0.0035	0.0037	0.0044	.....	.....	.....
10478	.....	1.3072	1.3172	1.3041	1.2926	1.2923	1.2850	.....	.....	1.2930
	.....	0.0038	0.0039	0.0041	0.0041	0.0039	0.0053	.....	.....	.....
9937	.....	.....	.....	1.3516	1.3556	1.3485	1.3430	1.3560	1.3498	1.3510
	.....	.....	.....	0.0041	0.0039	0.0039	0.0058	0.0043	0.0043	.....

* The root-mean-square error of observation is given below each value of log $I_\lambda(0)$ in the table. See text for its determination.

ments this list and gives the smoothed values of log $I_\lambda(0)$ for an equidistant set of wave lengths. The results are in satisfactory agreement with those of Peyturaux.[2] A comparison is given in Figure 7, which shows the measures of the author as circles and the mean results of Peyturaux as crosses. The observations show large deviations from a Planck-curve corresponding to $T = 6400°$ K. The hump at 16,000 A is remarkably sharp.

TABLE 2

SMOOTHED RELATIVE VALUES OF LOG $I_\lambda(0)$

Wave Length (A)	log $I_\lambda(0)$	Wave length (A)	log $I_\lambda(0)$	Wave Length (A)	log $I_\lambda(0)$
9,000	1.452	15,000	0.900	21,000	0.410
10,000	1.342	16,000	.832	22,000	0.335
11,000	1.242	17,000	.752	23,000	0.262
12,000	1.148	18,000	.658	24,000	0.192
13,000	1.059	19,000	.570	25,000	0.125
14,000	0.973	20,000	0.488	26,000	0.060

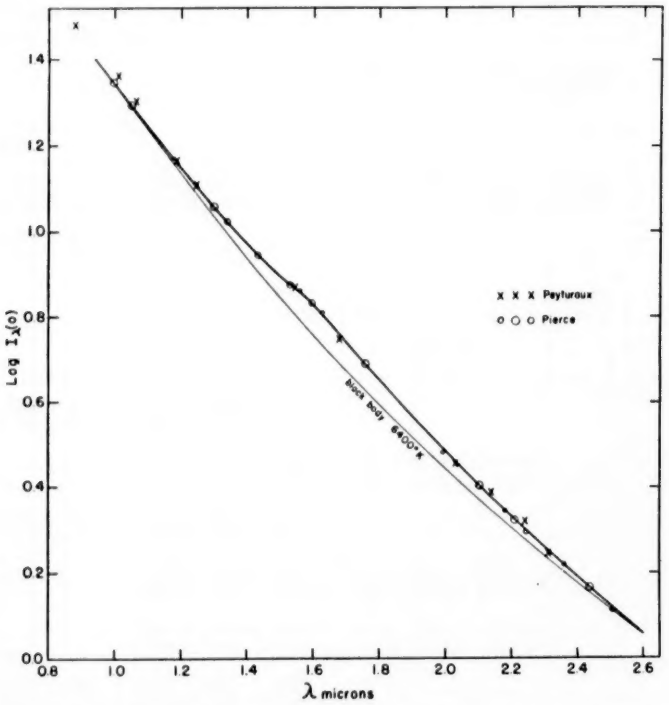

FIG. 7.—Relative solar-energy distribution. The black-body curve for $T = 6400°$ K is drawn in only for comparison and has been fitted to the end-points of the observed solar curve by shifting it vertically.

ERROR ANALYSIS

The root-mean-square error in these determinations is distributed as follows: The error of reading the temperature of the black body is estimated as 3° C. As this is random for each observation and each wave length, application of Wien's law gives 0.0020 as the estimated error in log $I_\lambda(BB)$ at λ 15000 A. The percentage error in finding the transmission of the quartz window is $\frac{1}{4}$ per cent, and hence the error in log T_λ is 0.0010. The deflection error of the recorder, for observations of the black body, is compounded of the errors of the linearity calibration, noise of the trace, and error of reading. If we adopt somewhat arbitrarily a value of $\frac{1}{2}$ per cent, then the error in log $\delta_\lambda(BB)$ is 0.0020. Likewise, the error in the logarithm of the reflectivity ratio of the mirrors is taken to be 0.0020. The standard deviation of the extrapolated secant z-curves, i.e., the error in log $\delta_\lambda(\text{sun})_{M=0}$, was directly determined by the least-squares solutions. The values center about the figure 0.0020, with an extreme range between 0.0007 to 0.0090.

If one estimates the root-mean-square error from these error limits, one finds from the formula of propagation of errors that the root-mean-square error of a single observation of log $I_\lambda(0)$ is about 0.0040, or about 1 per cent of the intensity. The individual values are given in Table 1. An examination of the table shows some systematic trends, whose cause is unknown to the writer. Hence the final smoothed values of log $I_\lambda(0)$, as determined from a large-scale plot of the observations, have an estimated precision of 0.0050 for log $I_\lambda(0)$.

In addition to the errors discussed above, the final result is affected by the following influences: the error of absolute calibration of the optical pyrometer, whose estimated maximum uncertainty is 5° C; the deviations of the furnace from true black-body conditions; the variations in the long-time stability of the equipment; and the systematic errors in the determination of the transmission of the quartz window, the reflectivity of the mirrors, and the calibration of the amplifier gain and linearity.

EXTINCTION OF THE EARTH'S ATMOSPHERE

Direct radiation from the sun is diminished by three main sources of extinction:[17] (1) molecular scattering—about proportional to λ^{-4}; (2) obscuration by haze and dust; and (3) band or line absorption by molecules at selected wave lengths.

Except for certain wave lengths near strong water-vapor bands, we have tried to select regions free of molecular absorption. In Figure 8 we have plotted van de Hulst's calculation of the extinction coefficient of pure air for the reduced atmosphere (H = 6.44 km) of Mount Wilson. This curve is based on a slight modification of the original Rayleigh scattering theory, which in a first approximation makes the extinction almost exactly proportional to λ^{-4}. In the figure the irregular lines above the pure air-curve give the observed values for several days of observation. It is of interest to note the general increase in the extinction as the warmer weather and hazy conditions of summer approached. We also note that even on the best day, May 7, the extinction in the near infrared is primarily due to "dust" and that the observed extinction is $\tau = 0.005$, which corresponds to a vertical transmission of 99.5 per cent.

SOME REMARKS ON HIGH-DISPERSION SPECTRAL PHOTOMETRY

We have shown in the introduction that, as one extends the observations to shorter wave lengths, the problem of calibration becomes more difficult. In some earlier work the author fell into the error of using too narrow a slit in an effort to "get in between" the absorption lines in the violet. The error introduced is that of a variable width-diffraction pattern on the collimator as a function of wave length. The possibility of this

[17] H. C. van de Hulst in G. P. Kuiper, *The Atmospheres of the Earth and Planets* (Chicago: University of Chicago Press, 1948), p. 55.

error has been pointed out by G. Harrison[18] but seems to be missing in the astronomical literature.

Further, suppose that one observes the spectrum of the sun or of a star with a suitable imaging system, so that the collimator is geometrically filled with light. In practice, with narrow slits, there will be diffraction effects at the edges of the collimator. The use of a calibrating source which will more than fill the collimator, such as a lamp just before

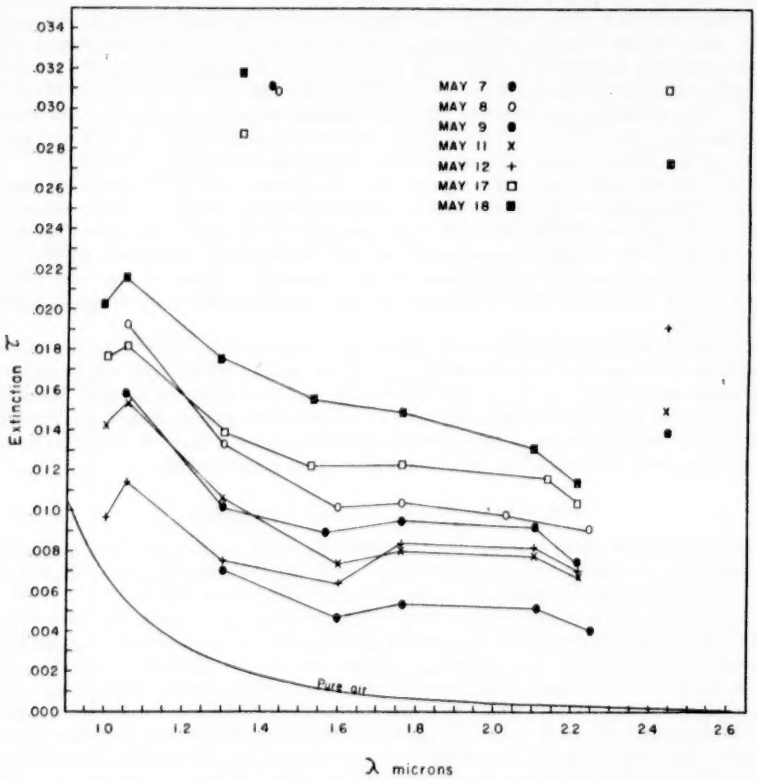

FIG. 8.—Atmospheric extinction at Mount Wilson. The smooth curve labeled *Pure air* is from van de Hulst and follows the Rayleigh λ^{-4} law. The broken curves are the observed values of extinction. Scattered points with high extinction are in water-vapor bands.

the slit, or one which fails to fill the collimator introduces errors of calibration with wave length due to diffraction. That is, when one wishes to make a spectrophotometric comparison, the star and comparison source must be imaged at the same f/ratio on the collimator unless the collimator is much larger than the diffracted or geometrical beams from each.

The author's original program extended to ultraviolet wave lengths, and a number of observations were made. It was found that polarization differences between comparison and solar paths introduced errors larger than the 1 per cent below 8000 A, while no de-

[18] *J. Opt. Soc. America*, **24**, 60, 1934.

tectable error from this cause was found above 8000 A. This arose from the changing angle of illumination of the coelostat, from the action of the grating as an analyzer of the incident radiation, and from the dip in the reflectivity-curve of aluminum at about 8000 A. The action of the grating as a polarizer varies with wave length and appeared visually to be strongest in regions farthest removed from the blaze. It is, of course, realized that these effects play no role if the solar and comparison paths can be made identical. This condition is difficult to fulfil for large-scale instruments, in which a collimator as large as the imaging mirror is desirable. In addition, a suitable mounting must be used.

It is a pleasure to express my thanks to Dr. Robert R. McMath. His interest and direction made possible this investigation. I owe debts of gratitude to Messrs. William Livingston and Dale Vrabec, who, as McMath-Hulbert staff observers at Mount Wilson, shared with me the burden of the observing program. I am grateful to Dr. Robert B. Leighton for permission to draw electrical power for the black body from mains operating the cosmic-ray installation at the Snow building, and to members of the research staff of the Detroit Edison Company, who loaned electrical equipment for the problem. From Dr. McMath's and the author's rough sketches, the detailed design of black-body arc, mirror supports, etc., was the work of Mr. John T. Brodie. Mr. Herbert E. Sanderson constructed the mechanical parts and helped instal them at Mount Wilson. I wish also to thank Dr. Ira S. Bowen for his kindness in making available the Snow telescope.

THE FORMATION OF ATMOSPHERIC O_2 EMISSION IN THE AIRGLOW

JOSEPH W. CHAMBERLAIN*
Geophysics Research Directorate, Air Force Cambridge Research Center
Received November 9, 1953

ABSTRACT

A suggestion by Bates, that absorption of the O_2 Atmospheric 0–0 band followed by emission of 0–1 may be an important source of the observed airglow O_2 emission, is investigated quantitatively. An approximate equation of radiative transfer is solved and applied to a model atmosphere. In the limiting case of no collisional de-excitation, Bates's fluorescent mechanism could account for about 75 per cent of the observed emission, and this portion would arise from a layer at about 50 km. The low rotational temperatures that have been determined for the 0–1 band are tentatively interpreted as an effect of collisional de-excitation and thus may not represent kinetic temperatures.

I. INTRODUCTION

The O_2 Atmospheric ($b\,^1\Sigma_g^+ \rightarrow X\,^3\Sigma_g^-$) band system was first observed in emission by Kaplan[1] in a laboratory afterglow, and shortly afterward the 0–1 band at 8645 A was identified by Meinel[2] in the airglow. The observations by Krassovsky,[3] who used a photoelectric image-converter, have shown a number of emissions longward of the photographic infrared. Although Krassovsky[4] did not believe that the Atmospheric system was present in this region, J. Dufay[5] has suggested that these observations may show the 0–2 band at 9976 A blended with an *OH* band. However, the transition probabilities indicate that 0–2 would be extremely weak. As we might expect from the strong A band in solar spectra, the 0–0 transition (λ 7596) is completely absorbed below the emitting layer and is not observed in emission. Also no bands arising from $v' \geq 1$ have been observed.

So far, the height of the emitting layer has not been determined from precise measurements of the variation of intensity with zenith angle. Meinel[6] noted that the 0–1 band intensity varied with zenith angle at about the same rate as the neighboring *OH* bands; this implied that the effective emitting layer is in the neighborhood of 70 km, the height for *OH*.[7] Moreover, Meinel's[6] rotational temperature of 150° K seemed to be fairly consistent with this height. A recent analysis[8] of rocket data, however, lists the minimum atmospheric temperature as 205° K at a height of 80 km. Since the Atmospheric bands arise from a forbidden transition, the rotational temperature at any one level should ap-

* Now at Yerkes Observatory.

[1] *Nature*, **159**, 673, 1947; *Phys. Rev.*, **71**, 274, 1947.

[2] *Trans. Amer. Geophys. Union*, **31**, 21, 1950.

[3] *Doklady Acad. Sci., S.S.S.R.*, **70**, 999, 1950. Observations of the photoelectric infrared spectrum have also been made by Kron (*Pub. A.S.P.*, **62**, 264, 1950) and more recently by A. V. Jones (*Nature*, **172**, 496, 1953).

[4] *Op. cit.*, **73**, 679, 1950.

[5] *Ann. de géophys.*, **7**, 1, 1951.

[6] *Ap. J.*, **112**, 464, 1950.

[7] F. E. Roach, H. B. Pettit, and D. Williams, *J. Geophys. Res.*, **55**, 183, 1950. This height is probably more reliable than the 300 km of Hurukata (*Rep. Ionosph. Res. Japan*, **4**, 137, 1950) or the 150 km of Berthier (*C.R.*, **237**, 928, 1953). Berthier deduced 130 km for the O_2 band but did not adequately discuss the effects of atmospheric scattering on the reductions of his observations.

[8] The Rocket Panel, *Phys. Rev.*, **88**, 1027, 1951.

proximate the kinetic temperature. This expectation has been roughly verified for fairly high densities by the laboratory rotational temperatures obtained by Branscomb.[9] The low rotational temperature in the airglow was confirmed by J. and M. Dufay,[10] who pointed out that if the *OH*- and O_2-emitting layers coincided, then either the *OH* temperatures (which average about 260° K at middle latitudes) or those of O_2 must depart for some reason from the kinetic temperature.

Bates[11] has called attention to the fact that absorption of the 0–0 band continually populates the $v' = 0$ level, which may then emit the 0–1 band. Thus some of the 0–0 emission will ultimately be converted into the 0–1 band, which may then have an effective emitting height appreciably lower than the height of the primary emission. The 0–0 band has a transition probability about fourteen times that of 0–1. Hence the former will be scattered numerous times before it is transformed into 0–1, and much of the 0–0 radiation will be scattered out of the atmosphere. A solution of the transfer equation in Section II shows that the 0–1 fluorescence will be approximately three times as intense as the 0–1 primary emission.

In this paper we shall attempt a quantitative discussion of the formation of the 0–1 band by the fluorescence mechanism. An approximate transfer equation is solved in the next section and applied to a model atmosphere in Section III. Finally, we shall discuss the roll of collisional de-excitation and an alternate transfer mechanism in an attempt to understand the observed rotational temperatures.

II. THE EQUATION OF RADIATIVE TRANSFER

We consider here a plane-parallel layer emitting at frequency ν in the 0–0 Atmospheric band at an undetermined height above the absorbing atmosphere. In passing through the atmosphere, the intensity, $I_\nu^{(0)}$, will be diminished in proportion to the number of molecules per cubic centimeter, N_ν, in the ground state capable of absorbing frequency ν and to the absorption coefficient per molecule, a_ν. We assume that every absorption at ν is followed by p_0 isotropic re-emissions in the same frequency and by p_1 transitions in the corresponding frequency of the 0–1 band. The p's represent relative vibrational transition probabilities for the two bands. Thus our equation of transfer for the 0–0 band is

$$-\cos\theta \frac{dI_\nu^{(0)}(x,\theta)}{dx} = -N_\nu a_\nu I_\nu^{(0)}(x,\theta) + p_0 N_\nu a_\nu J_\nu^{(0)}(x), \tag{1}$$

where θ is the angle the light-ray makes with the downward vertical, x is the linear height measured positively upward, and $J_\nu^{(0)}$ is the intensity averaged over all directions.

If we define the optical depth, τ_ν, by $d\tau_\nu = -N_\nu a_\nu dx$ and let $\mu = \cos\theta$, equation (1) becomes

$$\mu \frac{dI_\nu^{(0)}(\tau_\nu,\mu)}{d\tau_\nu} = -I_\nu^{(0)}(\tau_\nu,\mu) + p_0 J_\nu^{(0)}(\tau_\nu). \tag{2}$$

The corresponding equation for 0–1 emission, which does not suffer any absorption, is

$$\mu \frac{dI_\nu^{(1)}(\tau_\nu,\mu)}{d\tau_\nu} = p_1 J_\nu^{(0)}(\tau_\nu), \tag{3}$$

and the mean intensity is given by

$$J_\nu^{(0)}(\tau_\nu) = \frac{1}{2}\int_{-1}^{+1} I_\nu^{(0)}(\tau_\nu,\mu)\,d\mu. \tag{4}$$

[9] *Phys. Rev.*, **86**, 258, 1952.

[10] *C.R.*, **232**, 426, 1951.

[11] *The Earth as a Planet*, ed. G. P. Kuiper, chap. xii. (To be published by the University of Chicago Press.)

Equation (2) is to be solved subject to the boundary conditions (*a*) that the downward intensity just below the emitting layer is $I_\nu^{(0)}(0, +\mu) = p_0 E_\nu/\mu$ and (*b*) that $I_\nu^{(0)}(\tau_\nu, \mu) \to 0$ as $\tau_\nu \to \infty$. Once equation (2) is solved, equation (3) may be readily integrated with the boundary conditions that $I_\nu^{(1)}(0, +\mu) = p_1 E_\nu/\mu$ and $I_\nu^{(1)}(\infty, -\mu) = 0$. Here E_ν represents the energy distribution in the primary emission. The vibrational transition probabilities have recently been computed by Fraser, Jarmain, and Nicholls.[12] They find $p_0 = 0.933$ and $p_1 = 0.065$.

Integrodifferential equations having the form of equation (2) have been discussed fully by Chandrasekhar,[13] and we shall omit details of the solution here. Suffice it to say that Chandrasekhar has presented a series solution for $I_\nu(\tau_\nu, \mu)$ that is based on replacing equation (2) with $2n$ linear differential equations. In principle, the accuracy of the solution can be increased indefinitely as n is increased; in practice, it is not usually necessary to carry the solution to a high order of approximation. A numerical solution for equation (2) has been obtained with the first, second, and third approximations, and there is very little difference in the results from one solution to the next. Solving equations (2) and (3) with the first approximation, we obtain, for the downward flux in the 0–1 band at optical depth τ_ν,

$$2\pi \int_0^{+1} I_\nu^{(1)}(\tau_\nu, \mu)\, \mu d\mu = 2\pi p_1 E_\nu \left[1 + 2.86\,(1 - e^{-0.45\tau_\nu})\right]. \tag{5}$$

It may be seen from this equation that, as $\tau_\nu \to \infty$, the ratio of fluorescence to primary emission becomes 2.86/1. A partial check on the computations and on the accuracy of the approximation is provided by the condition that the total net (downward and upward) flux in the 0–0 and 0–1 bands must remain constant at all depths.

III. THE 0–1 BAND IN THE AIRGLOW

In order to apply equation (5) to the atmosphere, we must relate the optical depth, τ_ν, to height in the atmosphere. The faction of O_2 molecules in each rotational level of the ground state ($v'' = 0$) has been computed from the Boltzmann excitation equation for a mean atmospheric temperature of 200° K. Below 80 km the O_2 densities were taken as 21 per cent of the total particle densities determined from rocket flights;[8] and Miss Kallman's[14] semiempirical densities, based on assumed oxygen dissociation between 80 and 120 km, were used above 80 km.

In the upper atmosphere collisional broadening of lines is negligible, and lines arising from forbidden transitions with long lifetimes for the upper states suffer very little natural broadening. Hence we need consider only the Doppler broadening of each rotational line. Inasmuch as the intensity of a Doppler line follows an error function,[15] only a small fraction of the line lies outside the range $\pm \Delta\nu$, where the absorption coefficient, α_ν, falls to half its value at the line center. Strictly speaking, our calculations will apply to the centers of the lines, but for most practical purposes we may regard an entire line as being formed at approximately the same height as its center.

The absorption coefficient also varies from one line to the next, so that, in general,

$$\alpha_\nu(J''J') = \alpha_0 \frac{S(J''J')}{2J'' + 1}\, \delta_\nu. \tag{6}$$

Here δ_ν is the Doppler function, S is the line strength, and α_0 is the absorption coefficient

[12] *Ap. J.*, **119**, 286, 1954.

[13] *Radiative Transfer* (Oxford: Clarendon Press, 1950).

[14] *J. Geophys. Res.*, **58**, 209, 1953.

[15] For details see L. H. Aller, *The Atmospheres of the Sun and Stars* (New York: Ronald Press, 1953).

for the entire 0–0 band. From his study of the solar A band, van de Hulst[16] deduced $a_0 = 1.30 \times 10^{-11}$ cm²/sec. This value corresponds to an Einstein coefficient of spontaneous emission, $A(v'v'')$, of 0.18 sec^{-1} and is in fair accord with the value found in the laboratory by Childs and Mecke.[17]

The proportionality constant that usually appears in equation (6) is unity if the relative strengths are chosen so that the sum of the strengths of all lines originating from a common lower level *equals* the statistical weight of that level. The relative strengths (which are frequently called "intensity factors" in the literature) have been computed by Schlapp.[18] It should be pointed out in this respect that the strengths used[6] to determine

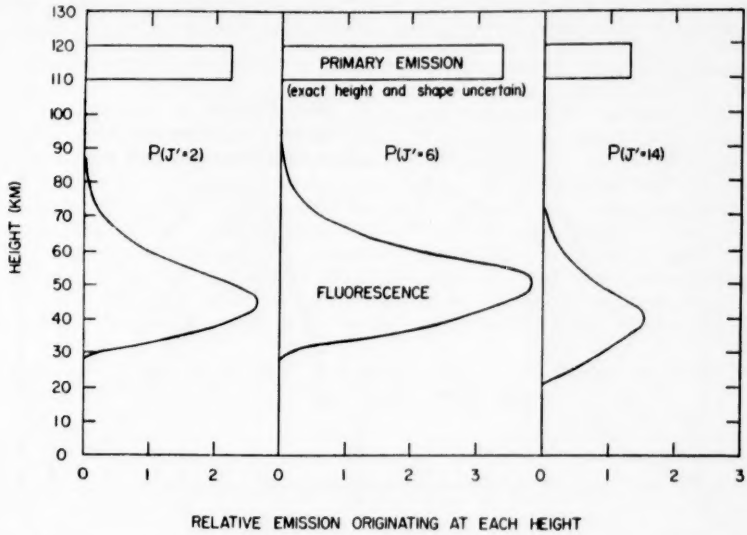

FIG. 1.—The formation of three lines in the 0–1 band. These heights of formation are also applicable to the $R(4)$, $R(8)$, and $R(16)$ lines, respectively, except that the relative intensities of the three lines will be slightly different from those in the P branch. The ^pQ and ^qQ lines are formed at slightly different heights from the corresponding P and R lines, but the difference is completely negligible for all but the first few lines in the band.

temperatures from the observed band profiles were in error, as they were calculated before it became known that the Atmospheric system arises from a magnetic dipole, rather than an electric dipole, transition. The numerical error involved is fortunately quite small and, indeed, affects the P-form and R-form branches in opposite manners, so that the derived temperatures may be accepted uncorrected.

With these data the emission formed at each level has been computed by evaluating equation (5) for various heights and an isothermal atmosphere at 200° K; the results are shown in Figure 1. The fact that the temperature of the atmosphere actually varies over the heights in question would have the effect of making only slight modifications in the computed levels of formation. Also, with the transfer equation employed here the rela-

[16] *Ann. d'ap.*, **8**, 12, 1945.

[17] See G. Herzberg, *Spectra of Diatomic Molecules* (2d ed.; New York, Toronto, and London: D. Van Nostrand Co., 1950), p. 278.

[18] *Phys. Rev.*, **51**, 342, 1937.

tive intensities of the different lines would still be governed entirely by the temperature of the primary-emission layer.

To a first approximation, the combined intensity from two emitting layers varies with zenith angle at about the same rate as emission from a single intermediate layer. Hence Meinel's[6] estimated effective height of 70 km implies that the primary emission originates at a somewhat higher level.

IV. THE ROTATIONAL TEMPERATURE

In the foregoing treatment we have made two physical simplifications regarding collisional phenomena, either one of which could conceivably affect the intensity profile. First of all, we have neglected collisional de-excitation. Strong laboratory discharges

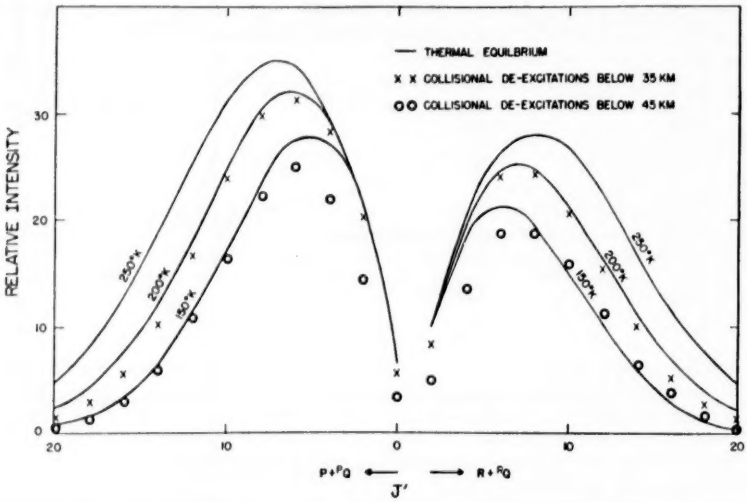

FIG. 2.—The effect of collisional de-excitation on the 0–1 band intensity profile. The primary emission is assumed to have $T_{rot} = 200°$ K. Thus the relative depressions of the computed points below the curve for 200° K represent the fraction of energy lost in each line because of collisional de-excitations.

and afterglows have beeen observed[9, 19] in pure O_2 at pressures of several cm *Hg*. The absence of wall effects and the presence of "impurities" such as nitrogen may modify considerably the behavior of metastable O_2, but it seems plausible, at least, that collisional de-excitation could become important at heights of 30–50 km. Hence we have computed by equation (5) the downward fluxes in the individual rotational lines at 35 and 45 km. The results are shown in Figure 2, along with the normal intensity distributions for three temperatures. The distortion of the profiles by the superelastic collisions is quite striking, and it is apparent that the resultant rotational "temperature" could be considerably lower than the atmospheric kinetic temperature.

Meinel[6] observed on one occasion that the O_2 band was greatly enhanced and that the rotational temperature was increased to 200° K. Detailed calculations for several temperatures indicate that collisional de-excitation below 45 km would have the effect of lowering the rotational "temperature" by approximately 50° K; thus the enhanced O_2 may actually have a temperature of the order of 250° K. One infrared plate obtained

[19] R. Herman and C. Weniger, *CR.*, **230**, 940, 1950.

recently by the author at Yerkes Observatory on a region near the northern horizon shows the O_2 band greatly enhanced relative to *OH*, whereas the O_2 observed simultaneously in the zenith was quite normal. The former spectrum also possessed, besides the *OH* bands, very weak *O* I and Meinel N_2^+ bands. Although Meinel did not observe any auroral emissions accompanying his enhanced O_2, the author's plate suggests that O_2 is extremely sensitive to auroral excitation and that enhanced O_2 may merely indicate a weak aurora. The possibility of a substantial change in the airglow emission cannot, of course, be definitely excluded on the basis of this one plate.

A second effect that has been neglected is that the re-emission in each line of the 0–0 band is probably not strictly proportional to the number of absorptions in the same line, as we have assumed with our transfer equations (2) and (3). Actually, there must be some redistribution of the relative populations before re-emission occurs. In the limiting case the relative intensities of the lines emitted at each height are governed purely by the local kinetic temperature, and at each frequency ν the emission produced at a given height is weighted according to the *total* amount of absorption at that height. Hence, if most of the absorption occurs in the 40–60-km region, we would expect to find rotational temperatures of the order of 250° K. Collisional de-excitations would not alter the relative intensities with this model, except in so far as they might eliminate some of the fluorescence and thereby emphasize the intensity profile of the primary emission. Thus the assumption of thermal equilibrium within the excited state, which a priori may appear to be the most likely situation, does not seem to give a satisfactory explanation of the observed rotational temperature. More accurate data on the collision phenomena will be needed before the effects of fluorescence can be definitely ascertained; and it may well be that the relative intensities cannot be ascribed to the de-excitation mechanism.

I wish to thank Drs. D. R. Bates, S. Chandrasekhar, G. P. Kuiper, and A. B. Meinel for reading the manuscript and offering several helpful suggestions.

MULTIPLE-STAR SYSTEMS IN EMISSION NEBULAE

STEWART SHARPLESS*
Mount Wilson and Palomar Observatories
Received October 2, 1953

ABSTRACT

A number of O-type multiple-star systems in emission nebulae are reproduced and discussed. Some of these are shown to be surrounded by a clustering of fainter stars. The presence of the latter is discussed in the light of the dynamical instability of these multiple systems.

INTRODUCTION

Emission nebulae often contain, in addition to the O-type stars which cause the ionization of the nebular material, fainter B-type stars as well. The fact that the latter do not contribute appreciably to the ionization of the nebula has been demonstrated by Strömgren.[1] However, their concentration within the borders of a nebula is, in many cases, such as to leave no doubt of their physical connection with it.

The existence of extremely compact clusterings of early-type stars has been noted by several observers. W. W. Morgan,[2] on the basis of visual observations made with the 40-inch refractor, concluded that a large percentage of O-type stars are found to be at the center of a compact clustering of fainter stars. Ambarzumian[3] has drawn attention to the fact that all O-associations contain nuclear clusters which are characterized by a type of multiple-star system similar to the Trapezium of Orion. The term "multiple system" will be used here to designate such compact clusterings, in order to avoid confusion with the more familiar type of galactic cluster in which they are often found. Ambarzumian has pointed out that these multiple systems differ from the familiar type of multiple star, in that the separations of their components are all of the same order of magnitude. Considerations of the dynamical instability of these systems have led him to the conclusion that they are necessarily very young, i.e., 10^6–10^7 years.

In the course of compiling a catalogue of emission nebulae from 48-inch Schmidt plates, the writer selected a number of nebulae containing multiple-star systems for study on a somewhat larger scale. These were rephotographed at the Newtonian focus of the 60-inch telescope on Mount Wilson and are reproduced and individually discussed in the next section. All the photographs are 10- or 15-minute exposures on Eastman 103*a*-O emulsion. The nebulae and the galactic clusters which some of them contain are designated by the NGC number or that of the author's catalogue,[4] prefixed by the letter *E*. Most of the spectral types given here were determined from slit spectrograms obtained with the Cassegrain spectrograph attached to the 60-inch telescope.

EXAMPLES OF MULTIPLE-STAR SYSTEMS IN EMISSION NEBULAE

IC 410 ($l = 141°$; $b = -1°$).—This nebula lies in the direction of the anticenter at a distance of about 2000 parsecs.[5] It contains a cluster of five O-type stars ranging in

* Carnegie Fellow, 1952–1953. Now at the United States Naval Observatory.

[1] *Ap. J.*, **108**, 242, 1948.

[2] Private communication.

[3] *Abh. Deutsche Akad. Wiss., Kl. Naturw.*, No. 2, 1950; see also *Astronomical Newsletter*, No. 64, and references given there.

[4] *Ap. J.*, **118**, 362, 1953.

[5] *Sky and Telescope*, **11**, 138, 1952.

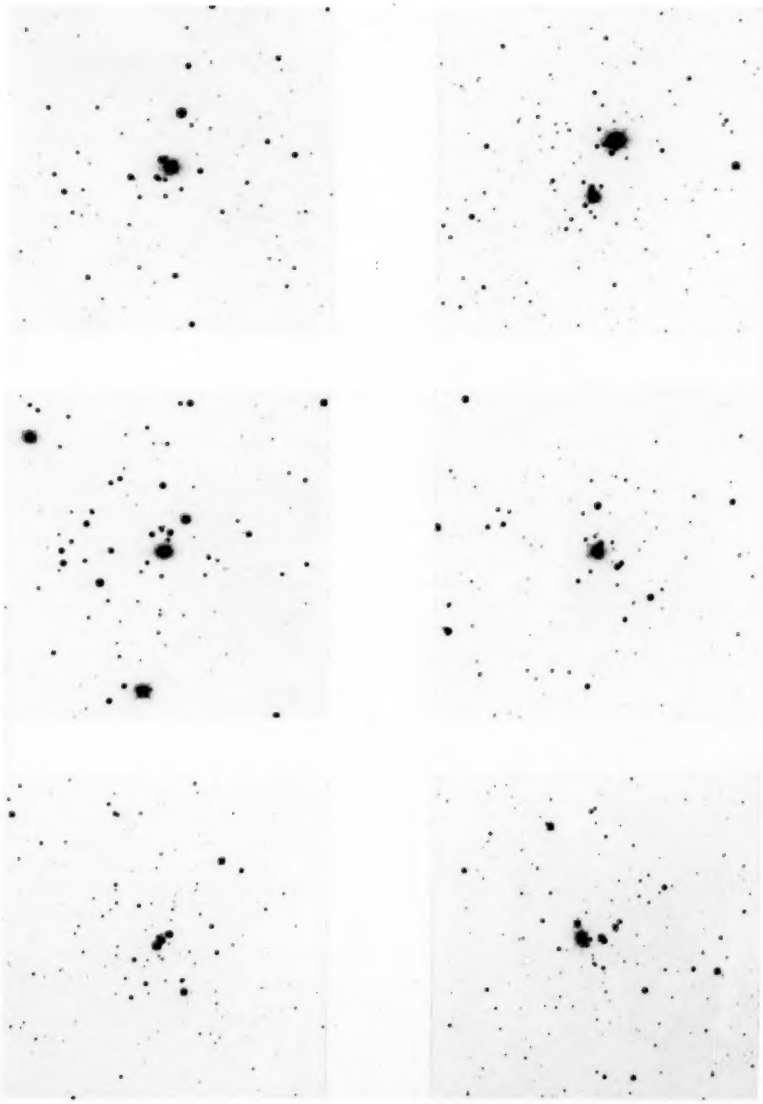

FIG. 1.—Multiple star systems in emission nebulae: HD 18326 (*upper left*), HD 17505 and HD 17520 (*upper right*), HD 15558 (*middle left*), HD 5005 (*middle right*), BD +22°3782 (*lower left*), HD 167971 (*lower right*). The scale is 1".3 mm.

spectral type from O5 to O8, and several B0 stars. These are all within a radius of approximately 6′, or 4 parsecs. The surrounding nebulosity is about 1° in diameter. The ninth-magnitude multiple system BD + 33°1026 lies near the center of the cluster in a region of higher-than-average density of faint stars. Table 1 lists the separations and

TABLE 1

COMPANIONS OF BD+33°1026

Components	r	θ	Components	r	θ
ab.....	10″.2	113°	ad.....	14″.7	204°
ac.....	11.6	333	ae.....	23.3	119

position angles of the components as measured from the photograph. The image of the primary suggests several other partially resolved fainter companions. The spectral type of the primary is O7.

Anon No. 1 ($l = 106°$; $b = +2°$).—The objects Anon No. 1, IC 1848, and IC 1805 are probably at very nearly the same distance, judging from their proximity in the sky and their similarity of appearance. Their distance is approximately 2000 parsecs.[5] The nebulosities of Anon No. 1 and IC 1848 are contiguous but are excited by different stars. The single exciting star of Anon No. 1, HD 18326, is a multiple system, as shown in Figure 1. Its spectral type is O7, and its magnitude, 7.9. Table 2 lists the positions of the

TABLE 2

COMPANIONS OF HD 18326

Components	r	θ	Δm	Components	r	θ	Δm
ab.....	10″.9	3°	5^m	af.....	27″.2	152°	4^m
ac.....	13.3	331	5	ag.....	34.4	136	5
ad.....	23.4	27	4	ah.....	35.0	122	3
ae.....	25.9	51	3				

components and their approximate magnitudes, referred to that of the primary. The star density in the vicinity of HD 18326 appears to be higher than elsewhere on the plate within a radius of several minutes of arc.

IC 1848 ($l = 105°$; $b = +2°$).—This is a cluster of four O-type stars of spectral types O7–O8 which are distributed over an angle of about 40′. Of these, three are the primary components of multiple systems: BD + 60°586, HD 17505, and HD 17520. The components of HD 17505 are shown in Figures 1 and 2. Figure 2 combines visual data on the inner components taken from Aitken's double-star catalogue,[6] with measurements of the fainter components obtained from the photographs. The spectral type of the primary is O7, and its magnitude, 7.1. The positions and magnitude differences of the components are given in Table 3. The capital-letter designations are those of Aitken's catalogue.

The multiple system, HD 17520, is shown in Figures 1 and 2. Its spectral type is O8, and its magnitude, 8.7. Table 4 contains the positions of the components and their magnitude differences.

[6] *New General Catalogue of Double Stars* (Washington, D.C.: Carnegie Institution of Washington, 1932).

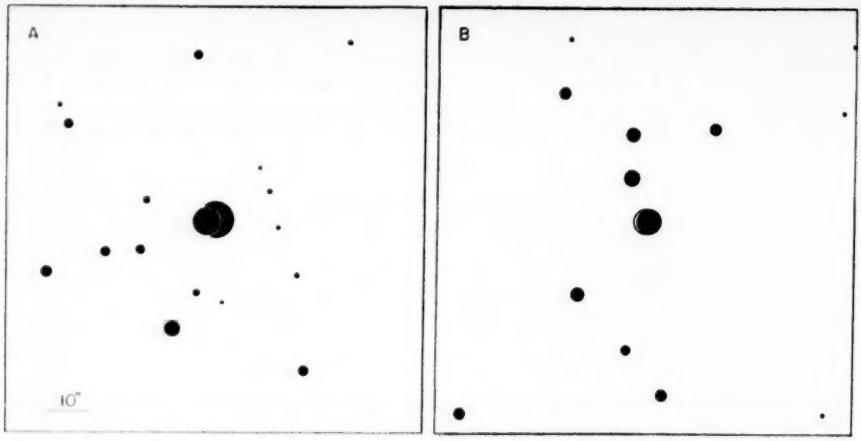

FIG. 2.—The components of *a*, HD 17505; *b*, HD 17520

TABLE 3

COMPANIONS OF HD 17505 = ADS 2161

Components	ADS	r	θ	Δm
ab	AB	2".1	93°	1^m.9
ac		14.4	297	7
ad		15.0	263	7
ae		16.1	320	7
af	AD	17.0	74	6.7
ag		17.6	165	7
ah		19.0	185	8
ai	AE	19.2	112	6.4
aj		23.6	235	7
ak	AF	27.4	106	5.9
al	AC	27.5	157	4.4
am		39.0	7	6
an		41.4	211	6
ao		42.1	107	6
ap		42.1	58	6

TABLE 4

COMPANIONS OF HD 17520 = ADS 2165

Components	ADS	r	θ	Δm
ab	AB	0".3	290°	0^m.0
ac	AB–C	10.7	20	2.3
ad	AB–D	20.2	10	2.8
ae		23.8	137	4
af		27.3	323	4
ag		30.4	171	5
ah		35.9	33	4
ai		40.9	186	4

IC 1805 ($l = 102°$; $b = +2°$).—This cluster contains five O-type stars and several known B-type stars within a radius of 12′. Of these, the seventh-magnitude O5f star, HD 15558, is the only known multiple system. It is shown in Figures 1 and 3. Data concerning its components are given in Table 5. It is noteworthy that a cluster of approximately fifteen stars having magnitudes between 11 and 13 surrounds this multiple system. The radius of this cluster is approximately 5′. The other O-type stars in IC 1805 have no such clustering associated with them.

NGC 281 ($l = 91°$; $b = -6°$).—The NGC number here refers to the nebulosity around HD 5005. The nebula is 20′ in diameter and lies at a distance of about 2000 parsecs.[5] The magnitude and spectral type of HD 5005 are 7.7 and O6. The close components as listed in Aitken's catalogue and the fainter components appearing on the photograph are plotted in Figure 3. A portion of the photograph is reproduced in Figure 1. Table 6 contains the positions and magnitudes of the components referred to the primary.

E 117 ($l = 85°$; $b = +3°$).—This is a spherical nebula centered on the ninth-magnitude O8 star, BD + 63°2093. Observations of the individual components of this star are summarized in Table 7. A total of nine stars is visible on the plate within a radius of 50″ of the O-type star.

E 109 ($l = 80°$; $b = -1°$).—Eccentrically placed in this nebula is the WN5 star HD 219460. This system (not shown) contains at least ten components within a radius of 45″.

E 91 ($l = 71°$; $b = -1°$).—The brightest part of this nebula is 20′ in diameter, with

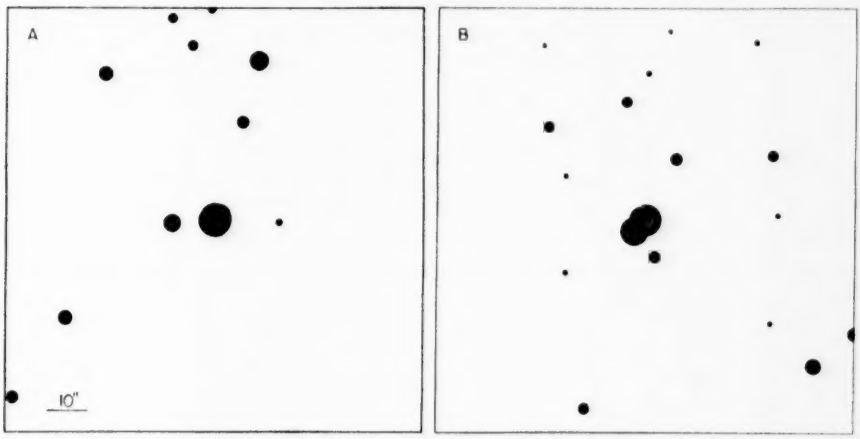

FIG. 3.—The components of *a*, HD 15558; *b*, HD 5005

TABLE 5

COMPANIONS OF HD 15558 = ADS 1920

Components	ADS	r	θ	Δm
ab	AB	10″.2	95°	3^m.7
ac	.....	15.3	268	8
ad	.....	24.1	344	7

faint extensions out to 60′ from the center. Its distance is approximately 2800 parsecs.[5] There are about ten ninth-magnitude stars in the brightest part of the nebula, but only one is a known early-type star. Its spectral type is listed as Ob in the *Henry Draper Catalogue*. A multiple system, BD + 55°2722, lies near the center of the nebula and is shown in Figure 4. Its magnitude is 9.5. This system shows a marked similarity to the

TABLE 6

COMPANIONS OF HD 5005 = ADS 719

Components	ADS	r	θ	Δm
ab	AB	1″.4	81°	2^m.0
ac	AC	3.9	134	0.8
ad	AD	8.9	193	1.4
ae	AE	15.7	333	4.4
af	.....	21.7	61	5
ag	.....	23.0	123	5
ah	.....	28.1	10	4
ai	.....	31.9	273	5
aj	.....	32.3	47	4
ak	.....	33.8	297	4

TABLE 7

COMPANIONS OF BD+63°2093 = ADS 17171

Components	ADS	r	θ	Δm
ab	AB	1″.7	290°	1^m.2
ac	.....	9.6	265	5
ad	.....	13.8	313	3
ae	.....	17.6	135	4

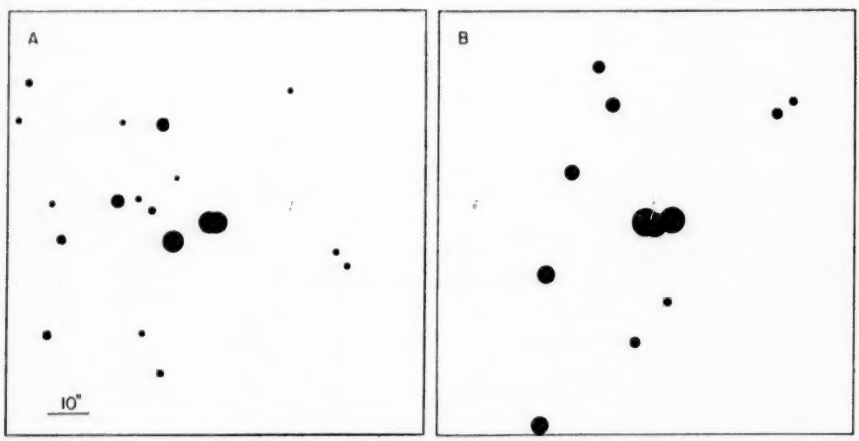

FIG. 4.—The components of *a*, BD+55°2722; *b*, BD+46°2972

Trapezium of Orion not only in the apparent arrangement of its components but also in the fact that they are of more nearly equal brightness than in the case of some of the systems discussed above. Data on the components as derived from the photograph are given in Table 8 in combination with the visual data from Aitken's double-star catalogue.

E 82 ($l = 53°$; $b = +3°$).—This nebula is 50′ in diameter, and the multiple system, BD + 46°2972, is eccentrically placed with respect to it. The components are shown in Figure 4, and the positions and magnitudes, referred to the primary, are given in Table 9. The magnitude of the primary is 8.7.

NGC 6823 ($l = 27°$; $b = -1°$).—This nebula contains three known early-type stars within a radius of 10″. The multiple system, BD + 22°3782, is unique thus far, in that it consists of a chain of several compact systems. It is reproduced in Figure 1. This system is in the center of a sparse cluster approximately 5′ in diameter. This cluster is noteworthy for the fact that it contains practically no stars whose magnitudes are near the plate limit. Table 10 contains data on the components as derived from the photograph.

TABLE 8

COMPANIONS OF BD+55°2722 = ADS 15834

Components	ADS	r	θ	Δm
ab	AB	1″.5	91°	0^m.2
ac	AC	11.5	114	0.0
ad		14.5	24	5
ae		15.9	80	4
af		19.7	73	4
ag	AD	24.3	78	3.3
ah	AE	30.4	39	3.3

TABLE 9

COMPANIONS OF BD+46°2972 = ADS 14010

Components	ADS	r	θ	Δm
ab	AB	2″.3	250°	1^m.8
ac	AC	6.3	266	1.0
ad		19.5	196	5
ae		21.4	57	3
af		26.8	117	3
ag		28.6	174	4
ah		29.2	17	3

TABLE 10

COMPANIONS OF BD+22°3782

Components	r	θ	Δm	Components	r	θ	Δm
ab	7″.6	248°	3^m	ai	26.8	279	4
ac	9.8	303	3	aj	31.0	321	4
ad	17.6	341	2	ak	31.2	310	4
ae	17.8	307	3	al	33.1	334	5
af	21.8	320	4	am	36.8	318	3
ag	23.1	292	5	an	37.6	309	1
ah	25.4	333	4				

NGC 6604 ($l = 346°$; $b = 0°$).—This nebula contains six known early-type stars, of which the O8f star, HD 167971, forms part of a multiple system. This system, shown in Figure 1, is somewhat larger than the others in angular size. It contains about twenty stars within a radius of $60''$. Another multiple system (not shown) is HD 167834, located about 13′ from HD 167971. Data concerning the components of HD 167971 are given in Table 11.

TABLE 11

COMPANIONS OF HD 167971

Components	r	θ	Δm	Components	r	θ	Δm
ab	16.″0	189°	7.m	aj	50.0	261	5
ac	17.6	257	5	ak	50.5	349	6
ad	19.2	213	6	al	64.0	254	7
ae	29.6	19	4	am	70.2	279	7
af	38.2	11	7	an	71.0	306	7
ag	39.8	268	3	ao	71.5	286	4
ah	43.8	299	7	ap	83.5	291	5
ai	44.5	257	6				

DISCUSSION

It appears from the foregoing examples that it is not uncommon for the stars associated with an emission nebula to number at least one multiple system among them. Little can be said about the relative frequency of such systems, since some of them may be below the visual resolving power of large telescopes. However, of a group of emission nebulae in which at least one associated early-type star is known,[4] about 40 per cent are known also to contain a multiple system. In general, the number of components of the system is considerably greater than the number listed in Aitken's catalogue.

The spectral types of eleven of the primary components of the multiple systems described above have been determined from slit spectrograms. The two of earliest spectral type have been classified as O5f and WN5, respectively. Of the remaining, there is one O6, six O7, and one O8f star. Evidently, there is a strong tendency for the bright components of such systems to be of earlier spectral type than O9. A number of brighter O-

TABLE 12

OTHER O-TYPE MULTIPLE SYSTEMS

HD	ADS	m	Sp.*	No. of Components	Nebula
164492	10991	6.9	O8	7	NGC 6514
190429	13312	6.7	O5f	4	P Cyg nebula
190864	13361	7.8	O6	4	P Cyg nebula
190918	13374	7.0	O9.5 III+WN5	8	P Cyg nebula
193443	13686	7.7	O9 III	3	P Cyg nebula
206267	15184	5.6	O6	4	IC 1396
λ Ori	4179	3.7	O8	4	λ Ori nebula†
θ′ Ori	4186	5.4	O6	9	NGC 1982
46150	5165	6.8	O6	5	NGC 2244
S Mon	5322	4.7	O7	8	NGC 2264
τ CMa	5977	4.4	O9 III	4	NGC 2362

*The spectral types were taken from N. G. Roman, *Ap. J.*, **116**, 492, 1951, and W. W. Morgan, *Pub. Obs. U. Michigan*, **10**, 33, 1951.

†*Ap. J.*, **118**, 89, 1952.

type stars are also known to be multiple systems on the basis of visual data. These are listed in Table 12, the columns of which contain the star designations in the *Henry Draper Catalogue* and Aitken's catalogue, the apparent magnitude and spectral type of the primary, the number of components listed in Aitken's catalogue, and the emission nebula with which the system is associated.

It has been shown by Ambarzumian[3] that these multiple systems must, as a result of their dynamical instability, be very young. Consider a system consisting of an early O-type star and a number of main-sequence B-type stars. If the mass and radius of the system are $100\odot$ and 0.1 parsec, respectively, the average Keplerian period of the secondary components is about 3×10^5 years. Over several such periods, encounters between member stars will occur, resulting in an exchange of energy and, in many cases, in the ejection from the system of one of the stars. This process of ejection will continue

TABLE 13

OBSERVATIONS OF FAINT STARS SURROUNDING HD 15558

Star	m	Sp.	Star	m	Sp.	Star	m	Sp.
1	12.09	B2	5	11.17	O–B0	9	10.02	Indeterminate
2	11.39	B1	6	11.64	B1			
3	9.49	O–B0	7	11.70	O–B0			
4	11.26	B2	8	11.16	O–B0			

TABLE 14

OBSERVATIONS OF FAINT STARS SURROUNDING BD+22°3782

Star	m	Sp.	Star	m	Sp.
1	11.80	B5	6	11.95	B5
2	11.33	Indeterminate	7	11.89	B3
3	11.46	O–B0	8	12.03	B5
4	11.66	O–B0	9	11.51	O–B0
5	9.64	O–B0	10	9.37	Indeterminate

until a stable configuration, e.g., one in which the separations of the components are not of the same order of magnitude, is reached. The velocity of escape from a multiple system of the type described above is about 3 km/sec. This is of the same order as the velocities of expansion observed for the ζ Persei[7] and Lacerta[8] aggregates. It is of interest to note that the integrated absolute magnitude of the known members of the ζ Persei aggregate is -6.7. Some apparently single O-stars are known to have absolute magnitudes at least as bright. The photographs reproduced suggest that some multiple systems are surrounded by a clustering of fainter stars, although the surface density of such a cluster is not much greater than that of the surrounding field. In order to establish the stellar content of these clusterings, photoelectric observations in three colors were made of stars immediately surrounding HD 15558 (in IC 1805) and BD + 22°3782 (in E 65). These observations were made with a conventional photoelectric photometer attached to the 40-inch telescope of the United States Naval Observatory. All stars brighter than the twelfth magnitude and within 5′ of the two multiple systems were observed. The methods of observation were the same as those described earlier.[9] Spectral types were derived from the colors after the method of Johnson and Morgan.[10] The colors themselves will be

[7] A. Blaauw, *B.A.N.*, No. 433, 1952.

[8] A. Blaauw and W. W. Morgan, *Ap. J.*, **117**, 256, 1953.

[9] *Ap. J.*, **116**, 251, 1952.

[10] *Ap. J.*, **117**, 313, 1953.

discussed in detail in a later paper dealing with the parallaxes of these objects. The apparent visual magnitudes and spectral types of the faint stars surrounding HD 15558 and BD + 22°3782 are listed in Tables 13 and 14, respectively. The stars are identified in Figure 5. The preponderance of early B-type stars within 5′ of the two multiple systems weighs strongly in favor of the physical reality of these clusterings.

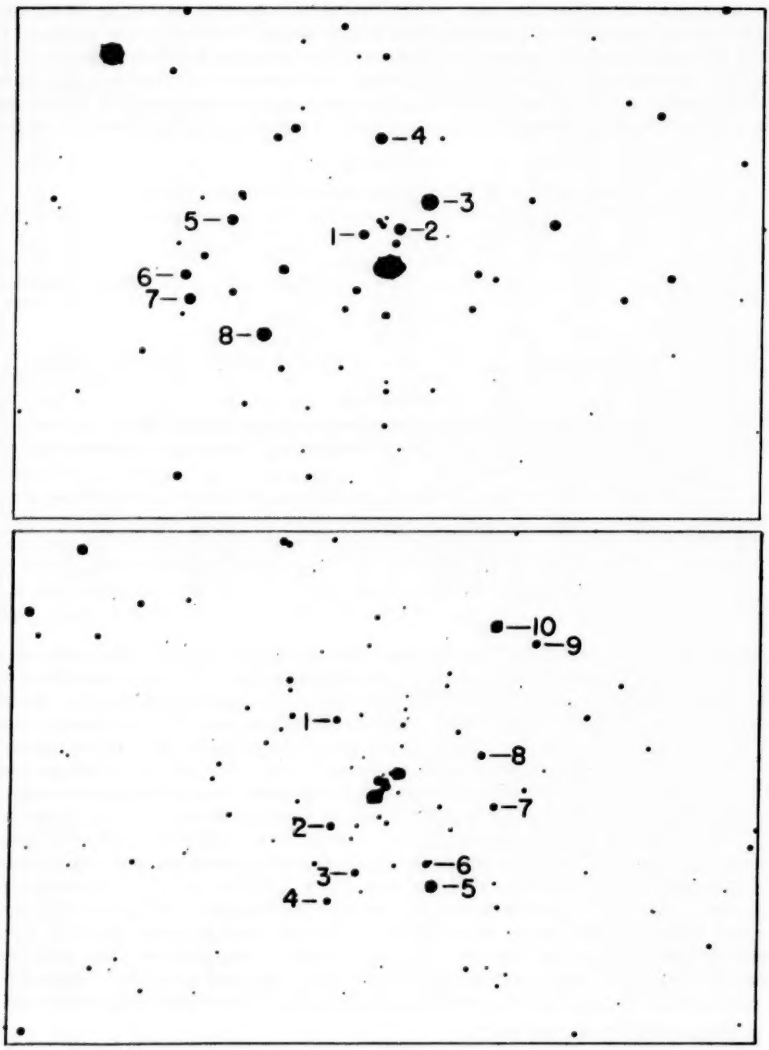

FIG. 5.—Identification charts for stars listed in Table 13 (*upper*), and Table 14 (*lower*)

Examination of the photographs and diagrams reproduced here reveals that there is not always a sharp boundary between the multiple system and the clustering of faint stars around it, if the latter exists. In some cases, e.g., Anon No. 1, IC 1805, and NGC 281, it is impossible to tell where the multiple-star system ends and the surrounding cluster begins. In view of this fact and in view of the ejection process occurring in such systems, it is not unreasonable to assume that all the fainter stars immediately surrounding the O-type star may have formed concurrently with it and in its immediate vicinity, i.e., within a radius of less than 10^4 A.U., corresponding to approximately 5″ for the objects discussed here. The velocity of escape from these systems is such that a cluster containing ten or twenty stars could expand from the immediate neighborhood of the O-type star into a sphere 5 parsecs in diameter in less than 10^6 years as a result of the ejection process.

The existence of a multiple-star system of the type described here is evidently transitory. In earlier stages the system must have been more compact, whereas in later stages many of the components will have escaped with part of the kinetic energy of the system, leaving a compact and stable double or multiple star. Since it is not unreasonable to expect that systems in both earlier and later stages of evolution exist today, many apparently single O-type stars may have one or more unresolved companions. The question arises as to whether the multiplicity of such a star would ordinarily be detected. Consider a representative system consisting of an O5 star, an O7 star, and ten B5 stars, and assume that this system has only recently been formed. Since interactions between the secondary components have not yet taken place, the system will be very compact and probably unresolved. The B5 stars will not contribute appreciably to the light and therefore will not be detectable spectroscopically. The blended spectrum of the O5 and O7 stars could not easily be distinguished from that of a single star of intermediate spectral type. The total absolute magnitude of this system will be about 0.9 brighter than that of a single O6 star. A spread of at least this amount occurs in the absolute magnitudes of O-type stars as determined differentially from associated B-type stars.[11] Although many multiple systems cannot be detected as such spectroscopically, nevertheless, certain combinations of early-type stars will exhibit composite spectra. Such systems exist, e.g., HD 190918, which has been classified as WN5 + O9.5 III by Miss Roman.[11] In any case, the possibility of the multiplicity of many O-type stars which are apparently single and which do not exhibit composite spectra cannot be ruled out on the basis of ordinary spectroscopic and photometric evidence.

[11] Nancy G. Roman, *Ap. J.*, **114**, 499, 1951; Stewart Sharpless, *Ap. J.*, **116**, 267, 1952.

A HEAVILY OBSCURED O-ASSOCIATION IN CYGNUS

H. L. JOHNSON AND W. W. MORGAN
Lowell Observatory; Yerkes Observatory
Received October 7, 1953

ABSTRACT

The clustering of blue giant stars near γ Cygni discovered at the Tonantzintla Observatory by L. Münch and Morgan has been observed photometrically and spectroscopically. It is shown to be an O-association of considerable interest because of the large number of O stars and the great interstellar absorption; the latter reaches a value of between 6 and 7 mag. on the V system of Johnson and Morgan. The distance of the association is around 1500 parsecs.

A group of blue giant stars northeast of γ Cygni was discovered recently at the Tonantzintla Observatory by L. Münch and W. W. Morgan.[1] The identification map published by them is defective; it should be replaced by Figure 1. The latter is from a plate taken by H. M. Johnson with a Meinel-Pearson F1 Schmidt camera of 8-inch aperture. Eastman 103*a*-E emulsion was used, together with a red filter.

The blue giants identified in Figure 1 have been observed with a photoelectric photometer by H. L. Johnson at the Lowell Observatory; slit spectrograms were obtained by W. P. Bidelman with the 82-inch telescope of the McDonald Observatory and by Morgan with the Yerkes 40-inch refractor; these have been classified on the revised Yerkes atlas system by Morgan. We are greatly indebted to Dr. Bidelman for the McDonald spectrograms.

The photometric and spectroscopic data are given in Table 1. The columns give: first, the number from the paper by Münch and Morgan; in the case of star No. 8, which is quadruple (ADS 14,000), the notation is that of the Aitken double-star catalogue; second to fourth, the magnitudes (V) and colors ($B-V$) and ($U-B$), on the photometric system described by Johnson and Morgan;[2] fifth, the spectral types on the revised system of the Yerkes spectral atlas.[2] Types followed by an interrogation mark (?) are uncertain and may be in error by an appreciable amount. The sixth column gives the color excesses on the ($B-V$) system; the seventh lists the values of V_0, the magnitudes on the V system corrected for interstellar absorption by a factor of $3E_{(B-V)}$.[3] The eighth column gives the true distance moduli; these are uncertain because of the preliminary nature of the calibration of the luminosity classes for the O stars; in addition, a deviation from the mean reddening law could cause error. A mean luminosity of $M_V = -6.5$ has been adopted for the Of stars.

The last column gives values of

$$Q = (U-B) - \frac{E_{(U-B)}}{E_{(B-V)}}(B-V),$$

whose characteristics have been described.[2] For the quantity $E_{(U-B)}/E_{(B-V)}$, a value of 0.886 has been adopted.[3]

The values of Q in Table 1 indicate that all the stars with the exception of No. 2 are probably O stars. The spectral types confirm this result; in the case of several of the stars, however, the spectrograms are so weak that the determination of an accurate spectral type was not possible.

[1] *Ap. J.*, **118**, 161, 1953.

[2] *Ap. J.*, **117**, 313, 1953.

[3] *Ap. J.*, **118**, 92, 1953.

FIG. 1.—Field of association northeast of γ Cygni. North is at top; the field is about 40′ square. No. 8 is BD+40°4227; its position is $\alpha(1900) = 21^h29^m.5$; $\delta(1900) = +41°58'$. Plate by H. M. Johnson with Meinel-Pearson F1 Schmidt camera.

The color excesses on the $(B-V)$ system range from 1.41 to 2.26 mag.; the reddest stars in this clustering are therefore probably the most heavily obscured of any now known. It is interesting to note that if there were no interstellar absorption in the direction of the association, the latter would have the approximate appearance to the naked eye of the Pleiades; the brightest stars would then be of the fourth magnitude.

TABLE 1

PHOTOMETRIC AND SPECTROSCOPIC DATA

MM	V	$B-V$	$U-B$	MK	$E_{(B-V)}$	V_0	V_0-M^*	Q
1	11.09	+1.42	+0.31	O9 V?	1.73	5.90	10.1	−0.95
2	10.61	+1.15	+ .13	B1 *Ib*?	1.41	6.38	11.9	−0.89
3	10.22:	+1.61	+ .47	O9?	1.92	4.46:	.....	−0.96
4	10.22	+1.17	+ .09	O8	1.48	5.78	.....	−0.95
5	9.1 (var)	+1.67	+ .55	O7f	1.99	(3.8)†	10.3	−0.93
6	10.67	+1.216	+ .175	O8 (V)	1.53	6.08	10.6	−0.90
7	10.50	+1.44	+ .30	O6f	1.76	5.22	11.7	−0.98
8 A	8.98	+1.287	+ .138	O6f	1.61	4.15	10.7	−1.00
8 B	10.31:	+1.35:	.....	O8?	1.66:	5.33:	.....	.....
8 C	10.08	+1.347	+ .104	O6?	1.66	5.10	.....	−1.09
8 D	11.93	+1.43	+ .30	O9?	1.74	6.71	.....	−0.97
9	10.80	+1.93	+ .65	O5f	2.26	4.02	10.5	−1.06
10	9.88	+1.52	+ .40	O9.5 I*a*	1.83	4.42	11.4	−0.95
11	10.04	+1.43	+0.25	O6f	1.75	4.79	11.3	−1.02

* The mean value of the distance modulus is 10.9.

† Eclipsing binary; magnitude corrected by +0.7 mag. for duplicity.

If it is assumed that the association has a diameter of the order of 0°.5, the true diameter is about 13 parsecs. This is considerably smaller than the average size of the nearest associations; however, the heavy absorption may prevent the discovery of outlying members of the group.

Star No. 5 is an eclipsing binary of considerable interest.[4] Star No. 4 is part of a multiple system having at least five components; the latter are arranged in a small semicircular arc having a diameter of the order of 20″.

[4] G. R. Miczaika, *Pub. A.S.P.*, **65**, 141, 1953; earlier references are given there.

THE RADIAL VELOCITY OF DELTA SCUTI*

G. F. PADDOCK AND OTTO STRUVE
Lick Observatory and Berkeley Astronomical Department, University of Califorina
Received September 18, 1953

ABSTRACT

The radial velocities measured on 246 spectrograms, taken on twenty-eight nights, were used to confirm E. A. Fath's photometric fundamental period of 0.193770 day. The mean velocity of the star is −44.6 km/sec and was constant throughout the period covered by the observations. The range of the individual velocity-curves varied between 6.5 km/sec and 15.2 km/sec. A plot of the values of $2K$ against the time suggests the existence of a beat period of 0.838066 day, which agrees with one of the two beat periods discovered by Fath from his photoelectric observations. The range of the fundamental oscillation is $2K_1 = 10.5$ km/sec, and the range of the secondary oscillation is $2K_2 = 2.5$ km/sec.

In 1935 A. Colacevich[1] discovered the fundamental period of δ Scuti from radial velocity measurements made at the Lick Observatory between 1899 and 1935. This period was found to be approximately 4^h40^m. During the same year E. A. Fath[2] found that δ Scuti varied in brightness with an amplitude of about 0.2 mag. and in a period identical with that of the radial-velocity oscillation. During the years 1936 and 1937 Fath[3] secured additional photoelectric observations that enabled him to refine the fundamental period to $P = 0.19377$ day. He was also able to show that the amplitudes of the individual light-curves vary with a beat period of either $P' = 0.838066$ day or $P'' = 5.24774$ days. The shorter beat period gave only about one-half the amount of scatter found for the 5.2 days beat period; hence, Fath accepted as the true beat period 0.838066 day.

Table 1 lists the radial velocities of δ Scuti, including those of 1935 obtained by Colacevich. The observations of 1936 and 1937 were made at Lick Observatory by Paddock, and those of 1953 by Struve with the coudé spectrograph of the 100-inch telescope of Mount Wilson Observatory.

Figures 1*a* and 1*b* give the individual velocity-curves for all dates except June 1, 1953, when only a single spectrogram was obtained. The variation of the radial velocity follows closely the fundamental period determined by Fath, $P = 0.193770$ day. This period represents the observations of 1953 sufficiently well, as may be seen from the (O−C) values in Table 2.

The individual velocity-curves show that the ranges vary between about 6.5 km/sec and 15.2 km/sec. The change in $2K$ appears to be periodic, as may be seen from the observations on six consecutive nights, June 21 until June 26, 1937. The corresponding values of $2K$ are consistent with either a beat period of 5.2 days or with one of 0.84 day. There is a strong indication that the shorter beat period is the correct one. This conclu-

* *Contributions from the Lick Observatory*, Ser. II, No. 51. The radial velocities of δ Scuti in 1935 were obtained by A. Colacevich with the Mills spectrograph of the Lick Observatory. Those of 1936 and 1937 were obtained by G. F. Paddock with the same instrument. Mr. Paddock also revised some of the measurements previously made by Mr. Colacevich. The observations of 1953 were made by Mr. Struve, as guest investigator, with the coudé spectrograph of the Mount Wilson 100-inch reflector. The Lick spectrograms have a dispersion of 10 A/mm, the Mount Wilson spectrograms on June 1 and June 3, 1953, have a dispersion of 4.5 A/mm and those of June, 1953, have a dispersion of 10 A/mm. The Mount Wilson spectrograms were measured by Mr. C. R. Lynds and Miss V. L. Vasilevskis.

[1] *Lick Obs. Bull.*, **17**, 171, 1935 (No. 478).

[2] *Lick Obs. Bull.*, **17**, 175, 1935 (No. 479).

[3] *Ibid.*, **18**, 77, 1937 (No. 487); **19**, 77, 1940 (No. 501).

TABLE 1

RADIAL VELOCITIES OF δ SCUTI

Gr. Civil Date	Julian Day (Geocentric) 242+	Radial Velocity (Km/Sec)
1935		
June 26...	7979.716	−38.8
	.757	−46.6
	.793	−48.6
	.829	−46.0
	.865	−40.0
	.902	−40.8
	.941	−45.8
	.984	−50.3
June 27...	7980.713	−44.8
	.755	−49.6
	.798	−42.6
	.833	−41.1
	.868	−40.4
	.904	−43.4
	.941	−49.1
	.979	−47.4
July 18...	8001.691	−49.4
	.726	−46.1
	.760	−40.3
	.794	−40.2
	.828	−42.1
	.860	−51.0
	.898	−50.6
July 26...	8009.701	−41.0
	.737	−42.1
	.770	−42.5
	.805	−47.8
	.840	−48.1
	.874	−43.3
	.911	−40.2
Aug. 16...	8030.670	−42.8
	.708	−46.1
	.745	−50.8
	.784	−46.8
	.824	−40.8
	.865	−43.5
Sept. 10...	8055.649	−38.4
	.682	−43.1
	.709	−45.6
	.737	−48.3
	.765	−47.2
	.793	−43.9
1936		
July 14...	8363.695	−45.6
	.730	−41.8
	.762	−40.3
	.792	−42.9
	.821	−45.8
	.852	−51.3
	.883	−47.6
1936		
July 24...	8373.697	−50.0
	.727	−52.0
	.756	−48.5
	.784	−44.0
	.811	−40.8
	.840	−40.0
	.870	−45.9
July 30...	8379.679	−43.2
	.708	−47.4
	.737	−53.3
	.763	−49.1
	.788	−42.7
	.814	−38.0
	.842	−40.2
	.871	−44.7
Aug. 1....	8381.676	−49.5
	.704	−44.4
	.730	−41.0
	.755	−39.5
	.781	−40.4
	.808	−49.4
	.837	−49.6
	.868	−47.4
	.898	−45.8
Aug. 7....	8387.675	−47.2
	.703	−47.9
	.730	−44.6
	.758	−40.6
	.786	−41.8
	.813	−45.4
	.841	−46.8
	.870	−47.2
1937		
June 21...	8705.750	−39.1
	.777	−39.4
	.803	−49.3
	.828	−48.9
	.850	−49.6
	.873	−46.6
	.898	−44.1
	.921	−39.0
	.944	−38.0
	.969	−41.9
	.999	−48.1
June 22...	8706.722	−42.3
	.753	−47.0
	.780	−48.4
	.803	−49.5
	.825	−46.9
	.847	−44.5
	.869	−39.9
1937		
June 22...	8706.892	−41.0
	.916	−42.5
	.942	−45.3
	.969	−49.1
	7.001	−48.7
June 23...	8707.715	−44.5
	.773	−47.0
	.797	−44.1
	.819	−42.4
	.862	−40.6
	.884	−41.4
	.906	−45.2
	.929	−47.7
	.956	−48.7
	.989	−46.6
June 24...	8708.729	−48.5
	.759	−44.9
	.788	−45.2
	.815	−42.7
	.864	−42.9
	.887	−43.1
	.910	−44.8
	.932	−46.0
	.955	−47.7
	.984	−46.9
June 25...	8709.712	−49.9
	.745	−48.5
	.777	−42.2
	.806	−42.0
	.833	−39.3
	.859	−40.5
	.880	−45.6
	.903	−48.8
	.928	−47.9
	.955	−45.9
	.986	−41.2
June 26...	8710.709	−49.5
	.743	−45.6
	.775	−37.9
	.804	−39.4
	.829	−41.7
	.853	−46.3
	.879	−46.5
	.905	−46.0
	.934	−45.7
	.966	−37.8
	11.002	−36.2
July 1....	8715.699	−48.6
	.728	−49.3
	.755	−45.7
	.780	−43.9
	.804	−44.2

TABLE 1—*Continued*

Gr. Civil Date	Julian Day (Geocentric) 242+	Radial Velocity (Km/Sec)	Gr. Civil Date	Julian Day (Geocentric) 242+	Radial Velocity (Km/Sec)	Gr. Civil Date	Julian Day (Geocentric) 242+	Radial Velocity (Km/Sec)
1937			1937			1937		
July 1...	8715.827	−38.6	July 21...	8735.682	−49.8	July 24...	8738.681	−38.9
	.849	−41.3		.707	−52.0		.709	−40.4
	.873	−44.6		.730	−44.7		.735	−46.3
	.897	−48.3		.753	−41.9		.755	−50.2
	.922	−49.4		.755	−39.8			
	.949	−48.1		.797	−39.1	Aug. 19...	8764.663	−43.3
	.980	−42.5		.819	−41.8		.688	−47.4
				.841	−42.8		.709	−50.0
July 19...	8733.705	−46.6		.863	−49.8		.731	−49.7
	.733	−48.3		.887	−48.3		.753	−48.1
	.759	−46.8		.913	−47.2		.777	−47.2
	.781	−46.3		.945	−44.2		.800	−45.8
	.803	−41.4					.825	−40.4
	.825	−38.9	July 22...	8736.678	−47.4		.854	−40.0
	.846	−41.8		.704	−44.3		.885	−44.0
	.869	−45.2		.731	−39.6			
	.893	−45.6		.759	−39.0	1953	243+	
	.917	−46.7		.784	−41.5	June 1...	4529.821	−34.1
	.942	−46.4		.809	−49.0			
	.969	−43.8		.832	−52.8	June 3...	4531.790	−39.5
				.858	−51.7		.816	−36.4
July 20...	8734.686	−46.8		.887	−46.7		.840	−38.3
	.712	−45.3		.915	−42.2		.865	−45.6
	.736	−47.5		.948	−36.5		.890	−48.8
	.758	−46.9					.916	−48.3
	.779	−43.8	July 23...	8737.680	−41.9		.942	−47.1
	.801	−43.6		.706	−37.4		.973	−45.2
	.822	−41.6		.729	−38.1			
	.844	−42.5		.753	−46.4	June 4...	4532.812	−42.1
	.869	−46.6		.779	−50.1		.834	−46.4
	.892	−48.4		.804	−47.8		.845	−50.0
	.917	−46.1		.845	−47.3		.878	−51.2
	.944	−45.8		.890	−39.7		.901	−48.0
				.927	−39.6		.924	−45.6
				.962	−50.0		.947	−42.2
							.972	−38.8

sion may be drawn from several nights' observations that clearly show a change in $2K$ between successive cycles. For example, the very accurate Mount Wilson observations of June 3, 1953, which were obtained with a dispersion of 4.5 A/mm, show that the beginning of the curve is considerably above the end, despite the fact that they are separated by almost exactly one complete cycle of 4^h40^m.

The values of $2K$ are plotted against phase for a beat period of 0.838066 day in Figure 2. In Figure 3 the same values of $2K$ are plotted against phase for a beat period of 5.24774 days. The shorter beat period shows a periodic variation but with a considerable scatter. The material is not sufficient to improve this shorter beat period; however, it seems probable that the scatter cannot be entirely explained in terms of observational errors. It will be noticed that the observations of 1936 and 1937 agree much better with the beat hypothesis than those of 1935. It is possible, therefore, that one of the two oscillations, probably the smaller ones, is itself variable.

From the observations in Figure 2 we estimate:

$$2(K_1 + K_2) = 13.0 \text{ km/sec}, \qquad 2(K_1 - K_2) = 8.0 \text{ km/sec}.$$

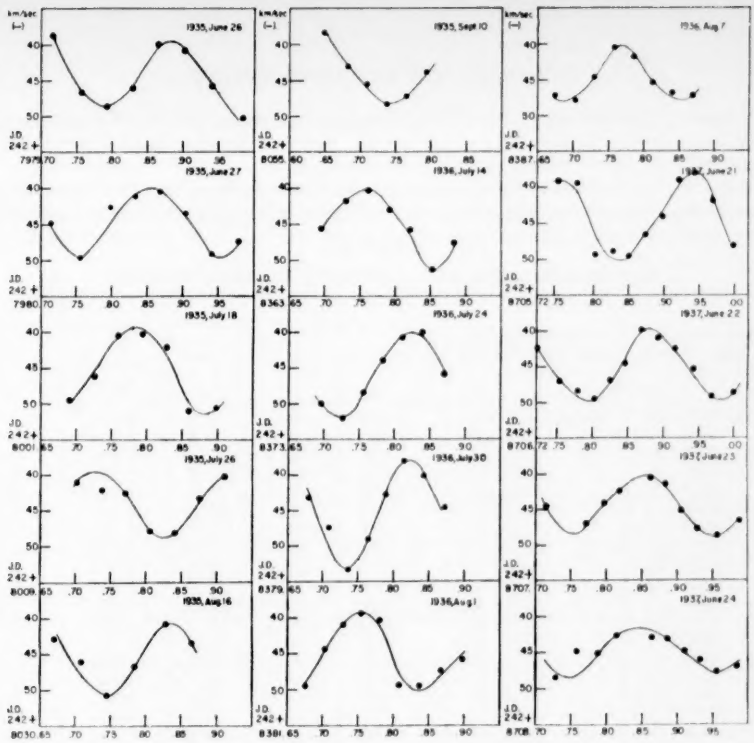

FIG. 1*a*.—Individual velocity-curves of Delta Scuti

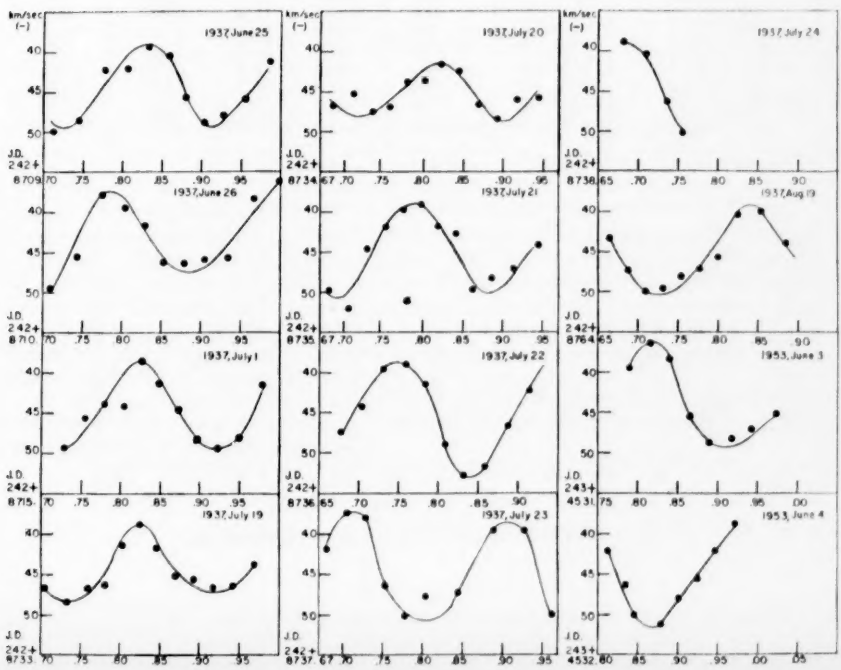

FIG. 1*b*.—Individual velocity-curves of Delta Scuti

From these values we obtain for the fundamental oscillation $2K_1 = 10.5$ km/sec and, for the secondary oscillation, $2K_2 = 2.5$ km/sec. Figure 3 shows so much scatter that we can probably exclude the beat period of 5.24774 days.

Table 2 lists the values of the mean velocity for each cycle, γ, and the corresponding values of $2K$. The scatter in γ is very small. Figure 4 is a plot of γ against $2K$. There

TABLE 2*

EPOCHS OF MAXIMUM RADIAL VELOCITY, $2K$, AND γ OF δ SCUTI

Observed Epoch Max. Radial Velocity (E)	Computed Epoch of Max. Radial Velocity ($E'+nP$)	O−C	γ	$2K$	Phase $E-(E'+nP'')$ (Days)	Phase $E-(E'+nP')$ (Days)
JD 242 7979.886	JD 242 7979.886	0.000	−44.2	9.0	0	0
7980.855	7980.855	.000	−44.7	9.8	0.969	0.131
8001.787	8001.782	+ .005	−45.4	12.2	0.910	.111
8009.726	8009.727	− .001	−44.8	10.3	3.601	.508
8030.840	8030.848	− .008	−45.6	10.0	3.724	.670
8055.837	8055.844	− .007	.....	(10.0)	2.483	.525
8363.760	8363.744	+ .016	−45.8	11.2	0.789	.040
8373.824	8373.820	+ .004	−45.9	11.7	0.358	.047
8379.828	8379.827	+ .001	−45.6	15.2	1.114	.185
8381.748	8381.765	− .017	−44.8	11.0	3.034	.428
8387.772	8387.772	.000	−44.0	7.6	3.810	.586
8705.748	8705.748	.000	−44.6	11.2	1.674	.097
8705.942	8705.942	.000	−44.1	12.2	1.868	.291
8706.887	8706.911	− .024	−44.6	10.1	2.813	.401
8707.856	8707.880	− .024	−44.5	8.7	3.782	.529
8708.849	8708.849	.000	−44.9	6.5	4.775	.684
8709.823	8709.818	+ .005	−44.2	10.5	0.501	.820
8710.786	8710.786	.000	−42.5	10.0	1.464	.106
8715.819	8715.824	− .005	−44.5	10.0	1.249	.111
8733.827	8733.845	− .018	−43.3	9.0	3.514	.520
8734.814	8734.814	.000	−45.0	7.1	4.501	.669
8735.789	8735.783	+ .006	−44.7	11.4	0.228	.806
8736.747	8736.752	− .005	−45.9	14.2	1.186	.087
8737.714	8737.720	− .006	−44.0	13.5	2.153	.216
8737.907	8737.914	− .007	−44.6	12.2	2.346	.409
8764.832	8764.848	− .016	−44.7	11.3	3.033	.516
243 4531.815	243 4531.831	− .016	−42.9	13.1	2.752	.767
4532.965	4532.994	−0.029	.....	(14.0)	3.899	0.241

* $P = 0.193770$ day; $E' =$ JD 2,427,979.886; $P'' = 5.24774$ days; $P' = 0.838066$ day.

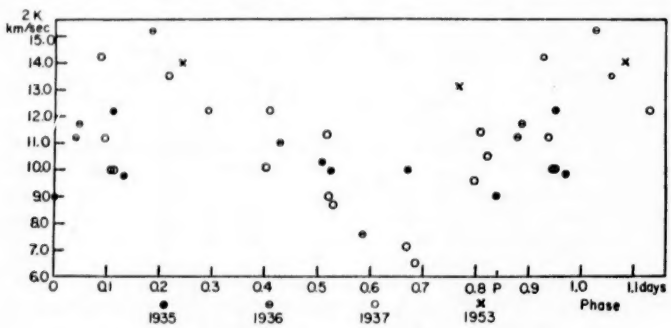

FIG. 2.—Plot of $2K$ against the beat period of 0.838066 day

is no systematic trend. We conclude that the mean velocity is probably constant and has a value of −44.6 km/sec.

The photoelectric observations by Fath had already shown that the maximum brightness of δ Scuti occurs very close to the minimum of the radial velocity. Fath concluded from two nights of simultaneous observing with the photoelectric photometer and the Mills spectrograph, in 1935, that the maximum light precedes the minimum radial

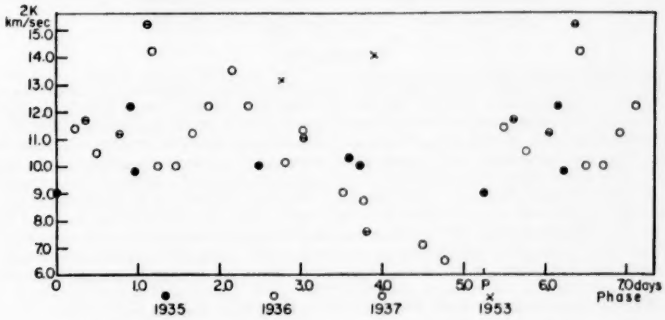

FIG. 3.—Plot of $2K$ against a possible beat period of 5.24774 days

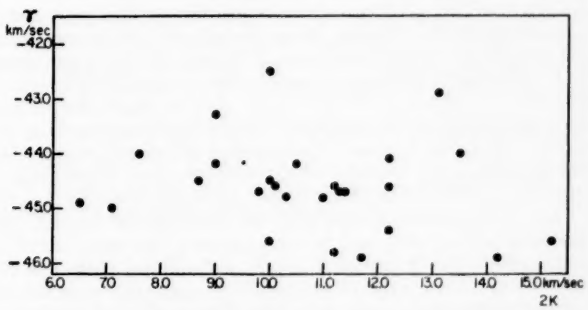

FIG. 4.—Plot of γ against $2K$

velocity by approximately 0.023 day. Photoelectric observations made by A. D. Williams at Lick Observatory, in 1953, when combined with the radial velocity observations of the same year, indicate that within the errors of the observations the maximum brightness and the minimum radial velocity occur at the same time. In this respect δ Scuti agrees with the classical cepheid variables and the cluster-type variables. In the β Canis Majoris variables maximum brightness occurs approximately in the middle of the descending branch of the velocity-curve.

The high-dispersion spectrograms of 1953 show that the absorption lines of δ Scuti are slightly broader near the middle of the descending branch of the velocity-curve than near the middle of the ascending branch.

AERODYNAMIC MOTIONS OF INTERSTELLAR GAS CLOUDS

G. C. McVittie
University of Illinois Observatory, Urbana, Illinois
Received July 8, 1953; revised September 18, 1953

ABSTRACT

A new method for solving the equations of gas dynamics, which depends on the Newtonian approximation to Einstein's equations of general relativity, is described for the case of one-dimensional motion. The resulting equations take account of the pressure-gradient force in the gas and of the force due to the gravitational self-attraction of the mass of gas under consideration. The motion of a thin interstellar cloud, bounded by two parallel planes that are shock waves and moving perpendicularly to these planes, is considered. It is shown that such a cloud can move as an entity held together by its gravitational self-attraction. The motion may be either with constant velocity or subject to an acceleration that is either constant or varies with the time. Outside the cloud, there may be either a vacuum or a gas at relatively low density. When the velocity is either constant or subject to a constant acceleration, adiabatic motion of the cloud is possible. When the acceleration varies with the time, the cloud may be losing energy by radiation. The width of the cloud, in the direction of its motion, is calculable in terms of the density and temperature at the densest portion of the cloud. Numerical values for the widths range from 45 to $\frac{1}{4}$ parsecs, according to the circumstances postulated at the densest portion.

I. INTRODUCTION AND SUMMARY

It is well known that the problem of the nonturbulent flow of a compressible gas presents great mathematical difficulties when the velocity of the gas is not, as in the theory of sound, regarded as being infinitesimal. Aerodynamics, or gas dynamics, treats of the aspects of this problem relating to the flow of air past aerofoils, the disturbances of the atmosphere caused by violent explosions, such as those due to atomic bombs, and other terrestrial gas motions. Analogous problems in astronomy occur in solar surges, in nova outbursts, and in the motions of interstellar gas clouds, where the phenomena are, aerodynamically speaking, probably of the simplest type. These large masses of gas move at high speeds, and it is often the case that the dynamical effects of radiation may be neglected. Thus their motions should obey the equations of classical gas dynamics,[1] except that the internal gravitational self-attraction of the gas, usually neglected in terrestrial aerodynamics, can be expected to play a significant part. The classical methods of aerodynamics are, however, mathematically complicated, even the most tractable case—that of one-dimensional motion—involving Riemann's partial differential equation and applications of the theory of the complex variable. Recently[2] the present author has shown that, whether the motion is in one, two, or three dimensions, a relatively simpler method of solving the equations of gas dynamics exists. It is found by taking the Newtonian approximation to Einstein's equations of general relativity, equations that may be briefly described thus. Let

$$ds^2 = g_{\mu\nu}dx^\mu dx^\nu \tag{1}$$

be the metric of a space-time that corresponds to a distribution of perfect fluid of density ρ, pressure p, and velocity 4-vector u^μ ($\mu = 1, 2, 3, 4$), whose energy tensor may be written

$$T^{\mu\nu} = \left(\rho + \frac{p}{c^2}\right)u^\mu u^\nu - g^{\mu\nu}\frac{p}{c^2}.$$

[1] See, on this point, J. M. Burgers, *Nederl. Akad. Wetensch.*, **49**, 589, 1946; also *Problems of Cosmical Aerodynamics* (Dayton, Ohio: Central Air Documents Office, 1951).

[2] *Quart. Appl. Math.*, **11**, 327, 1953.

Then, if $T^{\mu}_{\nu} = g_{\nu\alpha}T^{\mu\alpha}$, Einstein's equations are

$$-8\pi G T^{\mu}_{\nu} = R^{\mu}_{\nu} - \tfrac{1}{2}\delta^{\mu}_{\nu}R\,, \tag{2}$$

where G is the constant of gravitation, R^{μ}_{ν} and R are, respectively, the mixed contracted Riemann-Christoffel tensor and the scalar curvature for the metric (1), and δ^{μ}_{ν} is the Kroenecker delta. The velocity 4-vector is a unit vector and so satisfies the identity

$$1 = g_{\mu\nu}u^{\mu}u^{\nu}\,. \tag{3}$$

Since R^{μ}_{ν} and R can be calculated in terms of the $g_{\mu\nu}$ and their derivatives by the rules of the tensor calculus, it follows that the ten equations (2) are algebraic equations for ρ, p, and u^{μ} in terms of the $g_{\mu\nu}$. Thus if a practical method for using this fact could be devised, explicit expressions for the density, pressure, and velocity of a perfect fluid (gas or liquid) in terms of the space and time co-ordinates would result. But this is precisely the end aimed at in aerodynamic theory. In Section II it will be shown how this can be achieved for the case of one-dimensional motion, including gravity. However, the reader who is not interested in this aspect of the matter may pass directly to Section III and content himself with verifying that equations (24) do, in fact, satisfy the classical equations of continuity and of motion, (25) and (26).

As an example of the use of the new method, the motion of a thin interstellar gas cloud is considered in Sections IV and V. Specific cases are worked out in which the cloud moves either with constant velocity or with constant acceleration, its motion being adiabatic under these conditions. If the cloud loses energy by radiation, the motion being nonadiabatic, the acceleration is a function of the time. In all cases the thickness of the cloud parallel to its direction of motion may be calculated in terms of the density and temperature at the densest portion of the cloud (cf. eqs. [42], [49], and [62] below), and numerical values of cloud widths are given in Table 1 (p. 360).

II. EINSTEIN'S EQUATIONS AND NEWTONIAN GAS DYNAMICS

It has been proved by A. H. Taub[3] that, if x, y, and z are three spatial co-ordinates with the physical dimensions of length and t is a time co-ordinate, the metric of a space-time corresponding to a one-dimensional field is of the form

$$ds^2 = e^{2f}dt^2 - \frac{1}{c^2}\left(e^{2f}dx^2 + e^{2h}dy^2 + e^{2h}dz^2\right), \tag{4}$$

where f and h are functions of x and t. The calculation of Einstein's equations for such a case may be performed by the use of Dingle's formulae,[4] the index 4 being assigned to t, while 1, 2, and 3 refer to x, y, and z, respectively. The coefficients of the metric in Dingle's notation are

$$D = A\,c^2 = e^{2f}, \qquad B = C = \frac{e^{2h}}{c^2}; \tag{5}$$

and, since ρ and p are supposed to be expressed in grams per cubic centimeter and dynes per square centimeter, his constant 8π must be replaced by $8\pi G$, where G is the constant of gravitation in c.g.s. units. Inspection of the formulae for T^{12}, T^{13}, T^{23}, T^{24}, and T^{34} shows, in virtue of equation (5), that all these components are identically zero. This implies that $u^2 = 0$ and $u^3 = 0$, and the identity satisfied by the velocity 4-vector, therefore, becomes

$$1 = D\,(u^4)^2 - A\,(u^1)^2\,. \tag{6}$$

[3] *Ann. Math.*, **53**, 472, 1951.

[4] *Proc. Nat. Acad. Sci.*, **19**, 559, 1933.

It is also convenient to introduce the following symbols:

$$L = e^{f}u^{4}, \qquad U = e^{f}u^{1}, \qquad \sigma = \rho + \frac{p}{c^2}, \qquad \kappa = \frac{8\pi G}{c^2}, \tag{7}$$

and to denote partial derivatives of f and h with respect to x and t by subscripts. The surviving Einstein equations given below correspond to the energy-tensor components T^{11} T^{22} (or T^{33}), T^{44}, and T^{14} $(=T^{41})$, respectively:

$$\kappa(\sigma U^2 + p) = e^{-2f}\{-2h_{tt} + c^2(h_x^2 + 2h_x f_x) - (3h_t^2 - 2h_t f_t)\}, \tag{8}$$

$$\kappa p = e^{-2f}\{-h_{tt} - f_{tt} + c^2(h_{xx} + f_{xx}) + c^2 h_x^2 - h_t^2\}, \tag{9}$$

$$-\kappa\left(\sigma L^2 - \frac{p}{c^2}\right) = e^{-2f}\left\{2h_{xx} + 3h_x^2 - 2h_x f_x - \frac{1}{c^2}(h_t^2 + 2h_t f_t)\right\}, \tag{10}$$

$$-\kappa\sigma UL = 2e^{-2f}\{-h_{xt} - h_x h_t + h_x f_t + h_t f_x\}, \tag{11}$$

while equation (6) is

$$1 = L^2 - \frac{U^2}{c^2}. \tag{12}$$

Equation (9) may be used in equations (8) and (10) to express σU^2 and σL^2 in terms of the derivatives of f and h; then σ, U, and L may be eliminated in turn by using equation (11). The result is a *consistency relation* which f and h must satisfy if equations (8)–(11) are to be algebraically consistent. This relation is

$$4\{h_{xt} + h_x h_t - f_t h_x - f_x h_t\}^2$$
$$= \frac{1}{c^2}\{h_{tt} - f_{tt} + c^2(h_{xx} + f_{xx} - 2f_x h_x) + 2(h_t^2 - f_t h_t)\} \tag{13}$$
$$\times\{h_{tt} + f_{tt} + c^2(h_{xx} - f_{xx} + 2h_x^2 - 2f_x h_x) - 2f_t h_t\}.$$

If f and h satisfy this relation, σ may be found by elimination of p, U^2, and L^2 from equations (9), (10), and (12), and hence ρ itself may be determined, since equation (9) gives p. Again equations (8) and (9) give σU^2; thus the five equations (8)–(12) are equivalent to equation (13), together with

$$\kappa\rho = e^{-2f}\left\{f_{xx} - h_{xx} + \frac{1}{c^2}(h_{tt} - f_{tt}) - 3h_x^2 + \frac{3}{c^2}h_t^2\right\}, \tag{14}$$

$$\kappa p = e^{-2f}\{c^2(f_{xx} + h_{xx}) - (h_{tt} + f_{tt}) + c^2 h_x^2 - h_t^2\}, \tag{15}$$

$$\kappa U^2 = \frac{e^{-2f}}{\sigma}\{-c^2(f_{xx} + h_{xx}) - (h_{tt} - f_{tt}) + 2c^2 f_x h_x - 2h_t^2 + 2f_t h_t\}, \tag{16}$$

$$L^2 = 1 + \frac{U^2}{c^2}, \tag{17}$$

where, in equation (16), σ may be eliminated with the help of

$$\kappa\sigma = \frac{2e^{-2f}}{c^2}\{c^2 f_{xx} - f_{tt} - c^2 h_x^2 + h_t^2\}. \tag{18}$$

To obtain the Newtonian approximation, we proceed as follows. Let

$$f = -\frac{\kappa}{2}\phi + \kappa^2 F, \qquad h = -\frac{\kappa}{2}\chi + \kappa^2 H,$$

where ϕ, χ, F, and H are functions of x and t, and powers of κ higher than the second are to be neglected. Since the partial derivatives of f and h are then at least of order κ, it is sufficient to put $e^{-2f} = 1 + \kappa\phi$. The consistency relation (13) may then be written

$$\begin{aligned} 4\kappa^2\{ &-\tfrac{1}{2}\chi_{xt} + \kappa(H_{xt} + \tfrac{1}{4}\chi_x\chi_t - \tfrac{1}{4}\phi_t\chi_x - \tfrac{1}{4}\phi_x\chi_t)\}^2 \\ &= \kappa^2\Big[-\tfrac{1}{2}(\chi-\phi)_{tt} - \frac{c^2}{2}(\chi+\phi)_{xx} + \kappa\{c^2(H+F)_{xx} + (H-F)_{tt} \\ &\quad - \frac{c^2}{2}\phi_x\chi_x + \tfrac{1}{2}\chi_t^2 - \tfrac{1}{2}\phi_t\chi_t\}\Big]\Big[-\frac{1}{2c^2}(\chi+\phi)_{tt} - \tfrac{1}{2}(\chi-\phi)_{xx} \\ &\quad + \kappa\Big\{(H-F)_{xx} + \frac{1}{c^2}(H+F)_{tt} + \tfrac{1}{2}\chi_x^2 - \tfrac{1}{2}\chi_x\phi_x - \frac{1}{2c^2}\chi_t\phi_t\Big\}\Big]. \end{aligned} \tag{19}$$

The approximation carried out so far refers to κ $(=8\pi G/c^2)$, but it is not sufficient to produce the Newtonian theory because it does not guarantee that all velocities will be small compared with that of light. A second approximation is therefore required, which consists in neglecting terms proportional to $1/c^2$. In order to carry it out, we first write

$$\chi = \frac{1}{c^2}\Phi - \phi, \tag{20}$$

and we suppose that Φ, ϕ, F, and H contain no terms of order c^2. Substituting in equation (19) and then neglecting all terms with a factor $1/c^2$, we find

$$\phi_{xt}^2 = \phi_{xx}\{\phi_{tt} - \tfrac{1}{2}\Phi_{xx} + 8\pi G(\tfrac{1}{2}\phi_x^2 + H_{xx} + F_{xx})\},$$

in which the term in $8\pi G$ $(=\kappa c^2)$ is now to be reckoned as a term of the second order compared with the others. Hence, equating to zero the first- and second-order terms separately, we have

$$\tfrac{1}{2}\Phi_{xx} = \phi_{tt} - \frac{\phi_{xt}^2}{\phi_{xx}} \quad \text{and} \quad (H+F)_{xx} = -\tfrac{1}{2}\phi_x^2. \tag{21}$$

The next step is to find the expressions for the density, pressure, and velocity of the fluid in the Newtonian approximation. The approximation with respect to κ gives, from equations (14) and (15),

$$\begin{aligned} \rho = \tfrac{1}{2}(\chi-\phi)_{xx} - \frac{1}{2c^2}(\chi-\phi)_{tt} + \kappa\Big\{&\frac{1}{c^2}(H-F)_{tt} - (H-F)_{xx} \\ &- \frac{1}{2c^2}\phi(\chi-\phi)_{tt} + \tfrac{1}{2}\phi(\chi-\phi)_{xx} - \tfrac{3}{4}\chi_x^2 + \frac{3}{4c^2}\chi_t^2\Big\}, \end{aligned}$$

$$\begin{aligned} p = \tfrac{1}{2}(\chi+\phi)_{tt} - \frac{c^2}{2}(\chi+\phi)_{xx} + \kappa\Big\{&c^2(F+H)_{xx} - (F+H)_{tt} \\ &- \frac{c^2}{2}\phi(\chi+\phi)_{xx} + \tfrac{1}{2}\phi(\chi+\phi)_{tt} + \tfrac{1}{4}c^2\chi_x^2 - \tfrac{1}{4}\chi_t^2\Big\}. \end{aligned}$$

Introducing equations (20) and (21) into these expressions and then neglecting all terms involving $1/c^2$, it follows that

$$\rho = -\phi_{xx}, \qquad p = -\phi_{tt} + \frac{\phi_{xt}^2}{\phi_{xx}} - 2\pi G\phi_x^2, \tag{22}$$

which are the expressions for the density and pressure in the Newtonian approximation, the time t now standing, of course, for the absolute Newtonian time. The velocity is most easily calculated from equation (11) as follows: Since, in equation (6), A is of order $1/c^2$ and D is of order unity in the Newtonian approximation, it follows that $u^4 = 1$; and, since $f = 0$ also, we have $L = 1$ in equation (7). The Newtonian velocity $u = dx/dt$ is therefore equal to the value of U when the $1/c^2$ approximation is made. Moreover, since p does not contain a term of order c^2, it also follows from equation (7) that $\sigma = \rho$. But now, when the κ approximation is made in equation (11), this equation becomes

$$\sigma UL = -\left(\frac{1}{c^2}\Phi - \phi\right)_{xt} + \kappa\,(2H_{xt} - \phi\chi_{xt} + \tfrac{1}{2}\chi_x\chi_t - \tfrac{1}{2}\phi_t\chi_x - \tfrac{1}{2}\phi_x\chi_t)\,;$$

hence the $1/c^2$ approximation, together with equation (22), gives

$$u = -\frac{\phi_{xt}}{\phi_{xx}}, \tag{23}$$

and therefore equations (22) and (23) express the density, pressure, and velocity of the fluid in terms of the single arbitrary function ϕ. The physical interpretation of this function will be explained in the next section.

III. ONE-DIMENSIONAL GAS DYNAMICS WITH GRAVITATION

In Section II it was shown that the Newtonian approximation to Einstein's equations of general relativity, when the coefficients of the metric depend on the time and on one linear spatial co-ordinate, leads to the following expressions for the density, pressure, and velocity of a classical perfect fluid:

$$\rho = -\phi_{xx}, \qquad p = -\phi_{tt} + \frac{\phi_{xt}^2}{\phi_{xx}} - 2\pi G\phi_x^2, \qquad u = -\frac{\phi_{xt}}{\phi_{xx}}, \tag{24}$$

where ϕ is an arbitrary function of x and t. But now in Newtonian hydrodynamics for one-dimensional motion these quantities satisfy the equation of continuity (conservation of mass),

$$\rho_t + (\rho u)_x = 0\,, \tag{25}$$

and the equation of motion (conservation of linear momentum),

$$u_t + uu_x = -\frac{1}{\rho}\,p_x + F_1\,, \tag{26}$$

where F_1 stands for the force per unit mass, excluding the pressure-gradient force. If expressions (24) are substituted in equation (25), this equation is identically satisfied for all ϕ. Substitution in equation (26) gives

$$F_1 = 4\pi G\phi_x\,; \tag{27}$$

and this formula for F_1, as well as the formula for ρ in terms of ϕ, show that $4\pi G\phi$ is the gravitational potential of the fluid due to its own self-attraction. This is a particular illustration of an implication regarding Einstein's equations of general relativity which is not usually drawn in the textbooks, viz., Einstein's equations are a generalization of the equations of Newtonian hydrodynamics for the case when the forces acting are the pressure gradient and the gravitational self-attraction of the material in question. A corollary is that Einstein's equations do not take account of what, in Newtonian theory, would be called "external forces": for example, in equation (26), the force F_1 has been shown to depend on ϕ; but this would not necessarily be the case if we had taken the

Newtonian equations (25) and (26) as our starting point, instead of Einstein's equations, because F_1 could then have been assigned arbitrarily.

Since ϕ is, in general, a function of both x and t, it follows that the density varies both in space and in time. Thus the fluid is a gas rather than a liquid, and thermodynamical considerations become important. If T is the temperature of the gas, c_v its specific heat at constant volume, k the ratio of specific heats, and dQ the change of heat content of unit mass of gas, then the first law of thermodynamics may be stated in the following form:

$$\frac{dS}{dt} = \frac{1}{c_v T}\frac{dQ}{dt} = \frac{d}{dt}\{\log p - k \log \rho\}, \tag{28}$$

where S is proportional to the entropy of the unit mass of gas and d/dt is the operator "following the motion" of the unit mass. A motion is *adiabatic* if

$$\frac{dS}{dt} = 0, \tag{29}$$

so that each unit mass conserves its entropy; but all unit masses do not necessarily have the same entropy. If the latter condition is fulfilled, the motion is *isentropic*, and the pressure and density are then related by

$$p = \eta \rho^k, \tag{30}$$

where η is a constant common to all unit masses.

A gas motion does not necessarily affect the entire mass of gas under consideration at the same moment. The boundary which will be used in the following discussion is a shock wave, defined as a plane normal to the x-axis, moving with velocity V, at which the following three conditions[5] hold:

$$\rho_1(u_1 - V) = \rho_0(u_0 - V) = m, \tag{31}$$

$$\rho_1 u_1(u_1 - V) + p_1 = \rho_0 u_0(u_0 - V) + p_0, \tag{32}$$

$$\rho_1\left(\tfrac{1}{2}u_1^2 + \frac{1}{k-1}\frac{p_1}{\rho_1}\right)(u_1 - V) + p_1 u_1 = \rho_0\left(\tfrac{1}{2}u_0^2 + \frac{1}{k-1}\frac{p_0}{\rho_0}\right)(u_0 - V) + p_0 u_0. \tag{33}$$

Here the subscript 1 denotes the value of a variable immediately to one side of the boundary, and the subscript 0 gives values on the other. Equation (31) expresses the conservation of mass, of amount m per unit area, flowing through the boundary; equation (32) expresses the conservation of linear momentum; and equation (33) that of energy. The last equation may also be written

$$m\left\{\tfrac{1}{2}(u_1 - V)^2 + \frac{k}{k-1}\frac{p_1}{\rho_1}\right\} = m\left\{\tfrac{1}{2}(u_0 - V)^2 + \frac{k}{k-1}\frac{p_0}{\rho_0}\right\}. \tag{34}$$

In the case of interstellar gas clouds, the boundary may separate the gas cloud proper from a region in which the density is so low that it may be idealized as a vacuum. If the side denoted by subscript 0 is the vacuum, equations (31)–(33) may be satisfied by

$$\rho_0 = 0, \quad p_0 = 0, \quad u_0 = 0, \quad m = 0, \quad p_1 = 0, \quad u_1 = V, \tag{35}$$

while ρ_1 remains undetermined but may, of course, also be chosen to be zero. Alternatively, we may idealize the situation outside the gas cloud in another way by assuming that

[5] See, e.g., R. Courant and K. O. Friedrichs, *Supersonic Flow and Shock Waves* (New York: Interscience Publishers, 1949), p. 123.

the external region is occupied by a gas of very small density ρ_0, but at a high temperature, so that p_0 is appreciable. In such a case equations (31) and (32) may be satisfied by

$$\rho_0 \simeq 0 , \qquad m \simeq 0 , \qquad u_0 = 0 , \qquad \rho_1 \neq 0 , \qquad u_1 = V , \qquad p_1 = p_0 , \tag{36}$$

while equation (33), in the form (34), is satisfied because m is negligibly small. In the following sections the simplified shock waves described by equations (35) and (36) will be used, chiefly for the sake of mathematical simplicity: it must not, however, be assumed that these simplified boundary conditions are the only ones applicable to equations (24).

IV. APPLICATION TO THE MOTION OF A THIN INTERSTELLAR GAS CLOUD

It is a well-known observational result that interstellar gas clouds occur whose cross-section is very small compared with their lateral extent. These clouds are in motion relative to the sun, with respect to which the co-ordinate system, x, y, and z, used in equation (4), may be taken to be at rest. We shall idealize the problem of the motion of such thin clouds by representing them as masses of gas, of infinite extent perpendicular to the x-axis, bounded by two planes normal to this axis at a finite distance apart. These planes are, of course, not rigid containing walls but merely mathematical surfaces, and the intervening gas cloud is held together by its gravitational self-attraction. The simplest way in which such a cloud could move would be with constant velocity with respect to the sun; the next degree of complexity would be to suppose that it had a constant acceleration relative to the sun; and so on. Motions of this kind are obtained if, in equation (24), it is assumed that

$$\phi = -\int \psi(X)\, dX - \int [\int P(t)\, dt]\, dt , \qquad X = x - \int v(t)\, dt , \tag{37}$$

where ψ, P, and v are arbitrary functions of their arguments. It is convenient to denote derivatives of these functions with respect to their arguments by primes, so that, for example,

$$\psi' = \frac{d\psi}{dX} , \qquad v' = \frac{dv}{dt} .$$

Using in equation (24) the expression for ϕ given by equation (37), it follows that

$$\rho = \psi' , \qquad p = P - v'\psi - 2\pi G\psi^2 , \qquad u = v ; \tag{38}$$

and therefore the velocity of the gas is a function of t alone, all elements of the gas moving, at any given instant, with the same speed. Since

$$\frac{dX}{dt} = \left(\frac{\partial}{\partial t} + u\frac{\partial}{\partial x}\right) X = -v + u = 0 ,$$

the rate of change "following the motion" of the entropy function S is

$$\frac{dS}{dt} = \frac{1}{p}\frac{dp}{dt} = \frac{P' - v''\psi}{P - v'\psi - 2\pi G\psi^2} . \tag{39}$$

Hence adiabatic motions of this kind[6] are possible if

$$P' = 0 \qquad \text{and} \qquad v'' = 0 ,$$

and in such motions

$$X = x - \tfrac{1}{2}\alpha t^2 - \beta t , \qquad \rho = \psi' , \qquad p = \Pi - \alpha\psi - 2\pi G\psi^2 , \qquad u = \alpha t + \beta , \tag{40}$$

[6] The isentropic case (eq. [30]), neglecting gravity, has been obtained by E. T. Copson, *Proc. Roy. Soc. London*, *A*, **216**, 539, 1953, using the theory of the complex variable.

where Π, α, and β are constants of integration and ψ is an arbitrary function of its argument. We shall now proceed to clarify the physical meaning of this general result by considering two particular cases of adiabatic motions.

i) GAS CLOUD MOVING WITH CONSTANT VELOCITY

An example of such a case is obtained by choosing in equations (40)

$$\psi = -\rho_c \frac{\lambda}{\pi} \cos \frac{\pi X}{\lambda}, \tag{41}$$

where ρ_c and λ are constants. The density, therefore, is

$$\rho = \rho_c \sin \frac{\pi X}{\lambda}$$

and is consequently zero at $X = 0$ and $X = \lambda$, having a maximum, ρ_c, at $X = \frac{1}{2}\lambda$. Thus at any instant t the cloud occupies the region between the planes $x = \frac{1}{2}\alpha t^2 + \beta t$ and $x = \frac{1}{2}\alpha t^2 + \beta t + \lambda$, its density vanishing at both these boundaries. It is therefore possible to fit the boundary conditions appropriate to having a vacuum outside the gas cloud, and it will be assumed that equations (35) hold at both faces of the cloud. But the pressure is, by equations (40) and (41),

$$p = \Pi + \alpha \rho_c \frac{\lambda}{\pi} \cos \frac{\pi X}{\lambda} - 2\pi G \rho_c^2 \frac{\lambda^2}{\pi^2} \cos^2 \frac{\pi X}{\lambda}$$

at any point within the cloud, and therefore, if it is to vanish at $X = 0$ and at $X = \lambda$, the constants Π, α, and λ must satisfy the two equations

$$0 = \Pi + \alpha \rho_c \frac{\lambda}{\pi} - 2\pi G \rho_c^2 \frac{\lambda^2}{\pi^2},$$

$$0 = \Pi - \alpha \rho_c \frac{\lambda}{\pi} - 2\pi G \rho_c^2 \frac{\lambda^2}{\pi^2}.$$

Hence

$$\alpha = 0 \qquad \text{and} \qquad \Pi = 2\pi G \rho_c^2 \frac{\lambda^2}{\pi^2},$$

and equations (40) take the form

$$X = x - \beta t, \qquad \rho = \rho_c \sin \frac{\pi X}{\lambda}, \qquad p = 2\pi G \rho_c^2 \frac{\lambda^2}{\pi^2} \sin^2 \frac{\pi X}{\lambda}, \qquad u = \beta.$$

The velocity, therefore, has a constant value β relative to the co-ordinate system that is being employed. Moreover, the maximum pressure, p_c, also occurs at $X = \frac{1}{2}\lambda$, and, if the temperature there is T_c, we have

$$p_c = R \rho_c T_c = 2\pi G \rho_c^2 \frac{\lambda^2}{\pi^2};$$

and therefore

$$\lambda = \pi \left(\frac{R}{2\pi G}\right)^{1/2} \left(\frac{T_c}{\rho_c}\right)^{1/2}, \tag{42}$$

which gives the width of the cloud. This width therefore depends on the temperature and density at the densest portion of the cloud. Since $\rho = \rho_c \sin(\pi X/\lambda)$, the average density across the cloud is $2\rho_c/\pi = 0.637\rho_c$. Now the observed average density of interstellar matter[7] in clouds of all kinds is of the order of 10^{-22} gm/cm^3 and is perhaps a thousand

[7] J. M. Burgers, *Nederl. Akad. Wetensch.*, **49**, 589, 1946.

times as large as this in the densest clouds.[8] Thus it is not unreasonable to suppose that ρ_c may have values lying between 10^{-21} and 10^{-19} gm/cm^3. Table 1 shows specimen values of cloud widths.

ii) GAS CLOUD MOVING WITH CONSTANT ACCELERATION

An illustration of motion of this kind is obtained by choosing, in equation (40),

$$\psi = \frac{4\rho_c(\frac{1}{2}\lambda X^2 - \frac{1}{3}X^3)}{\lambda^2} + \mu , \tag{43}$$

where ρ_c, λ, and μ are constants. The density, therefore, is

$$\rho = \psi' = \frac{4\rho_c X(\lambda - X)}{\lambda^2} , \tag{44}$$

TABLE 1

RANGE OF PHYSICAL PARAMETERS FOR INTERSTELLAR CLOUDS

T_c	ρ_c (Gm/Cm^3)	λ (Parsecs)
10,000°	10^{-21}	45.4
	10^{-20}	14.4
	10^{-19}	4.54
60°	10^{-21}	3.53
	10^{-20}	1.13
	10^{-19}	0.35

and so vanishes at $X = 0$ and $X = \lambda$, which may again be taken to be the boundaries of the cloud. If the region outside the cloud is again regarded as effectively a vacuum, equations (35) apply, and the vanishing of the pressure at the boundaries gives

$$0 = \Pi - a\psi(0) - 2\pi G\psi^2(0) , \qquad 0 = \Pi - a\psi(\lambda) - 2\pi G\psi^2(\lambda) , \tag{45}$$

where $\psi(0)$ and $\psi(\lambda)$ are the values of ψ at the boundaries $X = 0$ and $X = \lambda$, respectively. Hence $\psi(0)$ and $\psi(\lambda)$ are the roots of the quadratic equation in Z,

$$2\pi GZ^2 + aZ - \Pi = 0 ,$$

while their values are also directly obtainable from equation (43). Thus

$$\begin{aligned} \psi(0) &= \mu = -\frac{a + (a^2 + 8\pi G\Pi)^{1/2}}{4\pi G} , \\ \psi(\lambda) &= \tfrac{2}{3}\rho_c\lambda + \mu = -\frac{a - (a^2 + 8\pi G\Pi)^{1/2}}{4\pi G} , \end{aligned} \tag{46}$$

from which it follows that

$$\tfrac{1}{3}\rho_c\lambda = \frac{(a^2 + 8\pi G\Pi)^{1/2}}{4\pi G} . \tag{47}$$

The maximum value of the density from equation (44) is ρ_c and occurs at $X = \frac{1}{2}\lambda$; moreover, if expression (43) for ψ is substituted in the formula for p given in equations

[8] J. H. Oort, *M.N.*, **106**, 159, 1946.

(40), it is easy to show that the minimum values of p occur at the boundaries, while the maximum also occurs at $X = \frac{1}{2}\lambda$. Hence the maximum pressure is

$$p_c = \Pi - a\psi\left(\tfrac{1}{2}\lambda\right) - 2\pi G\psi^2\left(\tfrac{1}{2}\lambda\right),$$

where, by equations (43), (46), and (47),

$$\psi\left(\tfrac{1}{2}\lambda\right) = \tfrac{1}{3}\rho_c\lambda + \mu = -\frac{a}{4\pi G},$$

and therefore

$$p_c = \Pi + \frac{1}{2}\frac{a^2}{4\pi G}. \tag{48}$$

Thus if T_c is the central temperature and $p_c = R\rho_c T_c$, it is possible to eliminate Π and a from equations (47) and (48) and to obtain

$$\lambda = 3\left(\frac{R}{2\pi G}\right)^{1/2}\left(\frac{T_c}{\rho_c}\right)^{1/2} \tag{49}$$

for the width of the gas cloud, a formula that should be compared with equation (42). The numerical values for λ given in Table 1 are therefore not sensibly altered when ψ is given by equation (43) instead of by equation (41). Finally, eliminating Π from equations (46) and (48), we find

$$\mu = -\frac{a + (8\pi G p_c)^{1/2}}{4\pi G},$$

and therefore, by equations (40), the complete solution for the motion inside the gas cloud is given by equation (49), together with

$$\begin{aligned} X &= x - \tfrac{1}{2}at^2 - \beta t, \\ \psi &= \frac{4\rho_c\left(\frac{1}{2}\lambda X^2 - \frac{1}{3}X^3\right)}{\lambda^2} - \frac{a + (8\pi G p_c)^{1/2}}{4\pi G}, \\ \rho &= \frac{4\rho_c X(\lambda - X)}{\lambda^2}, \\ p &= p_c - \frac{a^2}{8\pi G} - a\psi - 2\pi G\psi^2, \\ u &= at + \beta. \end{aligned} \tag{50}$$

It is now possible to give a physical interpretation of the constant a in the following way: If equation (26) be multiplied throughout by ρ, it follows that the effective force on every unit volume of the gas is

$$\rho\frac{du}{dt} = \rho u_t = \rho a,$$

which is the form that would occur if a were the acceleration produced by a uniform gravitational field. But the pressure gradient is

$$-p_x = a\psi' + 4\pi G\psi\psi' = a\rho + 4\pi G\psi\rho,$$

while the gravitational force due to the gas cloud's self-attraction is, by equations (27) and (37),

$$\rho F_1 = 4\pi G\rho\phi_x = -4\pi G\psi\rho.$$

Thus the pressure gradient consists of two terms, one of which balances the uniform gravitational field that may be regarded as being external to the cloud, while the other balances the cloud's internal self-attraction. This indirect way of taking account of an external force, through the pressure gradient, is consistent with the limitation imposed on the nature of F_1 in equation (26) by deducing it from Einstein's equations.

V. NONADIABATIC MOTIONS

An interstellar gas cloud may lose internal energy by the emission of radiation, and the present theory can take this effect into account, provided that (*a*) the emission of radiation does not lead to any significant loss of mass, so that the equation of continuity is still (25), and (*b*) the emission produces no change in the momentum of the cloud, so that its equation of motion is still (26). The radiation loss means, under these conditions, that the adiabatic equation (29) or the isentropic relation (30) is no longer applicable. Instead, let it be assumed that E is the loss of energy in ergs per second per cubic centimeter of the gas; whence, by equation (28),

$$E = -J\rho\frac{dQ}{dt} = -Jc_vT\rho\frac{dS}{dt} = -\frac{p}{k-1}\frac{dS}{dt}, \tag{51}$$

where J is the mechanical equivalent of heat. Applying this to motions in which the density, pressure, and velocity are given by equation (38), it follows that

$$E = -\frac{P' - v''\psi}{(k-1)\psi'}\rho. \tag{52}$$

The simplest example of a motion of this kind is found by assuming that E/ρ is the same at all points in the cloud, which implies that this ratio is, at most, a function of t and may, of course, be a constant. Inspection of equation (52) shows that, in such a case,

$$P' = \mu v'' \quad \text{and} \quad \mu - \psi = \lambda\psi', \tag{53}$$

where λ and μ are positive constants; and therefore

$$\frac{E}{\rho} = -\frac{\lambda}{k-1}v''. \tag{54}$$

Thus there is a loss of energy by radiation if $v'' < 0$, since $k > 1$. The solutions of the two equations (53) are

$$P = \Pi + \mu v' \quad \text{and} \quad \psi = \mu - \sigma e^{-X/\lambda}, \tag{55}$$

where Π and σ are constants of integration. The expression for the density, therefore, is

$$\rho = \psi' = \frac{\sigma}{\lambda}e^{-X/\lambda},$$

and, consequently, ρ has a maximum, ρ_m, at $X = 0$, which is

$$\rho_m = \frac{\sigma}{\lambda}. \tag{56}$$

The expression for the pressure obtained from equations (38) and (55) is

$$p = \Pi + \mu v' - (\mu - \sigma e^{-X/\lambda})v' - 2\pi G(\mu - \sigma e^{-X/\lambda})^2$$

and therefore, if it is assumed that, at $X = 0$,

$$p = P = \Pi + \mu v',$$

it follows from the previous equation that $\mu = \sigma$. Moreover, λ is obviously of the physical dimensions of a length, and so the gas in motion may be taken to occupy the region $0 \leq X \leq \lambda$ as before. The solution for the motion within this region, consequently, becomes

$$\begin{aligned} X &= x - \int v\,(t)\,dt\,, \\ \rho &= \rho_m e^{-X/\lambda}\,, \\ p &= \Pi + \lambda \rho_m e^{-X/\lambda} v' - 2\pi G \lambda^2 \rho_m^2 (1 - e^{-X/\lambda})^2\,, \\ u &= v\,, \\ \frac{E}{\rho} &= -\frac{\lambda}{k-1} v''\,, \end{aligned} \tag{57}$$

the function $v(t)$ remaining arbitrary.

It is not possible to apply the boundary conditions given by equations (35) to motions of this kind, because, if there is to be loss of energy by radiation, v'' cannot be zero, and therefore v' cannot be constant. Hence it is impossible to satisfy the condition $p_1 = 0$ for all values of t at the boundaries of the cloud. Thus the region outside the cloud cannot be regarded as a vacuum; but it is possible to apply the boundary conditions (36), which imply that there is material at low density but high temperature outside the cloud. Let the plane $X = 0$ be denoted by B_1, while the plane $X = \lambda$ is called B_2, and suppose that, at each of these planes, the boundary conditions (36) hold good. Now since, by equations (57), the density just "inside" B_1 and B_2 cannot vanish, there must be a discontinuity of density at each boundary. Again, because of the continuity of "inside" and "outside" pressure at B_1 and at B_2, it follows that

$$\begin{aligned} (p_0)_1 &= \Pi + \lambda \rho_m v'\,, \\ (p_0)_2 &= \Pi + \lambda \rho_m \{ v' e^{-1} - 2\pi G \lambda \rho_m (1 - e^{-1})^2 \}. \end{aligned}$$

Since v'' must not be zero, v' cannot be constant, and so $(p_0)_1$ and $(p_0)_2$ must be functions of t. Thus the medium outside the region in which equations (57) apply cannot be in a steady state but must itself have a pressure that is changing with the time.

In order to see more clearly what is happening, we shall consider the case in which E/ρ decreases linearly with the time from the value ϵ at $t = 0$ to zero at $t = \tau$, i.e.,

$$\frac{E}{\rho} = \epsilon \left(1 - \frac{t}{\tau}\right). \tag{58}$$

Thus the motion described by equations (57) will be regarded as being limited in time to the interval $0 \leq t \leq \tau$, as well as being restricted in space to the values of x satisfying $0 \leq X \leq \lambda$. From equation (58) and the last equation of (57) it follows, on integration, that

$$\begin{aligned} v' &= \alpha + \frac{1}{2}\frac{\epsilon}{\lambda}(k-1)\,\tau \left(1 - \frac{t}{\tau}\right)^2, \\ v &= \beta + \alpha t - \frac{1}{6}\frac{\epsilon}{\lambda}(k-1)\,\tau^2 \left(1 - \frac{t}{\tau}\right)^3, \end{aligned} \tag{59}$$

where α and β are constants of integration. Hence the continuity of pressure at B_1 and B_2 gives

$$(p_0)_1 = \Pi + \lambda \rho_m \left\{ \alpha + \frac{1}{2}\frac{\epsilon}{\lambda}(k-1)\,\tau \left(1 - \frac{t}{\tau}\right)^2 \right\}, \tag{60}$$

$$(p_0)_2 = \Pi + \lambda\rho_m \left\{ a\, e^{-1} + \frac{1}{2}\frac{\epsilon}{\lambda}\, e^{-1}(k-1)\,\tau \left(1 - \frac{t}{\tau}\right)^2 - 2\pi G\lambda\rho_m (1 - e^{-1})^2 \right\}. \quad (61)$$

These two formulae show that the pressures at B_1 and B_2 decrease linearly with the time during the interval $0 \leq t \leq \tau$; on the other hand, the densities at these planes remain fixed at the values ρ_m and $\rho_m e^{-1}$, respectively. Let it therefore be assumed that, at $t = \tau$, the pressure at B_1 is p_m, which, by equation (60), is

$$p_m = \lambda\rho_m a + \Pi,$$

while the pressure at B_2 is Π. Hence, by equation (61),

$$a = 2\pi G\lambda\rho_m e\,(1 - e^{-1})^2;$$

and, since $p_m = R\rho_m T_m$, the last two formulae, when combined, give

$$\lambda^2 = \frac{e}{(e-1)^2}\frac{R}{2\pi G}\frac{T_m}{\rho_m} - \frac{\Pi e}{2\pi G(e-1)^2\rho_m^2}.$$

Thus, in this case, the maximum possible width of the cloud is

$$\lambda = \frac{e^{1/2}}{(e-1)}\left(\frac{R}{2\pi G}\right)^{1/2}\left(\frac{T_m}{\rho_m}\right)^{1/2} = 0.96\left(\frac{R}{2\pi G}\right)^{1/2}\left(\frac{T_m}{\rho_m}\right)^{1/2}, \quad (62)$$

which, on comparison with equations (42) and (49), reveals that the cloud width has been reduced to about one-third the previous values. Hence one consequence of permitting a linear decrease of loss of internal energy with time is to narrow the gas cloud as compared with the adiabatic motion. But, once again, the width of the cloud depends essentially on the square root of the ratio of the temperature to the density at the place where the density is a maximum. Another consequence of the loss of energy is to retard the motion of the cloud; for the acceleration of any unit mass is, by equation (59),

$$\frac{du}{dt} = v' = a + \frac{1}{2}\frac{\epsilon}{\lambda}(k-1)\,\tau\left(1 - \frac{t}{\tau}\right)^2$$

and therefore decreases from the value $a + \frac{1}{2}\epsilon(k-1)\tau/\lambda$ at $t = 0$ to a at $t = \tau$. Since radiation pressure and loss of momentum due to the departing radiation have not been included in our fundamental equations, this is purely an energy effect. The loss of internal energy has not led to a change in the width of the cloud—which remains equal to λ throughout the motion—or to a change of density at the boundaries B_1 and B_2. The fall of temperature in the cloud has not led to a collapse, but the total kinetic energy of the cloud has decreased instead.

The three examples given in Section IV, i and ii, and in Section V could be multiplied indefinitely by considering other functional forms for ψ in equations (38). But enough has probably been said to show that interstellar gas clouds with plane faces can move as entities held together by their internal gravitation, even when the cloud as a whole is subject to an acceleration, which, in general, may vary with the time but not with the spatial position of the cloud. Such motions may be expected to occur in regions sufficiently distant from other bodies for their gravitational field to be constant throughout the cloud. Moreover, it has proved possible to solve with comparative simplicity the problem of the nonadiabatic motion of a cloud, a question usually left open in classical aerodynamics.

TWO MODELS FOR THE INTERIOR OF THE SUN

PETER NAUR
Yerkes Observatory
Received October 16, 1953

ABSTRACT

Two models for the sun, based on the revised data for the proton-proton chain reaction and taking the opacity due to free-free transitions in hydrogen and helium into account, have been calculated. The models differ in the explicit opacity expressions used, but both yield a composition for the interior of the sun of about 0.75 per cent heavy elements, 75 per cent hydrogen, and 24 per cent helium.

In a recent paper Epstein and Motz[1] published a model for the interior structure of the sun, based on the most recent data for the rate of energy production by the proton-proton reaction. They arrive at a quite low abundance of the heavy elements, $Z = 0.002$, and a vanishing amount of helium but, in spite of this small value of Z, do not take the opacity due to the free-free transitions in hydrogen into account. In the present paper two different models for the sun, in which these free-free transitions are included approximately, are presented.

There exist, at present, no detailed computations of the opacity of mixtures of elements which include relatively large amounts of hydrogen and helium. There would be no particular difficulty in calculating such opacities, but for a first rough indication it was thought sufficient to use only a rather crude method for computing the opacity. The procedure used here consists simply in taking the sum of the opacities due to the heavy elements and to hydrogen and helium and then adding $\frac{3}{2}$ the opacity from the scattering on free electrons.

The opacity due to the group of heavy elements was computed by means of Morse's tables.[2] None of Morse's tables for the guillotine factor is computed for such high abundances of the elements of the oxygen group as those found in the atmosphere of the sun in recent investigations.[3] However, an inspection of the four tables given shows that, for the temperature and density range of the interior of the sun, the value of the guillotine factor is rather insensitive to changes in composition. It was therefore decided to use Morse's Table 3, case 1, for the guillotine factor.

The mixture of elements enters also through the "composition factor,"

$$\Gamma = \sum_{Z>2} \frac{c_Z Z^2}{M_Z},$$

where c_Z is the abundance, by weight, of the element of atomic number Z, relative to the heavy group as a whole, and M_Z is the atomic weight of the element. In this calculation Γ was taken to be 4.778, corresponding to a heavy group composed of 60 per cent oxygen and 40 per cent Russell mixture.

The opacity caused by free-free transitions in hydrogen and helium can also be computed by means of Morse's formula,[4] with a suitable interpretation of the quantities; $(1 - X - Y)$ in Morse's expression is the relative abundance of the heavy elements taken together. This factor must now be replaced by $(X + Y)$. The composition factor reduces to unity for any mixture of hydrogen and helium. The guillotine factor becomes

[1] *Ap. J.*, **117**, 311, 1953.
[2] *Ap. J.*, **92**, 27, 1940.
[3] *Trans. I.A.U.*, **7**, 460, 1950.
[4] *Op. cit.*, eq. (16).

the limit of Strömgren's function, $S(\infty) = 196.5$. The Gaunt factor was estimated from the expressions given by Maue[5] and Menzel and Pekeris[6] to be about 0.75. Finally, the scattering by free electrons is taken to contribute by $0.3\ (1 + X)$.

Collecting these results, we arrive at the following expression for the total opacity:

$$\kappa = 3.454 \times 10^{25} (1 + X) Z \rho T^{-3.5} \left(\frac{l}{g}\right)^{-1} + 2.74 \times 10^{22} (1 + X)(X + Y)\, \rho T^{-3.5} + 0.3\,(1 + X)\,. \tag{1}$$

This expression for the opacity could very well be used in the integration of the equations of equilibrium of the sun. However, it seemed well worth while to sacrifice some accuracy for the great simplification of the integration which follows if simplified expressions for the opacity are used. In this particular case such a procedure is further justified because expression (1) certainly cannot be expected to give very high accuracy.

In this investigation the method has been to divide the sun into an exterior region and an interior region, fitted together at some radius, r_f. In both these regions we take opacities of the form

$$\kappa = \kappa_0 \rho^{1-a} T^{-3-s}\,, \tag{2}$$

but the constants κ_0, a, and s take different values in the two regions. In what follows we shall distinguish the variables in the two regions by the subscripts i and e.

We shall always assume the opacity to be continuous at r_f, and thus a definite model of this kind is defined when a_i, s_i, a_e, s_e, and r_f/R are given, R being the radius of the star. These models permit of homology transformations, this property being one of the strongest arguments for using models of this kind.

An energy-production law of the form

$$\epsilon = \epsilon_0 \rho T^4 \tag{3}$$

has been used throughout.

Two different models of this kind have been calculated, adjusted so as to conform to the radius, mass, and luminosity of the sun, at the same time as having a run of the opacity which lies very close to that given by equation (1). In model I, which was calculated first, an opacity expression of the Kramers form was used in the exterior region, and the form introduced by M. Schwarzschild[7] in the interior. The opacity used in this model does not deviate from expression (1) by more than 32 per cent at any point in the model; but a marked trend in the deviations between the two opacities suggested that better agreement might be expected for a model with $(a_i, s_i) = (1, -2.1)$ and $(a_e, s_e) = (0, 0.8)$. This is model II.

Table 1 summarizes the properties of the two models. The arrangement is the one used by Chandrasekhar,[8] extended to cover the kind of model considered here. The numbers given are independent of any particular choice of the molecular weight or composition of the stellar material. Model I is unusual, in so far as it has no convective core. This, however, is not surprising, in view of the criterion for the absence of a convective core recently established by Naur and Osterbrock.[9] It was found that, in a model with energy production and opacity near the center given by $\epsilon = \epsilon_0 \rho T^\nu$, $\kappa = \kappa_0 \rho^{1-a} T^{-3-s}$,

[5] *Ann. d. Phys.*, **13**, 161, 1932.

[6] *M.N.*, **96**, 77, 1935.

[7] *Ap. J.*, **104**, 203, 1946.

[8] *Astrophysics: A Topical Symposium*, ed. J. A. Hynek (New York: McGraw-Hill Book Co., 1951), p. 626.

[9] *Ap. J.*, **117**, 306, 1953.

it is a necessary condition for the existence of a convective core that $6\nu - 10s - 15a > 21$. In model I this condition is violated, the left side of the inequality being $15\frac{1}{4}$.

The symbols appearing in Table 1 have the following meaning: Q gives the central temperature, T_c, by the formula

$$T_c = Q\mu MR^{-1} \times 10^6 \text{ degrees}, \tag{4}$$

where μ is the mean molecular weight and R and M are the radius and mass expressed in solar units.

There are two constants for the mass-luminosity relation, one for each of the two regions of opacity. The quantities given, C, are defined by

$$C = \frac{3\,\kappa_0}{4\,(4\pi)^{3-a}\,a\,c}\left(\frac{k}{GH}\right)^{7+s}\frac{LR^{3a+s}}{M^{5+s+a}}\frac{1}{\mu^{7+s}}, \tag{5}$$

TABLE 1

CONSTANTS OF THE MODELS INTEGRATED

	Model I	Model II
Opacity law { interior region	$\kappa_0\rho^{0.75}T^{-3.5}$	$\kappa_0 T^{-0.9}$
Opacity law { exterior region	$\kappa_0\rho T^{-3.5}$	$\kappa_0\rho T^{-3.8}$
Radius of opacity fit	0.487 R	0.482 R
Convective core { radius		0.050 R
Convective core { mass		0.007 M
Convective core { energy production		0.060 L
Polytropic index at center, n_c	1.981	1.5
Central density/average density $= \rho_c/\bar{\rho}$	66.6	60.8
Central temperature factor, Q	22.6	23.4
C_{interior}	3.12×10^{-6}	2.58×10^{-4}
C_{exterior}	2.35×10^{-6}	1.29×10^{-6}
$\epsilon_c ML^{-1}$	8.88	9.19

or, with R, M, and L expressed in solar units,

$$\log C = -27.0448 + 0.3274\,a - 7.3638\,s + \log\,\kappa_0 + \log\frac{LR^{3a+s}}{M^{5+s+a}\mu^{7+s}}.$$

The last quantity of Table 1 gives the concentration of the energy production toward the center, defined as the ratio of the central energy-production rate to the mean rate for the whole star.

Table 2 gives the results of applying the models to the sun. In Tables 3 and 4 the detailed variations of the physical parameters through the configurations are given. The two models have, of course, been chosen in such a way that they fit the sun as well as possible. Once the four exponents in the opacity laws have been chosen, only the value of r_f/R remains to be varied, i.e., for each choice of r_f/R the numbers given in Table 1 can be calculated. For each such choice it then remains to be decided whether any choice of the chemical composition will give the correct energy output and reproduce the run of the opacity through the star at the same time. It now turns out that, in the present situation, the condition of the fit of the energy generation almost solely determines the value of r_f/R. In fact, as the condition of fit of energy production, we use the equality of ϵ_c as determined, on the one hand, by the model,

$$\epsilon_{c,\,\text{model}} = \left(\epsilon_c ML^{-1}\right)_{\text{model}} LM^{-1}, \tag{6}$$

and, on the other hand, by the theory of the rate of the proton-proton reaction,[10]

$$\epsilon_{c,\ \text{physical}} = 0.99 \times 10^{-29} X^2 \rho_c T_c^4 , \tag{7}$$

which, with the use of the constants of the model, ρ_c and T_c/μ, can be written

$$\epsilon_{c,\ \text{physical}} = 0.99 \times 10^{-29} \rho_c \left(\frac{T_c}{\mu}\right)^4 X^2 \mu^4 . \tag{8}$$

Now, while both these expressions depend on the model, i.e., in our case on the value of r_f/R, the chemical composition enters only through the factor $X^2\mu^4$ of equation (8).

[10] E. E. Salpeter, *Ap. J.*, **116**, 649, 1952.

TABLE 2

THE SOLAR MODEL

		Model I	Model II
Abundances	hydrogen	0.74	0.76
	helium	0.25	0.23
	heavy elements	0.0075	0.0075
Mean molecular weight		0.598	0.589
Central density		94.0	85.7
Central temperature		13.5×10^6°K	13.8×10^6°K
Computed luminosity		1.007 L	1.006 L
log κ_0	interior	23.463	6.538
	exterior	23.421	25.252
Ratio: carbon cycle to proton-proton reaction	at the center	0.47	0.65
	for the whole star	0.09	0.13

TABLE 3

VARIATION OF PHYSICAL VARIABLES THROUGH THE MODELS (MODEL I)

r/R	ρ/ρ_c	T/T_c	M_r/M	L_r/L	ϵ/ϵ_c	κ_{phys}	Relative Contributions to κ			log ($\kappa_{model}/\kappa_{phys}$)
							Heavy	$H+He$	Electrons	
0.000	1.000	1.000	0.000	0.000	1.000	1.21	16	40	44	−0.10
.050	0.944	0.972	0.008	0.064	0.845	1.24	17	41	42	− .09
.091	0.829	0.913	0.045	0.290	0.576	1.31	18	42	40	− .06
.128	0.687	0.839	0.114	0.561	0.340	1.43	20	44	36	− .03
.184	0.467	0.716	0.267	0.849	0.123	1.67	24	44	32	+ .02
.230	0.307	0.614	0.419	0.953	0.044	1.94	30	43	27	+ .05
.276	0.192	0.525	0.561	0.987	0.015	2.32	39	38	23	+ .06
.334	9.98×10^{-2}	0.428	0.710	0.998	0.003	2.73	46	35	19	+ .08
.397	4.69×10^{-2}	0.343	0.826	1.000	0.001	3.40	56	29	15	+ .08
.482	1.66×10^{-2}	0.252	0.919	1.000	0.000	4.20	64	24	12	+ .12
.529	9.51×10^{-3}	0.211	0.948	1.000	0.000	5.14	69	21	10	+ .06
.570	5.62×10^{-3}	0.179	0.968	1.000	0.000	5.62	70	20	10	+ .05
.606	3.50×10^{-3}	0.155	0.979	1.000	0.000	5.71	71	20	9	+ .05
.637	2.31×10^{-3}	0.136	0.986	1.000	0.000	6.14	72	20	8	+ .04
.664	1.58×10^{-3}	0.121	0.990	1.000	0.000	6.44	72	20	8	+ .04
.687	1.12×10^{-3}	0.109	0.993	1.000	0.000	6.82	73	19	8	+ .02
.707	8.20×10^{-4}	0.099	0.995	1.000	0.000	7.21	74	19	7	+ .01
.742	4.70×10^{-4}	0.083	0.997	1.000	0.000	7.49	74	19	7	+ .01
.783	2.23×10^{-4}	0.066	0.999	1.000	0.000	8.64	77	17	6	− .03
0.820	1.06×10^{-4}	0.052	1.000	1.000	0.000	10.97	82	14	4	−0.10

But it so happens that, for the kind of chemical composition which is of interest, $Z \sim 0.01$ and $X \sim 0.8$, the factor $X^2\mu^4$ is quite insensitive to variations of X. Therefore, the equality of equations (6) and (8) can be achieved only through variations of the model and, on the other hand, this condition is sufficient to determine the model. With the model thus determined, one has to try to adjust the chemical parameters to make the opacity of the model, as computed from equation (2), with κ_0 given by equation (5), agree well with the opacity (1). At this stage it will also become apparent whether the choice of the exponents of the opacity laws has been a fortunate one.

The execution of the program thus outlined requires the integration of the equations of equilibrium from the center and outward, and from the surface and inward for a

TABLE 4

VARIATION OF PHYSICAL VARIABLES THROUGH THE MODELS (MODEL II)

r/R	ρ/ρ_0	T/T_c	M_r/M	L_r/L	ϵ/ϵ_c	κ_{phys}	Relative Contributions to κ			Log ($\kappa_{model}/\kappa_{phys}$)
							Heavy	$H+He$	Electrons	
0.000	1.000	1.000	0.000	0.000	1.000	1.14	15	38	47	+0.06
.050	0.956	0.971	0.007	0.060	0.850	1.18	17	38	45	+ .05
.091	0.860	0.907	0.042	0.278	0.582	1.28	18	40	42	+ .04
.128	0.734	0.828	0.107	0.547	0.345	1.43	20	43	37	+ .03
.184	0.518	0.699	0.259	0.843	0.124	1.75	25	45	30	+ .01
.230	0.348	0.594	0.415	0.952	0.043	2.10	30	44	25	.00
.276	0.218	0.504	0.562	0.987	0.014	2.51	37	41	21	− .02
.334	0.112	0.408	0.717	0.998	0.003	3.09	47	36	17	− .03
.397	5.16×10^{-2}	0.325	0.835	1.000	0.001	4.00	59	28	13	− .05
.482	1.75×10^{-2}	0.238	0.927	1.000	0.000	4.85	65	24	11	.00
.529	9.64×10^{-3}	0.199	0.956	1.000	0.000	5.45	69	22	10	− .01
.570	5.58×10^{-3}	0.169	0.973	1.000	0.000	5.83	70	21	9	− .01
.606	3.40×10^{-3}	0.146	0.982	1.000	0.000	5.92	71	20	9	+ .01
.637	2.19×10^{-3}	0.128	0.988	1.000	0.000	6.30	72	20	8	+ .01
.664	1.47×10^{-3}	0.114	0.992	1.000	0.000	6.51	72	20	8	+ .01
.687	1.02×10^{-3}	0.102	0.994	1.000	0.000	6.80	73	19	8	+ .02
.707	7.37×10^{-4}	0.093	0.996	1.000	0.000	7.08	74	18	8	+ .01
.742	4.12×10^{-4}	0.078	0.998	1.000	0.000	7.17	75	18	7	− .01
.783	1.88×10^{-4}	0.062	0.999	1.000	0.000	9.06	79	15	6	− .04
0.820	8.60×10^{-5}	0.049	1.000	1.000	0.000	10.74	82	13	5	−0.07

number of different initial conditions. In this respect the work has been greatly facilitated by the use of a large number of integrations from the center, which were carried out by means of the punched-card equipment of the International Business Machines Watson Laboratory, Columbia University, New York. These integrations will be described in detail elsewhere. Furthermore, the structure of the exterior region could, to quite a high degree of accuracy, be described by series expansions, and, altogether, only a comparatively small amount of work of integration was necessary for each model.

Table 2 shows that although quite different opacity laws are assumed in the models, the chemical composition comes out about the same. This agreement of the two models is probably rather significant where the hydrogen content is concerned, while it should be stressed that the value of Z is rather uncertain. This uncertainty is, unfortunately, a rather important feature of the whole situation. In fact, as seen from Table 3, the opacity is strongly dependent on the content of heavy elements only in the outer parts of the sun. Also the energy generation is largely independent of Z.

In the construction of the models the energy generation due to the carbon cycle has

been neglected. Table 2 gives the relative importance of this process, when the data corresponding to a low-energy resonance of the capture of protons by N^{14} are adopted.[11] Carbon and nitrogen were assumed to constitute one-seventh the weight of the heavy elements. The carbon-nitrogen cycle, though not very important for energy production as a whole, would probably be sufficiently effective near the center to produce a convective core. Also, since model II, which already has a convective core, gives the better opacity fit, the evidence presented supports the view that a small convective core is actually present in the sun.

We conclude that the inclusion of free-free transitions in the assumed opacity gives a comfortable abundance of helium in the interior of the sun, even if the new higher rate for the proton-proton reaction is used; further, that the proton-proton reaction contributes the bulk of the energy, even if a low-energy resonance in the capture cross-section of protons by N^{14} exists; and, finally, that a small convective core probably is present in the sun. However, in view of the uncertainties which still enter with all the fundamental physical data, the numerical results are still likely to be rather uncertain, and, in particular, the total abundance of the elements heavier than helium is quite poorly determined.

The author wishes to present his cordial thanks to Dr. B. Strömgren for advice and encouragement while this work was carried out. He also wants to thank the United States Educational Foundation in Denmark for a Fulbright Travel Grant, the International Astronomical Union for a grant which enabled him to work at the Watson Laboratory, and Dr. W. J. Eckert for placing the facilities of this laboratory at his disposal.

[11] Cf. D. B. Duncan and J. E. Perry, *Phys. Rev.*, **82**, 809, 1951; and also H. Bondi and E. E. Salpeter, *Nature*, **169**, 304, 1952.

RADIATIVE OPACITY OF STELLAR MATTER

HAROLD ZIRIN
Harvard College Observatory
Received May 18, 1953; revised November 9, 1953

ABSTRACT

The wave functions of free and bound electrons in the dense, highly ionized stellar material are calculated by a variational principle of Hulthen and by the Ritz principle, respectively. It is shown by a self-consistent type of calculation that one may regard the potential in the gas as the central potential of the nucleus, plus the potential of a uniformly distributed cloud of electrons. The free-free absorption in this shielded potential is calculated, and the Gaunt factor for this process is found to be generally less than unity.

The Rosseland mean opacity coefficient is computed for a grid of temperatures and densities, including the free-free absorption, photoelectric absorption (using Meyerott's cross-sections), and scattering. The line absorption is not taken into account. It is found that free-free absorption in hydrogen and helium overweighs that in the heavy elements, so long as $1 - X - Y$ is 0.2 or less. It is possible to give a power law only for the opacity in the limited high-density region where scattering is unimportant; there the opacity varies as $T^{-2.9}$, but the density variation is always irregular.

I. INTRODUCTION

The opacity of stellar matter is a quantity of fundamental importance in the equations of stellar structure. Unfortunately, observational evidence on the values of this quantity is lacking; we must rely on the predictions that our simple physical theory makes for the behavior of a complex, strongly interacting gas. The present work is a study of the opacity due to free-free absorption in the dense stellar material; we also combine the results of this with the photoelectric absorption coefficients obtained by others to compute a small table of opacities. The contribution of line absorption to the opacity has not been included because there is no conclusive evidence on its magnitude; it could quite possibly be significant.

The problem of free-free absorption in a pure coulomb field has been treated in great detail by Gaunt,[1] Maue,[2] Menzel and Pekeris,[3] and others and may be regarded as formally solved. It is evident, however, that the ions in the stellar interior are strongly shielded, and the free-electron wave functions are no longer coulombic. Thus the free-free absorption coefficient in the stellar interior may differ considerably from that in the atmosphere. We shall carefully investigate the character of the electron wave functions in the stellar gas, using a pseudo-Hartree type calculation. In particular, we shall show that it is possible to use here the wave functions of electrons moving in a uniform electron cloud about each atom. We shall determine these wave functions by variational means and introduce them into the formulae for the absorption coefficients.

II. DETERMINATION OF FREE ELECTRON WAVE FUNCTIONS

Consider a hot, dense gas mixture at a temperature of 10^7 degrees and density greater than water. The atoms of this gas are all ionized; there are an enormous number of free electrons produced by the ionization of hydrogen and helium (the principal constituents of the astrophysical mixture). The electrons obey the Fermi-Dirac statistics. We disregard the infrequent encounters between nuclei and state that we can approximate the potential field about each nucleus of charge Z by its own coulomb field plus that of a

[1] *Phil. Trans. R. Soc., London, A*, **229**, 163, 1930.
[2] *Ann. d. Phys.*, **13**, 161, 1932.
[3] *M.N.*, **96**, 77, 1935.

uniform cloud of Z electrons distributed in a sphere of radius a, viz.,

$$V(x) = Ze^2\left(\frac{1}{x}+\frac{1}{2a^3}x^2-\frac{3}{2a}\right) \qquad (x<a). \quad (1a)$$

This potential has zero slope and value at $x = a$. Outside this point we assume that the random effects of other nuclei and electrons average out to zero potential, i.e.,

$$V(x) = 0 \qquad (x>a). \quad (1b)$$

In Hartree's atomic units[4] the radial Schrödinger equation for an electron moving in this field is

$$\frac{d^2}{dx^2}\phi+\left[2Z\left(\frac{1}{x}+\frac{x^2}{2a^3}-\frac{3}{2a}\right)+k^2-\frac{l(l+1)}{x^2}\right]\phi=0 \qquad (x<a), \quad (2a)$$

$$\frac{d^2}{dx^2}\phi+\left[k^2-\frac{l(l+1)}{x^2}\right]\phi=0 \qquad (x>a), \quad (2b)$$

where k^2 is the total energy of the electron.

The three-dimensional wave function is, of course, the product of ϕ/x and a spherical harmonic Y_{lm}. The quantity l is the angular-momentum quantum number. Equation (2*a*) is insoluble analytically; we shall have to use variational techniques. The solution of equation (2*b*) is a linear combination of spherical Bessel functions,[5]

$$\phi_l(x) = A_l kx\,[j_l(kx)\cos\eta_l - n_l(kx)\sin\eta_l]. \quad (3)$$

Asymptotically (if $l = 0$ this holds for all x),

$$\phi_l(x) \underset{x\to\infty}{=} A_l \sin(kx-\tfrac{1}{2}l\pi+\eta_l). \quad (4)$$

Our problem now is to solve the inside wave equation (2*a*) and to join this to the outside solution (eq. [4]) by equating the logarithmic derivatives at $x = a$. In the actual stellar gas, the odds are that equation (4) is not really the true wave function outside the ion sphere, but on the average the potential outside must be zero, and hence this solution is a good approximation.

It is possible to solve equation (2*a*) by variational methods or by numerical integration. The former has the advantage of giving us analytic wave functions, and therefore will be more useful to us, inasmuch as we must carry out a variety of operations with our wave functions. Fortunately, it turns out that all the phase shifts η_l are small for $l > 0$. This is because the angular-momentum barrier keeps the electrons outside the region of the attractive potential. Thus we shall have to worry only about the **S**-wave.

We use the second variational principle of Hulthen[6] (an attempt was made using the first variational principle of Hulthen[7] with a polynomial trial function whose coefficients were determined by the boundary conditions at $x = a$; this failed for various reasons). In this case we use the trial function

$$\phi(x) = \sin(kx+\eta) - \sin\eta\cdot Y(x) \quad (5)$$

for $l = 0$, where the boundary conditions on $Y(x)$ are $Y(0) = 1$, $Y(a) = 0$. It turns out to be very difficult to choose a $Y(x)$ satisfying the second boundary condition; we finally simply let

$$Y = e^{-akx}, \quad (6)$$

[4] We use, however, the energy unit 13.54 e.v., or half of Hartree's.

[5] L. I. Schiff, *Quantum Mechanics* (New York: McGraw-Hill Book Co., 1949), p. 77.

[6] *Ark. f. mat., astr. och fysik*, Vol. **35A**, No. 25, 1948.

[7] *K. Fysiog. Sallsk. Lund Forhandl.*, **14**, 1944.

where α is a parameter to be varied, and we hope that αk will turn out large enough so that the boundary condition at $x = a$ is satisfied. This proves to be the case.

Hulthen shows that if

$$J = \int_0^\infty - Y'^2 + k^2 Y^2 + V(x)(\cos kx - Y)^2 dx , \tag{7a}$$

$$N = \int_0^\infty V(x) \sin kx (\cos kx - Y)\, dx , \tag{7b}$$

$$\lambda = \cot \eta , \qquad \delta \eta = 0 , \tag{7c}$$

then

$$\frac{\partial J}{\partial \alpha} + 2\lambda \frac{\partial N}{\partial \alpha} = 0 \tag{8}$$

and

$$N = k(1 - \eta_b \lambda) , \tag{9}$$

the relation (eq. [9]) being a general property of the phase shift. The condition (eq. [7c]) is the fundamental one; the phase is stationary for a solution of the Schrödinger equation. The quantity η_b is the Born-approximation phase shift. Equations (8) and (9) are sufficient to determine η and α. We may evaluate the quantities J and N by a series of fairly complicated integrations; in particular, we let the boundaries of all integrals linear in Y go to infinity. Substituting in equations (8) and (9), we obtain the following equation:

$$-\frac{K}{2Z\alpha}\frac{1}{2\alpha^2\beta} + \frac{1-\beta}{\alpha} + \frac{1}{2K^3}\left[\beta^3(3-4\beta) - \frac{3}{4\alpha^4}\right] + \frac{3}{2K}\left[2\beta(2\beta-1) + \frac{1}{2\alpha^2}\right]$$
$$+ \frac{\beta}{\eta_b}\left[1 + \frac{6\alpha\beta^2}{K^3}(1-2\beta) - \frac{3\alpha\beta}{K}\right]\left\{1 - \frac{2Z\alpha}{K}\left[C - \cot^{-1}\alpha - \frac{\beta^3(3-4\beta)}{2K^3} + \frac{3}{2K}\right]\right\} = 0 \tag{10}$$

where

$$C = \frac{1}{2}\left\{Si(2K) + \frac{1}{8K^3}[2K\sin 2K - (2K^2-1)\cos 2K - 1] - \frac{3}{4K}(1-\cos 2K)\right\} , \tag{11}$$

with $k\alpha = K$, and $\beta = (1 + \alpha^2)^{-1}$.

Equation (11) depends on $k\alpha$ and $Z\alpha$ only; these quantities determine the wave function. We therefore carry out the solutions over a two-dimensional grid of values of $Z\alpha$ and $k\alpha$. The solution must be done by an iterative procedure; it was carried out on an IBM Card Programmed Calculator.[8] The CPC was able to evaluate equation (10) for a given trial value of α, test for equality to zero, and adjust to a new α in fifty-four-card cycles, or 21.6 seconds. On the average, α converged in about eight iterations, or about one solution in 3 minutes. About twelve solutions could be obtained in 1 hour of running time. The phase shifts are all tabulated and are available upon request to anyone interested.

Hulthen gives a formula for improvement of the phase, which is actually not at a true stationary point when obtained from equation (10). This formula is

$$\lambda_0 = \lambda + \delta\lambda + \ldots = \lambda - \frac{\Delta}{k} - \eta_b\left(\frac{\Delta}{k}\right)^2 - \ldots \tag{12}$$

$$= J + \lambda N , \tag{13}$$

[8] Kindly made available by the Perkin-Elmer Corporation.

and λ_0 is the cotangent of the true stationary phase shift. It does not prove practicable on the CPC to evaluate and introduce this correction for each phase, but a determination of $\delta\eta$ for several cases will give us an idea of the accuracy of our phase shifts. These are given in Table 1 for $ka = 3$ and a series of values of Za. We have a further and very good check of our results by numerical integration, using the Gauss-Jackson method.[9]

TABLE 1

ERRORS OF VARIATIONAL PHASE SHIFTS

Za	Δ	Δ/k	$\delta\eta$	$\delta\eta/\eta$
1	−0.0008	−0.0002	.....	.....
2	−0.5473	− .1824	0.104	+0.114
3	−0.6893	− .2298	.234	+ .172
5	−0.243	− .0810	.0749	− .0398
7	+1.531	+0.510	0.297	+0.141

TABLE 2

PHASE SHIFTS FROM NUMERICAL INTEGRATIONS

Za	ka	Num.	Var.	Born
1	2	0.408	0.410	0.305
1	1	0.305	0.295	0.186
4	2	2.027	1.975	1.222
4	3	1.692	1.680	1.372
8	3	2.918	2.176	2.744

TABLE 3

COMPARISON OF NUMERICAL AND VARIATIONAL WAVE FUNCTIONS

x	$y_{num.}$	$y_{var.}$	y_{free}
0	0	0	+0.994
0.1	+0.542	+0.586	+ .917
0.2	+0.678	+ .648	+ .759
0.3	+0.559	+ .496	+ .533
0.4	+0.303	+ .247	+ .250
0.5	−0.010	− .034	− .038
0.6	−0.322	− .331	− .332
0.7	−0.598	− .596	− .596
0.8	−0.812	− .807	− .807
0.9	−0.949	− .945	− .945
1.0	−1.000	−0.999	−0.999

The results of some numerical integrations are given in the third column of Table 2; the fourth and fifth columns there give the variational and Born approximation phase shifts, respectively. The variational method seems to break down about $Za = 8$; but there the Born approximation seems fairly good. We shall limit our application, therefore, to Za less than 8. Still another check is provided by comparing our wave functions with a power-series expansion; the reader will be spared the results of this.

[9] N. F. Mott and H. S. W. Massey, *The Theory of Atomic Collisions* (London and New York: Oxford University Press, 1949), p. 130.

Finally, Table 3 gives the wave functions, point by point, for $Za = 4$, $ka = 3$, from the numerical integration and variational method. The point of our use of the trial solution (eq. [6]) is that the nucleus is well-enough shielded so that the wave function is almost free for some distance into the ion sphere. For this reason we have given the wave function $Y = \sin(kx + \eta)$ in the final column, to show how true this is. We see that the wave functions obtained by the variational method are reasonably accurate. They will be valuable in our calculations of absorption coefficients and should be useful in the computation of cross-sections for collisional excitations as well.

III. BOUND-STATE WAVE FUNCTIONS

The wave equation for the bound states is the same as equations (2*a*) and (2*b*), except that the energy is negative in this case. We may use a hydrogenic wave function, such as that used by Morse, Young, and Haurwitz,[10] as our trial function, and apply the Ritz principle as they do. For the K shell the trial function is

$$\psi_0 = 2A^{3/2} Y_{00} e^{-Ax}, \tag{14}$$

where A is the trial parameter to be determined by the variation. The expectation value of the energy is

$$\int \psi^* H \psi \, d\tau = \int \psi_0^* \left[-\nabla^2 + 2Z\left(\frac{1}{x} + \frac{x^2}{2a^3} - \frac{3}{2a}\right)\right] \psi_0 \, d\tau. \tag{15}$$

Simple integrations show that this is

$$\langle E_K \rangle = \frac{1}{a^2}\left\{ a^2 - Za\left[2a + \frac{3}{a^2} - 3 - e^{-2a}\left(3 + \frac{6}{a} + \frac{3}{a^2}\right)\right]\right\}, \tag{16}$$

where $a = Aa$. This quantity must be minimized, so we set its derivative with respect to a equal to zero:

$$\frac{\partial \langle E_K \rangle}{\partial a} = \frac{1}{a^2}\left\{ a - Za\left[1 - \frac{3}{a^3} + 3e^{-2a}\left(1 + \frac{2}{a} + \frac{1}{a^2} + \frac{1}{a^3}\right)\right]\right\} = 0. \tag{17}$$

To solve equation (17) it is simpler to start with an a and find the corresponding Za. We then interpolate in the (a, Za) table to find the a corresponding to a given Za and then compute the energy from equation (20). The results are given in Table 4. For values of Za greater than those given in the table, $E = Z^2(1 - 3/Za)$.

The trial function for the $2p$ electrons of the L shell is

$$\psi_{21} = \frac{2}{\sqrt{3}} Y_{10} B^{5/2} x e^{-cx}. \tag{18}$$

For states of $m = \pm 1$ we substitute Y_{11} or Y_{1-1} here. The integrations give for the energy

$$\langle E_L \rangle = \frac{1}{a^2}\left\{ \beta^2 - 2Za\left[\frac{\beta}{2} - \frac{3}{2} + \frac{15}{4\beta^2} - e^{-2\beta}\left(\frac{\beta^2}{2} + \frac{5\beta}{2} + 6 + \frac{15}{2\beta} + \frac{15}{4\beta^2}\right)\right]\right\}, \tag{19}$$

where $\beta = Ba$. Differentiating with respect to β and minimizing, we obtain

$$0 = \frac{\partial}{\partial \beta}\langle E_L \rangle = \frac{2\beta}{a^2} - \frac{2Z}{a}\left\{ \frac{1}{2} - \frac{30}{4\beta^3} - e^{-2\beta}\left[\beta^3 + 5\beta^2 + 11\beta + \frac{25}{2} + \frac{15}{\beta} + \frac{15}{2\beta^2} + \frac{15}{2\beta^3}\right]\right\}. \tag{20}$$

We carry out the solution as for the K shell; the values of β and E_L/Z^2 are given in Table 4. For values of $Za > 52$, the energy is given by $E_L = Z^2/4 \cdot (1 - 6/\beta)$. Note that there is no bound state at all for $Za < 12$.

[10] *Phys. Rev.*, **48**, 948, 1935.

The wave function for the $2s$ electron, because it must be orthogonal to the $1s$ state, is more complicated. Inasmuch as it is nearly degenerate with the $2p$ state, however, we may simply use the parameter and energy from our solution for that state. The wave function is, therefore,

$$\psi_{20} = 2\,Y_{00}B^{3/2}e^{-Bx}(1-Bx)\,. \tag{21}$$

We have not yet made allowance for the fact that if there are two bound K electrons, the electron distribution will be somewhat different from our uniform cloud approxima-

TABLE 4

BOUND ELECTRON WAVE FUNCTIONS FOR K AND L SHELLS

Za	$\alpha = A\alpha$	E_K/Z^3	$\beta = B\alpha$	E_L/Z^3
3	2.61	−0.106	.....	.....
4	3.79	− .299	.....	.....
5	4.88	− .425	.....	.....
6	5.92	− .510	.....	.....
7	6.94	− .580	.....	.....
8	7.95	− .631	.....	.....
9	8.96	− .677	.....	.....
10	9.97	− .703	.....	.....
12	11.97	− .751	5.58	−0.018
14	13.98	− .787	6.64	− .047
16	15.99	− .813	7.74	− .070
18	18.00	− .834	8.70	− .089
20	20.00	− .851	9.85	− .104
24	24.00	− .875	11.90	− .127
28	28.00	− .893	13.93	− .145
32	32.00	− .906	15.94	− .157
36	36.00	− .917	17.96	− .167
40	40.00	− .925	19.97	− .175
44	44.00	− .932	21.98	− .182
48	48.00	− .938	23.99	− .188
52	52.00	−0.942	26.00	−0.193

tion. The electronic repulsion energy of the L electrons due to the K electrons is given by Morse, Young, and Haurwitz as

$$V_{KL} = \beta\left[1 - \frac{\beta^4}{(\alpha+\beta)^4} - \frac{2\alpha\beta^4}{(\alpha+\beta)^5}\right] \sim \beta\left(1 - \tfrac{1}{81} - \tfrac{4}{243}\right)\,, \tag{22}$$

since $\alpha \sim 2\beta$. We see that if we simply subtract, in equation (19), the number of bound K electrons from Z, we have a good approximation; we now enter Table 4 with $(Z-2)a$ and obtain $E/(Z-2)^2$ in the last column.

We have not taken into account the repulsion between electrons in the same shell. This is because the use of the Fermi-Dirac statistics in computing occupation numbers will not allow us to include interactions between particles in the same state. We hopefully assume that the interactions not included are approximated by the uniform cloud potential. This will be true if the density is fairly high.

Note how strong is the effect of the electron cloud in depressing the energy. There are no bound K states for $Za < 3$, nor L states for $Za < 12$. And, where the bound states do exist, the energy of the levels is strongly decreased from its value in the isolated atom. This is the effect of pressure ionization; the uniform cloud approximation allows us to measure it in an extremely simple way.

IV. VERIFICATION OF THE UNIFORM CLOUD APPROXIMATION BY THE SELF-CONSISTENT FIELD

We have assumed that the potential about an ion of the intrastellar gas is of the form of equations (1*a*) and (1*b*) and have determined the electron wave functions in such a potential. We now are in a position to check back and see if the electron distribution corresponding to these wave functions produces a potential identical with that assumed. If it does, then our procedure is self-consistent (although not necessarily correct in an absolute sense). A similar calculation has been carried out by Miss Hsieh[11] for a pure hydrogen gas at zero temperature, with all the electrons concentrated in a thin shell. This potential does not have zero slope at $x = a$.

Slater[12] has shown that we may write the Hartree-Fock equations with only small loss of accuracy in the following form:

$$H_1 u_i(x_1) + \left\{ \sum_{k=1}^{n} \int u_k^*(x_2)\, u_k(x_2) \frac{e^2}{r_{12}}\, dx_2 - \frac{\sum_{j=1}^{n}\sum_{k=1}^{n} \int u_j^*(x_1)\, u_k^*(x_2)\, u_k(x_1)\, u_j(x_2) \frac{e^2}{r_{12}}\, dx_2}{\sum_{j=1}^{n} u_j^*(x_1)\, u_j(x_1)} \right\} u_i(x_1) = E_i u_i(x_1). \tag{23}$$

This is a Schrödinger equation for the wave function $u_i(x_i)$ of the ith electron. The first term is the ordinary Hamiltonian due to motion about the nucleus; the first term in the braces is the potential due to all electrons; the second term is the exchange potential. Note that the repulsion term includes the potential due to all electrons; this justifies our assumption in the trial potential (eqs. [1*a*] and [1*b*]) that Z electrons act on the one in question.

Equation (23) may be simplified by some rather accurate approximations. The first term in the braces is greatly simplified if the quantity $u_k^*(x_2)u_k(x_2)$, which is nothing more than the electron density $\rho(x_2)$, is spherically symmetrical. Then this term is a function of x_1 only; in fact, it is the potential due to a spherically symmetric distribution of charge of density

$$\rho(x_2) = \sum_{k=1}^{n} u_k^*(x_2)\, u_k(x_2). \tag{24}$$

Inasmuch as we have both free and bound states, equation (24) should be written as a sum over the bound states plus an integral over the continuum. The number of electrons in the former is very small, particularly in the light-elements which interest us most. We shall incur no great error by assuming all electrons are free. The distribution of electrons in the energy states of the continuum is given by the Fermi-Dirac statistics; the number of electrons of each energy k^2 at the point x_2 is given by the modulus squared of the wave function; therefore,

$$\rho(x_2) = \frac{3}{T_a^{3/2}} \int_0^\infty \frac{u_k^*(x_2)\, u_k(x_2)\, k^2 dk}{e^{k^2/T_a - \delta} + 1}, \tag{25}$$

[11] *Ap. J.*, **119**, 70, 1954.

[12] *Phys. Rev.*, **81**, 385, 1951.

where T_a is the temperature in atomic units and δ is found from the tables of MacDougall and Stoner.[13] The first term in the braces of equation (23) can therefore be written

$$A\left[\frac{1}{x_1}\int_0^{x_1}\rho(x_2)\,dx_2+\int_{x_1}^{b}\frac{\rho(x_2)\,dx_2}{x_2}\right], \tag{26}$$

with $\rho(x_2)$ defined by equation (31) and the neutral sphere radius b being given by

$$Z=4\pi\int_0^b x^2\rho(x)\,dx\,. \tag{27}$$

The constant A is a normalization factor which is determined by requiring that there be just one electron in a large sphere of radius R. The density of electrons at any point r is then given by the integral of $|\psi|^2$ over all states,

$$\rho(r)=\sum_l\sum_m\frac{4}{\pi}\int_0^\infty n_i(k)\,dk\,\frac{1}{4\pi}\int_0^{2\pi}\int_0^{\pi}|\psi_{lm}|^2\sin\vartheta\,d\vartheta\,d\phi\,, \tag{28}$$

TABLE 5

COEFFICIENT OF THE EXCHANGE POTENTIAL AT VARIOUS TEMPERATURES

T_a/k_m^2	4	2	0.991	0.5	0.2	0.0
$\beta(T_a, \rho_0)$	0.088	0.135	0.210	0.538	0.840	1.000

where $n_i(k)$ is the Fermi-Dirac distribution function. We integrate over the angles and sum over m and obtain

$$\tilde{\rho}(r)=\sum_l\frac{2l+1}{\pi^2}\int_0^\infty n_i(k)\,|\phi_l|^2dk\,. \tag{29}$$

The second half of the braces in equation (23) we replace by the exchange potential in a free-electron gas, which Slater has shown to be a good approximation. This potential was first evaluated by Dirac[14] for zero temperature and is

$$V_{ex}(x)=6\beta(T,\rho_0)\left[\frac{3\rho(x)}{8\pi}\right]^{1/3}. \tag{30}$$

The quantity β expresses the variation with temperature of this potential and has been tabulated elsewhere by the author[15] for various temperatures; it is given in Table 5.

Rather than solve the Schrödinger equation, we now determine the potential due to our electron distribution and compare it with the trial potential (eqs. [1*a*] and [1*b*]). We may alter the parameter a to produce a good fit. When this is done, we assert that the Schrödinger equation (23) has, in effect, been solved in Section II and use those solutions.

Table 6 shows how the correspondence of b with a varies with temperature. In actual application, of course, b is the given quantity, determined by the electron density. The quantity k_m^2 is the energy at the top of the Fermi band, a function of ρ only. Table 7 shows how the shape of the potential varies in these cases and gives the trial potential for comparison. In all cases given, $Z=1$, $a=1$. Table 6 shows clearly that even for $T_a k_m^2=0.5$ we already have essentially the nondegenerate case. The fit of the potentials

[13] *Phil. Trans.*, **237**, 67, 1936.

[14] *Proc. Cambridge Phil. Soc.*, **26**, 376, 1930.

[15] *Phys. Rev.*, **90**, 795, 1953.

is rather good and is best at high temperatures. Most of the results at hand at present for the b, ρ, and k_{max} corresponding to a given Z and a are given in Table 8.

The agreement of b with a is so good for the nondegenerate case that we may clearly assume that the two are equal; thus, for any given ρ_0 we simply take

$$a = b = \left(\frac{3Z}{4\pi\rho_0}\right)^{1/3}$$

and use the corresponding wave functions. For zero temperature we must make a more extensive table than Table 8 and interpolate inversely for a table of a's and b's. But we

TABLE 6

VARIATION OF SELF-CONSISTENT NEUTRAL SPHERE RADIUS WITH TEMPERATURE

Case	T_a	T_a/k_m^2	ρ_0	b	k_m
I.....	0	0	0.3356	0.8067	2.15
II.....	1.8417	0.5	.2243	0.9610	1.9142
III.....	3.6502	0.991	.2064	1.0178	1.9192
IV.....	7.3667	2.000	0.2212	1.0091	1.9192

TABLE 7

VARIATION OF SELF-CONSISTENT POTENTIAL WITH TEMPERATURE

R	Case				V_{tr}
	I	II	III	IV	
0.2	−3.706	−3.662	−3.518	−3.511	−3.520
0.4	−1.097	−1.054	−1.064	−1.074	−1.080
0.6	−0.300	−0.325	−0.349	−0.349	−0.347
0.8	−0.056	−0.073	−0.080	−0.078	−0.070
1.0	0	0	0	0	0

are principally interested in the nondegenerate region for astrophysical applications, so we will concern ourselves with it here. Should the degenerate case arise, we have the tools to handle it.

V. THE CALCULATION OF ABSORPTION COEFFICIENTS

The work of the preceding sections has placed us in a position to find the wave functions of the electrons of the intrastellar gas at given temperature and density. To obtain the atomic absorption coefficients we merely insert these wave functions in the standard quantum-mechanical formulae. The formula for free-free absorption is given by Gaunt:[16]

$$a(\omega, k_0)\, d\omega = \frac{256\pi^2}{3}\frac{Z^2e^2}{hc}\, a_0^5 \frac{1}{\omega^3}\sum_l l\{|\langle l, k_0^2|\ddot{x}|l-1, k_1^2\rangle|^2 + |\langle l-1, k_0^2|\ddot{x}|l, k_1^2\rangle|^2\}\,\mathrm{cm}^5 . \tag{31}$$

[16] *Phil. Trans. R. Soc., London, A*, **229**, 163, 1930.

Here $\ddot{x}$ is the acceleration in the radial co-ordinate, k_0^2 and k_1^2 the energies of the initial and final states. The acceleration matrix element must be used here because the equivalent dipole form would be indeterminate. The matrix elements are given by

$$(l,\ k_0^2|\ \ddot{x}\ |l-1,\ k_1^2) = -\int_0^a R_l(k_0x)\left(\frac{1}{x^2}-\frac{1}{a^3}\,x\right)R_{l-1}(k_1x)\,x^2dx\,, \tag{32}$$

where the R's are our radial wave functions from Section II and

$$\begin{aligned} R_0(kx) &= \frac{1}{kx}\left[\sin(kx+\eta) - e^{-akx}\sin\eta\right], \\ R_l(kx) &= j_l(kx) \qquad (l>0). \end{aligned} \tag{33}$$

TABLE 8

RESULTS OF SELF-CONSISTENT POTENTIAL MATCHING

Z	a	T_a/k_m^2	ρ_0	b	k_m
	I. High-Temperature–Nondegenerate Case				
1	0.25	4	1.9096	0.2498	7.677
1	0.50	4	1.528	0.5003	3.838
1	1.00	0.5	0.2243	0.9610	1.9192
1	1.00	0.991	0.2064	1.0178	1.9192
1	1.00	2.000	0.2212	1.0091	1.9192
2	0.50	2	3.615	0.5052	4.836
2	1.00	4	0.4600	1.0089	2.418
4	0.50	4	7.639	0.4992	6.093
	II. Zero-Temperature–Degenerate Case				
1	1.00	0	0.3356	0.8067	2.15
1	2.00	0	0.0660	1.25	1.25
2	0.50	0	4.35	0.471	5.05
2	1.00	0	0.4456	0.9203	2.363
4	0.50	0	7.295	0.4923	6.0930

The normalization of R has been taken care of in equation (31). The quantity $R_0(kx)$ may be rewritten as follows:

$$R_0(kx) = \cos\eta\cdot j_0(kx) + \sin\eta\cdot\left[j_{-1}(kx) - e^{-akx}\right]. \tag{34}$$

The absorption coefficient may be expressed in a form convenient for comparison with the Kramers absorption law. The latter is

$$\begin{aligned} a(\omega,\ k_0) &= \frac{4}{3\sqrt{3}\pi^2}Z^2\left(\frac{\hbar c}{e^2}\right)^4\left(\frac{\hbar}{mc}\right)^5\frac{1}{k_0\omega^3} \\ &= 2.30\times10^{-41}\frac{Z^2}{\omega^3k}\ \mathrm{cm}^5. \end{aligned} \tag{35}$$

Formula (31) can be written as

$$a(\omega,\ k_0) = 2.30\times10^{-41}\frac{Z^2}{\omega^3k_0}\,g(\omega,\ k_0)\ \mathrm{cm}^5, \tag{36}$$

where $g(\omega, k)$ is the Gaunt factor.

Evaluation of the matrix elements is done by parts intergrations of the various spherical Bessel functions that occur. The computation is too lengthy to give here. We note, however, the following features: The series in equation (31) is strongly convergent; in fact, all terms but the first are negligible. The reason for this is that electrons of appreciable angular momentum are kept outside the ion sphere by the centrifugal-force barrier. Hence, the value of the wave function is very small in the limits of integration, and the matrix element is correspondingly small. It further turns out that the contribution of the acceleration due to the electron cloud is quite small, except for very low frequencies, and may therefore be neglected. Thus the effect of the shielding enters only through the fact that we must cut off the integration in equation (32) at $x = a$ and through the wave functions themselves. The Gaunt factors are quite sensitive to the phase shifts η, because of the interference effect involved; fortunately, this is our best-determined parameter.

The Gaunt factors calculated for various cases are tabulated in Table 9. Inasmuch as the phase shifts for the heavy elements are not too accurate and the Gaunt factors do not change much between them, I have only given values for oxygen. If a is greater than 1, the Gaunt factors do not change appreciably from those for $a = 1.00$, and the latter may be used. Note that the Gaunt factor in no case equals unity. For hydrogen at $a = 0.25$, which corresponds, more or less, to the center of the sun, the average Gaunt factor is about one-third. The reason for this is twofold: first, the shielding makes the wave functions smaller in the region of interaction than the coulomb functions; and, second, the integration in the matrix element only proceeds as far as $x = a$, beyond which there is no acceleration. The free-free absorption coefficient, given in Table 10, is then determined by averaging the Gaunt factor over the Maxwellian distribution of absorbing electrons.

The free-free absorption coefficients computed above may now be used in calculating a table of opacities. For the photoelectric absorption coefficients we use the recent data of Meyerott.[17] The occupation numbers of bound states are computed from the energy levels determined in Section III, using the Fermi-Dirac statistics. The Thompson scattering is corrected for the Klein-Nishina formula, as tabulated by Morse,[18] as well as for the fact that there is no net stimulated emission from scattering, as pointed out by Maria G. Mayer.

We have calculated the Rosseland mean opacity under various conditions, using the following mixture of the heavy elements, suggested by L. H. Aller:[19] *O*, 0.874; *Mg*, 0.058; *Si*, 0.035; *Fe*, 0.0332. The Strömgren "*D*'s" have been added up for each process at a grid of frequencies and the Rosseland mean determined numerically. The procedure is identical with that outlined by Strömgren,[20] except that the *D*'s will now vary between absorption edges. The contribution from the free-free absorption is

$$D_{ff} = c_Z N_e a\,(T_a, \omega) \qquad \text{for } H, He,$$

$$D_{ff} = \Gamma\,(1 - X - Y)\, N_e a\,(T_a, \omega) \qquad \text{total}, Z > 2; \Gamma = \sum_{Z>2} c_Z \frac{Z^2}{m_Z},$$

where N_e is in cm^{-3} and c_Z is the proportion by weight of the element of charge Z, except that for the heavy elements it refers to the proportion in the hexvy mixture alone. The free-free absorption due to hydrogen and helium is as great as, or greater than, that of the heavy elements, because of the abundance of the former; this is contrary to the conclusion of Morse but evidently true, for the absorption from the two sources (except

[17] *Argonne National Lab. Bull.*, No. 5008, March, 1953.

[18] *Ap. J.*, **92**, 27, 1940.

[19] Private communication.

[20] *Zs. f. Ap.*, **4**, 118, 1932; **7**, 222, 1933.

TABLE 9

GAUNT FACTORS FOR HYDROGEN, HELIUM, AND OXYGEN

HYDROGEN

k	ω			
	0	500	1000	2000
	$a=0.25$			
0	0	0	0	0
2	0	0.036	0.068	0.049
4	0.002	.078	.118	.097
6	.070	.135	.200	.108
8	.169	.212	.207	.133
10	.280	.306	.280	.171
12	.450	.383	.305	.213
14	.437	.478	.336	.244
16	0.375	0.570	0.367	0.258

HELIUM

k	ω			
	0	500	1000	2000
	$a=0.25$			
0	0	0	0	0
2	0	0.050	0.101	0.080
4	0.120	.216	.212	.167
6	.229	.272	.310	.258
8	.354	.372	.379	.294
10	.501	.474	.447	.335
12	.340	.414	.489	.368
14	.372	.475	.579	.389
16	0.392	0.462	0.532	0.419

HYDROGEN

k	ω				
	0	100	200	300	500
	$a=0.50$				
0	0	0	0	0	0
2	0.044	0.397	0.200	0.182	0.353
4	.340	.571	.366	.333	.339
6	.513	.583	.498	.420	.364
8	.467	.583	.568	.487	.431
10	0.468	0.702	0.589	0.513	0.430
	$a=1.00$				
0	0	0	0	0	0
2	0.393	0.701	0.581	0.545	0.460
4	.426	.707	.673	.621	.551
6	.443	.675	.667	.638	.585
8	.425	.602	.560	.601	.559
10	0.434	0.571	0.583	0.593	0.609

HELIUM

k	ω				
	0	100	200	300	500
	$a=0.50$				
0	0	0	0	0	0
2	0.036	0.832	0.516	0.513	0.667
4	.312	.827	.617	.592	.618
6	.444	.710	.696	.599	.599
8	.400	.615	.684	.591	.570
10	0.409	0.615	0.659	0.586	0.514
	$a=1.00$				
0	0	0	0	0	0
2	0.139	0.910	0.828	0.760	0.659
4	.108	.675	.657	.623	.559
6	.137	.600	.609	.583	.537
8	.136	.523	.480	.547	.512
10	0.122	0.429	0.558	0.475	0.502

OXYGEN

k	ω				
	0	100	200	300	500
	$a=0.50$				
0	0	0	0	0	0
2	0.041	0.157	0.291	0.389	0.593
4	.175	.318	.488	.605	.744
6	.273	.306	.521	.525	.767
8	.252	.300	.514	.540	.807
10	0.259	0.299	0.531	0.527	0.609
	$a=1.00$				
0	0	0	0	0	0
2	0.007	0.455	0.673	0.715	0.788
4	.031	.257	.392	.507	.588
6	0.001	.210	.356	.452	.542
8	.....	.166	.248	.386	.465
10	.....	0.137	0.247	0.330	0.454

TABLE 10

THE FREE-FREE ABSORPTION COEFFICIENT*

HYDROGEN

	T_a		
	50	100	200
	$a=0.25$		
0	0.257	0.319	0.193
500	.359	.385	.357
1000	.409	.368	.315
2000	0.259	0.239	0.209

HELIUM

	T_a		
	50	100	200
	$a=0.25$		
0	0.597	0.464	0.343
500	.717	.539	.397
1000	.766	.563	.417
2000	0.602	0.451	0.342

HYDROGEN

	T_a			
	10	20	40	80
	$a=0.50$			
0	0.753	0.957	0.897	0.711
100	2.299	1.809	1.613	1.060
200	1.341	1.250	1.044	0.788
300	1.205	1.082	0.925	0.745
500	1.799	1.158	0.941	0.692
	$a=1.00$			
0	2.068	1.462	1.067	0.751
100	3.583	2.415	1.668	1.091
200	3.111	2.191	1.545	0.975
300	2.912	2.071	1.513	1.048
500	2.520	1.825	1.382	1.002

HELIUM

	T_a			
	10	20	40	80
	$a=0.50$			
0	0.667	0.812	0.784	0.627
100	4.196	2.542	1.853	1.203
200	2.843	2.100	1.588	1.133
300	2.760	1.963	1.445	1.018
500	3.342	2.211	1.518	0.995
	$a=1.00$			
0	0.677	0.461	0.326	0.222
100	4.266	2.621	1.637	.965
200	3.946	2.482	1.588	.959
300	3.665	2.339	1.537	.956
500	3.203	2.084	1.412	0.932

OXYGEN

	T_a				T_a			
	10	20	40	80	10	20	40	80
	$a=0.50$				$a=1.00$			
0	0.452	0.514	0.489	0.390	0.021	0.024	0.029	0.016
100	1.094	0.850	0.680	0.502	2.005	1.142	0.657	.361
200	1.809	1.444	1.154	0.852	3.039	1.744	1.034	.604
300	2.299	1.693	1.278	0.967	3.314	2.016	1.256	.747
500	3.282	2.397	1.765	1.183	3.702	2.300	1.479	0.927

* For unit electron density; units 10^{-18} cm^5; to be multiplied by $N_a C_a Z^2/M_a$.

for the Gaunt factors) will be in proportion with the ratio of $X + Y$ to $\Gamma\ (1 - X - Y)$.

Table 11 gives the absorption coefficients for two mixtures; the first with 10 per cent of heavy elements, the second with only 1 per cent, at various temperatures and pressures. It is immediately apparent that when the opacity due to scattering and free-free absorption in hydrogen and helium is included, the opacity is no longer proportional to $(1 - X - Y)$ but varies rather irregularly with this term. The amount of change in $\bar{k}$,

TABLE 11

THE MEAN OPACITY $\bar{k}$ FOR VARIOUS TEMPERATURES AND PRESSURES (CM^2/GM)

($O = 0.874$, $Mg = 0.058$, $Si = 0.035$, $Fe = 0.0332$)

	T_a/ρ				
	10	20	40	80	160
	$X = 0.60$, $Y = 0.30$, $1 - X - Y = 0.1$				
T (10^6 deg.)	1.57	3.14	6.28	12.56	25.12
100 gm/cm³	1251	180	24.79	3.46	0.764
10	337	116	10.38	3.660	0.427
1	183	39.3	3.38	3.418	0.313
	$X = 0.69$, $Y = 0.30$, $1 - X - Y = 0.01$				
100	483	61.8	7.98	1.436	0.525
10	119	19.8	1.89	0.5356	.351
1	33.4	5.32	0.792	0.346	0.303
	$X = 0.90$, $Y = 0.09$, $1 - X - Y = 0.01$				
100	971	180	16.6	1.90	0.55
10	222	104	5.72	0.76	0.41
1	45.5	19.5	1.66	0.40	.....
0.1	6.49	1.51	.....	.....	.....

the Rosseland mean opacity, resulting from a decrease in $(1 - X - Y)$ will depend on the relative importance of the photoelectric effect in determining $\bar{k}$. Finally, it may be noted by way of comparison that substitution of Russell mixture for the heavy-element mixture used here gives, for $\rho = 100$, $T_a = 40$, a value of $\bar{k} = 42.3$ cm^2/gm, compared with 24.8 cm^2/gm in Table 11. So the opacity is as sensitive to changes in the composition of the heavy mixture as it is to changes in over-all composition.

The first half of Table 11 is graphed in Figure 1, and this gives us an idea of the variation of $\bar{k}$ with temperature and density. For $\rho = 1$ and $\rho = 10$ it is difficult to give an approximation to the opacity; for $\rho = 100$, $\bar{k}$ appears to be well represented by the law $\bar{k} \propto T^{-2.9}$. This is because scattering is not so important in the latter case. The flattening of the curves around $T_a = 10$ is an effect due to the K-absorption of oxygen. There is no good rule for the density dependence of the opacity. The astrophysicist must face the fact that no simple power law can represent such a complicated quantity as the opacity. However, it is possible to compute tables of opacities quite rapidly and to use the actual opacities in calculations on the internal constitution of the stars.

I wish to thank Professor P. M. Morse, who suggested this investigation and many of the methods used and who was the source of continual encouragement. Mr. Arthur Kerman was associated with early stages of this work, and I had a number of stimulating discussions with Professor D. H. Menzel. Much of the final work reported on here was accomplished during my stay at the RAND Corporation, where many facilities were made available by Dr. E. H. Plesset.

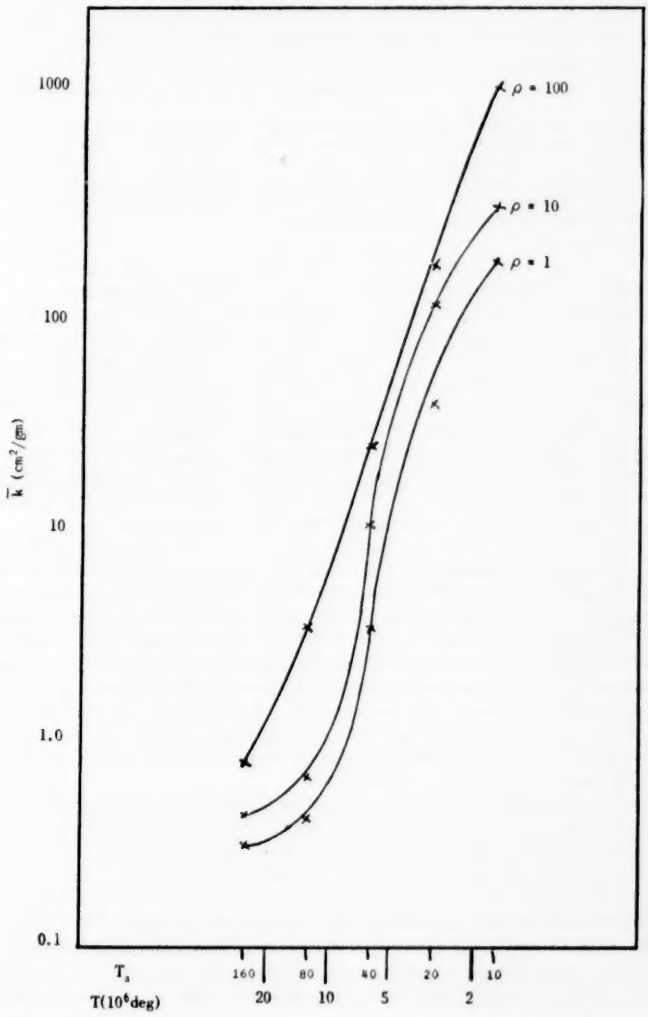

FIG. 1.—The Rosseland mean opacity $\bar{k}$ for the mixture of Table 4, $1 - X - Y = 0.1$, as a function of temperature for three densities.

THE GAUNT FACTOR FOR FREE-FREE TRANSITIONS IN PURE HYDROGEN*

RUSSELL M. KULSRUD
Yerkes Observatory
Received October 19, 1953

ABSTRACT

The Gaunt factor for free-free transitions of an electron in the interior of a star, assuming pure hydrogen, is computed, taking into account the overlapping of the coulomb fields of the hydrogen ions. It is found that the results originally obtained by Sommerfeld[1] for the case of a pure coulomb field must be altered by changing the normalization of his electronic wave functions at infinity. A simple analytic expression is found for the Gaunt factor, and its average over the Maxwell distribution of the initial velocities is carried out. The results are given in Table 1.

INTRODUCTION

The currently accepted heavy-element content in stellar interiors is so low that free-free transitions of electrons in the fields of the hydrogen ions have become important in calculating the opacity coefficient. Hence some care must be taken in evaluating the Gaunt factor connected with this process. Since the free-free transitions contribute strongly only near the center of the star, where high temperatures cut down the photoelectric effect, a high energy approximation is appropriate. The Gaunt factor was worked out in this approximation by Sommerfeld[1] and Maue[2] in 1932, for the case when a single nucleus is present. Since the coulomb field near the nucleus is proportional to Z, it is obvious that, as the density increases, this assumption of a pure coulomb field first breaks down for the hydrogen ion. Since at the time of their work the low heavy-element abundance of stellar interiors was not suspected, this was not serious.

In this paper the problem of free-free transitions of a single electron in the field of many hydrogen nuclei is considered. Since the electron moves with a speed which is the square root of eighteen hundred times the speed of an average proton, the calculation of the probability of a free-free transition is made under the assumption that all the protons are at rest. The probability thus found is averaged over all possible distributions of the positions of the protons. Since the kinetic energies of the protons are large compared to their interaction energies, the assumption that all possible distributions are equally likely is a good one and is made here. For convenience, the calculations are carried out in a box of volume Ω, on whose boundaries periodic conditions are satisfied and in which there are N protons, where N/Ω is the density of the protons. After the complete calculation is carried out, Ω will be set equal to infinity.

If, instead of a coulomb potential, a potential of the form $\exp(-ar)/r$ is used, a perturbation calculation (Born approximation) may be made. The result of this calculation gives the probability of a free-free transition as N times the probability of a free-free transition by a single proton with the others absent, plus an interaction term depending on the positions of all N of the protons. When the average over all the possible positions of the protons is carried out, it is found that this interaction term averages to zero and only the first term remains. However, it is found that the normalization generally used in

* Submitted to the Department of Physics of the University of Chicago in partial fulfilment of the requirements for the Ph.D. degree. The work was done while the author was a National Science Foundation Predoctoral Fellow.

[1] *Ann. d. Phys.*, **11**, 257, 1931.

[2] *Ann. d. Phys.*, **13**, 161, 1932.

the case of one proton present is no longer correct for the following reason: The wave function is disturbed near each nucleus, and, as the size of the box Ω is set equal to infinity, this small change in the wave function ordinarily may be neglected in the case of just one proton. In our case there are N protons, and N goes to infinity with Ω so that N/Ω is a constant. Hence the disturbance of the wave function remains important and must be taken into account through the correct normalization.

These results hold strictly only in the case of a potential $\exp(-\alpha r)/r$ rather than for the true coulomb case; but it is obvious that if α is small, the deviations are appreciable only for large r, and these deviations would be masked by the fields of the other protons. Hence it is expected that the general results should hold under the assumption of a coulomb field. For the single-proton case Sommerfeld obtains

$$g = \frac{\sqrt{3}}{\pi} \frac{2\pi n'}{e^{2\pi n'} - 1} \frac{2\pi n}{1 - e^{2\pi n}} \log \frac{k' + k}{k' - k}, \tag{A}$$

where $n = me^2/\hbar^2 k$, $n' = me^2/\hbar^2 k'$, k and k' are the wave numbers for the initial and final states and g is the Gaunt factor introduced to correct Kramer's original classical result to the quantum-mechanical result. Taking into account the normalization when N protons are present can be done fairly accurately by setting

$$g = \frac{\sqrt{3}}{\pi} \log \frac{k' + k}{k' - k}. \tag{B}$$

The actual calculation proceeds as follows.

THE CALCULATION

The probability for the free-free transition of an electron present in the box Ω is proportional to the square of the absolute value of the matrix element

$$\langle \psi' | e^{i\Gamma} \boldsymbol{p} \cdot \boldsymbol{A} | \psi \rangle ,$$

where ψ' and ψ are the wave functions for the final and initial states of the electron; $e^{i\Gamma} = \exp(i\boldsymbol{n} \cdot \boldsymbol{r}\omega/c)$ is the expression for the space dependence of the electromagnetic potenta representing the photon absorbed in the process; $\boldsymbol{A}$ is a unit vector in the direction of this potential; and $\boldsymbol{p} = -i\hbar\nabla$ is the momentum of the electron. The probability must, of course, be averaged over the initial state and summed over all final states.

The wave function ψ satisfies Schroedinger's equation

$$H\psi = \left(\frac{p^2}{2m} + \sum_{i=1}^{N} V_i(\boldsymbol{r}) \right) \psi = E\psi , \tag{1}$$

where V_i is the potential due to the ith proton at position $\boldsymbol{R}_i$,

$$V_i = -e^2 \frac{e^{-\alpha r_i}}{r_i} = -e^2 \frac{e^{-\alpha|\boldsymbol{r} - \boldsymbol{R}_i|}}{|\boldsymbol{r} - \boldsymbol{R}_i|}, \tag{2}$$

and E is the initial energy of the proton. The wave function ψ' satisfies a similar equation with final energy E'. The wave functions ψ and ψ' also satisfy periodicity conditions on the boundary of the box. Assuming that the average value of the potential energy is small compared to E, we may solve equation (1) by perturbation theory. Taking as the unperturbed Hamiltonian

$$H_0 = \frac{p^2}{2m},$$

we find, for the unperturbed wave functions,

$$\langle \boldsymbol{r} | \boldsymbol{k} \rangle = \frac{e^{i\boldsymbol{k}\cdot\boldsymbol{r}}}{\sqrt{\Omega}}, \tag{3}$$

where k is determined by the periodicity conditions,

$$k_x = \frac{2\pi n_x}{L}, \qquad k_y = \frac{2\pi n_y}{L}, \qquad k_z = \frac{2\pi n_z}{L},$$

and n_x, n_y, and n_z are integers running from $-\infty$ to $+\infty$. Expanding $|\psi\rangle$ as a series in e^2 and expressing the separate terms in terms of the unperturbed wave functions, we have

$$|\psi\rangle = |\boldsymbol{k}\rangle + |1\rangle + |2\rangle + \ldots, \tag{4}$$

$$|1\rangle = \sum_{\boldsymbol{k}''} \frac{\langle \boldsymbol{k}'' | \sum_i V_i | \boldsymbol{k} \rangle}{(E_k - E_{k''})} |\boldsymbol{k}''\rangle = \sum_{\boldsymbol{k}'', i} \frac{\langle \boldsymbol{k}'' | V_i | \boldsymbol{k} \rangle}{(E_k - E_{k''})} |\boldsymbol{k}''\rangle, \tag{5}$$

$$|2\rangle = \sum_{\boldsymbol{k}', \boldsymbol{k}''', i, j} \frac{\langle \boldsymbol{k}'' | V_i | \boldsymbol{k}''' \rangle \langle \boldsymbol{k}''' | V_j | \boldsymbol{k} \rangle}{(E_k - E_{k'''})(E_k - E_{k''})} |\boldsymbol{k}''\rangle.$$

Two modifications have been made in this perturbation calculation. First, the perturbed energy has been taken equal to the unperturbed energy, since we are not interested in such things as changes of energy. This eliminates certain awkward terms usually encounted when the energy spectrum is discrete. Second, the $|k\rangle$term in the expansions in terms of unperturbed functions, which is undetermined by the equations of perturbation theory, is set equal to zero. Normally, these terms are adjusted to normalize the perturbed wave function, but it is simpler to normalize the wave function at the end of the calculation.

The value of the matrix elements involved in equations (5) are

$$\begin{aligned} \langle \boldsymbol{k}'' | V_i | \boldsymbol{k}''' \rangle &= \frac{1}{\Omega} \int d\boldsymbol{r}\, e^{-i(\boldsymbol{k}'' - \boldsymbol{k}''')\cdot\boldsymbol{r}} \left(-e^2 \frac{e^{-a r_i}}{r_i} \right) \\ &= -\frac{4\pi e^2}{\Omega} \frac{e^{-i(\boldsymbol{k}'' - \boldsymbol{k}''')\cdot\boldsymbol{R}_i}}{|\boldsymbol{k}'' - \boldsymbol{k}'''|^2 + a^2}. \end{aligned} \tag{6}$$

The wave function $|\psi'\rangle$ is found to have a similar expansion, the unperturbed state being $|k'\rangle$. The energies are

$$E = \frac{\hbar^2 k^2}{2m}, \qquad E' = \frac{\hbar^2 k'^2}{2m}. \tag{7}$$

Substituting these series in the fundamental matrix element $\langle \psi' | e^{i\Gamma \boldsymbol{p}\cdot\boldsymbol{A}} | \psi \rangle$, and taking $\boldsymbol{A}$ in the y-direction, $\boldsymbol{n}$ in the x-direction, it is seen that only those terms are unequal to zero for which

$$-\boldsymbol{k}_1'' + \frac{\omega}{c}\boldsymbol{n} + \boldsymbol{k}'' = 0, \tag{8}$$

where $|k_1''\rangle$ is a term in the expansion of $|\psi'\rangle$, and $|k''\rangle$ is a term in the expansion of $|\psi\rangle$. Thus a typical term in the expansion of the matrix element would be

$$\frac{i k_x'' \langle \boldsymbol{k}' | V_i | \boldsymbol{k}_1''' \rangle \langle \boldsymbol{k}_1''' | V_j | \boldsymbol{k}_1^{(\mathrm{iv})} \rangle \ldots \langle \boldsymbol{k}_1^{(n)} | V_l | \boldsymbol{k}_1'' \rangle \langle \boldsymbol{k}'' | V_m | \boldsymbol{k}^{(m)} \rangle \ldots \langle \boldsymbol{k}''' | V_r | \boldsymbol{k} \rangle}{(E_{k'} - E_{k_1'''}) \ldots (E_{k'} - E_{k_1''})(E_k - E_{k''}) \ldots (E_k - E_{k'''})}, \tag{9}$$

where k_1'' and k'' satisfy condition (8). The physical significance of this is evident. The physical process in which the electron goes from state $|\psi\rangle$ to $|\psi'\rangle$, with the absorption of a photon in state $Ae^{i\Gamma}$, may be considered as the sum of virtual processes like those indicated in formula (9) (i.e., the electron goes from k to k''' by an interaction with proton R, etc., until it comes to k''; then it absorbs a photon going to k_1'' and, finally, by more interactions with the protons, proceeds to the final state k'). The matrix element for the physical process is the sum of the matrix elements for all such virtual processes given by formula (9).

In the square of the matrix element for the whole process it is seen that cross-terms appear which represent interference of the virtual processes. From the fact that the complex conjugate of formula (9) is the matrix element for the reverse process in which the electron starts in k' and ends in k, emitting a photon in state $Ae^{-i\Gamma}$, it is seen that

$$|\langle\psi'|\, e^{i\Gamma}\mathbf{p}\cdot\mathbf{A}\,|\psi\rangle|^2 = \langle\psi|\, e^{-i\Gamma}\mathbf{p}\cdot\mathbf{A}\,|\psi'\rangle\,\langle\psi'|\, e^{+i\Gamma}\mathbf{p}\cdot\mathbf{A}\,|\psi\rangle$$

is the sum of terms of the form

$$\frac{\langle k|V_s|k^{(\mathrm{iv})}\rangle\ldots\langle k^{(l)}|V_j|k'''\rangle\langle k_1'''|V_l|k_1^{(l)}\rangle\ldots\langle k^{(m)}|V_m|k'\rangle\ldots\langle k_1^{(n)}|V_p|k_1''\rangle\langle k''|V_q|k^{(n)}\rangle\ldots V_r|k\rangle}{\text{Energy denominator}}, \tag{10}$$

where this is the matrix element for the virtual process in which the electron starts in state k, proceeds to k', and thence goes back to k through interaction with the protons, and absorption and emission of a photon. It is seen from equation (6) that this matrix element (10) depends on the positions of the protons only through the phase factor,

$$\begin{aligned}\exp\{-i[&(k-k^{(\mathrm{iv})})\cdot R_s+\ldots+(k^{(l)}-k''')\cdot R_j+(k_1'''-k_1^{(l)})\cdot R_l+\ldots\\ &+(k_1^{(m)}-k')\cdot R_m+\ldots(k_1^{(n)}-k_1'')\cdot R_p+(k''-k^{(n)})\cdot R_q+\ldots(-k)\cdot R_r]\}.\end{aligned} \tag{11}$$

Using relation (8) with a similar relation between k''' and k_1''', formula (11) may be rewritten

$$\begin{aligned}\exp\{-i[&(k-k^{(\mathrm{iv})})\cdot R_s+\ldots+(k^{(l)}-k''')\cdot R_j+(k_1'''-k_1^{(l)})\cdot R_l+\ldots\\ &+(k_1^{(n)}-k'')\cdot R_p+(k''-k^{(n)})\cdot R_q+\ldots+(k^{(p)}-k)\cdot R_r]\}\\ &\times\exp\left\{i\frac{\omega}{c}\mathbf{n}\cdot(R_l-R_p)\right\}\end{aligned} \tag{12}$$

$$\begin{aligned}=\exp\{-i[&R_{sr}\cdot k+R_{ks}\cdot k^{(\mathrm{iv})}+\ldots+R_{lj}k'''+\ldots+R_{qp}\cdot k''\\ &+\ldots R_{sr}\cdot k^{(p)}]\}\exp\left(i\frac{\omega}{c}\mathbf{n}\cdot R_{lp}\right),\end{aligned}$$

where $R_{lp}=R_l-R_p$, etc.

Treating the expansion of the matrix element $|\langle\psi'|e^{i\Gamma}\mathbf{p}\cdot\mathbf{A}|\psi\rangle|^2$ term by term, each term must be first averaged over k and summed over k' and all the vector wave numbers for the intermediate states, and averaged over the direction $\mathbf{n}$ for the photon. Second, the result must be averaged over all possible distributions of the positions of the protons in the box Ω; and, finally, Ω must be set equal to infinity. If the calculation is carried out in the reverse order, averaging over the proton positions first, integrals appear which have no limit. However, since the calculation converges properly when carried out in one order, we may introduce a convergence factor $e^{-\gamma(|R_{sr}|+\ldots)}$, reverse the order of the calculation, carry out the integrations, and finally set $\gamma=0$. If in the virtual process (10) all the interactions occur with the same proton, the exponent in equation (12) becomes zero, and the phase factor becomes 1. Otherwise, in the case where two or more protons are involved, we will have at least one factor of the form

$e^{-iR_{ij}\cdot k''}$, which must be averaged over all admissible values of R. Setting $\Omega = \infty$, we have

$$\int d\boldsymbol{R}_{ij}\, e^{-\gamma|R_{ij}|}\, e^{-iR_{ij}\cdot k''} = 4\pi \int_0^\infty dR R\, e^{-\gamma R}\, \frac{\sin R|k''|}{|k''|}$$

$$= \frac{8\pi}{|k''|}\, \frac{\gamma}{\gamma^2+1} \to 0 \qquad \text{as} \qquad \gamma \to 0 .$$

Consequently, any terms involving more than one proton average to zero, leaving only those terms involving a single proton. Since there are N protons, the total contribution to a free-free transition is N times the contribution due to a single proton. That is, each proton acts separately on the initial wave function $e^{ik'\cdot r}/\sqrt{\Omega}$ to produce a free-free transition. The result for a single proton for the coulomb case is well known and yields the Gaunt factor given by equation (A) in the introduction. However, as pointed out above, we must multiply our unperturbed wave function by a factor which would make the perturbed wave function normalized, and hence Sommerfeld's result must be multiplied by the square of the two normalization factors for ψ and ψ', actually altering his result. In other words, the general result of the interaction of the fields of the protons is to alter the normalization at infinity that Sommerfeld uses.

These normalization factors are difficult to determine from the perturbation calculation, since the interaction of the different protons no longer averages out when the series is squared, and the limit processes must be performed very carefully. However, a good estimate of their values may be made in the following manner: The solution Sommerfeld obtains for ψ is a hypergeometric function whose absolute value at infinity is 1 and which increases monotonically to the value $[2\pi n/(1 - e^{2\pi n})]^{1/2}$ at the origin. Furthermore, at distance d (the average distance between the protons) the hypergeometric function has not attained its value at infinity for all cases of interest in a stellar interior. Hence the new normalization must reduce equation (A). On the other hand, if the wave function is normalized to 1 at the origin, the wave function will be everywhere less than 1, and the normalization will be too small. In the case of ψ' the wave function attains its asymptotic value considerably before d is reached, so its normalization should be fairly accurate. Considering these two extreme normalizations, Gaunt factors are found which lie roughly 20 per cent above and 15 per cent below the value given by the simpler expression (B). Consequently, since g should lie somewhere in between these extreme values, we may assume that equation (B) is accurate within 10 per cent at worst. Thus we will assume that

$$g = \frac{\sqrt{3}}{\pi} \log\left(\frac{k'+k}{k'-k}\right)$$

gives the Gaunt factor for free-free transitions sufficiently accurately in the interior of stars somewhat similar to the sun.

THE AVERAGE OVER THE INITIAL ENERGY

We have found the Gaunt factor g for a certain initial energy of the electron $\hbar^2k^2/2m$ and a certain frequency ν; g must be averaged over all initial energies of the electron for a constant frequency. Now k and k' are related by

$$\frac{\hbar^2k'^2}{2m} - \frac{\hbar^2k^2}{2m} = h\nu .$$

Furthermore, the probability of k is given by the distribution formula,

$$P(\boldsymbol{k})\, d\boldsymbol{k} = N e^{-\hbar^2k^2/2m\kappa T} d\boldsymbol{k} ,$$

where N is a normalization factor. Set $y^2 = \hbar^2k^2/2m\kappa T$, $y'^2 = y\hbar^2k'^2/2m\kappa T$, and $x = h\nu/\kappa T$. Then $y'^2 - y^2 = x$, and y has the distribution function,

$$P(y)\,dy = \frac{4}{\sqrt{\pi}}\, y^2 e^{-y^2} dy$$

and x is constant. Thus the average is given by

$$\bar{g} = \int_0^\infty \frac{g(y)}{y} P(y)\,dy \div \int_0^\infty \frac{1}{y} P(y)\,dy$$

$$= 2\,\frac{\sqrt{3}}{\pi} \int_0^\infty y\, e^{-y^2} \log\left(\frac{y'+y}{y'-y}\right),$$

since the cross-section is proportional to $g(y)/y$. It turns out that, for x between 3 and 7, this is approximated well by simply taking the value of g at $y = 0.87$ or $\hbar^2k^2/2m = 0.76\kappa T$. Table 1 gives the average value of g as a function of x. For other values of x

TABLE 1

THE GAUNT FACTOR AS A FUNCTION OF x

x	g	x	g	x	g
1.0	0.84	4.0	0.46	6.0	0.38
2.0	.63	4.5	.44	6.5	.37
3.0	.53	5.0	.42	7.0	0.36
3.5	0.49	5.5	0.40		

the approximation is not so good, but at these values the free-free transitions do not contribute strongly to the opacity. Also for lower temperatures the high-energy approximation of Sommerfeld and Maue breaks down; but before this happens, the contribution of the free-free transitions of hydrogen to the opacity will become insignificant. Hence the formula

$$\bar{g} = \frac{\sqrt{3}}{\pi} \log\left(\frac{(0.76+x)^{1/2} + 0.87}{(0.76+x)^{1/2} - 0.87}\right)$$

may be used everywhere throughout the star with reasonable accuracy.

DISCUSSION

Admittedly, the final answers obtained are crude. It was felt justified to use a perturbation treatment to indicate the structure of the problem, since (1) the regions of interest have energies large compared to the interaction energies with the protons, (2) the answer obtained is independent of the energies involved. That is, a recipe for calculating the Gaunt factor is obtained which states simply that the single-proton Gaunt factor must be modified by a change in normalization to give the correct result and does not involve the idea of a convergent series. The calculation of the normalization factors is not complete; so it seemed best to state a simple analytic formula which seemed to conform with proper normalization to reasonable accuracy. Until more accuracy is desired in the Gaunt factor, it did not seem sensible to cope with the difficulties attendant upon their calculation.

In the actual physical situation there are N electrons in the box rather than 1. The

effect of more than 1 electron being present is expected to be small, since it is known that electrons by themselves cannot produce free-free transitions. However, in addition to other effects, they may produce an additional modification in the normalization; and, to get the correct answer, these effects must be taken into account. This problem will be attempted in a later paper, using the methods outlined here.

I wish to express my thanks to Dr. Bengt Strömgren for suggesting this problem to ı. e. I am indebted to him and to Dr. Marvin Goldberger for discussions of it with me.

ON THE REFLECTION AND REFRACTION OF ALFVÉN WAVES*

V. C. A. FERRARO†
Queen Mary College, London, England
Received November 17, 1953

ABSTRACT

It is shown that plane harmonic hydromagnetic waves polarized at right angles to the plane of incidence can be reflected and refracted from a plane surface of separation of two infinitely conducting liquids. The general laws of reflection and refraction are derived, and it is shown that these depend on the orientation of the permanent uniform magnetic field with respect to the surface of separation and the plane of incidence.

The propagation of hydromagnetic waves in a horizontally stratified isothermal atmosphere lying over an infinitely conducting liquid is briefly discussed. It is shown that eventually the magnetic field associated with waves decreases with height proportionately to the density of the atmosphere.

1. *Introduction.*—The reflection and refraction of hydromagnetic waves from a surface of discontinuity of two liquids has been briefly considered by Walén,[1] Alfvén,[2] and Lundquist;[3] but, as far as the writer is aware, a detailed discussion has not yet been given. The problem is of interest in connection with Alfvén's theory of sunspots. In their discussion of the reflection of hydromagnetic whirls from the sun's surface, Alfvén and Walén appear to have considered that this surface acts like a rigid boundary. This procedure is questionable in so far as the density of the solar atmosphere decreases rapidly with height above the photosphere and the conditions there are approximate to those at a free surface.

In the first part of this paper we shall discuss in some detail the reflection and refraction of plane hydromagnetic waves at a surface of separation of two liquids of infinite extent for the case when the electrical conductivities of the liquids are infinite and the magnetic field is uniform. It will be shown that the modes of reflection and refraction depend on the orientation of the magnetic field with respect to both the surface of separation of the liquids and the plane of incidence of the waves. The general laws of reflection and refraction are derived, and these are especially simple in the case when the magnetic field is normal to the surface or the plane of incidence is normal to the plane normal to the surface of separation and parallel to the permanent magnetic field. The amplitudes of the reflected and refracted waves are simple functions of the ratio of the densities of the two liquids.

In the second part of this paper, we briefly consider the propagation of waves in a horizontally stratified atmosphere in contact with an infinitely conducting liquid, thus simulating the conditions obtaining in the region of demarcation between the photosphere and chromosphere. It is shown that, for a given value of the permanent magnetic field, the penetration of the waves into the atmosphere is greater, the greater the frequency of the waves, but that eventually the amplitudes of the waves must decrease directly as the density of the gas.

* The research reported in this paper has in part been supported by the Geophysics Research Directorate of the Air Force Cambridge Research Center, Air Research and Development Command, under Contract AF 19(604)-299 with the University of Chicago.

† Now on leave of absence at Yerkes Observatory.

[1] C. Walén, *Ark. f. Mat., Astr. o. Fys.*, Vol. **30A**, No. 15, 1944; Vol. **33A**, No. 18, 1946.

[2] H. Alfvén, *Cosmical Electrodynamics* (Oxford: Clarendon Press, 1950).

[3] S. Lundquist, *Ark. f. Fys.*, **5**, 297, 1952.

I. REFLECTION AND REFRACTION FROM THE SURFACE OF DISCONTINUITY OF TWO LIQUIDS

2. *The equations of hydromagnetic waves.*—We recall the relevant equations of hydromagnetic waves in an infinite conducting liquid of density ρ in the presence of a uniform magnetic field $\boldsymbol{H}_0$. Let $\boldsymbol{h}$ denote the magnetic field of the wave and $\boldsymbol{v}$ the velocity of the liquid particles; then the differential equations for $\boldsymbol{v}$ and $\boldsymbol{h}$ are,[2]

$$\frac{\partial \boldsymbol{h}}{\partial t} - (\boldsymbol{H}_0 \cdot \operatorname{grad})\, \boldsymbol{v} = (\boldsymbol{h} \cdot \operatorname{grad})\, \boldsymbol{v} - (\boldsymbol{v} \cdot \operatorname{grad})\, \boldsymbol{h}, \tag{1}$$

$$\frac{\partial \boldsymbol{v}}{\partial t} - \frac{1}{4\pi\rho}(\boldsymbol{H}_0 \cdot \operatorname{grad})\, \boldsymbol{h} = \boldsymbol{v} \times \operatorname{curl} \boldsymbol{v} - \frac{1}{4\pi\rho}(\boldsymbol{h} \times \operatorname{curl} \boldsymbol{h}) - \operatorname{grad}\left(\frac{p}{\rho} + \tfrac{1}{2}\boldsymbol{v}^2 + \frac{1}{4\pi\rho}\boldsymbol{H}_0 \cdot \boldsymbol{h}\right), \tag{2}$$

where p denotes the pressure in the liquid. These equations simplify in the two cases when either (i) $|\boldsymbol{h}|$ and $|\boldsymbol{v}|$ are small quantities or (ii) if

$$\boldsymbol{v} = \frac{\pm \boldsymbol{h}}{\sqrt{(4\pi\rho)}}, \tag{3}$$

as was first pointed out by Walén. This relation expresses the fact that in a hydromagnetic wave the kinetic and magnetic energies of the wave motion are equal. In the two cases mentioned above, equations (1) and (2) reduce, respectively, to

$$\frac{\partial \boldsymbol{h}}{\partial t} = (\boldsymbol{H}_0 \cdot \operatorname{grad})\, \boldsymbol{v}, \tag{4}$$

$$4\pi\rho \frac{\partial \boldsymbol{v}}{\partial t} = (\boldsymbol{H}_0 \cdot \operatorname{grad})\, \boldsymbol{h}, \tag{5}$$

provided also that

$$p + \tfrac{1}{2}\rho\boldsymbol{v}^2 + \frac{1}{4\pi}(\boldsymbol{H}_0 + \boldsymbol{h})^2 = \text{Const}. \tag{6}$$

These are the assumptions usually made in the theory; in the case of plane harmonic waves, equation (3) is identically satisfied, as will be shown in § 3, and this will be assumed here.

Eliminating $\boldsymbol{v}$ from equations (4) and (5), we find that

$$4\pi\rho \frac{\partial^2 \boldsymbol{h}}{\partial t^2} = (\boldsymbol{H}_0 \cdot \operatorname{grad})^2 \boldsymbol{h}, \tag{7}$$

which is Alfvén's equation for hydromagnetic waves. The same equation is also satisfied by $\boldsymbol{v}$.

Since $\boldsymbol{H}_0$ is uniform, we may take this to be parallel to the z-axis of a system of rectangular axes $O(x, y, z)$; equation (7) may then be written

$$\frac{\partial^2 \boldsymbol{h}}{\partial t^2} = \frac{H_0^2}{4\pi\rho}\frac{\partial^2 \boldsymbol{h}}{\partial z^2}. \tag{8}$$

The solution of this equation is

$$\boldsymbol{h} = \boldsymbol{f}(x, y, z - Vt) + \boldsymbol{g}(x, y, z + Vt) \tag{9}$$

where

$$V = \frac{H_0}{\sqrt{(4\pi\rho)}} \tag{10}$$

and f and g are arbitrary functions. This solution represents a pair of hydromagnetic waves traveling with equal and opposite velocities V in the direction of the magnetic field. They are further related by the condition that

$$\operatorname{div} \boldsymbol{h} = 0 . \tag{11}$$

3. *Plane harmonic waves.*—A train of plane harmonic waves of frequency $\omega/2\pi$ traveling in the direction of the magnetic field can be written as

$$\boldsymbol{h} = \boldsymbol{A} \exp\left\{i\omega\left(t - \frac{\boldsymbol{u}\cdot\boldsymbol{r}}{V}\right)\right\}, \tag{12}$$

where $\boldsymbol{A}$ is a constant vector, $\boldsymbol{r}$ is the position vector of a field point, and $\boldsymbol{u}$ is a constant vector. By equation (11) it then follows that

$$\boldsymbol{A}\cdot\operatorname{grad}(\boldsymbol{u}\cdot\boldsymbol{r}) = 0 , \tag{13}$$

i.e., $\boldsymbol{A}\cdot\boldsymbol{u} = 0$. Also $\boldsymbol{u}$ is a vector normal to the wave fronts, and thus the constant direction of the magnetic field of the wave is perpendicular to the wave fronts.

The phase velocity of the waves is given by

$$V_a = V\,|\,\boldsymbol{u}\,|^{-1/2} . \tag{14}$$

Again, by equation (5), it follows that $\boldsymbol{v} \propto \exp\{i\omega(t - \boldsymbol{u}\cdot\boldsymbol{r}/V)\}$; and, since $\boldsymbol{H}_0\cdot\operatorname{grad} = H_0\partial/\partial z$, equation (5) also shows that

$$\boldsymbol{v} = -\frac{\boldsymbol{h}}{\sqrt{(4\pi\rho)}}, \tag{15}$$

which is Walén's relation. For waves moving in a direction opposite to the field, the same relation holds with the positive sign.

4. *The reflection and refraction of plane waves.*—We now examine the reflection and refraction of plane waves traveling in a liquid of density ρ_1 occupying the region of space $z < 0$ and impinging on the plane surface of separation, $z = 0$, of a liquid of density ρ_2 occupying the region of space $z > 0$, where $O(x, y, z)$ is a system of rectangular axes. Let the magnetic field be uniform, of intensity $\boldsymbol{H}_0$, and inclined at an angle β to the plane $z = 0$. There is clearly no loss of generality in taking the (y, z) plane parallel to the field. Since the hydromagnetic waves in the two liquids are propagated along the field, the directions of motion of the waves in the incident, reflected, and refracted waves are all parallel to the direction

$$(0, l, m) , \tag{16}$$

where

$$l = \cos\beta , \qquad m = \sin\beta , \qquad l^2 + m^2 = 1 . \tag{17}$$

The amplitude of the waves is not necessarily constant; let $O(y', z')$ be axes in the (y, z) plane in which the y'-axis is in the direction of the field. Then the amplitudes are arbitrary functions of x and z', where

$$y' = ly + mz , \qquad z' = -my + lz . \tag{18}$$

Hence we may take the magnetic field in the incident wave to be

$$\boldsymbol{h}_0 = \boldsymbol{A}(x, z') \exp\left\{i\omega\left(t - \frac{y'}{V_1}\right)\right\}, \tag{19}$$

where $\boldsymbol{A}$ is an arbitrary function of x and z', and V_1 is the velocity of the waves in the liquid of density ρ_1, $\omega/2\pi$ being the frequency. Then the magnetic fields of the waves in

the two liquids are given by

$$\boldsymbol{h}_1 = \boldsymbol{A}(x, z') \exp\left\{i\omega\left(t - \frac{y'}{V_1}\right)\right\} + \boldsymbol{B}(x, z') \exp\left\{i\omega\left(t + \frac{y'}{V_1}\right)\right\} \qquad (z < 0), \quad (20)$$

and

$$\boldsymbol{h}_2 = \boldsymbol{C}(x, z') \exp\left\{i\omega\left(t - \frac{y'}{V^2}\right)\right\} \qquad (z > 0), \quad (21)$$

where V_2 is the velocity of the waves in the liquid of density ρ_2 and V_1 and V_2 are given by

$$V_1 = \frac{H_0}{\sqrt{(4\pi\rho_1)}}, \qquad V_2 = \frac{H_0}{\sqrt{(4\pi\rho_2)}}. \quad (22)$$

The second term in equation (20) represents the reflected wave, and equation (21) gives the refracted wave. In addition, we must have

$$\operatorname{div} \boldsymbol{h}_1 = 0, \qquad \operatorname{div} \boldsymbol{h}_2 = 0. \quad (23)$$

5. *The boundary conditions.*—The boundary conditions to be satisfied at the surface of separation, $x = 0$, are (i) the continuity of the electric and magnetic fields and (ii) the continuity of the normal velocity resolute of the liquid and of the pressure.[4]

The electric field associated with the waves in a liquid of infinite conductivity is given by

$$\boldsymbol{E} = -\frac{1}{c}\boldsymbol{v} \times \boldsymbol{H}, \quad (24)$$

where $\boldsymbol{H} = \boldsymbol{H}_0 + \boldsymbol{h}$ is the total field. Since in a harmonic plane wave equation (3) holds, this reduces to

$$\boldsymbol{E} = -\frac{1}{c}\boldsymbol{v} \times \boldsymbol{H}_0. \quad (25)$$

Let $\boldsymbol{v}_1$ and $\boldsymbol{v}_2$ be the particle velocities in the two liquids of densities ρ_1 and ρ_2, respectively; then conditions (*i*), (*ii*) require that

$$\boldsymbol{h}_1 = \boldsymbol{h}_2, \quad (26)$$

$$\boldsymbol{v}_1 \times \boldsymbol{H}_0 = \boldsymbol{v}_2 \times \boldsymbol{H}_0, \quad (27)$$

at $z = 0$. Let $\boldsymbol{k}$ denote a unit vector along Oz; then the continuity of the normal velocity resolute requires that

$$\boldsymbol{v}_1 \cdot \boldsymbol{k} = \boldsymbol{v}_2 \cdot \boldsymbol{k}. \quad (28)$$

Multiply equation (27) vectorially on the left by $\boldsymbol{k}$; then we get

$$(\boldsymbol{k} \cdot \boldsymbol{H}_0)\boldsymbol{v}_1 - (\boldsymbol{v}_1 \cdot \boldsymbol{k})\boldsymbol{H}_0 = (\boldsymbol{k} \cdot \boldsymbol{H}_0)\boldsymbol{v}_2 - (\boldsymbol{v}_2 \cdot \boldsymbol{k})\boldsymbol{H}_0. \quad (29)$$

Using equation (28), this reduces to

$$\boldsymbol{v}_1 = \boldsymbol{v}_2 \quad (30)$$

unless $\boldsymbol{k} \cdot \boldsymbol{H}_0 = 0$, i.e., the magnetic field is parallel to the plane $z = 0$. This case will be considered in § 9. Ignoring this case for the present, it follows that the velocities of the two liquids at the surface of separation must be continuous.

6. *The reflected and refracted waves.*—We first express $\boldsymbol{h}_1$ and $\boldsymbol{h}_2$ in terms of (x, y, z) by equation (18); we find

$$\boldsymbol{h}_1 = \boldsymbol{A}(x, -my + lz) \exp\left\{i\omega\left(t - \frac{ly + mz}{V_1}\right)\right\} + \boldsymbol{B}(x, -my + lz) \exp\left\{i\omega\left(t + \frac{ly + mz}{V_1}\right)\right\} \quad (31)$$

[4] The liquids are assumed to be inviscid in the theory.

and

$$\boldsymbol{h}_2 = \boldsymbol{C}(x, -my+lz)\exp\left\{i\omega\left(t-\frac{ly+mz}{V_2}\right)\right\}. \tag{32}$$

Then, omitting the time factor and arguments in $\boldsymbol{A}$, $\boldsymbol{B}$, $\boldsymbol{C}$, equation (26) gives, at $z = 0$,

$$\boldsymbol{A}\exp\left(-\frac{i\omega ly}{V_1}\right)+\boldsymbol{B}\exp\left(\frac{i\omega ly}{V_1}\right)=\boldsymbol{C}\exp\left(-\frac{i\omega ly}{V_2}\right), \tag{33}$$

and equation (30), at $z = 0$, gives

$$\sqrt{\rho_2}\left[\boldsymbol{A}\exp\left(-\frac{i\omega ly}{V_1}\right)-\boldsymbol{B}\exp\left(\frac{i\omega ly}{V_1}\right)\right]=\sqrt{\rho_1}\boldsymbol{C}\exp\left(-\frac{i\omega ly}{V_2}\right), \tag{34}$$

the negative sign in the second term on the left-hand side of equation (34) arising from the fact that in the incident and reflected waves opposite signs must be taken in equation (3). Solving equations (33) and (34), we find

$$\boldsymbol{B}=\frac{\sqrt{\rho_2}-\sqrt{\rho_1}}{\sqrt{\rho_2}+\sqrt{\rho_1}}\boldsymbol{A}\exp\left(-\frac{2i\omega ly}{V_1}\right),\quad \boldsymbol{C}=\frac{2\sqrt{\rho_2}}{\sqrt{\rho_2}+\sqrt{\rho_1}}\boldsymbol{A}\exp\left\{-i\omega ly\left(\frac{1}{V_1}-\frac{1}{V_2}\right)\right\}. \tag{35}$$

These are the expressions for $\boldsymbol{B}$ and $\boldsymbol{C}$ in terms of $\boldsymbol{A}$ over the plane $z = 0$. To obtain their general values, these must be expressed as functions of x and $-my + lz$ by replacing $-y$ by $(-y + lz/m)$ in equation (35). These become

$$\boldsymbol{B}=\frac{\sqrt{\rho_2}-\sqrt{\rho_1}}{\sqrt{\rho_2}+\sqrt{\rho_1}}\boldsymbol{A}(x, -my+lz)\exp\left\{\frac{2i\omega l}{mV_1}(-my+lz)\right\}, \tag{36}$$

$$\boldsymbol{C}=\frac{2\sqrt{\rho_2}}{\sqrt{\rho_2}+\sqrt{\rho_1}}\boldsymbol{A}(x, -my+lz)\exp\left\{\frac{i\omega l}{m}(-my+lz)\left(\frac{1}{V_1}-\frac{1}{V_2}\right)\right\}. \tag{37}$$

We next express $\boldsymbol{A}$ as a harmonic function of the form

$$\boldsymbol{A}(x, -my+lz)=\boldsymbol{A}_0\exp\left\{\frac{i}{V_1}[-kx+\omega_0(-my+lz)]\right\}, \tag{38}$$

where k and ω_0 are constants and $\boldsymbol{A}_0$ is a constant vector. Substituting in equations (31) and (32), we then have

$$\boldsymbol{h}_1=\boldsymbol{A}_0\exp\left\{i\left(\omega t-\frac{\boldsymbol{u}_0\cdot\boldsymbol{r}}{V_1}\right)\right\}+\boldsymbol{A}_0'\exp\left\{i\left(\omega t-\frac{\boldsymbol{u}_1\cdot\boldsymbol{r}}{V_1}\right)\right\}, \tag{39}$$

$$\boldsymbol{h}_2=\boldsymbol{A}_0''\exp\left\{i\left(\omega t-\frac{\boldsymbol{u}_2\cdot\boldsymbol{r}}{V_1}\right)\right\}, \tag{40}$$

where

$$\boldsymbol{A}_0'=\frac{\sqrt{\rho_2}-\sqrt{\rho_1}}{\sqrt{\rho_2}+\sqrt{\rho_1}}\boldsymbol{A}_0,\qquad \boldsymbol{A}_0''=\frac{2\sqrt{\rho_2}}{\sqrt{\rho_2}+\sqrt{\rho_1}}\boldsymbol{A}_0, \tag{41}$$

and the constant vectors $\boldsymbol{u}_0$, $\boldsymbol{u}_1$, and $\boldsymbol{u}_2$, are defined by

$$\boldsymbol{u}_0=(k, l\omega+m\omega_0, m\omega-l\omega_0), \tag{42}$$

$$\boldsymbol{u}_1=\left[k, l\omega+m\omega_0, -l\omega_0-(1+l^2)\frac{\omega}{m}\right], \tag{43}$$

$$\boldsymbol{u}_2=\left[k, l\omega+m\omega_0, -l\omega_0-\left(l^2-\frac{V_1}{V_2}\right)\frac{\omega}{m}\right]. \tag{44}$$

From equation (41) we see that the amplitudes of the reflected and refracted waves are as $(\sqrt{\rho_1}+\sqrt{\rho_2}):(\sqrt{\rho_2}-\sqrt{\rho_1}):2\sqrt{\rho_2}$, in agreement with the result found by Lundquist.[3]

We have yet to satisfy the conditions in equation (23); these give the relations

$$\boldsymbol{A}_0\cdot\boldsymbol{u}_0+\boldsymbol{A}_0'\cdot\boldsymbol{u}_1=0\,,\qquad \boldsymbol{A}_0''\cdot\boldsymbol{u}_2=0\,. \tag{45}$$

Using equations (41) and (42)–(44) we find, after some simplification, that

$$(\boldsymbol{A}_0\cdot\boldsymbol{k})\left(\sqrt{\frac{\rho_1}{\rho_2}}-\sqrt{\frac{\rho_2}{\rho_1}}\right)=0\,, \tag{46}$$

whence we must have

$$\boldsymbol{A}_0\cdot\boldsymbol{k}=0\,. \tag{47}$$

This result shows that the only waves that can be reflected or refracted are those in which the magnetic field of the waves and hence the particle velocity are parallel to the plane of separation. This remarkable result has an important bearing on Alfvén's theory of sunspots; this will be discussed elsewhere.

7. *The laws of reflection and refraction.*—By definition, the planes of incidence, reflection, and refraction are parallel to the respective rays in the incident, reflected, and refracted waves and also pass through the z-axis. The direction cosines of the normals to the plane of incidence, reflection, and refraction are thus of the form $(\lambda, \mu, 0)$; and the condition that these normals should be perpendicular to the rays of the respective waves by equations (42)–(44) leads to an equation the same for all three waves, namely,

$$\lambda k+\mu\,(l\omega+m\omega_0)=0\,. \tag{48}$$

Thus *the planes of incidence, reflection, and refraction coincide.* Let this common plane make an angle γ with the plane through the z-axis parallel to $\boldsymbol{H}_0$ (Fig. 1). Then we have

$$\lambda=\cos\gamma\,,\qquad \mu=\sin\gamma\,; \tag{49}$$

and, from equation (48), it follows that

$$\cos\gamma=\frac{l\omega+m\omega_0}{N}\,, \tag{50}$$

where

$$N=\{k^2+(l\omega+m\omega_0)^2\}^{1/2}\,. \tag{51}$$

Denote by θ, θ', and θ'' the angles which the directions of the rays in the incident, reflected, and refracted waves make with the plane of separation of the liquids, measured in the same sense. Then, from equations (47)–(49), it follows that

$$\tan\theta=-\frac{1}{N}\,(l\omega_0-m\omega)\,, \tag{52}$$

$$\tan\theta'=-\frac{1}{N}\left\{l\omega_0+(1+l^2)\,\frac{\omega}{m}\right\}, \tag{53}$$

$$\tan\theta''=-\frac{1}{N}\left\{l\omega_0+\left(l^2-\frac{V_1}{V_2}\right)\frac{\omega}{m}\right\}. \tag{54}$$

Adding equations (52) and (53), we find that

$$\tan\theta+\tan\theta'=-\frac{2l}{mN}\,(m\omega_0+l\omega)\,, \tag{55}$$

or, using equations (18) and (50),

$$\tan\theta + \tan\theta' = -2\cot\beta\cos\gamma\,. \tag{56}$$

This is the law of reflection for hydromagnetic waves. Using equations (52) and (54), we find, after some simplification, that

$$\tan\theta'' - \frac{V_1}{V_2}\tan\theta = -\left(1-\frac{V_1}{V_2}\right)\frac{l(l\omega + m\omega_0)}{mN}\,; \tag{57}$$

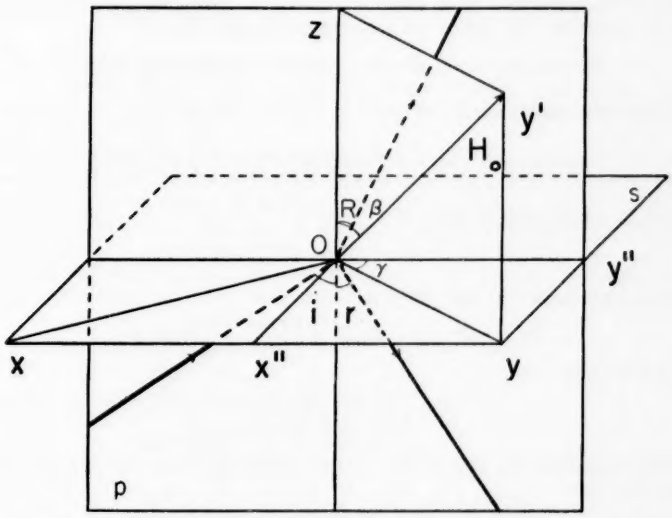

FIG. 1.—Illustrating the reflection and refraction of Alfvén waves polarized at right angles to the plane of incidence (p) and impinging on the surface of separation (s) of two infinite conducting liquids; i, r, and R are the angles of incidence, reflection, and refraction. The plane containing the z-axis and the magnetic field vector $\boldsymbol{H}_0$ is inclined at an angle γ to the plane of incidence, and $\boldsymbol{H}_0$ makes an angle β with the plane s. The heavier arrowed lines show the incident, reflected, and refracted rays.

and, using equations (18) and (50), we finally get

$$\tan\theta'' = \frac{V_1}{V_2}\tan\theta + \left(\frac{V_1}{V_2} - 1\right)\cot\beta\cos\gamma\,. \tag{58}$$

This is the law of refraction for hydromagnetic waves. It will be seen that the laws of reflection and refraction are by no means so simple as those in optics, since they depend on the orientation of the field with respect to the plane of incidence and the surface of separation of the two liquids.

However, they become especially simple in the case when the magnetic field is normal to the surface of separation ($\beta = \frac{1}{2}\pi$) or the plane of incidence is perpendicular to the (y, z) plane ($\gamma = \frac{1}{2}\pi$). It is also of interest to note that equation (56) can be obtained from equation (58) by putting $V_1/V_2 = -1$, as should be the case.

8. *Case when either β or γ is a right angle.*—In this case equations (56) and (58) reduce, respectively, to

$$\tan\theta + \tan\theta' = 0\,, \qquad \tan\theta'' = \frac{V_1}{V_2}\tan\theta\,. \tag{59}$$

The first equation gives $\theta' = \pi - \theta$, so that the angle of incidence $(\pi/2 - \theta)$ and reflection $(\theta' - \pi/2)$ are equal, as in optics. But Snell's law in optics is replaced by the tangent law, as in the case of refraction in a uniaxial crystal having its optic axis in the plane of incidence and in the surface of separation. If we denote the angles of incidence and refraction by i and R, respectively, equation (59) gives

$$\tan R = \frac{V_2}{V_1} \tan i . \tag{60}$$

9. *Transformation to axes in the plane of incidence.*—Take axes $O(x'', y'')$ in the surface of separation, so that Oy'' lies in the plane of incidence. Then

$$x'' = x \cos \gamma + y \sin \gamma , \qquad y'' = -x \sin \gamma + y \cos \gamma . \tag{61}$$

The incident wave may then be written

$$\boldsymbol{h}_0 = \boldsymbol{A}_0 \exp \left\{ i\omega t - i \frac{N}{V_1} \sec \theta \, (y'' \cos \theta + z \sin \theta) \right\} . \tag{62}$$

The apparent wave velocity, then, is

$$V_a = V_1 \frac{\omega}{N} \cos \theta . \tag{63}$$

Again, from equations (50) and (52),

$$\sec \gamma = N (l\omega + m\omega_0) = \left\{ \frac{m\omega - l\omega_0}{l\omega + m\omega_0} \right\} \cot \theta , \tag{64}$$

from which we find

$$\frac{\omega_0}{\omega} = \frac{\tan \beta - \tan \theta \sec \gamma}{1 + \tan \beta \tan \theta \sec \gamma} . \tag{65}$$

Substituting equation (65) in equation (63) and using equation (18), we find, after some simplification, that

$$V_a = V_1 (\cos \theta \cos \beta \cos \gamma + \sin \theta \sin \beta) , \tag{66}$$

in accordance with equation (14), since the coefficient of V_1 in equation (66) is equal to the cosine of the angle between the incident ray and the field $\boldsymbol{H}_0$. Hence equation (62) may be written

$$\boldsymbol{h}_0 = \boldsymbol{A}_0 \exp \left\{ i\omega t - \frac{i}{V_a} (y'' \cos \theta + z \sin \theta) \right\} . \tag{67}$$

Likewise, the apparent velocity of the reflected wave is

$$V_r = \frac{V_1 \omega}{N} \cos \theta' = V_a \cos \theta' \sec \theta , \tag{68}$$

and that of the refracted wave is

$$V_R = V_a \cos \theta'' \sec \theta . \tag{69}$$

Thus we may write the magnetic fields of the waves in the two liquids in the form

$$\boldsymbol{h}_1 = \boldsymbol{A}_0 \exp \{ i\omega t - i\boldsymbol{u}_0 \cdot \boldsymbol{r}'' / V_a \} + \boldsymbol{A}_0' \exp \{ i\omega t - i\boldsymbol{u}_1 \cdot \boldsymbol{r}'' / V_r \} , \tag{70}$$

$$\boldsymbol{h}_2 = \boldsymbol{A}_0'' \exp \{ i\omega t - i\boldsymbol{u}_2 \cdot \boldsymbol{r}'' / V_R \} , \tag{71}$$

where $\boldsymbol{r}''$ is the position vector referred to the axes $O(x'', y'', z)$ and the unit vectors $\boldsymbol{u}_0$,

$\boldsymbol{u}_1$, and $\boldsymbol{u}_2$, are now given by

$$\boldsymbol{u}_0 = (0, \cos\theta, \sin\theta), \qquad \boldsymbol{u}_1 = (0, \cos\theta', \sin\theta'), \qquad \boldsymbol{u}_2 = (0, \cos\theta'', \sin\theta''). \tag{72}$$

By equation (47) it follows that the z resolutes of $\boldsymbol{A}_0$, $\boldsymbol{A}_0'$, and $\boldsymbol{A}_0''$ vanish; the condition (23) then gives, in addition,

$$\boldsymbol{A}_0 \cdot \boldsymbol{j}'' = 0, \tag{73}$$

where $\boldsymbol{j}''$ is a unit vector along Oy''. Hence $\boldsymbol{A}_0$ *is perpendicular to the plane of incidence*, so that the magnetic fields of the incident reflected and refracted waves must all be perpendicular to this plane, i.e., the waves are polarized at right angles to the plane of incidence.

This is a necessary condition if reflection and refraction are assumed; it must be interpreted as implying that if there is a resolute of the magnetic field of the wave in the plane of incidence, this cannot be reflected or refracted. The conditions obtaining in this case will not be examined here.

Finally, we consider the case when the magnetic field $\boldsymbol{H}_0$ is parallel to the surface of separation of the liquids mentioned in § 5. In this case also it will be seen that there are no reflected or refracted waves. This can be seen from equation (33) and remembering that, since $l = 1$, $m = 0$ in this case, $\boldsymbol{A}$, $\boldsymbol{B}$, and $\boldsymbol{C}$ are now functions of x and z only. Clearly, equation (33) cannot be satisfied for all values of y in this case.

10. *General discussion of reflection and refraction.*—Let i, r, and R denote the angles of incidence, reflection, and refraction; then it follows that

$$i = \frac{\pi}{2} - \theta, \qquad r = \theta' - \frac{\pi}{2}, \qquad R = \frac{\pi}{2} - \theta''. \tag{74}$$

Hence equations (58) and (60) may be written

$$\cot r = \cot i + 2 \cot\beta \cos\gamma, \tag{75}$$

$$\cot R = \frac{V_1}{V_2} \cot i + \left(\frac{V_1}{V_2} - 1\right) \cot\beta \cos\gamma. \tag{76}$$

It will be seen that, provided that neither β nor γ is a right angle, there is an upper limit, r_m, to the value of the angle of reflection. For $i \leq \frac{1}{2}\pi$, so that $\tan r \leq \frac{1}{2} \tan\beta \sec\gamma$ or

$$r \leq r_m, \qquad \text{where} \qquad r_m = \tan^{-1}(\tfrac{1}{2} \tan\beta \sec\gamma). \tag{77}$$

Again, if the waves impinge on a denser liquid, there is also an upper limit, R_m, to the angle of refraction. For in this case $V_1/V_2 > 1$, so that, since $i \leq \frac{1}{2}\pi$, we have $\tan R \leq (V_1/V_2 - 1) \tan\beta \sec\gamma$ and

$$R \leq R_m, \qquad \text{where} \qquad R_m = \tan^{-1}\left\{\left(\frac{V_1}{V_2} - 1\right) \tan\beta \sec\gamma\right\}. \tag{78}$$

If the waves impinge on a lighter liquid, $V_1/V_2 < 1$, and the expression for $\cot R$ becomes negative for some value of i. This implies that R lies in the second quadrant, so that waves are refracted by more than a right angle. In this case R increases from zero to a right angle, after which it decreases from two right angles to a value R_c, given by

$$\cot R_c = -\left(1 - \frac{V_1}{V_2}\right) \cot\beta \cos\gamma. \tag{79}$$

11. *Energy considerations.*—The flow of energy across the unit area of a surface due to an electromagnetic field is given by the Poynting vector $c\boldsymbol{E} \times \boldsymbol{H}/4\pi$, where $\boldsymbol{E}$ and $\boldsymbol{H}$

are the (variable) parts of the electric and magnetic fields. Since in a hydromagnetic wave the electric field is given by equation (25), the flow of energy across a surface of unit area is given by

$$\boldsymbol{F} = \frac{1}{4\pi}\, \boldsymbol{h} \times (\boldsymbol{v} \times \boldsymbol{H}_0)\,. \tag{80}$$

Since $\boldsymbol{v} = \boldsymbol{h}/\sqrt{(4\pi\rho)}$, apart from a sign, this reduces to

$$\boldsymbol{F} = \frac{1}{(4\pi)^{3/2}\sqrt{\rho}}\,[\,(\boldsymbol{h}\cdot\boldsymbol{H}_0)\,\boldsymbol{h} - \boldsymbol{h}^2\boldsymbol{H}_0]\,. \tag{81}$$

The intensity of this flow is $|\boldsymbol{F}|$ or $(\boldsymbol{F}\boldsymbol{F}^*)^{1/2}$, where $\boldsymbol{F}^*$ is the conjugate complex of $\boldsymbol{F}$. Thus

$$|\boldsymbol{F}| = \{\,|\,(\boldsymbol{h}\cdot\boldsymbol{H}_0)\,|\,|\boldsymbol{h}| + \boldsymbol{h}^2|\boldsymbol{H}_0|\,\}\,. \tag{82}$$

Since a hydromagnetic wave is propagated in the direction of the field $\boldsymbol{H}_0$, the energy flow per unit area is proportional to $|\boldsymbol{F}|$. Using equations (41), (70), and (71), it follows that the energies in the incident, reflected, and transmitted waves are as

$$|\boldsymbol{A}_0|\,\rho_1^{-1/2} : |\boldsymbol{A}_0'|\,\rho_1^{-1/2} : |\boldsymbol{A}_0''|\,\rho_2^{-1/2}\,; \tag{83}$$

and, by equation (45), this becomes

$$(\sqrt{\rho_1} + \sqrt{\rho_2})^2 : (\sqrt{\rho_2} - \sqrt{\rho_1})^2 : 4\sqrt{(\rho_1\rho_2)}\,, \tag{84}$$

whence the principle of conservation of energy is seen to be satisfied.

12. *Numerical discussion of the results.*—To illustrate the results of the preceding analysis, we shall consider the variations of r and R with i in the case when $\tan\beta \sec\gamma = 1$ (say, $\beta = \pi/4$, $\gamma = 0$), and the two cases when $V_1/V_2 = 2$ and $\frac{1}{2}$, respectively. This corresponds to waves impinging on liquids whose densities are as 1:4 and 4:1, respectively. The results are shown in Table 1. The angle of refraction in the second row corresponds to the case of a wave impinging on the denser liquid. The energies of incident, reflected, and refracted waves are as 9:1:8 in this case, so that the greater part of the energy is transmitted.

TABLE 1

TAN β SEC γ = 1

i	0°	15°	30°	45°	60°	75°	90°
r	0°	11°56′	15°	18°34′	21°13′	23°48′	26°33′
R, $(V_1/V_2=2)$	0	7°09′	12°09′	18°26′	24°54′	33°04′	45°
R, $(V_1/V_2=\frac{1}{2})$	0	38°47′	69°52′	90°	168°04′	159°53′	153°26′

II. PROPAGATION OF HYDROMAGNETIC WAVES IN A HORIZONTALLY STRATIFIED ATMOSPHERE

13. *Propagation of hydromagnetic waves in a horizontally stratified atmosphere.*—In the foregoing sections we have considered the reflection and refraction of hydromagnetic waves from a surface of separation of two liquids. In connection with Alfvén's theory of sunspots, it is also of interest to consider the mode of propagation of such waves in a horizontally stratified isothermal atmosphere.

We shall here suppose that the permanent magnetic field $\boldsymbol{H}_0$ is vertical and that the wave fronts are horizontal. This assumption simplifies the discussion considerably. Fur-

ther, we restrict the waves to small amplitudes, so that equation (4) holds as before.

The equation of mechanical oscillations may then be written

$$\rho \frac{\partial \boldsymbol{v}}{\partial t} = -\operatorname{grad} p + \frac{1}{4\pi} (\operatorname{curl} \boldsymbol{h}) \times \boldsymbol{H}_0 + \rho \boldsymbol{g} , \tag{85}$$

where p is the pressure in the gas and $\boldsymbol{g}$ is the acceleration of gravity, assumed to be constant.

Let p_1 and ρ_1 refer to the undisturbed (equilibrium) values of the pressure and density, and let their values in a disturbed state be $p_1 + \delta p$ and $\rho_1 + \delta \rho$. The equation of hydrostatic equilibrium is

$$-\operatorname{grad} p_1 + \rho_1 \boldsymbol{g} = 0 . \tag{86}$$

Substituting for the pressure and density in equation (85) and using equation (86), retaining only first-order terms, we have, approximately,

$$\rho_1 \frac{\partial \boldsymbol{v}}{\partial t} = -\operatorname{grad} \delta p + \frac{1}{4\pi} (\operatorname{curl} \boldsymbol{h}) \times \boldsymbol{H}_0 + \delta \rho \boldsymbol{g} . \tag{87}$$

To the first order, the equation of continuity is

$$\frac{\partial \delta \rho}{\partial t} + \rho_1 \operatorname{div} \boldsymbol{v} = 0 ; \tag{88}$$

and, since the wave fronts are horizontal, $\boldsymbol{v}$ and $\boldsymbol{h}$ are perpendicular to $\boldsymbol{H}_0$. Supposing, further, that all variables depend solely on the co-ordinate z, measured vertically upward, we have div $\boldsymbol{v} = 0$, so that, by equation (88), $\delta \rho = 0$. For a gas for which p is a function of ρ only, $\delta p \propto \delta \rho$, so that equation (87) reduces to

$$\rho_1 \frac{\partial \boldsymbol{v}}{\partial t} = \frac{1}{4\pi} (\operatorname{curl} \boldsymbol{h}) \times \boldsymbol{H}_0 \tag{89}$$

or

$$\rho_1 \frac{\partial \boldsymbol{v}}{\partial t} = \frac{1}{4\pi} (\boldsymbol{H}_0 \cdot \operatorname{grad}) \boldsymbol{h} . \tag{90}$$

In terms of z, equations (4) and (90) may be written

$$\frac{\partial \boldsymbol{h}}{\partial t} = H_0 \frac{\partial \boldsymbol{v}}{\partial z} , \tag{91}$$

$$4\pi \rho_1 \frac{\partial \boldsymbol{v}}{\partial t} = H_0 \frac{\partial \boldsymbol{h}}{\partial z} . \tag{92}$$

Eliminating $\boldsymbol{v}$ between these equations, we obtain the equation of wave propagation

$$\frac{\partial^2 \boldsymbol{h}}{\partial t^2} = \frac{H_0^2}{4\pi} \frac{\partial}{\partial z} \left(\frac{1}{\rho_1} \frac{\partial \boldsymbol{h}}{\partial z} \right) ; \tag{93}$$

and, for harmonic waves of frequency $\omega/2\pi$, this reduces to

$$-\omega^2 \boldsymbol{h} = \frac{H_0^2}{4\pi} \frac{\partial}{\partial z} \left(\frac{1}{\rho_1} \frac{\partial \boldsymbol{h}}{\partial z} \right) . \tag{94}$$

Let us consider an isothermal atmosphere for which

$$\rho_1 = \rho_0 e^{-z/z_0} , \tag{95}$$

where z_0 is the scale height. Then, if we choose

$$\xi = e^{-z/z_0} \tag{96}$$

as a new independent variable, equation (94) becomes

$$\xi \frac{\partial^2 \boldsymbol{h}}{\partial \xi^2} + \sigma^2 \boldsymbol{h} = 0 , \tag{97}$$

where

$$\sigma = \frac{1}{H_0} [\omega z_0 \sqrt{(4\pi\rho_0)}] = \frac{\omega z_0}{V_0} \tag{98}$$

and $V_0 [= H_0(4\pi\rho_0)^{-1/2}]$ is the velocity of the Alfvén waves for a density ρ_0. The solution of equation (97), which is finite for $\xi = 0$ ($\rho_1 = 0$), is

$$\boldsymbol{h} = \boldsymbol{C} e^{i\omega t} \xi^{1/2} J_1(2\sigma\xi^{1/2}) , \tag{99}$$

where $\boldsymbol{C}$ is an arbitrary constant vector and J_1 is Bessel's function of order unity, of the first kind. This solution represents a standing wave, the wave length increasing with increasing height at first, and the amplitude eventually being proportional to the density.

Let us now examine the case of a hydromagnetic wave traveling in a liquid of density ρ_0 which merges with the isothermal atmosphere considered lying over the plane $z = 0$. In the region $z < 0$, the wave is given by

$$\boldsymbol{h} = \boldsymbol{A} e^{i\omega t} \cos\left(\frac{z\omega}{V_0} + \epsilon\right) = \boldsymbol{A} e^{i\omega t} \cos\left(\frac{\sigma z}{z_0} + \epsilon\right) \tag{100}$$

by equation (98); this represents a standing harmonic wave. To fit the two solutions (99) and (100) over the plane $z = 0$, we must insure that the electric and magnetic fields are continuous, i.e., that $\boldsymbol{h}$ and $\boldsymbol{v} \times \boldsymbol{H}_0$ will be continuous for $z = 0$. Since $\boldsymbol{v} \cdot \boldsymbol{H}_0 = 0$ by hypothesis, this implies that $\boldsymbol{v}$ is continuous at $z = 0$. It follows from equations (99) and (100) that $\boldsymbol{h}$ and $\partial\boldsymbol{h}/\partial z$ are continuous at the surface $z = 0$. These conditions give

$$\boldsymbol{A} \cos\epsilon = \boldsymbol{C} J_1(2\sigma) , \tag{101}$$

$$\boldsymbol{A} \sin\epsilon = \boldsymbol{C} J_0(2\sigma) \tag{102}$$

whence

$$\tan\epsilon = \frac{J_0(2\sigma)}{J_1(2\sigma)} , \tag{103}$$

an equation which determines ϵ in terms of σ. Furthermore,

$$|\boldsymbol{C}|^2 [J_0^2 + J_1^2] = |\boldsymbol{A}|^2 , \tag{104}$$

whence, from equations (99) and (100), we have

$$\boldsymbol{h}_- = \boldsymbol{A} e^{i\omega t} \cos\left(\frac{\sigma z}{z_0} + \epsilon\right), \qquad z < 0 , \tag{105}$$

$$\boldsymbol{h}_+ = \boldsymbol{A} e^{i\omega t} [J_0^2 + J_1^2]^{-1/2} \xi^{1/2} J_1(2\sigma\xi^{1/2}) , \qquad z > 0 , \tag{106}$$

where $\boldsymbol{h}_+$ and $\boldsymbol{h}_-$ denote the magnetic fields of the waves in the regions $z > 0$ and $z < 0$, respectively, and $\xi = e^{-z/z_0}$.

The penetration of the waves into the atmosphere thus depends essentially on the

parameter σ, i.e., on the frequency of the wave, the scale height of the atmosphere, and the Alfvén wave velocity in the region of constant density. When σ is small, we may replace $J_1(2\sigma\xi^{1/2})$ by $\sigma\xi^{1/2}$, since $\xi \leq 1$. In this case $h_+ \propto \xi = \rho_1/\rho_0$, and the magnetic field will decrease directly as the density. This is illustrated in Figure 2, which shows the variation in h_+ over the range $-12 \leq z/z_0 \leq 4$ for the case when $\sigma = 0.1$. In this case the transmitted wave is quickly extinguished. When σ is large compared with unity,

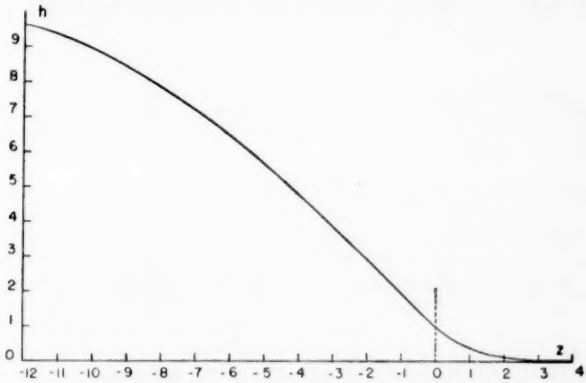

FIG. 2.—The figure illustrates the reflection of a wave traveling in an infinitely conducting liquid and impinging on a horizontally stratified isothermal atmosphere in contact with the liquid. The curve illustrates the variation of the amplitude, h, of the standing wave with height, and its rapid extinction in the atmosphere when the parameter σ (=0.05) is small compared with unity. The dotted line marks the surface of separation of liquid and gas, and the height z is measured in terms of a scale height as unit.

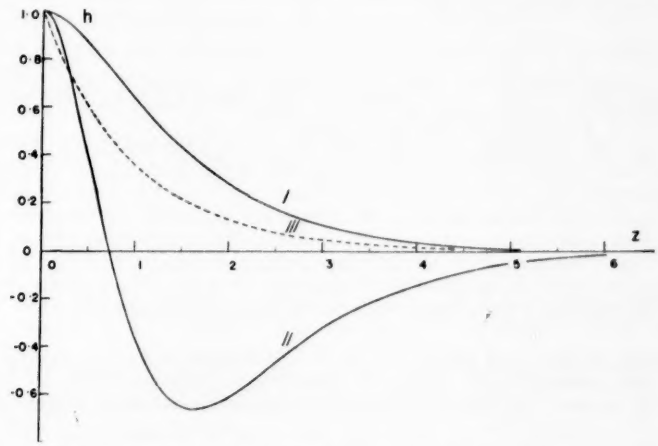

FIG. 3.—The figure illustrates the reflection of a wave traveling in an infinitely conducting liquid and impinging on a horizontally stratified isothermal atmosphere in contact with the liquid. The curves show the variation of the amplitude, h, of the standing wave with height in the cases when 2σ is equal to the first (curve *I*) and second (curve *II*) zeros of $J_0(x)$. The dotted curve (*III*) shows the variation of density with height x measured in terms of a scale height as unit.

so long as $\sigma\xi^{1/2}$ is large, we may use the asymptotic expansion for the Bessel functions. In this case the amplitude of the wave in the atmosphere varies as $\xi^{1/4}$, that is, as $\rho_1^{1/4}$. This agrees with the findings of Alfvén[2] and Walén,[1] but their discussion is seen to be valid only as long as $\sigma\xi^{1/2} \gg 1$. Since ξ decreases exponentially with height, this product eventually becomes small, and the wave will again be extinguished rapidly.

To illustrate the penetration of a hydromagnetic wave in the atmosphere in this case, curves have been drawn for the case when (i) $\epsilon = 0$ and (ii) $\epsilon = \pi/2$. By equation (103) it follows that $J_0(2\sigma) = 0$ in case (i) and $J_1(2\sigma) = 0$ in case (ii). Figure 3 shows these

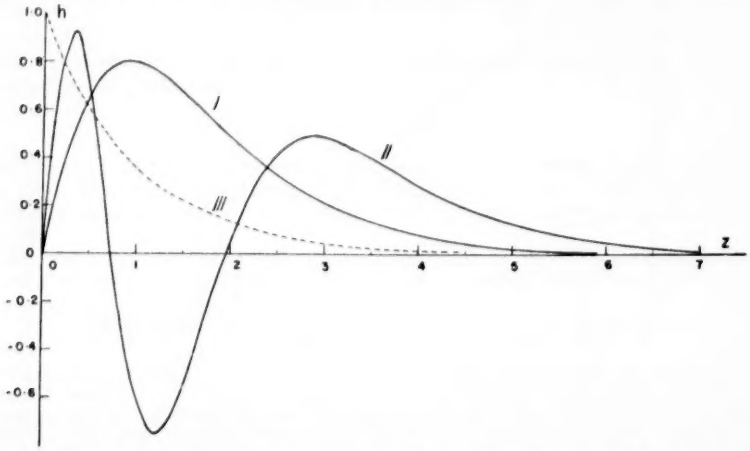

FIG. 4.—The same as Fig. 3 except that curves *I* and *II* now refer to the cases when 2σ is, respectively, equal to the first and third zeros of $J_1(x)$.

curves for values of σ corresponding to the first two zeros of J_0 and Figure 4, the curves for values of σ corresponding to the first and third zeros of J_1. These curves show clearly that the penetration of the wave increases with increasing values of σ but that this is accompanied by an increase in the "wave length."

As a numerical illustration, consider the case when the frequency $\omega = 3.16 \times 10^{-5}$, the "lowest transmitted frequency" just at the top of the photosphere,[2] corresponding to a short-lived sunspot of 2 days' duration. Taking also $z_0 = 1.5 \times 10^7$ cm as the scale height just above the photosphere, $H_0 = 1$ gauss, and $\rho_0 = 2 \times 10^{-5}$ gm/cm^3, we find $\sigma = 0.12$. This corresponds to the case illustrated in Figure 2, very nearly, so that the magnetic field of the sunspot on Alfvén's theory would decrease with height as the density. This result seems to conflict with observations. It is hoped to consider more fully elsewhere the bearing of these results of Alfvén's theory of sunspots.

The writer expresses his thanks to Dr. S. Chandrasekhar for the interest he has shown in this work. He also thanks the Geophysical Division of the Air Force for enabling him to carry out this research and to Yerkes Observatory for their kind hospitality.

ON THE EQUILIBRIUM OF MAGNETIC STARS*

V. C. A. FERRARO
Queen Mary College, London, England†
Received September 29, 1953

ABSTRACT

The necessary condition for the equilibrium of a liquid magnetic star is derived and the solution in a particular case given. It is shown, as was first pointed out by Chandrasekhar and Fermi,[1] that a magnetic field has the same effect as rotation, i.e., it tends to produce a flattening of the poles of the star. A formula for the ellipticity is derived.

1. *Introduction.*—The mechanical equilibrium of an ionized medium in which electric currents flow is of interest in connection with problems of cosmical magnetism. Chandrasekhar and Fermi[1] first pointed out that we must expect a magnetic field to produce the same effect as a rigid-body rotation. They showed that for a spheroidal liquid sphere, in which the magnetic field was uniform inside and like a dipole field outside, the ellipticity to be expected is given by the formula $\mathfrak{E} = (7/2)\mathfrak{M}/\mathfrak{W}$, where $\mathfrak{M}$ denotes the magnetic energy and $\mathfrak{W}$ the gravitational energy of the star.

We shall here consider the problem of the equilibrium of a rotating liquid star in which electric currents flow, restricting the discussion to the case of symmetry about the axis of rotation. It will be shown that the magnetic field in the star must satisfy a certain condition for equilibrium similar to that found by Stokes[2] for steady rotational motion in an incompressible fluid. No account is taken of the decay of currents through electrical resistance, since Cowling[3] has shown that this is extremely slow, and we can therefore consider the currents as effectively steady. Provided that the magnetic energy of the currents is small compared with the gravitational energy, the surface of the liquid will be a spheroid of small ellipticity whose value is given by a formula similar to that found by Chandrasekhar and Fermi. It is hoped to discuss the stability of the equilibrium in a future note.

2. *The equation of the problem.*—We consider a finite mass of liquid of density ρ rotating as a rigid body with constant angular velocity ω about a fixed axis. Let this be taken as the z-axis of a system of cylindrical polar co-ordinates (ϖ, φ, z). Let $\boldsymbol{H}$ be the magnetic field produced by a system of currents of density $\boldsymbol{j}$ flowing in the liquid. Then the field equations in the steady state are

$$\operatorname{div} \boldsymbol{H} = 0 , \tag{1}$$

$$\operatorname{curl} \boldsymbol{H} = 4\pi \boldsymbol{j} . \tag{2}$$

Since we assume axial symmetry, it follows from equation (1) that $\boldsymbol{H}$ is derivable from a stream function U, the resolute of $\boldsymbol{H}$ in the directions of ϖ and z increasing being given

* The research reported in this paper has in part been supported by the Geophysics Research Directorate of the Air Force Cambridge Research Center, Air Research and Development Command, under Contract AF 19(604)-299 with the University of Chicago.

† Now on leave of absence at Yerkes Observatory.

[1] *Ap. J.*, **118**, 116, 1953.

[2] G. G. Stokes, *Mathematical and Physical Papers of Sir George Stokes* (Cambridge, England, 1901), **1**, 15.

[3] T. G. Cowling, *M.N.*, **105**, 166, 1945.

by

$$H_\varpi = -\frac{1}{\varpi}\frac{\partial U}{\partial z}, \qquad H_z = \frac{1}{\varpi}\frac{\partial U}{\partial \varpi}, \tag{3}$$

respectively. Let p be the pressure in the liquid and Ω the gravitational potential; then the equation of mechanical equilibrium of the liquid is

$$\rho\boldsymbol{\omega} \times (\boldsymbol{\omega} \times \boldsymbol{r}) = -\operatorname{grad} P + \boldsymbol{j} \times \boldsymbol{H} \tag{4}$$

where $\boldsymbol{r}$ is the position vector of any point of the liquid relative to the origin and

$$P = p + \rho\Omega . \tag{5}$$

Using equation (3), the resolutes of equation (4) are

$$-\rho\omega^2\varpi = -\frac{\partial P}{\partial \varpi} + \frac{JH_z}{4\pi}, \tag{6}$$

$$0 = -\frac{\partial P}{\partial z} - \frac{JH_\varpi}{4\pi}, \tag{7}$$

where the quantity J is defined by

$$J = \frac{\partial H_\varpi}{\partial z} - \frac{\partial H_z}{\partial \varpi} \tag{8}$$

and is proportional to the intensity of the current density.

Since ρ is constant, it follows from equations (6) and (7) that

$$\frac{\partial^2 P}{\partial z \partial \varpi} = \frac{\partial}{\partial z}\left(\rho\omega^2\varpi + \frac{JH_z}{4\pi}\right) = -\frac{\partial}{\partial \varpi}\left(\frac{JH_\varpi}{4\pi}\right) \tag{9}$$

or

$$\frac{\partial}{\partial \varpi}(JH_\varpi) + \frac{\partial}{\partial z}(JH_z) = 0 . \tag{10}$$

Also, from equations (8) and (3),

$$J = -\frac{\Delta U}{\varpi}, \tag{11}$$

where

$$\Delta U = \varpi \frac{\partial}{\partial \varpi}\left(\frac{1}{\varpi}\frac{\partial U}{\partial \varpi}\right) + \frac{\partial^2 U}{\partial z^2} . \tag{12}$$

Substituting in equation (10), we find, after simplification, that

$$\frac{\partial(\varpi^{-2}\Delta U, U)}{\partial(\varpi, z)} = 0 , \tag{13}$$

where $\partial(f_1, f_2)/\partial(\varpi, z)$ represents the Jacobian of f_1 and f_2.

Equation (13) is the necessary condition which must be satisfied by U for equilibrium. It is clearly identically satisfied if $\Delta U = 0$, in which case there are no currents in the liquid and the magnetic field is of external origin. It is also satisfied if U is independent of ϖ or of z, the latter case being trivial. In general, equation (13) is satisfied, provided that

$$\Delta U = \varpi^2 f(U) , \tag{14}$$

where f is an arbitrary function. This condition is similar to that found by Stokes for the steady rotational motion of an incompressible fluid.[2]

Since the current density is proportional to J, and thus to $(\Delta U)/\varpi$ by equation (11), and the surfaces U = Constant are those obtained by revolving the magnetic lines of force about the axis of symmetry, equation (14) implies that the current density over any surface U = Constant varies directly as the distance from the axis. The currents thus tend to be concentrated near the surface.

3. *A particular solution in spherical polar co-ordinates.*—Clearly, further progress can be made only by assuming some special form for the arbitrary function f. The simplest case is that in which f is a constant, κ, say; equation (14) then becomes

$$\Delta U = \kappa \varpi^2 , \tag{15}$$

and, expressing this in spherical polar co-ordinates (r, θ, φ), in which we take the θ-axis along the axis of symmetry, we find that

$$\frac{\partial^2 U}{\partial r^2} + \frac{\sin \theta}{r^2} \frac{\partial}{\partial \theta} \left(\frac{1}{\sin \theta} \frac{\partial U}{\partial \theta} \right) = \kappa r^2 \sin^2 \theta . \tag{16}$$

Let us seek a solution of this equation of the form

$$U = F(r) \sin^2 \theta . \tag{17}$$

Substituting in equation (16), this gives

$$r^2 \frac{d^2 F}{d r^2} - 2F = \kappa r^4 . \tag{18}$$

The solution of this equation, which is finite at the origin, is

$$U = \left(C r^2 + \frac{\kappa}{10} r^4 \right) \sin^2 \theta , \tag{19}$$

where C is an arbitrary constant.

Outside the liquid, the stream function, U', say, must satisfy the equation

$$\Delta U' = 0 . \tag{20}$$

Assuming a solution of the form (17), the solution which is finite at infinity is

$$U' = \frac{D}{r} \sin^2 \theta , \tag{21}$$

where D is an arbitrary constant. As was to be expected, equation (21) represents the field of a magnetic dipole of strength D centered at the origin.

4. *Solution for a nearly spherical boundary.*—We shall now suppose that the surface of the liquid is very nearly spherical and of mean radius a; the condition to be satisfied at this surface is the continuity of the magnetic field. By equation (3) this implies that

$$\frac{\partial U}{\partial r} = \frac{\partial U'}{\partial r} , \qquad \frac{\partial U}{\partial \theta} = \frac{\partial U'}{\partial \theta} , \tag{22}$$

where $r = a$. From equations (19) and (21) we find, to the first order, that

$$2Ca + \tfrac{2}{5} \kappa a^3 = -\frac{D}{a^2} , \tag{23}$$

$$Ca^2 + \frac{\kappa}{10} a^4 = \frac{D}{a} , \tag{24}$$

giving

$$C = -\tfrac{1}{6}\kappa a^2, \qquad D = -\tfrac{1}{15}\kappa a^2. \tag{25}$$

Hence the required stream functions inside and outside the liquid are, respectively,

$$U = \kappa(\tfrac{1}{10}r^4 - \tfrac{1}{6}a^2r^2)\sin^2\theta, \tag{26}$$

$$U' = -\frac{\kappa a^5}{15r}\sin^2\theta. \tag{27}$$

The line of foci inside the liquid where $\boldsymbol{H} = 0$, is given by $\partial U/\partial r = 0 = \partial U/\partial\theta$; and from equations (26) and (27) we find this to be the equatorial circle

$$r = (\tfrac{5}{6})^{1/2}a, \qquad \theta = \tfrac{1}{2}\pi; \tag{28}$$

it lies close to the surface.

The expressions for U and U' may be more conveniently expressed in terms of the intensity of the magnetic field at the poles, which is easily found to be

$$H_p = \tfrac{2}{15}\kappa a^2. \tag{29}$$

Substituting in equations (26) and (27), we find

$$U = \frac{H_p}{4a^2}(3r^4 - 5a^2r^2)\sin^2\theta, \tag{30a}$$

$$U' = -\frac{H_p}{2r}a^3\sin^2\theta. \tag{30b}$$

The value of the magnetic-field intensity at the origin is $\frac{1}{3}\kappa a^2$ or $\frac{5}{2}H_p$, i.e., five times the value of the intensity at the equator. This contrasts with Cowling's decaying magnetic field,[8] the central intensity of which is eighty times the equatorial surface value. It seems probable that this field may not satisfy the general conditions of equilibrium, and in this case we should expect some turbulence to be set up in the interior of the star on this account.

5. *The equation of the free surface.*—At the free surface the pressure must vanish, i.e., $p = 0$ when $r = a$. From equations (6) and (7) we find

$$\rho\omega^2\varpi\,d\varpi = dP + \frac{\Delta U}{4\pi\varpi^2}\,dU, \tag{31}$$

which, by equation (15), can be integrated to give the pressure equation

$$p + \rho\Omega + \frac{\kappa U}{4\pi} = \tfrac{1}{2}\rho\omega^2\varpi^2 + \text{Const.}, \tag{32}$$

At the surface of the liquid we must, therefore, have

$$\rho\Omega_s + \frac{\kappa U_s}{4\pi} = \tfrac{1}{2}\rho\omega^2\varpi_s^2 + \text{Const.}, \tag{33}$$

where the subscript s refers to the values of the variables at the surface.

Now, to the first order, we find

$$U_s = -\tfrac{1}{2}H_p\varpi_s^2; \tag{34}$$

and it is then clear from equation (33) that the effect of the magnetic field is the same as that of an angular velocity. Hence the surface of the liquid is very nearly an oblate spheroid (of small eccentricity, e, say).

The gravitational potential of a uniform spheroidal mass is of the form

$$\Omega_s = G\pi\rho\,(\alpha_0\varpi^2 + \gamma_0 z^2)\,, \tag{35}$$

and, when e is small, the values of the constants α_0 and γ_0 are given by

$$\alpha_0 = \tfrac{2}{3} - \tfrac{2}{15}e^2\,, \qquad \gamma_0 = \tfrac{2}{3} + \tfrac{4}{15}e^2\,, \tag{36}$$

very nearly, G being the gravitational constant. Substituting equations (34)–(36) in equation (33) we find

$$\left\{(\tfrac{2}{3} - \tfrac{2}{15}e^2)G\pi\rho^2 - \tfrac{1}{2}\rho\omega^2 - \frac{15}{16\pi}\frac{H_p^2}{a^2}\right\}\varpi^2 + (\tfrac{2}{3} + \tfrac{4}{15}e^2)G\pi\rho^2 z^2 = \text{Const.}\,; \tag{37}$$

but, since this represents a spheroid of eccentricity e, it follows that the coefficients of ϖ^2 and z^2 are in the ratio $1 - e^2 : 1$. Hence we find, after some simplification, that

$$e^2 = \frac{15\omega^2}{8G\pi\rho} + \frac{225}{64}\frac{H_p^2}{G\pi^2\rho^2 a^2}\,. \tag{38}$$

By setting $\omega = 0$ in this equation, we see that the effect of the magnetic field alone produces an eccentricity e, given by

$$e^2 = \frac{225H_p^2}{64G\pi^2\rho^2 a^2}\,. \tag{39}$$

Since the gravitational energy of a liquid sphere of radius a is

$$\mathfrak{W} = \tfrac{16}{15}G\pi^2\rho^2 a^2\,, \tag{40}$$

equation (26) may be written as

$$e^2 = \frac{15}{4}\frac{H_p^2 a^3}{\mathfrak{W}}\,, \tag{41}$$

an expression similar to one first given by Chandrasekhar and Fermi.[4]

6. *Numerical illustration.*—Condition (41) may be expressed in terms of the magnetic energy $\mathfrak{M}$ instead of H_p. Now $\mathfrak{M} = \iiint (H^2/8\pi)dv$ integrated over all space; using equation (26), we find that

$$\mathfrak{M} = \tfrac{5}{14}H_p^2 a^3\,; \tag{42}$$

whence, substituting in equation (41), we find the *ellipticity* $\mathfrak{E}$ $(= \tfrac{1}{2}e^2)$ to be

$$\mathfrak{E} = \frac{21}{4}\frac{\mathfrak{M}}{\mathfrak{W}}\,. \tag{43}$$

This expression shows that the flattening will be appreciable only if $\mathfrak{M}$ is comparable with $\mathfrak{W}$. To illustrate the order of magnitude involved, consider, first, the case of a magnetic star such as Babcock's, for which

$$H_p = 10^4 \text{ gauss}\,, \qquad a \sim R_\odot\,, \qquad M \sim M_\odot\,, \tag{44}$$

[4] For the case considered by them, the numerical factor in eq. (41) is $\frac{1}{4}$, or one-third the value given here.

where M denotes the mass of the star. Substituting these values in equation (43), taking $R_\odot = 6.96 \times 10^{10}$ cm, and $M_\odot = 1.99 \times 10^{33}$ gm, we find

$$\mathfrak{E} \sim 4 \times 10^{-8} ; \tag{45}$$

so that the effect of the magnetic field on the equilibrium of the star is negligible in this case.

For an S-type star, however, the effect begins to be appreciable, as was pointed out by Chandrasekhar and Fermi. For this star Babcock finds that

$$H_p \sim 1000 \text{ gauss} , \qquad a \sim 300 R_\odot , \qquad M \sim 15 M_\odot ; \tag{46}$$

and, inserting these values in equation (43), we find, very nearly,

$$\mathfrak{E} = 0.01 , \tag{47}$$

corresponding to a flattening at the poles of one part in a hundred.

This work arose during the course of a discussion with Dr. S. Chandrasekhar, to whom the author wishes to express his indebtedness. He also wishes to express his grateful thanks to the Geophysical Research Division of the Air Force for enabling him to undertake this work and to Yerkes Observatory for their generous hospitality.

ON THE RADIAL PULSATIONS OF AN INFINITE CYLINDER WITH A MAGNETIC FIELD PARALLEL TO ITS AXIS

EJNAR LYTTKENS*
Yerkes Observatory
Received October 30, 1953

ABSTRACT

This paper deals with the periods of the radial adiabatic pulsations of an infinitely conducting cylinder under its own gravity and a magnetic field parallel to its axis. For the case in which the magnetic field is a normal decay field in the cylinder, the characteristic values are tabulated.

I. THE AMPLITUDE EQUATION

In a recent paper Chandrasekhar and Fermi[1] dealt with the general equation governing the adiabatic radial pulsations of an infinitely conducting, infinitely long cylinder, under its own gravity and with a magnetic field parallel to its axis. In this paper we shall consider the explicit solutions of the pulsation equation.

Let r be the distance from the axis of the cylinder; m the mass per unit length interior to r; δr the deviation of r from its equilibrium value; H the strength of the magnetic field; ρ the density; γ the ratio between the specific heats; and G the constant of gravity. According to Chandrasekhar and Fermi,[1] the radial pulsations are governed by the equation

$$\frac{\partial^2}{\partial t^2}\,\delta r = 4\pi^2 r\,\frac{\partial}{\partial m}\left\{\left(\gamma p + \frac{H^2}{4\pi}\right)\rho\,\frac{\partial}{\partial m}(r\,\delta r)\right\} + \frac{4Gm}{r^2}\,\delta r\,, \tag{1}$$

where the magnetic permeability is assumed to be 1. Denoting by P the total pressure in radial direction,

$$P = p + \frac{H^2}{8\pi}, \tag{2}$$

we can rewrite equation (1) in the form

$$\left(\omega^2 + \frac{4Gm}{r^2}\right)\delta r = -4\pi^2 r\,\frac{d}{dm}\left\{\left[\gamma P + (2-\gamma)\frac{H^2}{8\pi}\right]\rho\,\frac{d}{dm}(r\,\delta r)\right\}, \tag{3}$$

in case all the physical variables vary with time like $e^{i\omega t}$. In equation (3) the boundary conditions are[1]

$$\delta r = 0 \qquad \text{for} \qquad r = 0\,, \tag{4}$$

$$\delta P = \left[\gamma p + (2-\gamma)\frac{H^2}{8\pi}\right]\rho\,\frac{d}{dm}(2\pi r\,\delta r) = 0 \qquad \text{for} \qquad r = R\,, \tag{5}$$

where δP means the amplitude of pulsations of the total pressure and R is the radius of the cylinder. If the space outside the cylinder is empty and if no magnetic field is present outside the cylinder, we have $P = 0$ for $r = R$; and therefore, according to equation (2), $H = 0$ for $r = R$. Then the boundary conditions are satisfied if the amplitude δr and its derivative are finite for $r = R$.

* On leave of absence from the Astronomical Observatory of the University of Uppsala, Uppsala, Sweden.

[1] *Ap. J.*, **118**, 116, 1953.

Now we consider the special case where the density is constant. Then

$$m = \pi \rho r^2 , \tag{6}$$

and

$$P = -\int_r^R \rho \frac{2Gm}{r}\, dr = \pi G \rho^2 (R^2 - r^2) , \tag{7}$$

where R is the radius of the cylinder.

Introducing expressions (6) and (7) for m and P into equation (3) and choosing r as the independent variable, we have

$$(\omega^2 + 4\pi G\rho)\, \delta r = -\frac{1}{\rho}\frac{d}{dr}\left\{\left[\gamma G\pi\rho^2 (R^2 - r^2) + (2-\gamma)\frac{H^2}{8\pi}\right]\frac{1}{r}\frac{d}{dr}(r\,\delta r)\right\}. \tag{8}$$

Letting

$$\frac{1}{\gamma}\left(\frac{\omega^2}{\pi G\rho} + 4\right) = A , \tag{9}$$

$$\left(\frac{2}{\gamma} - 1\right)\frac{H^2}{8\pi^2\rho^2 R^2 G} = f , \tag{10}$$

and introducing the new variables

$$x = \frac{r}{R}, \qquad \Psi = \frac{\delta r}{R} , \tag{11}$$

the differential equation takes the form

$$A\Psi = -\frac{d}{dx}\left\{(1 - x^2 + f)\frac{1}{x}\frac{d}{dx}(x\Psi)\right\}. \tag{12}$$

Introducing a function Φ, defined by

$$\frac{d\Phi}{dx} = \Psi , \tag{13}$$

and integrating, the equation can be rewritten in the form

$$A\Phi = -(1 - x^2 + f)\frac{1}{x}\frac{d}{dx}\left(x\frac{d\Phi}{dx}\right). \tag{14}$$

II. THE CHARACTERISTIC VALUES WITHOUT A MAGNETIC FIELD

At first we consider the pulsations when no magnetic field is present. Then equation (14) reduces to

$$A\varphi = -(1 - x^2)\frac{1}{x}\frac{d}{dx}\left(x\frac{d\varphi}{dx}\right), \tag{15}$$

where we use φ in order to distinguish it from the case where the magnetic field is present. This equation resembles the corresponding equation for a sphere.[2]

Seeking a solution of this equation in a power series of the form

$$\varphi = \sum_{k=0}^{k=\infty} a_k x^k , \tag{16}$$

[2] Cf. S. Rosseland, *The Pulsation Theory of Variable Stars* (Oxford: Clarendon Press, 1949), p. 28.

we obtain the following recurrence formula for the coefficients:

$$a_{k+2} = \frac{k^2 - A}{(k+2)^2}\, a_k . \tag{17}$$

Remembering that the amplitude $\delta r = 0$ for $r = 0$, we have

$$\frac{d\varphi}{dx} = 0 \qquad \text{for} \qquad x = 0 . \tag{18}$$

Thus $a_1 = 0$, and from formula (17) it is seen that all a_n with odd indices vanish as well, so that series (16) contains only even powers of x. Therefore, we rewrite formula (17) as follows:

$$\frac{a_{2j+2}}{a_{2j}} = \frac{j^2 - A^2/4}{j^2 + 2j + 1} . \tag{19}$$

From this formula it is seen that series (16) converges according to Gauss's criterion,[3] even when $x = 1$. For the derivative of series (16) the ratio between two consecutive nonvanishing coefficients is

$$\frac{(2j+2)\, a_{2j+2}}{2j a_{2j}} = \frac{j^3 + j^2 - (j+1)\, A^2/4}{j^3 + 2j^2 + j} . \tag{20}$$

Here the difference between the coefficients for the next highest power of j in the denominator and that in the numerator is only 1, and therefore the series is generally divergent. The only exception is when A is the square of an even number, for series (16) then bounds at $k = \sqrt{A}$. The characteristic values for A, when no magnetic field is present are, therefore,

$$A_1 = 4, \qquad A_2 = 16, \qquad A_3 = 36, \ldots, \; A_n = 4n^2, \ldots . \tag{21}$$

Let the nth characteristic function of equation (15) be denoted by φ_n; the corresponding amplitude is then given by

$$\psi_n = \frac{d\varphi_n}{dx} . \tag{22}$$

The amplitudes are subject to the following orthogonality relation:

$$\int_0^1 \psi_j \psi_k x\, dx = 0 , \tag{23}$$

which can be considered a special case of that given by Chandrasekhar and Fermi.[1] By partial integration we have (cf. eq. [22])

$$\int_0^1 \psi_j \psi_k x\, dx = -\int_0^1 \varphi_k \frac{d}{dx}\left(x \frac{d\varphi_j}{dx}\right) dx . \tag{24}$$

Remembering that the jth characteristic value of equation (15) is $4j^2$, we have

$$\int_0^1 \psi_j \psi_k x\, dx = 4 j^2 \int_0^1 \frac{\varphi_j \varphi_k}{1 - x^2}\, x\, dx . \tag{25}$$

Since this formula must be valid even if j and k are interchanged, the integrals vanish if $j \neq k$. Further, we choose the arbitrary factor in the characteristic functions so that

[3] Cf. E. Goursat, *A Course in Mathematical Analysis* (Boston: Athenaeum Press, 1904), I, 344.

we have

$$\int_0^1 \psi_j \psi_k x\,dx = 4\,j^2 \int_0^1 \frac{\varphi_j \varphi_k}{1-x^2}\,x\,dx = \begin{cases} 1 & \text{if} \quad j = k \\ 0 & \text{if} \quad j \neq k\,. \end{cases} \tag{26}$$

Characteristic functions, normalized in this fashion, are

$$\begin{aligned} \varphi_1 &= 1 - x^2\,, \\ \varphi_2 &= \frac{1}{\sqrt{2}}\,(1 - 4x^2 + 3x^4)\,, \\ \varphi_3 &= \frac{1}{\sqrt{3}}\,(1 - 9x^2 + 18x^4 - 10x^6)\,, \\ &\cdots\cdots\cdots\cdots \end{aligned} \tag{27}$$

while the corresponding amplitudes are

$$\begin{aligned} \psi_1 &= -2x\,, \\ \psi_2 &= -\frac{1}{\sqrt{2}}\,(8x - 12x^3)\,, \\ \psi_3 &= -\frac{1}{\sqrt{3}}\,(18x - 72x^3 + 60x^5)\,, \\ &\cdots\cdots\cdots\cdots \end{aligned} \tag{28}$$

III. A SIMPLE ASSUMPTION CONCERNING THE MAGNETIC FIELD

If the magnetic field is proportional to the square root of the pressure, i.e.,

$$f(x) = B\,(1 - x^2)\,, \tag{29}$$

where B is a constant, equation (14) takes the form

$$\frac{A}{1+B}\,\Phi = -\,(1-x^2)\,\frac{d}{dx}\left(x\,\frac{d\Phi}{dx}\right). \tag{30}$$

By comparing this equation with equation (15) it is immediately seen that the characteristic functions are the same as in the case of no magnetic field, while the characteristic values are multiplied by the factor $(1 + B)$. Thus, with the aid of relation (21), we obtain

$$A_n = 4\,n^2\,(1+B)\,. \tag{31}$$

IV. A DECAY FIELD

In dealing with the pulsations we assume that the electrical conductivity is infinite. In this section, however, we shall investigate a field subject to secular changes so slow that they do not affect the pulsations. Neglecting displacement currents, Maxwell's equations can be written, if electromagnetic units are used, as follows:

$$\begin{aligned} \frac{d\boldsymbol{H}}{dt} &= -\,\mathrm{curl}\,\boldsymbol{E}\,, \\ \mathrm{curl}\,\boldsymbol{H} &= 4\pi\sigma\boldsymbol{E}\,, \end{aligned} \tag{32}$$

where $\boldsymbol{H}$ is the magnetic field strength, $\boldsymbol{E}$ the electric field strength, and σ the electric conductivity. Eliminating $\boldsymbol{E}$, we obtain, on using the condition div $\boldsymbol{H} = 0$,

$$\frac{d\boldsymbol{H}}{dt} = \frac{1}{4\pi\sigma}\nabla^2\boldsymbol{H}\,. \tag{33}$$

If $\boldsymbol{H}$ is proportional to $e^{-t/\tau}$, t denoting the time and τ being a constant, we get

$$\nabla^2\boldsymbol{H} = -\frac{4\pi\sigma}{\tau}\boldsymbol{H}\,, \tag{34}$$

in accordance with Elsasser.[4] In cylindrical co-ordinates the magnetic field being an axial symmetric one in the direction of the axis, we have

$$\frac{d^2H}{dr^2} + \frac{1}{r}\frac{dH}{dr} + k^2H = 0\,, \tag{35}$$

where

$$k^2 = \frac{\tau}{4\pi\sigma}\,. \tag{36}$$

The solution of this equation appropriate to the problem on hand is

$$H = CJ_0(kr)\,, \tag{37}$$

where J_0 denotes the zero-order Bessel function. The constant k is to be chosen so that the field vanishes for $r = R$. Evidently, the lowest value of k, and therefore the longest decay time, is obtained if J_0 reaches its *first* zero on the surface of the cylinder, and this case will be especially considered. Then

$$H = CJ_0(xx_1)\,, \tag{38}$$

where x_1 is the first zero of the function $J_0(x)$.

With the notation used in equation (14), we put

$$f = BJ_0^2(xx_1)\,, \tag{39}$$

so that the equation can be written as follows:

$$A\Phi = [1 - x^2 + BJ_0^2(xx_1)]\frac{1}{x}\frac{d}{dx}\left(x\frac{d\Phi}{dx}\right). \tag{40}$$

V. CHARACTERISTIC FUNCTIONS AND CHARACTERISTIC VALUES

In the case of a magnetic field proportional to the square root of the pressure, it has been shown in Section III that the characteristic functions are the same as if there were no magnetic field. For even functions $f(x)$, it therefore seems reasonable that an expression of the form

$$\Phi = c_1\varphi_1 + c_2\varphi_2 + \ldots + c_n\varphi_n \tag{41}$$

should yield a good approximation of the characteristic functions if the constants c_1, c_2, . . . , c_n are suitably chosen. The corresponding expression for the amplitude is

$$\Psi = c_1\psi_1 + c_2\psi_2 + \ldots + c_n\psi_n\,. \tag{42}$$

Letting

$$x\Psi = U\,, \tag{43}$$

[4] *Phys. Rev.*, **69**, 106, 1946.

we can write equation (12) in the form

$$\frac{A}{x}\,U = -\frac{d}{dx}\left\{(1-x^2+f)\frac{dU}{dx}\right\}, \tag{44}$$

while the characteristic functions of this equation are approximated by

$$U = c_1 x\psi_1 + c_2 x\psi_2 + \ldots + c_n x\psi_n\,. \tag{45}$$

Following Rietz's method, we choose the constants $c_1, c_2, \ldots, c_n$ so as to minimize the quotient:

$$\mathfrak{A} = \frac{\int_0^1 U\,\frac{d}{dx}\left\{(1-x^2+f)\frac{dU}{dx}\right\}dx}{\int_0^1 \frac{1}{x}\,U^2 dx}\,. \tag{46}$$

Substituting expression (45) for U and differentiating with respect to c_j, we obtain

$$\frac{\partial \mathfrak{A}}{\partial c_j} = \frac{2\sum_{k=1}^{k=s} c_k \int_0^1 x\psi_j \frac{d}{dx}\left\{(1-x^2+f)\frac{d}{dx}(x\psi_k)\right\}dx - 2\mathfrak{A}\sum_{k=1}^{k=s} c_k \int_0^1 \psi_j\psi_k x\,dx}{\sum_{j=1}^{j=s}\sum_{k=1}^{k=s} c_j c_k \int_0^1 \psi_j\psi_k x\,dx}\,. \tag{47}$$

This expression should vanish when $\mathfrak{A}$ is minimum. Since the functions ψ_n are orthogonal and normalized (see eq. [26]), the foregoing reduces to the relation

$$\mathfrak{A}\,c_j + \sum_{k=1}^{k=s} c_k \int_0^1 x\psi_j \frac{d}{dx}\left\{(1-x^2+f)\frac{1}{x}\frac{d}{dx}(x\psi_k)\right\}dx = 0\,. \tag{48}$$

On integrating this equation by parts and remembering that f vanishes for $x = 1$, we obtain

$$\mathfrak{A}\,c_j - \sum_{k=1}^{k=s} c_k \int_0^1 (1-x^2+f)\frac{1}{x}\frac{d}{dx}\left(x\frac{d\varphi_k}{dx}\right)\frac{d}{dx}\left(x\frac{d\varphi_j}{dx}\right)dx = 0\,, \tag{49}$$

where we have replaced ψ_n by the derivative of φ_n. Making use of equation (15), the nth characteristic value of which is shown to be $4n^2$, and applying the relation (26), we get

$$(\mathfrak{A} - 4j^2)\,c_j - \sum_{k=1}^{k=s} 16\,j^2k^2\,c_k \int_0^1 \frac{\varphi_j\varphi_k}{(1-x^2)^2}\,x\,f\,dx = 0\,. \tag{50}$$

Combining the equations for $j = 1, 2, \ldots, s$, we get a linear homogeneous equation system for the coefficients c_j. In order to get a nonvanishing solution, $\mathfrak{A}$ must be chosen so that the determinant of the system vanishes. The n values of $\mathfrak{A}$ for which this condition is fulfilled are upper limits to the n first characteristic values.

If only the first characteristic function is retained in equation (50), we get

$$\mathfrak{A}_1 = 4 + 16\int_0^1 x\,f\,dx \tag{51}$$

as an approximation to the first characteristic value. With the aid of the definition equations (9) and (10) for $\mathfrak{A}$ and f, the same result is obtained from Chandrasekhar and Fermi's formula,[1]

$$\omega^2 \int_0^M r^2 dm = 2(\gamma - 1) GM^2 + (2 - \gamma) \int_0^R H^2 r \, dr . \tag{52}$$

In both cases the amplitude of the first characteristic function is treated as if it were proportional to the distance from the axis of the cylinder.

Returning to the decay field (39),

$$f = BJ_0^2(xx_1) ,$$

and writing

$$a_{jk} = 16 j^2 k^2 \int_0^1 \frac{x\varphi_j\varphi_k}{(1-x^2)^2} J_0^2(xx_1) \, dx , \tag{53}$$

we obtain from equation (50) the following system of equations, if the first three characteristic functions are retained:

$$\begin{cases} (Ba_{11} + 4 - \mathfrak{A})\, c_1 + Ba_{12} c_2 + Ba_{13} c_3 = 0 , \\ Ba_{12} c_1 + (Ba_{22} + 16 - \mathfrak{A})\, c_2 + Ba_{23} c_3 = 0 , \\ Ba_{13} c_1 + Ba_{23} c_2 + (Ba_{33} + 36 - \mathfrak{A})\, c_3 = 0 . \end{cases} \tag{54}$$

It should be noted that the expression

$$\frac{x\varphi_j\varphi_k}{(1-x^2)^2} \tag{55}$$

reduces to an odd polynomial of degree $2j + 2k - 3$. In order to compute the quantity a_{jk}, given by formula (53), we need the integral

$$\int_0^1 x^n J_0^2(xx_1) \, dx . \tag{56}$$

For the derivation, the following easily verified relations are required:

$$\frac{d}{dx}\left\{\frac{x^2}{2}[J_0^2(xx_1) + J_1^2(xx_1)]\right\} = xJ_0^2(xx_1) , \tag{57}$$

$$\frac{d}{dx}\{xJ_0(xx_1)J_1(xx_1)\} = xx_1\{J_0^2(xx_1) - J_1^2(xx_1)\} , \tag{58}$$

where J_1 denotes the first-order Bessel function. Integrating expression (56) partially, remembering that x_1 is a zero of J_0, and writing $J_0^2 - (J_0^2 - J_1^2)$ instead of J_1^2 under the sign of integration, we have

$$\int_0^1 x^n J_0^2(xx_1) \, dx = \tfrac{1}{2} J_1^2(x_1) - (n-1) \int_0^1 x^n J_0^2(xx_1) \, dx + \frac{n-1}{2} \int_0^1 x^n [J_0^2(xx_1) - J_1^2(xx_1)] \, dx . \tag{59}$$

If the last term is integrated partially twice and if the expression thus obtained is solved for the wanted integral, we get

$$\int_0^1 x^n J_0^2(xx_1) \, dx = \frac{1}{2n} J_1^2(x_1) - \frac{(n-1)^3}{4nx_1^2} \int_0^1 x^{n-2} J_0^2(xx_1) \, dx . \tag{60}$$

When this formula is used for odd values of n, in which we are interested, we start with $n = 1$, in which case we have

$$\int_0^1 x J_0^2(x x_1)\, dx = \tfrac{1}{2} J_1^2(x_1)\,. \tag{61}$$

The first three characteristic values, as calculated from the vanishing determinant of equation system (54), are found in the second column of Table 1. The ratios between

TABLE 1*

CHARACTERISTIC VALUES AND RATIOS BETWEEN EXPANSION COEFFICIENTS, WHEN CHARACTERISTIC FUNCTIONS ARE APPROXIMATED BY LINEAR EXPRESSIONS IN FIRST THREE CHARACTERISTIC FUNCTIONS WITHOUT MAGNETIC FIELD

FIRST CHARACTERISTIC VALUE

B	$\mathfrak{A}_1$	q_1	l_1	c_2/c_1	c_3/c_1
0.1	4.21199	4.21199	4.21199	−0.01682	−0.00135
0.2	4.41737	4.41737	4.41737	− .03203	− .00206
0.3	4.61696	4.61696	4.61696	− .04663	− .00226
0.4	4.81142	4.81141	4.81141	− .05996	− .00205
0.5	5.00127	5.00126	5.00126	− .07242	− .00151
0.6	5.18698	5.18697	5.18696	− .08412	− .00070
0.7	5.36900	5.36891	5.36890	− .09514	+ .00033
0.8	5.54745	5.54741	5.54740	− .10557	+ .00154
0.9	5.72280	5.72276	5.72274	− .11544	+ .00288
1.0	5.89524	5.89519	5.89517	− .12483	+ .00435
1.1	6.06497	6.06493	6.06491	− .13376	+ .00591
1.2	6.23220	6.23216	6.23214	− .14229	+ .00754
1.3	6.39708	6.39704	6.39703	− .15044	+ .00923
1.4	6.55976	6.55974	6.55973	− .15824	+ .01096
1.5	6.72039	6.72038	6.72037	− .16572	+ .01273
1.6	6.87909	6.87908	6.87908	− .17290	+ .01452
1.7	7.03597	7.03596	7.03596	− .17980	+ .01632
1.8	7.19112	7.19111	7.19111	− .18645	+ .01814
1.9	7.34466	7.34463	7.34462	− .19285	+ .01996
2.0	7.49665	7.49660	7.49658	−0.19902	+0.02178

SECOND CHARACTERISTIC VALUE

B	$\mathfrak{A}_2$	q_2	l_2	c_1/c_2	c_3/c_2
0.1	16.6863	16.6861	16.6859	+0.01678	−0.02871
0.2	17.3473	17.3470	17.3467	+ .03219	− .05526
0.3	17.9861	17.9857	17.9855	+ .04645	− .07978
0.4	18.6052	18.6050	18.6049	+ .05975	− .10245
0.5	19.2070	19.2070	19.2069	+ .07224	− .12342
0.6	19.7938	19.7935	19.7932	+ .08403	− .14283
0.7	20.3673	20.3660	20.3649	+ .09520	− .16084
0.8	20.9293	20.9261	20.9232	+ .10584	− .17756
0.9	21.4812	21.4748	21.4690	+ .11600	− .19312
1.0	22.0242	22.0132	22.0027	+ .12573	− .20761
1.1	22.5594	22.5422	22.5250	+ .13507	− .22114
1.2	23.0877	23.0627	23.0363	+ .14405	− .23380
1.3	23.6101	23.5753	23.5368	+ .15270	− .24565
1.4	24.1271	24.0806	24.0269	+ .16105	− .25678
1.5	24.6395	24.5793	24.5066	+ .16912	− .26723
1.6	25.1477	25.0718	24.9760	+ .17692	− .27708
1.7	25.6522	25.5586	25.4351	+ .18448	− .28637
1.8	26.1535	26.0401	25.8838	+ .19180	− .29514
1.9	26.6519	26.5167	26.3220	+ .19891	− .30344
2.0	27.1477	26.9887	26.7495	+0.20580	−0.31130

TABLE 1—*Continued*

THIRD CHARACTERISTIC VALUE

B	$\mathfrak{A}_3$	q_3	l_3†	c_1/c_3	c_2/c_3
0.1	37.529	37.507	37.477	+0.00183	+0.02869
0.2	39.090	39.007	38.876	+ .00384	+ .05514
0.3	40.679	40.499	40.187	+ .00596	+ .07951
0.4	42.293	41.984	41.395	+ .00816	+ .10196
0.5	43.928	43.464	42.481	+ .01039	+ .12267
0.6	45.583	44.938	43.418	+ .01262	+ .14177
0.7	47.255	46.408	44.173	+ .01484	+ .15943
0.8	48.942	47.873	44.698	+ .01702	+ .17576
0.9	50.642	49.333	44.928	+ .01915	+ .19089
1.0	52.354	50.788	.....	+ .02123	+ .20491
1.1	54.077	52.239	.....	+ .02325	+ .21800
1.2	55.808	53.686	.....	+ .02521	+ .23016
1.3	57.549	55.129	.....	+ .02711	+ .24151
1.4	59.296	56.568	.....	+ .02893	+ .25212
1.5	61.051	58.002	.....	+ .03070	+ .26204
1.6	62.811	59.432	.....	+ .03241	+ .27135
1.7	64.577	60.858	.....	+ .03404	+ .28009
1.8	66.348	62.280	.....	+ .03561	+ .28830
1.9	68.123	63.698	.....	+ .03713	+ .29605
2.0	69.903	65.111	.....	+0.03859	+0.30336

* $\mathfrak{A}_1$, $\mathfrak{A}_2$, $\mathfrak{A}_3$ = the three zeros of the determinant of eqs. (54), upper limits of the first three characteristic values. c_1, c_2, c_3 = expansion coefficients, determined from eqs. (54). q_2 = the quotient (79); for the first characteristic value, also an upper limit. l_1, l_2, l_3 = lower limits of the characteristic values.

† The lower limit 44.928 is adopted also when $B > 0.9$.

the corresponding coefficients, c_1, c_2, and c_3, are found in the last two columns of the same table.

VI. LOWER LIMITS OF THE CHARACTERISTIC VALUES

From equation (14) we form the quotients

$$q_1 = \frac{\int_0^1 (1 - x^2 + f)\frac{1}{x}\left\{\frac{d}{dx}\left(x\frac{d\Phi}{dx}\right)\right\}^2 dx}{\int_0^1 \Phi\frac{d}{dx}\left(x\frac{d\Phi}{dx}\right)dx}, \tag{62}$$

$$q_2 = \frac{\int_0^1 \Phi\frac{d}{dx}\left(x\frac{d\Phi}{dx}\right)dx}{\int_0^1 \frac{x}{1 - x^2 + f}\Phi^2 dx}. \tag{63}$$

If Φ is a two-times differentiable function, which satisfies the boundary conditions, we have

$$A_1 \leqq q_2 \leqq q_1 . \tag{64}$$

The boundary conditions, implying zero amplitude at the axis and vanishing δP (see eq. [5]) at the surface of the cylinder, give, when applied to equation (14),

$$\frac{d\Phi}{dx} = 0 \qquad \text{for} \qquad x = 0 , \tag{65}$$

$$\Phi = 0 \qquad \text{for} \qquad x = 1 . \tag{66}$$

If just the first characteristic function is introduced, the equality signs of relation (64) are valid. If l_2 is a lower limit for the second characteristic value, we have

$$q_2 - \frac{q_1 - q_2}{(l_2/q_2) - 1} \leqq A_1 , \tag{67}$$

provided that Φ approximated the first characteristic function so well that

$$q_2 < l_2 . \tag{68}$$

Generally, if L_{n-1} is an upper limit for the $(n-1)$th characteristic value and l_{n+1} a lower limit for the $(n+1)$th characteristic value and if

$$L_{n-1} < q_2 < l_{n+1} , \tag{69}$$

the upper and lower limits of the nth characteristic value are given by Temple's condition,[5]

$$q_2 - \frac{q_1 - q_2}{(l_{n+1}/q_2) - 1} \leqq A_n \leqq q_2 - \frac{q_1 - q_2}{(L_{n-1}/q_2) - 1} . \tag{70}$$

As a first trial, let $\Phi = \varphi_n$ (φ_n being the nth characteristic function, when no magnetic field is present), when the nth characteristic value is considered. Using equation (15) (the nth characteristic value of which is $4n^2$) and the normalization condition as given by relation (26), we have, from formulae (62) and (63),

$$q_1 = 4n^2 + 16n^4 \int_0^1 \frac{x\varphi_n^2}{(1-x^2)^2} f\,dx , \tag{71}$$

$$q_2 = \frac{1}{\int_0^1 \frac{x\varphi_n^2}{1-x^2+f}\,dx} . \tag{72}$$

For the first characteristic value the expression for q_1 is identical with approximation (51). For the special case

$$f = BJ_0^2(xx_1) ,$$

we have

$$\begin{aligned} q_1 &= 4 + 2.1561B \quad \text{for} \quad \Phi = \varphi_1 , \\ q_1 &= 16 + 6.9987B \quad \text{for} \quad \Phi = \varphi_2 , \\ q_1 &= 36 + 15.1187B \quad \text{for} \quad \Phi = \varphi_3 , \\ &\cdots\cdots\cdots\cdots\cdots\cdots \end{aligned} \tag{73}$$

It has already been pointed out that, for the first characteristic value, q_1 is identical with approximation (51). For the higher characteristic values, q_1 lies between the limits given by relation (70). Therefore, q_1 is a convenient approximation for the characteristic values for small values of B. The upper and lower limits of the first three characteristic values, obtained by using the corresponding characteristic functions without magnetic field, are given in Table 2. By calculating q_2 from expression (72), the Euler-MacLaurin formula for numerical integration was used. As upper limit of the first characteristic value, the quantity q_2 was used. Then upper limits of the second and third characteristic values could be obtained successively from relation (70). As lower limit of the fourth charac-

[5] Cf. L. Collatz, *Numerische Behandlung von Differentialgleichungen* (Berlin: Springer-Verlag, 1951), p. 172.

teristic value, we took the characteristic value without the magnetic field, namely, 64. Then upper limits for the third, second, and first characteristic values could be obtained successively from relation (70).

Combining formulae (13) and (43), we have

$$U = x\frac{d\Phi}{dx}. \tag{74}$$

If this value of U is introduced into the quotient (46) and if the expression thus obtained is integrated partially in the numerator as well as in the denominator, a comparison with formula (62) shows that

$$\mathfrak{A} = q_1 . \tag{75}$$

TABLE 2

CHARACTERISTIC VALUES, OBTAINED IF CHARACTERISTIC FUNCTIONS ARE CONSIDERED UNCHANGED BY MAGNETIC FIELD

B	First Characteristic Value			Second Characteristic Value			Third Characteristic Value		
	Linear Approximation	Upper Limit	Lower Limit	Linear Approximation	Upper Limit	Lower Limit	Linear Approximation	Upper Limit	Lower Limit
0.1	4.216	4.213	4.212	16.70	16.71	16.66	37.51	37.55	37.41
.2	4.431	4.421	4.417	17.40	17.43	17.26	39.02	39.16	38.60
.3	4.647	4.624	4.617	18.10	18.16	17.80	40.54	40.83	39.59
.4	4.862	4.824	4.811	18.80	18.90	18.28	42.05	42.55	40.34
0.5	5.078	5.021	5.000	19.50	19.65	18.72	43.56	44.33	40.86

In order to get closer limits for the characteristic values, we assume

$$\Phi = c_1\varphi_1 + c_2\varphi_2 + \ldots + c_s\varphi_s , \tag{76}$$

and when the nth characteristic value is concerned, take for $c_1, c_2, \ldots, c_s$ the values determined by putting $A = A_n$ into equations (50). Since $\mathfrak{A}_n$ is an upper limit of the nth characteristic value, we have in this case a better upper limit than that given by (70); thus

$$q_2 - \frac{q_1 - q_2}{(l_{n+1}/q_2) - 1} \leqq A_n \leqq q_1 = \mathfrak{A}_n . \tag{77}$$

In order to determine q_2, we use the same approximation for Φ in formula (63):

$$q_2 = \frac{\sum_{j=1}^{j=s'}\sum_{k=1}^{k=s'} c_j c_k \int_0^1 \varphi_j \frac{d}{dx}\left(x\frac{d\varphi_k}{dx}\right)dx}{\sum_{j=1}^{j=s}\sum_{k=1}^{k=s} c_j c_k \int_0^1 \frac{x}{1-x^2+f}\varphi_j\varphi_k dx} . \tag{78}$$

Making use of equation (15) and remembering that the kth characteristic value of that

equation is $4k^2$, we get, with the aid of condition (26),

$$q_2 = \frac{\sum_{j=1}^{j=s} c_j^2}{\sum_{j=1}^{j=s}\sum_{k=1}^{k=s} c_j c_k \int_0^1 \frac{x}{1-x^2+f}\varphi_j\varphi_k dx}. \tag{79}$$

In the case of the decay field (39), $f = BJ_0^2(xx_1)$, the upper limits for the first three characteristic values, together with the corresponding values of the constants c_1, c_2, and c_3, have already been found from the equation system (54). Then, for the approximate characteristic functions thus obtained, q_2 was computed with the aid of formula (79), the integrals being evaluated with the aid of the Euler-MacLaurin formula. The values of q_2 are given in the third column of Table 2. For the first characteristic value, q_2 is also an upper limit. For the second characteristic value, q_2 would be an upper limit, if the expression for the first characteristic function were exact. Since the first characteristic function seems to be well approximated, we may expect that the second characteristic value does not exceed q_2 by any appreciable amount. However, it should be stated that this argument is not rigorous. The lower limit of the third characteristic value, as calculated from relation (70), by using the lower limit 64 of the fourth characteristic value, reached the value 44.928 for $B = 0.9$; but from $B = 1.0$, lower values of that limit are obtained. Since the characteristic values increase with B, we have adopted the value 44.928 for the lower limit of the third characteristic value when $B \geqq 0.9$. Thereafter, lower limits for the second and first characteristic values were obtained successively from relation (70).

At least for the first and second characteristic values, the linear approximation (73) gives the order of magnitude rather well; for $B = 2.0$, the error is about 10 per cent.

Finally, I wish to thank Dr. S. Chandrasekhar, who suggested this investigation to me, for his encouraging interest and valuable advice during the performance of this work. Also I would like to express my gratitude to the Royal Swedish Academy of Science and to the Sweden-America Foundation for fellowships, which made my stay at Yerkes Observatory possible.

COMPTON SCATTERING BY ELECTRON ATMOSPHERES
II. PROBLEMS WITH INCIDENT NORMAL FLUX

FRANK N. EDMONDS, JR.
Department of Mathematics and Astronomy, University of Texas, Austin, Texas
Received October 12, 1953

ABSTRACT

The problem of the transfer of radiation in an atmosphere of free electrons is solved in the first approximation for two sets of boundary conditions involving an incident normal flux, that of the planetary nebula problem and that of no incident diffuse radiation field. In the solution, account is taken of the noncoherent character of the electron scattering due to the Doppler shifts arising from a Maxwellian distribution of thermal velocities, the red shift of the Compton effect, and a non-Doppler blue shift arising from thermal motions and first pointed out by Dirac. The latter two effects, designated as "Compton scattering," are shown to produce asymmetries in spectral lines which would be very difficult to detect for very high temperatures, as they are much smaller than the thermal broadening. In an appendix, application of the solutions obtained to multiple Compton scattering of low-energy gamma radiation is considered.

I. INTRODUCTION

In an earlier paper[1] the transfer of radiation in an atmosphere of free electrons was analyzed under the conditions of the standard Schuster problem of line formation. In this analysis account was taken of the noncoherent character of the electron scattering due to three effects: the Doppler shifts arising from a Maxwellian distribution of thermal velocities, the red shift of the Compton effect, and a non-Doppler blue shift arising from the thermal motions and first pointed out by Dirac.[2] The latter two effects, designated as "Compton scattering," as well as the first, are accounted for by the spectral-distribution function for scattered radiation as determined in the second approximation.[3]

When the electron atmosphere is sufficiently far removed from the source of incident radiation, the applicability of the Schuster problem boundary conditions is questionable. Therefore, in this paper the transfer of radiation in an atmosphere of free electrons under conditions of an incident normal flux will be investigated in a manner analogous to the investigation of the Schuster problem in Paper I. Two different boundary conditions will be considered: those of no incident diffuse radiation field and those of the planetary nebula problem.[4] The appropriate equation of transfer, using the second-approximation spectral-distribution function, is solved in the first approximation, subject to these two sets of boundary conditions; and the solution for radiation emerging from the atmosphere is used to determine the changes produced in the profiles of spectral lines by the noncoherent scattering. As for the Schuster problem, it is shown that the changes produced by Compton scattering will be difficult to detect even under the most favorable conditions of a high-temperature atmosphere (7.5×10^5 ° K). Although the non-Doppler blue shift is about fifty-five times the Compton red shift, the resulting asymmetry to the blue is less than 5 per cent of the thermal broadening, which for

[1] F. N. Edmonds, Jr., *Ap. J.*, **119**, 58, 1953. This paper will be referred to as "Paper I" and equations in this paper will be designated by prefixing "I," e.g., "equation I (4)."

[2] *M.N.*, **85**, 825, 1925.

[3] F. N. Edmonds, Jr., *Ap. J.*, **117**, 298, 1953.

[4] Cf. E. A. Milne, *Zs. f. Ap.*, **1**, 98, 1930. The term "planetary nebula" is used here not just to designate a class of galactic objects but as the more general designation of any spherically symmetric shell surrounding a star at a distance much larger than the stellar radius.

such high temperatures should effectively mask a shift of the center of the line of approximately 0.5 A.

In an appendix to this paper computational problems involved in the application of the solutions for emergent radiation to the problem of multiple Compton scattering of low-energy gamma radiation are briefly discussed.

II. EMISSION COEFFICIENTS AND TRANSFORMATION OF THE EQUATION OF TRANSFER

It will be supposed that a flux is normally incident on the inner surface of a plane-parallel atmosphere of finite optical thickness and consisting of free electrons in thermal motion. This flux, $\pi F(\nu)$, has a known flux density distribution in frequency ν, and the thermal motions of the electrons are described by a Maxwellian distribution of velocities associated with a kinetic temperature, T, which is constant throughout the atmosphere. There is an incident diffuse radiation field only for the planetary nebula problem and only on the inner surface. This radiation field is symmetric with respect to the outward normal and is determined completely as to intensity distribution in frequency and direction.[4]

The incident normal flux introduces an additional term in the source function of the equation of transfer which represents the scattering by electrons in the atmosphere of $\pi F(\nu)$. The corresponding emission coefficient is

$$j'(\nu, \tau, \mu) = N_e \sigma_e \tfrac{3}{4}(1 + \cos^2\Theta) \int_0^\infty \pi F(\nu')\, e^{-(\tau_1 - \tau)} \psi(\nu, \Theta, \nu')\, d\nu' , \tag{1}$$

where N_e is the number of free electrons per cubic centimeter, σ_e the electron-scattering coefficient (eq. I [2]), Θ the angle of scattering, τ the optical depth (eq. I [1]), τ_1 the optical thickness of the atmosphere, and $\psi(\nu, \Theta, \nu')$ the spectral-distribution function for scattered radiation (eq. I [6]). The exponential factor in the integrand of equation (1) represents the reduction in the flux by electron scattering as it passes through the atmosphere. Since this flux is in the direction of the outward normal of the atmosphere,

$$\cos\Theta = \cos\theta = \mu , \tag{2}$$

where θ is the polar angle with respect to the outward normal. The transformation of variables, given by equations I (8) and equations (2) and I (6), changes equation (1) to

$$j'(a, \tau, \mu) = \frac{N_e \sigma_e}{4\sqrt{\pi}} \frac{\tfrac{3}{4}(1 + \mu^2)}{(1 - \mu)^{1/2}} \int_{-\infty}^{\infty} F(a')\, e^{-(\tau_1 - \tau)} \left[1 - \frac{3}{2} \left(\frac{4kT}{mc^2} \right)^{1/2} (a' - a) \right] \times \exp\left\{ \frac{-(a' - a)^2}{1 - \mu} + 2 \left(\frac{mc^2}{4kT} \right)^{1/2} \frac{h\nu_0}{mc^2} (a' - a) \right\} da' . \tag{3}$$

The equation of radiative transfer for the electron atmosphere is

$$\mu \frac{\partial I(a, \tau, \mu)}{\partial \tau} = I(a, \tau, \mu) - \frac{1}{N_e \sigma_e} [\, j(a, \tau, \mu) + j'(a, \tau, \mu) \,] , \tag{4}$$

where the emission coefficient for scattering of the diffuse radiation field within the atmosphere $j(a, \tau, \mu)$ is given by equation I (10). The emission coefficient $j'(a, \tau, \mu)$ makes equation (4) inhomogeneous in $I(a, \tau, \mu)$. The boundary conditions for the planetary nebula problem are

$$I(a, 0, -\mu) \equiv 0 , \qquad I(a, \tau_1, \mu) = I(a, \tau_1, -\mu) \qquad (\mu \geq 0) ; \tag{5}$$

and for no incident diffuse radiation field they are

$$I(a, 0, -\mu) \equiv I(a, \tau_1, \mu) \equiv 0 \qquad (\mu \geq 0) . \tag{6}$$

As in Paper I, it will be necessary to transform the equation of transfer in order to remove the mixing of frequencies in the emission coefficients which prevents solution of the equation by normal methods. Multiplication by $e^{i\xi\alpha}/\sqrt{(2\pi)}$ and integration over α transforms equation (4) to the following form:

$$\mu \frac{\partial \chi(\xi, \tau, \mu)}{\partial \tau} = \chi(\xi, \tau, \mu) - \int \frac{d\omega'}{4\pi} \chi(\xi, \tau, \mu') \tfrac{3}{4}(1+\cos^2\Theta)$$
$$\times [1 + i\tfrac{3}{2}\beta\gamma(1-\cos\Theta)\xi] \exp\{-(1-\cos\Theta)(\tfrac{1}{4}\xi^2 + i\tfrac{3}{2}\beta\xi)\} \quad (7)$$
$$-\tfrac{3}{4}(1+\mu^2) G(\xi)\, e^{-(\tau_1-\tau)} [1 + i\tfrac{3}{2}\beta\gamma(1-\mu)\xi] \exp\{-(1-\mu)(\tfrac{1}{4}\xi^2 + i\tfrac{3}{2}\beta\xi)\},$$

where γ and β are parameters defined by equations I (25) and I (26), respectively; $\chi(\xi, \tau, \mu)$ is the Fourier transform of intensity as given by equation I (14); and

$$G(\xi) = \frac{1}{\sqrt{(2\pi)}} \int_{-\infty}^{\infty} e^{i\xi\alpha} \tfrac{1}{4} F(\alpha)\, d\alpha \quad (8)$$

is the Fourier transform of incident flux. The third term on the right-hand side of equation (7), which represents the scattering of the incident flux, makes this equation inhomogeneous in $\chi(\xi, \tau, \mu)$. The use of equation I (30) and

$$G(\xi) = G^{(r)}(\xi) + iG^{(i)}(\xi) \quad (9)$$

allows the separation of equation (7) into its real and imaginary parts and gives

$$\mu \frac{\partial \chi^{(r)}(\xi, \tau, \mu)}{\partial \tau} = \chi^{(r)}(\xi, \tau, \mu)$$
$$-\frac{3}{8}\int_{-1}^{1} [\chi^{(r)}(\xi, \tau, \mu') p_r(\xi, \mu, \mu') + \chi^{(i)}(\xi, \tau, \mu') p_i(\xi, \mu, \mu')]\, d\mu' \quad (10)$$
$$-[G^{(r)}(\xi) q_r(\xi, \mu) - G^{(i)}(\xi) q_i(\xi, \mu)]\, e^{-(\tau_1-\tau)}$$

and

$$\mu \frac{\partial \chi^{(i)}(\xi, \tau, \mu)}{\partial \tau} = \chi^{(i)}(\xi, \tau, \mu)$$
$$-\frac{3}{8}\int_{-1}^{1} [\chi^{(i)}(\xi, \tau, \mu') p_r(\xi, \mu, \mu') + \chi^{(r)}(\xi, \tau, \mu') p_i(\xi, \mu, \mu')]\, d\mu' \quad (11)$$
$$-[G^{(i)}(\xi) q_r(\xi, \mu) + G^{(r)}(\xi) q_i(\xi, \mu)]\, e^{-(\tau_1-\tau)},$$

where $p_r(\xi, \mu, \mu')$ and $p_i(\xi, \mu, \mu')$ are phase functions resulting from integration over the azimuthal angle and given by equations I (16)–(24), while

$$q_r(\xi, \mu) = \tfrac{3}{4}(1+\mu^2)\, e^{-(1-\mu)\xi^3/4}$$
$$\times [\cos\tfrac{3}{2}(1-\mu)\beta\xi + \tfrac{3}{2}(1-\mu)\beta\gamma\xi \sin\tfrac{3}{2}(1-\mu)\beta\xi] \quad (12)$$

and

$$q_i(\xi, \mu) = -\tfrac{3}{4}(1+\mu^2)\, e^{-(1-\mu)\xi^3/4}$$
$$\times [\sin\tfrac{3}{2}(1-\mu)\beta\xi - \tfrac{3}{2}(1-\mu)\beta\gamma\xi \cos\tfrac{3}{2}(1-\mu)\beta\xi]$$

are phase functions for the inhomogeneous terms. Finally, the boundary conditions for

these transformed equations of transfer are

$$\left.\begin{aligned} &\chi^{(r)}(\xi, 0, -\mu) \equiv \chi^{(i)}(\xi, 0, -\mu) \equiv 0 , \\ &\chi^{(r)}(\xi, \tau_1, \mu) = \chi^{(r)}(\xi, \tau_1, -\mu) , \qquad \chi^{(i)}(\xi, \tau_1, \mu) = \chi^{(i)}(\xi, \tau_1, -\mu) \end{aligned}\right\} (\mu \geq 0) \quad (13)$$

for the planetary nebula problem and

$$\left.\begin{aligned} &\chi^{(r)}(\xi, 0, -\mu) \equiv \chi^{(i)}(\xi, 0, -\mu) \equiv 0 , \\ &\chi^{(r)}(\xi, \tau_1, \mu) \equiv \chi^{(i)}(\xi, \tau_1, \mu) \equiv 0 \end{aligned}\right\} (\mu \geq 0) \quad (14)$$

for no incident diffuse radiation field.

III. SOLUTIONS OF THE TRANSFORMED EQUATION OF TRANSFER IN THE FIRST APPROXIMATION

Equations (10) and (11) can now be solved by the standard approximate methods of radiation-transfer theory,[5] in which they are replaced by a system of linear differential equations. For reasons given in Section III of Paper I, these equations will be solved in the first approximation, where they take the form

$$\frac{1}{\sqrt{3}} \frac{\partial \chi_{+1}^{(r)}(\xi, \tau)}{\partial \tau} = \chi_{+1}^{(r)}(\xi, \tau) - M(\xi) \chi_{+1}^{(r)}(\xi, \tau) - N(\xi) \chi_{-1}^{(r)}(\xi, \tau) \} \quad (15)$$
$$+ L(\xi) \chi_{+1}^{(i)}(\xi, \tau) + K(\xi) \chi_{-1}^{(i)}(\xi, \tau) - [C_1(\xi) G^{(r)}(\xi) - C_2(\xi) G^{(i)}(\xi)] e^{-(\tau_1 - \tau)} ;$$

$$-\frac{1}{\sqrt{3}} \frac{\partial \chi_{-1}^{(r)}(\xi, \tau)}{\partial \tau} = \chi_{-1}^{(r)}(\xi, \tau) - M(\xi) \chi_{-1}^{(r)}(\xi, \tau) - N(\xi) \chi_{+1}^{(r)}(\xi, \tau) \quad (16)$$
$$+ L(\xi) \chi_{-1}^{(i)}(\xi, \tau) + K(\xi) \chi_{+1}^{(i)}(\xi, \tau) - [C_3(\xi) G^{(r)}(\xi) - C_4(\xi) G^{(i)}(\xi)] e^{-(\tau_1 - \tau)} ;$$

$$\frac{1}{\sqrt{3}} \frac{\partial \chi_{+1}^{(i)}(\xi, \tau)}{\partial \tau} = \chi_{+1}^{(i)}(\xi, \tau) - M(\xi) \chi_{+1}^{(i)}(\xi, \tau) - N(\xi) \chi_{-1}^{(i)}(\xi, \tau) \quad (17)$$
$$- L(\xi) \chi_{+1}^{(r)}(\xi, \tau) - K(\xi) \chi_{-1}^{(r)}(\xi, \tau) - [C_2(\xi) G^{(r)}(\xi) + C_1(\xi) G^{(i)}(\xi)] e^{-(\tau_1 - \tau)} ;$$

$$-\frac{1}{\sqrt{3}} \frac{\partial \chi_{-1}^{(i)}(\xi, \tau)}{\partial \tau} = \chi_{-1}^{(i)}(\xi, \tau) - M(\xi) \chi_{-1}^{(i)}(\xi, \tau) - N(\xi) \chi_{+1}^{(i)}(\xi, \tau) \quad (18)$$
$$- L(\xi) \chi_{-1}^{(r)}(\xi, \tau) - K(\xi) \chi_{+1}^{(r)}(\xi, \tau) - [C_4(\xi) G^{(r)}(\xi) + C_3(\xi) G^{(i)}(\xi)] e^{-(\tau_1 - \tau)} .$$

The phase functions $M(\xi)$, $N(\xi)$, $L(\xi)$, and $K(\xi)$ are given by equations I (38)–(42), while the phase functions of the inhomogeneous term are

$$C_1(\xi) = q_r\left(\xi, \frac{1}{\sqrt{3}}\right), \qquad C_2(\xi) = q_i\left(\xi, \frac{1}{\sqrt{3}}\right),$$
$$C_3(\xi) = q_r\left(\xi, \frac{-1}{\sqrt{3}}\right), \qquad C_4(\xi) = q_i\left(\xi, \frac{-1}{\sqrt{3}}\right). \quad (19)$$

Equations (15)–(18) constitute a fourth-order set of linear inhomogeneous differential equations with coefficients which are constant, since ξ may be considered a pa-

[5] Cf. S. Chandrasekhar, *Radiative Transfer* (Oxford: Clarendon Press, 1950), chap. ii.

rameter. Equations of the same general form have previously been solved,[6] and substitution of the trial solutions MA II (21) in equations (15)–(18) yields a fourth-order set of linear inhomogeneous equations in $\mathfrak{g}_{+1}^{(r)}(\xi)$, $\mathfrak{g}_{-1}^{(r)}(\xi)$, $\mathfrak{g}_{+1}^{(i)}(\xi)$, and $\mathfrak{g}_{-1}^{(i)}(\xi)$ with the solution

$$\sigma(\xi)\,\mathfrak{g}_{+1}^{(r)}(\xi) = -k_2(\xi)G^{(r)}(\xi) - k_4(\xi)G^{(i)}(\xi), \tag{20}$$

$$\sigma(\xi)\,\mathfrak{g}_{-1}^{(r)}(\xi) = k_1(\xi)G^{(r)}(\xi) + k_3(\xi)G^{(i)}(\xi), \tag{21}$$

$$\sigma(\xi)\,\mathfrak{g}_{+1}^{(i)}(\xi) = k_4(\xi)G^{(r)}(\xi) - k_2(\xi)G^{(i)}(\xi), \tag{22}$$

$$\sigma(\xi)\,\mathfrak{g}_{-1}^{(i)}(\xi) = -k_3(\xi)G^{(r)}(\xi) + k_1(\xi)G^{(i)}(\xi); \tag{23}$$

$$k_1(\xi) = -B_2(\xi)C_3(\xi) - B_4(\xi)C_4(\xi) + B_5(\xi)C_1(\xi) + B_6(\xi)C_2(\xi), \tag{24}$$

$$k_2(\xi) = B_1(\xi)C_1(\xi) + B_3(\xi)C_2(\xi) - B_5(\xi)C_3(\xi) - B_6(\xi)C_4(\xi), \tag{25}$$

$$k_3(\xi) = B_2(\xi)C_4(\xi) - B_4(\xi)C_3(\xi) - B_5(\xi)C_2(\xi) + B_6(\xi)C_1(\xi), \tag{26}$$

$$k_4(\xi) = -B_1(\xi)C_2(\xi) + B_3(\xi)C_1(\xi) + B_5(\xi)C_4(\xi) - B_6(\xi)C_3(\xi); \tag{27}$$

$$B_1(\xi) = \left(M - 1 - \frac{1}{\sqrt{3}}\right)\left[(M-1)^2 - N^2 + K^2 - \tfrac{1}{3}\right] + \left(M - 1 + \frac{1}{\sqrt{3}}\right)L^2 - 2NLK \tag{28}$$

$$B_2(\xi) = \left(M - 1 + \frac{1}{\sqrt{3}}\right)\left[(M-1)^2 - N^2 + K^2 - \tfrac{1}{3}\right] + \left(M - 1 - \frac{1}{\sqrt{3}}\right)L^2 - 2NLK, \tag{29}$$

$$B_3(\xi) = L\left[\left(M - 1 - \frac{1}{\sqrt{3}}\right)^2 + N^2 + L^2 - K^2\right] - 2\left(M - 1 - \frac{1}{\sqrt{3}}\right)NK, \tag{30}$$

$$B_4(\xi) = L\left[\left(M - 1 + \frac{1}{\sqrt{3}}\right)^2 + N^2 + L^2 - K^2\right] - 2\left(M - 1 + \frac{1}{\sqrt{3}}\right)NK, \tag{31}$$

$$B_5(\xi) = N\left[(M-1)^2 - N^2 - L^2 - K^2 - \tfrac{1}{3}\right] + 2(M-1)LK, \tag{32}$$

$$B_6(\xi) = -K\left[(M-1)^2 + N^2 - L^2 + K^2 - \tfrac{1}{3}\right] + 2(M-1)NL; \tag{33}$$

$$\sigma(\xi) = \left[(M-1)^2 - N^2 - L^2 + K^2 - \tfrac{1}{3}\right]^2 + 4\left[L(M-1) - NK\right]^2. \tag{34}$$

Since the homogeneous parts of equations (15)–(18) are the analogous equations for the Schuster problem, I (34)–(37), the complementary solution is that found for the Schuster problem. The most general solution, i.e., the combination of the particular solution and complementary solution, is given by equations MA II (27)–(30), where the characteristic roots $k'(\xi)$ and $k''(\xi)$ are defined by equations I (43) and I (44), and the functions $E_1(\xi)$, $E_2(\xi)$, $E_3(\xi)$, and $E_4(\xi)$ by equations I (45)–(48), respectively.

The determination from the boundary conditions of the arbitrary functions $D_1(\xi)$, $D_2(\xi)$, $D_3(\xi)$, and $D_4(\xi)$, appearing in the most general solution, will be identical to that given in the Moving Atmosphere II paper, as the forms of the solutions are identical. For the planetary nebula problem the boundary conditions are given by equation Ma II

[6] F. N. Edmonds, Jr., *Ap. J.*, **112**, 307 and 324, 1950. These papers will be referred to as "Moving Atmosphere I" and "Moving Atmosphere II," respectively, with equations in these papers designated by prefixing "MA I" or "MA II," respectively, e.g., "equation MA II (21)."

(31), and the expressions for the arbitrary functions by equations MA II (32)–(42). For no incident diffuse radiation field the boundary conditions are

$$\chi_{+1}^{(r)}(\xi, \tau_1) \equiv \chi_{+1}^{(i)}(\xi, \tau_1) \equiv 0\,, \qquad \chi_{-1}^{(r)}(\xi, 0) \equiv \chi_{-1}^{(i)}(\xi, 0) \equiv 0\,, \tag{35}$$

and equations MA II (32)–(36) and MA II (39)–(42) apply, with equations MA II (37) and MA II (38) replaced by

$$\begin{aligned} g_1(\xi) &= -\,\mathfrak{g}_{+1}^{(r)}(\xi)\,, & g_2(\xi) &= -\,\mathfrak{g}_{+1}^{(i)}(\xi)\,, \\ g_3(\xi) &= \mathfrak{g}_{-1}^{(r)}(\xi)\, e^{-\tau_1} & g_4(\xi) &= \mathfrak{g}_{-1}^{(i)}(\xi)\, e^{-\tau_1}\,, \end{aligned} \tag{36}$$

and

$$\begin{aligned} H_1(\xi) &= e^{k'\tau_1}\cos k''\tau_1\,, & H_2(\xi) &= e^{k'\tau_1}\sin k''\tau_1\,, \\ H_3(\xi) &= e^{-k'\tau_1}\cos k''\tau_1\,, & H_4(\xi) &= e^{-k'\tau_1}\sin k''\tau_1\,. \end{aligned} \tag{37}$$

These solutions have the required symmetry in ξ to insure that their inverse Fourier transforms will give a real function; and the validity of the application of the Fourier transform can be established within the scheme of the first approximation by placing the integrable-square requirement on $G^{(r)}(\xi)$ and $G^{(i)}(\xi)$. The coefficients of $G^{(r)}(\xi)$ and $G^{(i)}(\xi)$ are bounded for all values of τ and ξ,[7] and the solutions fall off exponentially in ξ^2, as indicated by equations (12) and (19).

The solution for radiation emerging from the electron atmosphere at the outer surface $\tau = 0$ is given by

$$\chi_{+1}^{(r)}(\xi, 0) = \Lambda_1 G^{(r)}(\xi) - \Lambda_2 G^{(i)}(\xi)\,, \qquad \chi_{+1}^{(i)}(\xi, 0) = \Lambda_2 G^{(r)}(\xi) + \Lambda_1 G^{(i)}(\xi)\,, \tag{38}$$

where, for the planetary nebula problem,

$$\eta'\sigma\Lambda_1 = (k_1+k_2)\,A_1 - (k_3+k_4)\,A_2 + e^{-\tau_1}(k_1A_3 - k_3A_4 - k_2\eta')\,, \tag{39}$$

$$\eta'\sigma\Lambda_2 = -\,(k_3+k_4)\,A_1 - (k_1+k_2)\,A_2 - e^{-\tau_1}(k_3A_3 + k_1A_4 - k_4\eta')\,; \tag{40}$$

$$A_1 = \eta\Gamma_1 + 2\,(E_4-E_2)\cosh k'\tau_1 \sin k''\tau_1 - 2\,(E_1-E_3)\sinh k'\tau_1\cos k''\tau_1\,, \tag{41}$$

$$A_2 = -\,\eta\Gamma_2 - 2\,(E_1-E_3)\cosh k'\tau_1 \sin k''\tau_1 - 2\,(E_4-E_2)\sinh k'\tau_1\cos k''\tau_1\,, \tag{42}$$

$$\begin{aligned} A_3 = {} & 2\,(E_1+E_3+2E_1E_3)\cosh 2k'\tau_1 \\ & - [\,(E_1+E_3)^2 + (E_4-E_2)^2 + 2\,(E_1+E_3)\,]\cos 2k''\tau_1\,, \end{aligned} \tag{43}$$

$$\begin{aligned} A_4 = {} & 2\,(E_4-E_2)\sinh 2k'\tau_1 + 2E_1E_4\,e^{2k'\tau_1} + 2E_2E_3\,e^{-2k'\tau_1} + [\,(E_1-E_3) \\ & \times (E_1+E_3+2) - (E_3^2+E_4^2)\,]\sin 2k''\tau_1 - 2\,(E_2E_3+E_1E_4)\cos 2k''\tau_1\,; \end{aligned} \tag{44}$$

$$\begin{aligned} \eta' = {} & 2\,(E_1E_3-E_2E_4)\cosh 2k'\tau_1 + (E_3^2+E_4^2+2E_3)\,e^{2k'\tau_1} \\ & + (E_1^2+E_2^2+2E_1)\,e^{-2k'\tau_1} + 2\,(E_1E_4-E_2E_3+E_4-E_2)\sin 2k''\tau_1 \\ & - 2\,[\,(E_1^2+E_2^2)(E_3^2+E_4^2) + E_1E_3+E_2E_4+E_1+E_3]\cos 2k''\tau_1\,; \end{aligned} \tag{45}$$

and, for no incident diffuse radiation field,

$$\eta\sigma\Lambda_1 = k_2A_1' - k_4A_2' + e^{-\tau_1}(k_1A_3' - k_3A_4' - k_2\eta)\,, \tag{46}$$

[7] To show this, requires evaluating the indeterminate form of the solution at $\xi = 0$ (cf. Paper I, n. 9).

$$\eta\sigma\Lambda_2 = -k_4 A_1' - k_2 A_2' - e^{-\tau_1}(k_3 A_3' + k_1 A_4' - k_4\eta)\,; \tag{47}$$

$$A_1' = \eta\Gamma_1\,, \tag{48}$$

$$A_2' = -\eta\Gamma_2\,; \tag{49}$$

$$\begin{aligned}(K^2+N^2)\,A_3' = {} & 2\,[KL + N(M-1)\,](\cosh 2k'\tau_1 - \cos 2k''\tau_1) \\ & - 2\left(\frac{Kk''}{\sqrt{3}} + \frac{Nk'}{\sqrt{3}}\right)\sinh 2k'\tau_1 - 2\left(\frac{Nk''}{\sqrt{3}} - \frac{Kk'}{\sqrt{3}}\right)\sin 2k''\tau_1\,,\end{aligned} \tag{50}$$

$$\begin{aligned}(K^2+N^2)\,A_4' = {} & 2\,[NL - K(M-1)\,](\cosh 2k'\tau_1 - \cos 2k''\tau_1) \\ & - 2\left(\frac{Nk''}{\sqrt{3}} - \frac{Kk'}{\sqrt{3}}\right)\sinh 2k'\tau_1 + 2\left(\frac{Kk''}{\sqrt{3}} + \frac{Nk'}{\sqrt{3}}\right)\sin 2k''\tau_1\,.\end{aligned} \tag{51}$$

In these equations Γ_1, Γ_2, and η are given by equations MA I (66)–(68) with N^2 replaced by $N^2 + K^2$.

For values of ν_0 and T of astrophysical interest, $\beta < 10^{-2}$, as shown by equation I (29), and considerable simplification of the solutions for emergent radiation is possible for this range of values of β. Neglecting terms involving the second and higher powers of β, equations (24)–(27) and (34) become

$$k_1(\xi) = [(M-1)^2 - N^2 - \tfrac{1}{3}]\left[N e^{-(1-1/\sqrt{3})\xi^3/4} - \left(M - 1 + \frac{1}{\sqrt{3}}\right) e^{-(1+1/\sqrt{3})\xi^3/4}\right], \tag{52}$$

$$k_2(\xi) = [(M-1)^2 - N^2 - \tfrac{1}{3}]\left[\left(M - 1 - \frac{1}{\sqrt{3}}\right) e^{-(1-1/\sqrt{3})\xi^3/4} - N e^{-(1+1/\sqrt{3})\xi^3/4}\right], \tag{53}$$

$$\begin{aligned}k_3(\xi) = {} & \left\{2LN(M-1) - K[(M-1)^2 + N^2 - \tfrac{1}{3}]\right. \\ & - \frac{3}{2}\left(1 - \frac{1}{\sqrt{3}}\right)\beta(\gamma-1)\,\xi N[(M-1)^2 - N^2 - \tfrac{1}{3}]\Big\}\, e^{-(1-1/\sqrt{3})\xi^3/4} \\ & + \left\{2KN\left(M - 1 + \frac{1}{\sqrt{3}}\right) - L\left[\left(M - 1 + \frac{1}{\sqrt{3}}\right)^2 + N^2\right]\right. \\ & + \frac{3}{2}\left(1 + \frac{1}{\sqrt{3}}\right)\beta(\gamma-1)\,\xi\left(M - 1 + \frac{1}{\sqrt{3}}\right)[(M-1)^2 - N^2 - \tfrac{1}{3}]\Big\}\, e^{-(1+1/\sqrt{3})\xi^3/4},\end{aligned} \tag{54}$$

$$\begin{aligned}k_4(\xi) = {} & -\left\{2KN\left(M - 1 - \frac{1}{\sqrt{3}}\right) - L\left[\left(M - 1 - \frac{1}{\sqrt{3}}\right)^2 + N^2\right]\right. \\ & + \frac{3}{2}\beta\left(1 - \frac{1}{\sqrt{3}}\right)(\gamma-1)\,\xi\left(M - 1 - \frac{1}{\sqrt{3}}\right)[(M-1)^2 - N^2 - \tfrac{1}{3}]\Big\}\, e^{-(1-1/\sqrt{3})\xi^3/4} \\ & - \left\{2LN(M-1) - K[(M-1)^2 + N^2 - \tfrac{1}{3}]\right. \\ & + \frac{3}{2}\beta\left(1 + \frac{1}{\sqrt{3}}\right)(\gamma-1)\,\xi N[(M-1)^2 - N^2 - \tfrac{1}{3}]\Big\}\, e^{-(1+1/\sqrt{3})\xi^3/4},\end{aligned} \tag{55}$$

$$\sigma(\xi) = [(M-1)^2 - N^2 - \tfrac{1}{3}]\,, \tag{56}$$

where $M(\xi)$, $N(\xi)$, $L(\xi)$, $k'(\xi)$, and $k''(\xi)$ are given by equations I (58)–(61) and

$$2K(\xi)\, e^{\xi^3/3} = V_0(z) - \tfrac{1}{3} U_1(z) - \tfrac{1}{6} V_2(z) + \tfrac{1}{12}\beta\xi\Big[(26\gamma - 24)\, I_0\Big(\frac{\xi^2}{6}\Big) - (21\gamma - 8)\, I_1\Big(\frac{\xi^2}{6}\Big) + (6\gamma - 4)\, I_2\Big(\frac{\xi^2}{6}\Big) - \gamma I_3\Big(\frac{\xi^2}{6}\Big)\Big], \tag{57}$$

with $U_n(z)$ and $V_n(z)$ the real and imaginary parts, respectively, of Bessel functions of the first kind, of order n, and of complex argument

$$z = \beta\xi - \frac{i\xi^2}{6}. \tag{58}$$

Also equations (39) and (41)–(45) of the emergent-radiation solution for the planetary nebula problem become (eq. [40] remaining unchanged)

$$\eta'\sigma\Lambda_1 = (k_1 + k_2)\, A_1 + e^{-\tau_1}(k_1 A_3 - k_2\eta'), \tag{59}$$

$$\tfrac{1}{4} N^2 A_1 = \tfrac{1}{3} k'^2 \cosh k'\tau_1 - \Big(\frac{k'}{\sqrt{3}}\Big)(M - 1 + N)\sinh k'\tau_1, \tag{60}$$

$$\tfrac{1}{4} N^2 A_2 = -\Big(\frac{k'}{\sqrt{3}}\Big)(K + L)\sinh k'\tau_1, \tag{61}$$

$$\tfrac{1}{4} N^2 A_3 = N(M - 1 + N)(\cosh 2k'\tau_1 - 1) - \tfrac{1}{3} k'^2, \tag{62}$$

$$\tfrac{1}{4} N^2 A_4 = [L(M - 1) - KN](\cosh 2k'\tau_1 - 1) + \Big(\frac{k'}{\sqrt{3}}\Big)(K + L)\sinh 2k'\tau_1, \tag{63}$$

$$\tfrac{1}{4} N^2 \eta' = N(M - 1 + N)(\cosh 2k'\tau_1 - 1) + \tfrac{1}{3} k'^2 \cosh 2k'\tau_1 - \Big(\frac{k'}{\sqrt{3}}\Big)(M - 1 + N)\sinh 2k'\tau_1, \tag{64}$$

while equations (46), (48)–(51), and MA I (68) of the corresponding solution for no incident diffuse radiation field become (eq. [47] remaining unchanged)

$$\eta\sigma\Lambda_1 = k_2 A_1' + e^{-\tau_1}(k_1 A_3' - k_2\eta), \tag{65}$$

$$\tfrac{1}{4} N^2 A_1' = \tfrac{1}{3} k'^2 \cosh k'\tau_1 - \Big(\frac{k'}{\sqrt{3}}\Big)(M - 1)\sinh k'\tau_1, \tag{66}$$

$$\tfrac{1}{4} N^2 A_2' = -\Big(\frac{k'}{\sqrt{3}}\Big) L \sinh k'\tau_1, \tag{67}$$

$$\tfrac{1}{2} N^2 A_3' = N(M - 1)(\cosh 2k'\tau_1 - 1) - \Big(\frac{k'}{\sqrt{3}}\Big) N \sinh 2k'\tau_1, \tag{68}$$

$$\tfrac{1}{2} N^2 A_4' = [NL - K(M - 1)](\cosh 2k'\tau_1 - 1) + \Big(\frac{k'}{\sqrt{3}}\Big) K \sinh 2k'\tau_1, \tag{69}$$

$$\tfrac{1}{2} N^2 \eta = [(M - 1)^2 + \tfrac{1}{3} k'^2] \cosh 2k'\tau_1 - 2\Big(\frac{k'}{\sqrt{3}}\Big)(M - 1)\sinh 2k'\tau_1 - N^2. \tag{70}$$

As in the Schuster problem, to the approximation in which second and higher powers of β are neglected, Λ_1 represents only the effects of the Doppler shifts in scattering due to thermal motions of the electrons, and Λ_2 only the effects of Compton scattering.

Application of these solutions for emergent radiation requires knowledge of Λ_1 and Λ_2 for $\xi = 0$, where they become indeterminate. These indeterminate forms can be

evaluated by expanding the expressions for Λ_1 and Λ_2 in powers of ξ and passing to the limit $\xi = 0$, with the following results:

$$\Lambda_1 \to \frac{k_1 + k_2}{\sigma}(1 - e^{-\tau_1}), \qquad \Lambda_2 \to 0 \qquad \text{as} \qquad \xi \to 0 \tag{71}$$

for the planetary nebula problem, and

$$\sigma\Lambda_1 \to \frac{k_2 - \frac{1}{2}k_1\tau_1 e^{-\tau_1}\sqrt{3}}{1 + \frac{1}{2}\tau_1\sqrt{3}} - k_2 e^{-\tau_1}, \qquad \Lambda_2 \to 0 \qquad \text{as} \qquad \xi \to 0 \tag{72}$$

for no incident diffuse radiation field.

IV. THE INVERSE TRANSFORM OF THE SOLUTIONS FOR EMERGENT RADIATION

The inverse Fourier transform of the solutions for emergent radiation is, by equations (38),

$$\begin{aligned} I_{+1}(a, 0) &= \frac{1}{\sqrt{(2\pi)}}\int_{-\infty}^{\infty} e^{-ia\xi}(\Lambda_1 + i\Lambda_2)[G^{(r)}(\xi) + iG^{(i)}(\xi)]\, d\xi \\ &= \frac{1}{4}\int_{-\infty}^{\infty} F(\epsilon)[\Delta'_{TB}(\tau_1; a - \epsilon) + \Delta'_{CS}(\tau_1, T, \nu_0; a - \epsilon)]\, d\epsilon, \end{aligned} \tag{73}$$

where

$$\Delta'_{TB}(\tau_1, x) = \frac{1}{\pi}\int_0^{\infty} \Lambda_1 \cos x\xi\, d\xi \tag{74}$$

and

$$\Delta'_{CS}(\tau_1, T, \nu_0; x) = \frac{1}{\pi}\int_0^{\infty} \Lambda_2 \sin x\xi\, d\xi. \tag{75}$$

The final form of equation (73) follows from the use of the Parseval formula I (68), which in turn requires that $G^{(r)}(\xi) + iG^{(i)}(\xi)$, $\Delta'_{TB}(\tau_1; x)$, and $\Delta'_{CS}(\tau_1, T, \nu_0; x)$ be integrable with respect to their arguments. This condition is satisfied for $G^{(r)}(\xi) + iG^{(i)}(\xi)$, since $G^{(r)}(\xi)$ and $G^{(i)}(\xi)$ are required to be integrable-square, and for $\Delta'_{CS}(\tau_1, T, \nu_0; x)$, since by equation (75) it is an odd function in x. That $\Delta'_{TB}(\tau_1; x)$ is also integrable with respect to x follows from an integral admitted by the original equation of transfer (4). The derivation of this integral is given in Section VI of Moving Atmospheres II, and equation MA II (68), together with $\Delta'_{CS}(\tau_1, T, \nu_0; x)$, being an odd function in x, gives

$$\int_{-\infty}^{\infty} \Delta'_{TB}(\tau_1; x)\, dx = (2\sqrt{3})(1 - e^{-\tau_1}). \tag{76}$$

The fact that Λ_1 is an even function in ξ and Λ_2 an odd function in ξ has been used in obtaining equations (74) and (75).

Physically, the right-hand side of equation (73) represents that portion of the incident flux $\pi F(a)$ which has suffered at least one scattering process in traversing the atmosphere, the integral over ϵ indicating the noncoherent nature of the electron scattering. Hence $\Delta'_{TB}(\tau_1; a - \epsilon) + \Delta'_{CS}(\tau_1, T, \nu_0; a - \epsilon)$ represents the spectral distribution of emergent scattered radiation arising from incident monochromatic flux at a frequency ϵ and of unit flux density. The function $\Delta'_{TB}(\tau_1; x)$ expresses the noncoherency resulting from Doppler shifts due to thermal motions when terms involving the second and higher powers of β are neglected, as only Λ_1 appears in equation (74). The function $\Delta'_{CS}(\tau_1, T, \nu_0; x)$ to a similar approximation expresses the noncoherency resulting from the effects of Compton scattering; i.e., the red Compton shift, which accounts for the parametric dependence on ν_0, and the non-Doppler blue shift due to thermal motions, which accounts for the dependence on T.

In equations (74) and (75) the integration over ξ represents the taking of the inverse Fourier transform of the solution for emergent radiation. Since Λ_1 and Λ_2 decrease exponentially to zero for large ξ, the integration need not be performed beyond values of ξ which are not large, and the convergence of the integral is assured. Because of the complicated dependence of Λ_1 and Λ_2 on ξ, numerical integration is necessary, with the values of the integrand for $\xi = 0$ being given by equations (71) or (72).

Most astrophysical applications of equation (73) for either the planetary nebula problem or no incident diffuse radiation field would involve small values of τ_1, where the effects of multiple scattering should not differ markedly from those of single scattering. In such cases the single-scattering spectral-distribution function $\psi(\nu, \Theta, \nu')$ may be substituted in equation (73) for both sets of boundary conditions, as follows:

$$\Delta'_{TB}(\tau_1; x) = \frac{2\tau_1\sqrt{3}}{[\pi(1-1/\sqrt{3})]^{1/2}} \exp\left\{\frac{-x^2}{1-1/\sqrt{3}}\right\} \tag{77}$$

and

$$\Delta'_{CS}(\tau_1, T, \nu_0; x) = -\left[1 + 3\beta\gamma x - \exp\left\{\frac{h\nu_0}{mc^2}\frac{x}{\beta\gamma}\right\}\right]\Delta'_{TB}(\tau_1; x). \tag{78}$$

Equations (77) and (78) were derived from equation I (6), using the transformation of co-ordinates I (8) and I (9), letting

$$\cos\Theta = \frac{1}{\sqrt{3}}, \tag{79}$$

and accounting for the difference in normalization with respect to integration over frequency variables. The function $\psi(\nu, \Theta, \nu')$ is normalized to $1/4\pi$ and $\Delta'_{TB}(\tau_1; x)$ as given by equation (76). It has been assumed that τ_1 is sufficiently small that terms involving the second and higher powers of τ_1 can be neglected. This allows neglecting the scattered radiation from the incident diffuse-radiation field in the planetary nebula problem, which would be of the order of τ_1^2.

The function $\Delta'_{TB}(\tau_1; x)/\tau_1$ has been calculated subject to this simplifying assumption for small τ_1, both for single scattering, using equation (77), and for multiple scattering, using equations (74), (52)–(56), and (59)–(64). The results are compared in Table 1, the agreement being well within the accuracy expected of a first-approximation solution, for small x. For large x, the multiple scattering, $\Delta'_{TB}(\tau_1; x)$, decreases to zero less rapidly, as would be expected. However, the two calcuations should produce discrepancies of less than 10 per cent in the application of $\Delta'_{TB}(\tau_1; x)$ in equation (73). The multiple-scattering calculations can be checked for accuracy against equation (76), with the result that numerical integration of $\Delta'_{TB}(\tau_1; x)/\tau_1$ over x gives 3.55, while equation (76) gives 3.46.

In view of the agreement between the single-scattering and the multiple-scattering calcuations of $\Delta'_{TB}(\tau_1; x)$, equation (78) should give, except for large x, a fair representation of the multiple scattering, $\Delta'_{CS}(\tau_1, T, \nu_0; x)$, for small τ_1. For an atmosphere at a temperature $T = 7.5 \times 10^5$ ° K and for $\lambda_0 = 3600$ A, corresponding to $\beta = 2 \times 10^{-4}$ and $\gamma = 56.2$, $\Delta'_{CS}(\tau_1, T, \nu_0; x)$ is less than 5 per cent of $\Delta'_{TB}(\tau_1; x)$ for $|x| < 1$, according to single-scattering calculations.

V. CHANGES PRODUCED IN PROFILES OF SPECTRAL LINES

An application of the solutions for emergent radiation of astrophysical importance is when the incident flux is the residual flux of a spectral line,

$$R(a) = \frac{F(a)}{F^{(c)}}, \tag{80}$$

where $\pi F^{(c)}$ is the flux of the incident continuum. As discussed in Section VII of the Moving Atmosphere II paper, the assumption of constancy of $\pi F^{(c)}$ over the limited fre-

quency range of the spectral line transforms equation (73) to the following expression for the emergent residual intensity $r_{+1}(a)$:

$$(2\sqrt{3})(1-e^{-\tau_1})\, r_{+1}(a) = \int_{-\infty}^{\infty} R(\epsilon)\, \Delta'_{TB}(\tau_1;\, a-\epsilon)\, d\epsilon + \int_{-\infty}^{\infty} R(\epsilon)\, \Delta'_{CS}(\tau_1, T, \nu_0;\, a-\epsilon)\, d\epsilon. \tag{81}$$

The first term on the right-hand side of equation (81) represents the thermal broadening by electron scattering of the profile for emergent radiation; the second term the asymmetry due to Compton scattering. Integration of equation (81) over a shows that the equivalent width of the spectral line is unchanged by the scattering.

TABLE 1

THE FUNCTION $\Delta'_{TB}(\tau_1; x)/\tau_1$ FOR SMALL τ_1, $T = 7.5 \times 10^5$° K AND $\lambda_0 = 3600$ A

	x				
	0	0.25	0.50	1.0	2.0
Multiple scattering	2.28	2.04	1.61	0.55	0.06
Single scattering	2.22	1.91	1.23	0.21	0.002

As for the Schuster problem discussed in Section V of Paper I, the detection of the asymmetry due to Compton scattering in astronomical spectra will be extremely difficult. As mentioned in the previous section, single-scattering expressions for Δ'_{TB} and Δ'_{CS} can be used with fair accuracy, and certainly the atmosphere considered with $T = 7.5 \times 10^5$° K and $\lambda_0 = 3600$ A should provide most favorable conditions for detection, as the non-Doppler blue shift is $\gamma = 56.2$ times the red Compton shift. However, the second term in equation (81) will be less then 5 per cent of the first, since Δ'_{CS} is less than 5 per cent of Δ'_{TB} for such an atmosphere. The thermal broadening of a line corresponding to such a high temperature should effectively mask both the asymmetry and the shift of the center of the line due to the Compton scattering term. As pointed out in Section V of Paper I, the shift of the center of the line should be of the order of magnitude of that associated with the spectral distribution function $\psi(\nu, \Theta, \nu')$, which is about 0.5A.[8]

I wish to thank the University Research Institute of the University of Texas for support of the computations and Mrs. LaNelle Janca Kahlbau for performing the computations.

APPENDIX

MULTIPLE COMPTON SCATTERING OF LOW-ENERGY GAMMA RADIATION

A problem of physical rather than astrophysical interest is the multiple scattering of low energy ($h\nu_0 \ll \frac{1}{2}$Mev) gamma radiation[9] involving room temperatures and frequencies of the order of 10^{19}, for which

$$\beta \sim 10^2, \qquad \gamma \sim 10^{-6}.$$

[8] F. N. Edmonds, Jr., *Ap. J.*, **117**, 298, eq. (28), 1953.

[9] R. C. O'Rourke, *Phys. Rev.*, **85**, 881, 1952.

The emergent-radiation solution obtained for no incident diffuse radiation field as given by equations (73)–(75), (46)–(51), (24)–(34), (19), and (12), is probably applicable in the first approximation to this problem for many physical situations. However, such application involves serious computational problems in performing the integrations indicated by equations (74) and (75). The functions $C_1(\xi)$ through $C_4(\xi)$, $M(\xi)$, $N(\xi)$, $L(\xi)$, and $K(\xi)$, which appear in the expressions for Λ_1 and Λ_2, all contain trigonometric factors with arguments $\delta\beta\xi$, where $\delta > \frac{1}{2}$. Hence these functions, the characteristic roots $k'(\xi)$ and $k''(\xi)$ and Λ_1 and Λ_2, will oscillate rapidly for variations in ξ, when β is large. Although the numerical integrations of equations (74) and (75) will be carried out to only moderate values of ξ, these integrations will be extremely laborious, as the rapid oscillations will require evaluation of the integrand for very small intervals in ξ. A small compensation lies in the fact that, for this range of large β, terms involving γ can be neglected in equations I (38)–(41) for $M(\xi)$, $N(\xi)$, $L(\xi)$, and $K(\xi)$.

Another difficulty involves determining $U_n(z)$ and $V_n(z)$, which appear in equations I (38)–(41). For large β and moderate ξ,

$$\rho = |z| \simeq \beta\xi ;$$

and hence large values of the modulus ρ will be involved. The functions $U_n(z)$ and $V_n(z)$ are tabulated[10] for the first and second order, and Lagrangian interpolation should give three-significant-figure accuracy out to about $\rho = 7$ for large β (for which z runs close to the real axis). Beyond this range, asymptotic expansions of these functions to three terms should give comparable accuracy. These asymptotic expansions[11] are

$$\begin{aligned}
U_n(z) = \frac{\cos\beta\xi}{\sqrt{(2\pi\rho)}}\Big\{ & C_n\Big(1+\frac{\beta\xi}{\rho}\Big)^{1/2}\cosh\tfrac{1}{6}\xi^2 - S_n\Big(1-\frac{\beta\xi}{\rho}\Big)^{1/2}\sinh\tfrac{1}{6}\xi^2 - \frac{4n^2-1}{8\rho} \\
& \times\Big[S_n\Big(1-\frac{2\beta\xi}{\rho}\Big)\Big(1+\frac{\beta\xi}{\rho}\Big)^{1/2}\cosh\tfrac{1}{6}\xi^2 - C_n\Big(1+\frac{2\beta\xi}{\rho}\Big)\Big(1-\frac{\beta\xi}{\rho}\Big)^{1/2}\sinh\tfrac{1}{6}\xi^2\Big] \\
& + \frac{(4n^2-1)(4n^2-3)}{128\rho^2}\Big[C_n\Big(1+\frac{2\beta\xi}{\rho}-\frac{4\beta^2\xi^2}{\rho^2}\Big)\Big(1+\frac{\beta\xi}{\rho}\Big)^{1/2}\cosh\tfrac{1}{6}\xi^2 \\
& - S_n\Big(1-\frac{2\beta\xi}{\rho}-\frac{4\beta^2\xi^2}{\rho^2}\Big)\Big(1-\frac{\beta\xi}{\rho}\Big)^{1/2}\sinh\tfrac{1}{6}\xi^2\Big]\Big\} \\
& + \frac{\sin\beta\xi}{\sqrt{(2\pi\rho)}}\Big\{S_n\Big(1+\frac{\beta\xi}{\rho}\Big)^{1/2}\cosh\tfrac{1}{6}\xi^2 + C_n\Big(1-\frac{\beta\xi}{\rho}\Big)^{1/2}\sinh\tfrac{1}{6}\xi^2 + \frac{4n^2-1}{8\rho} \\
& \times\Big[C_n\Big(1-\frac{2\beta\xi}{\rho}\Big)\Big(1+\frac{\beta\xi}{\rho}\Big)^{1/2}\cosh\tfrac{1}{6}\xi^2 + S_n\Big(1+\frac{2\beta\xi}{\rho}\Big)\Big(1-\frac{\beta\xi}{\rho}\Big)^{1/2}\sinh\tfrac{1}{6}\xi^2\Big] \\
& + \frac{(4n^2-1)(4n^2-3)}{128\rho^2}\Big[S_n\Big(1+\frac{2\beta\xi}{\rho}-\frac{4\beta^2\xi^2}{\rho^2}\Big)\Big(1+\frac{\beta\xi}{\rho}\Big)^{1/2}\cosh\tfrac{1}{6}\xi^2 \\
& + C_n\Big(1-\frac{2\beta\xi}{\rho}-\frac{4\beta^2\xi^2}{\rho^2}\Big)\Big(1-\frac{\beta\xi}{\rho}\Big)^{1/2}\sinh\tfrac{1}{6}\xi^2\Big]\Big\}
\end{aligned}$$

and

$$\begin{aligned}
V_n(z) = \frac{\cos\beta\xi}{\sqrt{(2\pi\rho)}}\Big\{ & C_n\Big(1-\frac{\beta\xi}{\rho}\Big)^{1/2}\cosh\tfrac{1}{6}\xi^2 + S_n\Big(1+\frac{\beta\xi}{\rho}\Big)^{1/2}\sinh\tfrac{1}{6}\xi^2 + \frac{4n^2-1}{8\rho} \\
& \times\Big[S_n\Big(1+\frac{2\beta\xi}{\rho}\Big)\Big(1-\frac{\beta\xi}{\rho}\Big)^{1/2}\cosh\tfrac{1}{6}\xi^2 + C_n\Big(1-\frac{2\beta\xi}{\rho}\Big)\Big(1+\frac{\beta\xi}{\rho}\Big)^{1/2}\sinh\tfrac{1}{6}\xi^2\Big]
\end{aligned}$$

[10] Mathematical Tables Project, *Table of the Bessel Functions $J_0(z)$ and $J_1(z)$ for Complex Arguments* (New York: Columbia University Press, 1943).

[11] G. N. Watson, *Treatise on the Theory of Bessel Functions* (New York: Macmillan Co., 1945), p. 202.

$$+\frac{(4n^2-1)(4n^2-3)}{128\rho^2}\left[C_n\left(1-\frac{2\beta\xi}{\rho}-\frac{4\beta^2\xi^2}{\rho^2}\right)\left(1-\frac{\beta\xi}{\rho}\right)^{1/2}\cosh\tfrac{1}{6}\xi^2\right.$$

$$\left.+S_n\left(1+\frac{2\beta\xi}{\rho}-\frac{4\beta^2\xi^2}{\rho^2}\right)\left(1+\frac{\beta\xi}{\rho}\right)^{1/2}\sinh\tfrac{1}{6}\xi^2\right]\Bigg\}$$

$$+\frac{\sin\beta\xi}{\sqrt{(2\pi\rho)}}\Bigg\{S_n\left(1-\frac{\beta\xi}{\rho}\right)\cosh\tfrac{1}{6}\xi^2-C_n\left(1+\frac{\beta\xi}{\rho}\right)\sinh\tfrac{1}{6}\xi^2-\frac{4n^2-1}{8\rho}$$

$$\times\left[C_n\left(1+\frac{2\beta\xi}{\rho}\right)\left(1-\frac{\beta\xi}{\rho}\right)^{1/2}\cosh\tfrac{1}{6}\xi^2-S_n\left(1-\frac{2\beta\xi}{\rho}\right)\left(1+\frac{\beta\xi}{\rho}\right)^{1/2}\sinh\tfrac{1}{6}\xi^2\right]$$

$$+\frac{(4n^2-1)(4n^2-3)}{128\rho^2}\left[S_n\left(1-\frac{2\beta\xi}{\rho}-\frac{4\beta^2\xi^2}{\rho^2}\right)\left(1-\frac{\beta\xi}{\rho}\right)^{1/2}\cosh\tfrac{1}{6}\xi^2\right.$$

$$\left.-C_n\left(1+\frac{2\beta\xi}{\rho}-\frac{4\beta^2\xi^2}{\rho^2}\right)\left(1+\frac{\beta\xi}{\rho}\right)^{1/2}\sinh\tfrac{1}{6}\xi^2\right]\Bigg\},$$

where

$$\frac{C_n}{\sqrt{2}}=\cos\tfrac{1}{2}(n+\tfrac{1}{2})\pi\,,\qquad\frac{S_n}{\sqrt{2}}=\sin\tfrac{1}{2}(n+\tfrac{1}{2})\pi\,.$$

Application of the solution of the Schuster problem discussed in Paper I for large values of β would involve more serious difficulties in computation. The integrations indicated by equations I (66) and I (67) must be carried out analytically for large ξ as the contribution from this range cannot be neglected. Usable asymptotic expressions for the integrand can be obtained only for $\xi \gg \beta$, which would require numerical integration out to large values of ξ. In spite of the simpler integrands involved, this increases the labor of the computations by nearly the factor β.

THE PHYSICAL THEORY OF METEORS. V. THE MASSES OF METEOR-FLARE FRAGMENTS

HENRY J. SMITH
Boyden Station, Harvard College Observatory
Received August 24, 1953

ABSTRACT

The masses of particles contributing to meteor flares have been computed from their observed durations, by applying the classical equations of meteor ballistics. The flare masses determined in this way are of the order of 10^{-6} gm. This value is 10^{-3}–10^{-4} times smaller than the flare masses computed by Jacchia from the total light generated by the flare. It is concluded that a typical meteor flare consists of the simultaneous emission of several thousand microscopic particles rather than the fracture of the parent-body into a few larger pieces.

The flares observed along the trajectories of visual and photographic meteors are probably the result of irregular increases in the rate of mass loss. The theory of meteors indicates that the luminosity of a meteor is proportional to the rate of mass loss, to the square of the velocity of the meteor, and to its luminous efficiency coefficient.[1] During a flare a meteor's luminosity often increases by 1–2 mag. It is difficult to envisage any mechanism which could impart a momentary velocity of sufficient magnitude to produce this effect; in fact, all observations of meteor velocities point to a monotonic deceleration of small magnitude. Moreover, no theoretical argument suggests that the luminous efficiency should change erratically for a given meteor.

Jacchia's study of the light-curves of meteors[2] shows, in general, that the observed light-curve of a meteor without flares is closely represented by the theoretical light-curve. In the case of a flaring meteor, however, the observed light-curve falls off more rapidly at the end, leading to a shorter duration than required by the theoretical light-curve. Thus the shorter duration of such meteors is easily understood in terms of an accelerated mass loss through fragmentation or some similar mechanism during the flares.

The only accessible observational data on flares are their light-curves (light versus position on the trail of the parent-meteor). Jacchia has determined the masses of flare particles for 65 flares on 32 meteors for which complete data were available. His method was to apply the mass-luminosity relation,

$$m_f = \frac{2}{\tau_0} \int_i^e \frac{I}{V^3}\, dt, \tag{1}$$

to the light, I, of the flare alone; m_f is the flare mass, V the instantaneous particle velocity, and τ_0 the luminous efficiency coefficient. The integral extends over the luminous lifetime of the flare.

In the present study an alternative method is applied to determine the masses, based on the observed durations of the flares. The known data are:

H_i = the height at which the flare begins;
H_e = the height at which the flare ends;
V_i = the velocity of the flare mass at initial appearance; and
ρ = the atmospheric density along the trail.

[1] F. L. Whipple, *Proc. Am. Phil. Soc.*, **79**, 499, 1938.

[2] *Harvard Reprints*, Ser. II, No. 21, 1949.

By applying these data to the drag and mass equations, the initial mass can be determined. The boundary value problem requires the solution of the equations

$$\frac{dV}{dt} = -\Gamma A m^{-1/3} \rho V^2, \qquad \frac{dm}{dt} = -\frac{\Lambda A}{2\zeta} m^{2/3} \rho V^3, \tag{2}$$

the first of which is the drag equation, the second the mass equation; in these equations Γ is the drag coefficient, ζ the heat of vaporization or fusion of the flare material, Λ its coefficient of heat transfer, and $Am^{2/3}$ the effective cross-sectional area of the flare particle. In the solution the boundary conditions are

$$V(t_i) = V_i, \quad \text{and} \quad m(t_e) = 0,$$

where t_i = time of appearance and t_e = time of disappearance.

The initial condition is well determined; the meteor velocity is the most accurately determined parameter. The terminal condition is less certain. It will be assumed that the meteor flare remains visible up to the instant the mass is exhausted. This assumption has

TABLE 1

DECELERATIONS IN KM/SEC²

m (Gm)	V (Km/Sec)							
	$H = 65$ km; $\rho = 2.3 \times 10^{-7}$ Gm/Cm³				$H = 85$ km; $\rho = 2.2 \times 10^{-8}$ Gm/Cm³			
	10	25	40	65	10	25	40	65
1	1.2	2.6	18.4	48.6	0.1	0.2	1.7	4.5
0.5	1.5	3.3	23.3	61.1	0.1	0.3	2.2	5.7
0.1	2.5	5.6	39.6	105	0.2	0.5	3.7	9.8
0.05	3.1	7.0	50.0	132	0.3	0.7	4.7	12.4
0.01	5.4	12.0	85.5	226	0.5	1.1	8.0	21.1
0.005	6.7	17.5	107	284	0.6	1.7	10.1	26.6
0.001	11.5	25.9	184	486	1.1	2.4	17.3	45.4

been tested by numerical integration of the drag, mass, and luminosity equations for sample cases. The terminal masses prove to be negligible.

It is possible to derive a solution of the mass and drag equations for the mass, expressed in terms of the time or distance by means of exponential integrals. Unfortunately, the resultant expression for the flare mass involves the terminal velocity, which is unknown. Consequently, it is necessary to use a method of approximations. The drag equations must be integrated to find the deceleration as a function of mass, velocity, and height. Then the mass equation is to be integrated for various masses, the velocity along the trail being calculated from the known deceleration for each mass. The mass of the flaring particle is found by adjusting the initial mass in the mass equation so that the total mass is exhausted in the observed duration. The numerical calculations are greatly simplified without loss of accuracy by assuming a constant atmospheric density for each flare. Sample integrations for the decelerations as functions of V, m, and H are given in Table 1.

The observed durations of flares (0.1 second or less, on the average) indicate that the velocity of the flare mass will not depart much from the original velocity during its lifetime. Hence, as a first approximation, we can consider the velocity to be constant in the mass equation.

With these approximations, the mass equation can be integrated, as follows:

$$3\, m_f^{1/3} = \frac{\Lambda A}{2\zeta} \int_i^e \rho\,(t)\; V^3\,(t)\; dt$$

or

$$m_f = \left(\frac{\Lambda A}{6\zeta} \tilde{V}^3 \tilde{\rho}\, [S_e - S_i] \right)^3, \tag{3}$$

where $[S_e - S_i]$ represents the duration of the flare, while $\tilde{V} = V_i$ and $\tilde{\rho}$ is the atmospheric density at the mid-point of the trail.

The neglected deceleration introduces an error of less than 5 per cent in the mass. Numerical integration of the mass and drag equations shows that the terminal mass of a flare particle amounts to about 10^{-7} gm, which may be 1–10 per cent of the total mass in most cases. But the accuracy of equation (3) is limited chiefly by the difficulty of measuring the end-point of flares, since their light decreases exponentially. It appears likely that the measured durations are systematically underestimated, though this error will be partly compensated by neglecting the terminal mass. While it is difficult to estimate accurately the magnitude of all these uncertainties, the resultant masses may be expected to be correct to within 25–50 per cent.

The value adopted for the coefficient in equation (3) in c.g.s. units is

$$\frac{\Lambda A}{6\zeta} = 2.04 \times 10^{-13},$$

based on recent values of the ballistics constants communicated privately by F. L. Whipple. The atmospheric densities used in this study are those given in the N.A.C.A. tables.[3] These densities are in good agreement with those derived directly from the meteor trails by Jacchia.[4]

The present work deals with three meteors from the Harvard collection for which double-station observations are available and whose trajectories have been analyzed. Pertinent data for these meteors are listed in Table 2. The masses entered in Table 2 are

TABLE 2

FUNDAMENTAL METEOR DATA

No.	Shower	Plate No.	H_c (Km)	log $\rho(H_c)$	V_c (Km/Sec)	m_∞ (Gm)
828	Sporadic	{AI34591 / FA 2766}	81.4	−7.424	32.6	0.292
1173	Perseid	{AI36712 / FA 6771}	85.5	−7.701	59.6	.0097
1241	Sporadic	{AI39253 / FA 8683}	79.[illegible]	−7.330	29.1	0.543

Jacchia's, reduced by a factor of 0.0571 to conform to the system of ballistic constants adopted in this paper. Since only the ratios of masses are involved in the present discussion, the absolute system is not important. In fact, the absolute system of masses is extremely sensitive to ballistic constants and the assumed specific density of the meteoroid.[5] The present system corresponds to measured meteorite densities.

[3] Warfield, National Advisory Committee on Aeronautics, Technical Note No. 1200, pp. 1–50, 1947.

[4] *Harvard Reprints*, Ser. II, No. 32, 1949.

[5] F. L. Whipple, *A.J.*, **57**, 28, 1952 (abstr.).

TABLE 3

METEOR FLARE MASSES

Flare and Plates	τ_f (Sec)	H_e (Km)	ρ_e (Gm/Cm^2 $\times 10^6$)	V_k (Km/Sec)	m_f(HS) (Gm $\times 10^6$)	m_f(LJ) (Gm)	Ratio m_f(LJ)/m_f(HS) $\times 10^{-3}$
	Meteor No. 828						
a AI	0.0280	80.90	4.04	32.6	0.52	0.026	50
FA	.0337	80.83	4.09	.....	0.94	.....	.....
b AI	.0332	78.13	6.08	34.2	2.8	.032	10
FA	.0434	78.00	6.16	.....	6.6	.....	.....
c AI	.0301	76.72	7.14	32.3	3.2	.016	5
FA	.0430	76.55	7.28	.....	8.6	.....	.....
d AI	.0173	73.38	10.27	31.9	1.5	.....	.....
FA	.0384	73.11	10.55	.....	20.0	.....	.....
e AI	.0313	72.21	11.59	31.7	13.1	.068	150
FA	.0371	72.13	11.69	.....	22.7	.....	.....
f AI	.0253	71.10	12.94	31.3	8.6	.....	.....
FA	.0271	71.08	12.96	.....	10.7	.....	.....
g AI	.0056	67.00	19.14	30.0	0.23	0.008	40
FA	0.0040	67.02	19.10	.....	0.10	.....	.....
	Meteor No. 1173						
a AI	0.0210	88.21	1.30	59.9	1.8	0.0021	1
FA	.0129	88.36	1.27	.....	0.37	.....	.....
b AI	.0156	82.87	3.01	59.3	8.4	0.0016	0.2
FA	0.0158	82.87	3.01	.....	8.7	.....	.....
	Meteor No. 1241						
a AI	0.0075	77.28	6.70	29.0	0.02	0.060	300
FA	.0068	77.28	6.70	.....	0.01	.....	.....
b AI	.0360	76.20	7.57	28.9	2.5	.070	20
FA	.0199	76.37	7.43	.....	0.34	.....	.....
c AI	.0370	75.26	8.40	28.7	3.3	.038	10
FA	.0212	75.44	8.24	.....	0.58	.....	.....
d AI	.0247	74.22	9.40	28.4	1.30	.076	50
FA	.0103	74.36	9.27	.....	0.07	.....	.....
e AI	0.0135	72.53	11.21	27.6	0.24	0.011	5

The reduction of a double-station meteor observation provides the following necessary data: the time, t, and distance, S, along the trail for each successive break, both measured from the first visible break; the initial mass, m_∞, and velocity, V_∞; their values m_e and V_e at the middle of the trail; and the deceleration at the mid-point. In order to find the duration and initial height and velocity of a flare, it is necessary only to measure the position of its beginning and end relative to the breaks and then to interpolate in the $S(t)$- and $V(t)$-curve.

The raw measures of a plate give the co-ordinates of the breaks and the beginning and end-points of the flares, in microns. The durations, τ, are then to be expressed in fictional units of time. These will closely approximate the actual durations of the flares, so long as the decelerations of the flare masses are not excessive. The durations can then be converted to trajectory lengths from the data of the meteor trajectory.

Measures were made on both the AI and FA series. The FA camera produces softer images, which are more difficult to measure. Where large discrepancies are found between durations measured on AI and on FA plates, those of the AI are to be preferred.

In Table 3 are listed the important data for each flare included in this study, and the mass of each, m_f(HS), computed in the manner described above. The last two columns of Table 3 contain the masses m_f(LJ) of these same flares as computed by Jacchia and the ratio of Jacchia's masses to those computed in the present paper. The latter range from 0.1 to 20×10^{-6} gm. A flare mass of about 10^{-6} is representative. For particles with a density of 4 gm/cm^3, the diameters are 10^{-3} cm.

Masses computed by formula (2) are, on the average, 10^{-3}–10^{-4} times smaller than flare masses computed by Jacchia from the luminosity equation (1). The discrepancy suggests that the total mass ejected during a flare is in the form of a spray of thousands of microscopic fragments. The luminosity equation gives the integrated mass of the flare, while the masses determined by equation (3) represent an average value for the individual fragments. This conclusion is confirmed by constructing theoretical light-curves for the appropriate numbers of particles with masses derived in the present paper. Such light-curves have been constructed for flare *b* of meteor No. 1173 and for flare *d* of meteor No. 1241 and are in satisfactory agreement with the observed light-curves.

As a further check on the accuracy of the flare-mass computations by equation (3), numerical integrations of the mass and drag equations (2) were carried out for these same two flares, in the manner described above. The results indicate that the accuracy of the mass determinations is severely limited by the small precision with which one can measure the end of a flare. Nevertheless, the numerical integrations confirm the small masses within about 50 per cent.

The author takes pleasure in acknowledging his gratitude to F. L. Whipple, who originally suggested this problem and who has generously assisted in its pursuit. Plate measurements were made on a Mann micrometer at the Massachusetts Institute of Technology Computing Bureau, through the kindness of L. Jacchia.

A STOCHASTIC MODEL OF A FLUCTUATING DENSITY FIELD

ALLADI RAMAKRISHNAN
Department of Physics, University of Madras, India
Received August 18, 1953

ABSTRACT

In this paper a stochastic model of a fluctuating density field is developed. On this model, functions expressing the correlation between the densities at n points are derived. These correlation functions are used in treating the problem of the fluctuations in brightness of the Milky Way in the light of the new picture of the continuous distribution of interstellar matter. The results of Chandrasekhar and Münch are extended to the higher moments of the probability distribution of the brightness of the Milky Way. In the course of the study a few theorems relating to the stochastic theory of the stationary state are derived.

The present study has been stimulated by the introduction of the concept of a fluctuating density field by Chandrasekhar and Münch[1] in connection with the astrophysical problem of fluctuations in brightness of the Milky Way. The mathematical and statistical implications of such a field are of considerable interest, since it introduces the notion of the addition of infinitesimal random variables.

Suppose $\rho(\boldsymbol{t})$ is a stochastic variable associated with a point in space denoted by the position vector $\boldsymbol{t}$, and let its probability distribution function be $\Pi(\rho; \boldsymbol{t})$. If the physical problem requires the quantity $M(V) = \int_V \rho dv$, where V is the domain of integration and $dv = dt^{(1)}dt^{(2)} \ldots dt^{(n)}$, where $t^{(1)}, t^{(2)}, \ldots, t^{(n)}$ are the components of the n-dimensional vector $\boldsymbol{t}$, then $M(V)$ is also a stochastic variable. In Section I we shall enunciate a theorem of general validity connecting the moments of M with the functions expressing the correlation between the ρ's at various points in space. There are difficulties in setting up an actual consistent mechanism in two or more spatial dimensions which will enable us either to determine the correlation between ρ's at various points in space or generate the moments of M in a fluctuating density field.[2] The purpose of this paper is to develop a model of a stochastic field in a space of *one* dimension and determine the correlation functions. It seemed worth while to develop such a model, since it is useful in extending the recent results of Chandrasekhar and Münch to higher moments. In modern theories of turbulence the functions defining the correlation of densities at two or three points are *assumed;* but in this paper we shall derive the function defining the correlation of densities at n points on the basis of a proposed stochastic model.

I. MOMENTS OF THE STOCHASTIC VARIABLE M

Since $M(V) = \int_V \rho dv$, we write formally $\rho dv_1 = dM(v_1), dv_1 = dt_1^{(1)}dt_1^{(2)} \ldots dt_1^{(n)}$. We split the domain of integration into N parts, $dv_1, dv_2, \ldots, dv_N$, arbitrarily and write

$$M(V) = \sum_{i=1}^{N} dM(v_i) \qquad \text{as} \qquad N \to \infty . \tag{1}$$

The procedure is similar to that adopted in the definition of Riemann integration. If

[1] *Ap. J.*, **115**, 103, 1952.

[2] A comprehensive formalism of such a field is given in terms of the characteristic functional in a long and fundamental paper by E. Hopf "Statistical Hydromechanics and Functional Calculus," *Journal of Rational Mechanics and Analysis*, Vol. 1, No. 1 (January, 1952).

the nth moment of M is $\epsilon\{M^n\}$, then[3]

$$\epsilon\{M^n(V)\} = \epsilon\{dM(v_1) + dM(v_2) \ldots + dM(v_N)\}^n \qquad \text{as} \quad N \to \infty , \tag{2}$$

$$\epsilon\{M(V)\} = \epsilon\{dM(v_1)\} + \epsilon\{dM(v_2)\} \ldots + \epsilon\{dM(v_N)\} \qquad \text{as} \quad N \to \infty , \tag{3}$$

i.e.,

$$\epsilon\{M(V)\} = \int_V \epsilon\{\rho(t_1)\}\, dv_1 \tag{4}$$

since

$$\epsilon\{dM(v_i)\} = \epsilon\{\rho(t_i)\}\, dv_i . \tag{5}$$

We shall assume that $\epsilon\{dM(v_i)dM(v_j)\} = O(dv_i dv_j)$ (including $i = j$) and write it as $\epsilon\{\rho(t_i)\rho(t_j)\}dv_i dv_j$. Thus $\epsilon\{\rho(t_i)\rho(t_j)\}$ expresses the density correlation between two points t_i and t_j. In a similar way we write

$$\epsilon\{dM(v_1)\, dM(v_2) \ldots dM(v_n)\} = \epsilon\{\rho(t_1)\, \rho(t_2) \ldots \rho(t_n)\}\, dv_1 dv_2 \ldots dv_n . \tag{6}$$

Hence as $N \to \infty$, i.e., as the dv's tend to zero, we get Theorem I.

THEOREM I

$$\epsilon\{M^n(V)\} = \int_V \int_V \ldots \int_V \epsilon\{\rho(t_1)\, \rho(t_2) \ldots \rho(t_n)\}\, dv_1 dv_2 \ldots dv_n .$$

Correlations of degree less than n do not enter into $\epsilon\{M^n(V)\}$, since if we expand $[dM(v_1) + dM(v_2) + \ldots + dM(v_N)]^n$ and pass to the limit as N tends to infinity, the summation of terms which are not products of n different infinitesimal dM's yields quantities which are of order dv or higher.

The above result may seem surprising, since in the case of certain correlation functions known as "product densities" formulated by the author in an earlier paper[4] the nth moments of the stochastic variable involve integrals of correlation functions of degree less than or equal to n. We shall not only compare the results but derive them from the theorem relating to product densities. In doing so, we will be passing from the "particle" to the "fluid" concepts of density.

Recalling the definition of product densities in the case of particles distributed in the t-space, we define $f_n(t_1, t_2, \ldots, t_n)$ as the product density of degree n, so that $f_n(t_1, t_2, \ldots, t_n)dv_1 dv_2 \ldots dv_n$ represents the probability that there is one particle in dv_1, one in $dv_2, \ldots$, and one in dv_n, irrespective of the number elsewhere. If we let $N(V)$ denote the stochastic variable expressing the number of particles in V, then

$$\epsilon\{N^n(V)\} = \sum_{s=1}^{n} \int_V \int_V \ldots \int_V C_s^n f_s(t_1, t_2, \ldots, t_s)\, dv_1 dv_2 \ldots dv_s , \tag{7}$$

where C_s^n are coefficients defined in the earlier paper. Here we shall need only C_n^n and C_{n-1}^n:

$$C_n^n = 1 , \qquad C_{n-1}^n = \frac{n(n-1)}{2} . \tag{8}$$

We call $f_1(t)$ the mean density of particles at the point t. We shall now establish the connection between the stochastic variables $M(V)$ and $N(V)$. Let us associate with each particle a mass m. Then, if $M(V)$ be the mass in the volume V, $M(V)$ is a stochastic variable, since $M(V) = mN(V)$. The nth moment of $M(V)$ according to the theory of

[3] Throughout this paper ϵ denotes expectation value.

[4] *Proc. Cambridge Phil. Soc.*, **46**, 595, 1950.

product densities is given by

$$\epsilon\{M^n(V)\} = \sum_{s=1}^{n} \int_V \int_V \cdots \int_V m^n C_s^n f_s(t_1, t_2, \ldots, t_s)\, dv_1 dv_2 \ldots dv_s . \tag{9}$$

We can call $mf_1(t_1)$ the "mean mass density." Let us assume that $m \to 0$ and $f_1, f_2, \ldots, f_n \to \infty$ in such a manner that

$$m f_1(t_1) \to \epsilon\{\rho(t_1)\}, \qquad m^2 f_2(t_1, t_2) \to \epsilon\{\rho(t_1)\rho(t_2)\}, \ldots,$$

and

$$m^n f_n(t_1, t_2, \ldots, t_n) \to \epsilon\{\rho(t_1)\rho(t_2)\ldots\rho(t_n)\}. \tag{10}$$

In such a case

$$\epsilon\{M^n(V)\} \to \int_V \int_V \cdots \int_V \epsilon\{\rho(t_1)\rho(t_2)\ldots\rho(t_n)\}\, dv_1 dv_2 \ldots dv_n , \tag{11}$$

since the other terms are of the order of $m, m^2, \ldots, m^n$. If we now assume m to be so small that only m^2 and higher powers of m can be neglected, we find that

$$\epsilon\{M^n(V)\} = \int_V \int_V \cdots \int_V \epsilon\{\rho(t_1)\rho(t_2)\ldots\rho(t_n)\}\, dv_1 dv_2 \ldots dv_n + m\,\frac{n(n-1)}{2} \int_V \int_V \cdots \int_V \epsilon\{\rho(t_1)\rho(t_2)\ldots\rho(t_{n-1})\}\, dv_1 dv_2 \ldots dv_{n-1} + O(m^2) . \tag{12}$$

We shall find this approximation useful in connection with the astrophysical problem.

We immediately note the following very interesting result. If we assume that

$$\epsilon\{\rho(t_1)\rho(t_2)\ldots\rho(t_n)\} = \epsilon\{\rho(t_1)\}\epsilon\{\rho(t_2)\}\ldots\epsilon\{\rho(t_n)\} \tag{13}$$

for all n, i.e., the density at one point is independent of the density at another, then

$$\epsilon\{M^n(V)\} = [\epsilon\{M(V)\}]^n , \tag{14}$$

i.e., $M(V)$ is no longer a statistical variable and is deterministic! This may seem a paradox at first sight, but we shall show that this is consistent not only with the results already obtained but also with the physical facts. The deeper mathematical significance of assuming equation (12) will be clearly brought out in the next section. We can observe that the condition corresponding to formula (13) in regard to product densities is

$$f_n(t_1, t_2, \ldots, t_n) = f_1(t_1) f_1(t_2) \ldots f_1(t_n) , \tag{15}$$

i.e., $N(V)$ has a Poisson distribution. But if $\epsilon\{N(V)\}, \epsilon\{N^2(V)\}, \ldots, \epsilon\{N^n(V)\}$ tend to infinity in such a manner that only $M(V) = mN(V)$ has a physical significance, then, since, according to the Poisson distribution,

$$\epsilon\{N^n(V)\} = \sum_s C_s^n [\epsilon\{N(V)\}]^s , \tag{16}$$

we shall have

$$\epsilon\{M^n(V)\} \to [\epsilon\{M(V)\}]^n + O(m) \qquad \text{as} \qquad m \to 0 . \tag{17}$$

If we neglect terms only of order m^2 and higher, we have

$$\epsilon\{M^n(V)\} = [\epsilon\{M(V)\}]^n + \frac{n(n-1)}{2}\, m\, [\epsilon\{M(V)\}]^{n-1} + O(m^2) . \tag{18}$$

We have now established a complete correspondence between the "particle" and the

"fluid" concepts of density. In what follows we shall be concerned only with the "fluid" concept, i.e., with the ρ's. The determination of the correlation functions is a very difficult problem. Even in turbulence theory, functions of degrees 2 and 3 are assumed a priori but are not "derived." In stochastic theory the correlation between two statistical variables is obtained normally through their joint distribution. To determine the joint probability $\Pi(\rho_2, \rho_1; t_2, t_1)d\rho_2 d\rho_1$ that $\rho(t_1) = \rho_1$ and $\rho(t_2) = \rho_2$, we have to know the conditional probability[5] $\Pi(\rho_2 | \rho_1; t_2, t_1)d\rho_2$ that $\rho(t_2) = \rho_2$, given that $\rho(t_1) = \rho_1$. In the theory of stochastic processes, if t is a continuous parameter, $\Pi(\rho_2 | \rho_1; t_2, t_1)$ is determined only in the case when t is one-dimensional (and in this case we write it as t) and Π is homogeneous and Markovian with respect to t, i.e., a function only of $t_2 - t_1$ $(t_2 > t_1)$. If

$$\Pi(\rho_2 | \rho_1; t_2 - t_1) \to R(\rho_2 | \rho_1)(t_2 - t_1) \qquad \text{as} \qquad t_2 - t_1 \to 0 \quad (\rho_2 \neq \rho_1),$$

then $\Pi(\rho_2 | \rho_1; t_2 - t_1)$ can be expressed in terms of $R(\rho_2 | \rho_1)$.

We note that the essential feature of the foregoing method is that the parameter t is ordered (this is possible only if t is one-dimensional) and the probability distribution of $\rho(t_2)$ is determined if the "state" at t_1, i.e., the probability distribution of $\rho(t_1)$ is known $(t_1 < t_2)$. Such a stochastic "field" we call a "process" to denote the "evolution" of the probability distribution with increasing t. The characteristic feature of a "process" is that the state at t is completely determined by the state "prior" to t and "boundary" conditions have to be satisfied at $t' < t$. We shall come to understand the full significance of this statement in the next section.

If t is n-dimensional, t cannot be ordered, and it is mathematically difficult to define transition probabilities for infinitesimal changes in t. The situation seems difficult, at least from the point of view of the physicist.

One way of getting around the difficulty is to consider the joint distribution $\Pi(\rho_n, \rho_{n-1}, \ldots, \rho_1; t_n, t_{n-1}, \ldots, t_1)$ to be functions of another parameter, τ, which can be ordered and then to consider transition probabilities for infinitesimal changes in τ; i.e., we assume that the stochastic "field" with respect to t is a "process" with respect to τ.

Incidentally, it must be noted that we can define joint distribution only at enumerable points. Since the t-space is a continuum, it is mathematically difficult to define the joint distribution of all points, though from a physical point of view such a distribution exists; and we leave its formal definition to the pure mathematician. We must be content with the joint distribution at n points (n can be made as large as we please), and this helps us to determine the nth integral moment of the stochastic variable $M(V)$. In the following section, we shall consider the case when t is one-dimensional and can be denoted simply by t. Our stochastic model will help us determine the joint distributions.

II. TWO THEOREMS ON INVERSE PROBABILITY IN RELATION TO MARKOFF PROCESSES

Let us consider the case of a stochastic process progressing with respect to t and defined by the probability distribution function at t of a stochastic variable $\rho(t)$. If the process is homogeneous and Markovian with respect to t, we ask: What is the conditional probability $\Pi(\rho_2 | \rho_1; t_2, t_1)d\rho_2 \equiv \Pi(\rho_2 | \rho_1; t_2 - t_1)d\rho_2 \, (t_2 > t_1)$ that the stochastic variable $\rho(t_2) = \rho_2$, given that $\rho(t_1) = \rho_1$? The process "evolves" with increasing t; the state at t_2 is determined completely by the state prior to t_2, and no boundary conditions at $t' > t_2$ need be satisfied when we wish to determine the state at t_2. Since the process is Markovian, if we are given the boundary conditions at t_1 and t_0 $(t_0 < t_1, t_2)$, the boundary conditions at t_0 are irrelevant. We shall call Π the "forward" transition probability.

Is it possible to obtain the "backward" transition probability, $P(\rho_1 | \rho_2; t_1, t_2)d\rho_1$ that $\rho(t_1) = \rho_1$, given that $\rho(t_2) = \rho_2$ $(t_2 > t_1)$? We note that P, unlike Π, is not homo-

[5] In this paper we use Π for a probability distribution function. If the functions are different, the difference will be apparent from the way in which the variables are written inside the brackets. In Sec. II, only in the case of backward transition probabilites do we use the symbol P.

geneous in t_2 and t_1, i.e., it is not completely determined by the interval $t_2 - t_1$. The moment we ask what is the state at t_1, we have tacitly assumed that the process started at some $t_0 < t_1$, i.e., the process is homogeneous in the three variables t_0, t_1, and t_2, which is to say it is a function of $t_1 - t_0$, $t_2 - t_1$, $t_2 - t_0$. In other words, the boundary conditions at $t_2 > t_1$ do not determine the state at t_1 uniquely. In addition, the boundary condition at $t_0 < t_1$ has to be specified. Thus we must speak of the backward transition probability $P(\rho_1 | \rho_2, \rho_0; t_1, t_2, t_0)d\rho_1$, the probability that $\rho(t_1) = \rho_1$, given that $\rho(t_2) = \rho_2$, $\rho(t_0) = \rho_0$ $(t_0 < t_1 < t_2)$.

We shall now prove that if we are given the boundary conditions at t_2 and t_3, the boundary condition at t_3 $(t_1 < t_2 < t_3)$ is irrelevant to determine the state at t_1.

THEOREM II

If a stochastic process, defined by the probability distribution of a stochastic variable $\rho(t_1)$ at $t = t_1$, is Markovian with respect to t, $t < t_1$, it is also Markovian with respect to $t > t_1$.

Proof:

Consider the joint probability[6] $\mathfrak{P}(\rho_3, \rho_1 | \rho_2, \rho_0; t_3, t_1, t_2, t_0)d\rho_3 d\rho_1$ that $\rho(t_3) = \rho_3$ and $\rho(t_1) = \rho_1$, given that $\rho(t_2) = \rho_2$ and $\rho(t_0) = \rho_0$ $(t_0 < t_1 < t_2 < t_3)$. By definition,

$$\begin{aligned}\mathfrak{P}(\rho_3, \rho_1 | \rho_2, \rho_0; t_3, t_1, t_2, t_0) &= P(\rho_1 | \rho_2, \rho_0; t_1, t_2, t_0)\,\Pi(\rho_3 | \rho_2, \rho_1, \rho_0; t_3, t_2, t_1, t_0) \\ &= P(\rho_1 | \rho_2, \rho_0; t_1, t_2, t_0)\,\Pi(\rho_3 | \rho_2; t_3, t_2)\,. \end{aligned} \tag{19}$$

By definition of joint probability, this is also equal to

$$\begin{aligned}&\Pi(\rho_3 | \rho_2, \rho_0; t_3, t_2, t_0)\,P(\rho_1 | \rho_3, \rho_2, \rho_0; t_1, t_3, t_2, t_0) \\ &\qquad = \Pi(\rho_3 | \rho_2; t_3, t_2)\,P(\rho_1 | \rho_3, \rho_2, \rho_0; t_1, t_3, t_2, t_0)\,. \end{aligned} \tag{20}$$

Equating equations (19) and (20), we obtain

$$P(\rho_1 | \rho_2, \rho_0; t_1, t_2, t_0) = P(\rho_1 | \rho_3, \rho_2, \rho_0; t_1, t_3, t_2, t_0) \qquad (t_0 < t_1 < t_2 < t_3)\,, \tag{21}$$

which proves our theorem.

We shall now express P in terms of Π. This immediately follows from the definition of the joint probability that $\rho(t_1) = \rho_1$, $\rho(t_2) = \rho_2$, given that $\rho(t_0) = \rho_0$ $(t_0 < t_1 < t_2)$:

$$\begin{aligned}\Pi(\rho_1, \rho_2 | \rho_0; t_1, t_2, t_0) &= \Pi(\rho_1 | \rho_0; t_1, t_0)\,\Pi(\rho_2 | \rho_1; t_2, t_1) \\ &= \Pi(\rho_2 | \rho_0; t_2, t_0)\,P(\rho_1 | \rho_2, \rho_0; t_1, t_2, t_0)\,. \end{aligned} \tag{22}$$

Therefore,

$$P(\rho_1 | \rho_2, \rho_0; t_1, t_2, t_0) = \frac{\Pi(\rho_1 | \rho_0; t_1, t_0)\,\Pi(\rho_2 | \rho_1; t_2, t_1)}{\Pi(\rho_2 | \rho_0; t_2, t_0)}\,. \tag{23}$$

If the process is homogeneous in t, $\Pi(\rho_1 | \rho_0; t_1, t_0)$ is a function of $t_1 - t_0$, $\Pi(\rho_2 | \rho_1; t_2, t_1)$ of $t_2 - t_1$, $\Pi(\rho_2 | \rho_0; t_2, t_0)$ of $t_2 - t_0$; and so $P(\rho_1 | \rho_2, \rho_0; t_1, t_2, t_0)$ is a function of $t_1 - t_0$, $t_2 - t_1$, and $t_2 - t_0$.

According to stochastic theory, under certain circumstances, as $t_2 \to t_1$, i.e., as $t_2 - t_1, \to +0$,

$$\Pi(\rho_2 | \rho_1; t_2 - t_1) \to R(\rho_2 | \rho_1)\,\Delta t + \delta(\rho_2 - \rho_1)\,\phi(\Delta t)\,, \tag{24}$$[7]

[6] Here we use the symbol $\mathfrak{P}$, since it is neither a backward nor a forward transition probability, but a "mixture" of the two.

[7] Hereafter, for the sake of brevity, we shall omit the δ-function part of the limit, though it will be taken into consideration in computing Π. Also δ denotes the Dirac delta function.

where $\Delta t = t_2 - t_1$ and $\phi(\Delta t) = 1 - \Delta t \int_{\rho_2} R(\rho_2 | \rho_1) d\rho_2$; and where such a limit exists, Π satisfies the well-known equation:

$$\frac{\partial \Pi(\rho_2 | \rho_1; t_2 - t_1)}{\partial t_2} = -\Pi(\rho_2 | \rho_1; t_2 - t_1) \int_{\rho'} R(\rho' | \rho_2)\, d\rho' + \int_{\rho'} \Pi(\rho' | \rho_1; t_2 - t_1) R(\rho_2 | \rho')\, d\rho' . \tag{25}$$

As $t_2 \to t_1$, i.e., as $t_2 - t_1 \to +0$, we get

$$P(\rho_1 | \rho_2, \rho_0; t_1, t_2, t_0) \to R_1(\rho_1 | \rho_2, \rho_0; t_1 - t_0) \, | t_2 - t_1 | = \frac{\Pi(\rho_1 | \rho_0; t_1 - t_0) R(\rho_2 | \rho_1)}{\Pi(\rho_2 | \rho_0; t_2 - t_0)} \, | t_2 - t_1 | . \tag{26}$$

As $t_1 \to t_0$, i.e., as $t_1 - t_0 \to +0$, we get

$$P(\rho_1 | \rho_2, \rho_0; t_1, t_2, t_0) \to R_2(\rho_1 | \rho_2, \rho_0; t_2 - t_0) \, | t_1 - t_0 | = \frac{R(\rho_1 | \rho_0) \Pi(\rho_2 | \rho_1; t_2 - t_1)}{\Pi(\rho_2 | \rho_0; t_2 - t_0)} \, | t_1 - t_0 | . \tag{27}$$[8]

It is possible to write integrodifferential equations for P exactly similar to equation (25) in terms of either R_1 or R_2, but we shall be concerned only with the special case, in which

$$\Pi(\rho_2 | \rho_1; t_2 - t_1) \to \psi(\rho_2) \qquad \text{as} \qquad t_2 - t_1 \to \infty , \tag{28}$$

i.e., *when* $\Pi(\rho_2 | \rho_1; t_2 - t_1)$ *tends to a stationary distribution independent of the state at the starting point.* In this case the above expressions reduce to

$$R_1(\rho_1 | \rho_2, \rho_0; t_1 - t_0) \to \frac{\psi(\rho_1) R(_2\rho | \rho_1)}{\psi(\rho_2)} \qquad \text{as} \qquad t_1 - t_0 \to \infty , \tag{29}$$

and

$$R_2(\rho_1 | \rho_2, \rho_0; t_2 - t_0) \to R(\rho_1 | \rho_0) \qquad \text{as} \qquad t_2 - t_0 \to \infty . \tag{30}$$

Note that the existence of the limits for R_1 and R_2 given in expressions (29) and (30) presupposes a stationary state, while R exists whether or not Π reaches a stationary state. It is not surprising that, when the limit of R_2 exists, $R_2(\rho_1 | \rho_2, \rho_0; t_2 - t_0) \to R(\rho_1 | \rho_0)$ as $t_2 - t_0$ tends to infinity, since R_2 differs from R, in that an additional boundary condition at $t_2 > t_0$ has to be satisfied, and, when $t_2 - t_0$ tends to infinity, the boundary condition becomes irrelevant.

A very interesting result follows from expressions (29) and (30). It is reasonable to suppose that in the stationary state, since all the differential coefficients of Π vanish in equation (25), we can write[9]

$$\psi(\rho_1) R(\rho_2 | \rho_1) = \psi(\rho_2) R(\rho_1 | \rho_2) . \tag{31}$$

Hence, from expressions (29) and (30),

$$R_2(\rho' | \rho) \equiv R_1(\rho' | \rho) \equiv R(\rho' | \rho) , \tag{32}$$

where $R_2(\rho' | \rho)$ and $R_1(\rho' | \rho)$ are the limits of R_2 and R_1 according to equations (29) and (30), i.e., the backward and forward transition probabilities per unit change in the parameter are identical in the stationary state. We state the above result in a more precise form as Theorem III.

[8] Note that in eq. (26) $t_2 - t_0 = t_1 - t_0$ and in eq. (27), $t_2 - t_1 = t_2 - t_0$.

[9] This is called the "principle of detailed balance" in statistical mechanics.

THEOREM III

If a stochastic process progressing with respect to a one-dimensional parameter t is Markovian and homogeneous with respect to t and can be represented by a function $\Pi(\rho_2|\rho_1; t_2, t_1) = \Pi(\rho_2|\rho_1; t_2 - t_1)$, which expresses the probability that $\rho(t_2) = \rho_2$, given that $\rho(t_1) = \rho_1 (t_2 > t_1)$, then, if $P(\rho_1|\rho_2, \rho_0; t_1, t_2, t_0) = P(\rho_1|\rho_2, \rho_0; t_1 - t_0, t_2 - t_0, t_2 - t_1)$ denotes the probability that $\rho(t_1) = \rho_1$, given that $\rho(t_2) = \rho_2$ and $\rho(t_0) = \rho_0$ $(t_0 < t_1 < t_2)$, and if

$$P(\rho_1|\rho_2, \rho_0; t_1 - t_0, t_2 - t_0, t_2 - t_1) \to R_1(\rho_1|\rho_2)\,|t_2 - t_1|$$

as

$$t_1 - t_0 \to \infty \qquad \text{and} \qquad t_2 \to t_1 \tag{33}$$

and

$$P(\rho_1|\rho_2, \rho_0; t_1 - t_0, t_2 - t_0, t_2 - t_1) \to R_2(\rho_1|\rho_0)\,|t_1 - t_0|$$

as

$$t_2 - t_0 \to \infty \qquad \text{and} \qquad t_1 \to t_0\,,$$

then it follows that

$$R_1(\rho'|\rho_1)\,|\Delta t_1| = R_2(\rho'|\rho_1)\,|\Delta t_1| = R(\rho'|\rho_1)\,|\Delta t_1|\,. \tag{34}$$

In equation (34) $\Delta t_1 = t' - t_1$; in R_2 and R we make it tend to $+0$, and in R_1 we make it tend to -0; but the infinitesimal intervals occurring in each of the three terms must have the same magnitude. We use the symbol t' instead of some t_i, since we want $t' - t_1 \to +0$ in the case of R_2 and R and $t' - t_1 \to -0$ in the case of R_1. Note that R_1 is the limit as $t_1 - t_0 \to +\infty$, where t_0 is the origin of the process, i.e., it is the backward transition probability per unit change in parameter in the *stationary state*. The above theorem is merely a generalization of the observations of Feller and Bartlett[10] to continuous time.

III. CALCULATION OF THE CORRELATION FUNCTIONS

In the case of a process, Markovian and homogeneous with respect to t, the joint probability that $\rho(t_n) = \rho_n$, $\rho(t_{n-1}) = \rho_{n-1}, \ldots,$ and $\rho(t_1) = \rho_1$, given that $\rho(t_0) = \rho_0$, is given by

$$\begin{aligned}&\Pi(\rho_n, \rho_{n-1}, \ldots, \rho_1|\rho_0; t_n, t_{n-1}, \ldots, t_1, t_0)\\ &\quad = \Pi(\rho_1|\rho_0; t_1 - t_0)\,\Pi(\rho_2|\rho_1; t_2 - t_1) \ldots \Pi(\rho_n|\rho_{n-1}; t_n - t_{n-1})\,,\end{aligned} \tag{35}$$

where $\Pi(\rho_i|\rho_{i-1}; t_i, t_{i-1})$ is the probability that $\rho(t_i) = \rho_i$, given that $\rho(t_{i-1}) = \rho_{i-1}$. Hence

$$\begin{aligned}\epsilon\{\rho(t_1)\,\rho(t_2) \ldots \rho(t_n)\} = &\int_{\rho_n}\int_{\rho_{n-1}} \ldots \int_{\rho_1} \rho_1\rho_2 \ldots \rho_n \Pi(\rho_1|\rho_0; t_1 - t_0)\\ &\times \Pi(\rho_2|\rho_1; t_2 - t_1) \ldots \Pi(\rho_n|\rho_{n-1}; t_n - t_{n-1})\,(d\rho_1 d\rho_2 \ldots d\rho_n)\,.\end{aligned} \tag{36}$$

If ρ_1 has a stationary distribution as $t_1 - t_0 \to \infty$,

$$\begin{aligned}\epsilon\{\rho(t_1)\,\rho(t_2) \ldots \rho(t_n)\} = &\int_{\rho_n}\int_{\rho_{n-1}} \ldots \int_{\rho_1} \rho_1\rho_2 \ldots \rho_n \psi(\rho_1) \Pi(\rho_2|\rho_1; t_2 - t_1)\\ &\times \Pi(\rho_3|\rho_2; t_3 - t_2) \ldots \Pi(\rho_n|\rho_{n-1}; t_n - t_{n-1})\,d\rho_1 d\rho_2 \ldots d\rho_n\,.\end{aligned} \tag{37}$$

Thus we have formally determined the correlation function of degree n, where n is a positive integer which can be made as large as we please.

In view of Theorems II and III, the backward and forward transition probabilities are identical as long as we assume that $t_1 - t_0 \to \infty$. Thus we could have assumed that

[10] W. Feller, *An Introduction to Probability and Its Applications* (New York: John Wiley & Sons, 1950), Sec. 15.11; M. S. Bartlett, *J. R. Statistical Soc.*, **13**, 11, 265.

$t_i - t_0 \to \infty$, i.e., the distribution at t_i is stationary where $i = n, n-1, \ldots, 1$ and the joint probability $\Pi(\rho_n, \rho_{n-1}, \ldots, \rho_1; t_n, t_{n-1}, \ldots, t_1)$ will still be the same, i.e., the stochastic "process" is now "a stochastic field isotropic with respect to t."

We must remember that this isotropic stochastic field is Markovian. We shall show that the field adequately describes all the features of the "wildly" fluctuating density field of Chandrasekhar and Münch.

IV. STOCHASTIC MODEL OF A FLUCTUATING DENSITY FIELD

Let us assume that $\Pi(\rho' \mid \rho; \mid t' - t \mid) \to R(\rho' \mid \rho) \mid t' - t \mid$ as $\mid t' - t \mid \to 0$. We assume that $R(\rho' \mid \rho)$ is only a function of ρ' and write $R(\rho' \mid \rho) = X(\rho')$. Notice that

$$\int_{\rho'} R(\rho' \mid \rho)\, d\rho' = \int_{\rho'} X(\rho')\, d\rho' = a\,,$$

i.e., the total probability that some transition takes place from ρ is independent of ρ. Therefore, Π satisfies the equation

$$\begin{aligned} \frac{\partial \Pi(\rho' \mid \rho; \mid t' - t \mid)}{\partial \mid t' - t \mid} &= -\Pi(\rho' \mid \rho; \mid t' - t \mid)\, a + \int_{\rho''} \Pi(\rho'' \mid \rho; \mid t' - t \mid)\, X(\rho')\, d\rho'' \\ &= -\Pi(\rho' \mid \rho; \mid t' - t \mid)\, a + X(\rho')\,, \end{aligned} \tag{38}$$

since

$$\int_{\rho''} \Pi(\rho'' \mid \rho; \mid t' - t \mid)\, d\rho'' = 1\,.$$

Hence

$$\Pi(\rho' \mid \rho; \mid t' - t \mid) = \frac{X(\rho')}{a}(1 - e^{-a \mid t' - t \mid}) + \delta(\rho' - \rho)\, e^{-a \mid t' - t \mid}\,, \tag{39}$$

where δ is the Dirac delta function.

As

$$\mid t' - t \mid \to \infty\,, \qquad \Pi(\rho' \mid \rho; \mid t' - t \mid) \to \frac{X(\rho')}{a} = \psi(\rho')\,. \tag{40}$$

Using in equation (37) the expression given in equation (39), we get:

$$\epsilon\{\rho(t)\, \rho(t')\} - [\epsilon\{\rho\}]^2 = [\epsilon\{\rho^2\} - (\epsilon\{\rho\})^2]\, e^{-a \mid t' - t \mid} \tag{41}$$

where

$$\epsilon(\rho^n) = \int_0^\infty \rho^n \psi(\rho)\, d\rho\,.$$

Now let us assume that a is very large. Then Π tends to the stationary state very rapidly. It is easily seen that, when a is very large, for $\mid t' - t \mid \gg 1/a$, $\Pi \to \psi$, and hence in this case the distribution at t' is independent of the distribution at t. But, however large a may be, the densities are not independent in the range $0 < \mid t' - t \mid < 1/a$. The quantity $1/a$ is well known in turbulence as the "mixing length." In fact, as $\mid t' - t \mid \to 0$, $\Pi(\rho' \mid \rho; t' - t) \to \delta(\rho' - \rho)$. Herein lies the answer to the apparent paradox mentioned in Section I. However "wild" be the density fluctuation, i.e., however large a may be, densities at two points separated by a distance less than $1/a$ are correlated. We shall later establish a connection between $1/a$ and the quantity m occurring in the limiting process of product densities.

We note that the Markovian stochastic field described above has all the features of the "wildly" fluctuating density field of Chandrasekhar and Münch. A wildly fluctuating field where correlation tends to zero, with increasing distance between two points, can be approximated by a Markovian field. In order to see this, consider the joint distribu-

tion of densities at three points, t_1, t_2, and t_3. Then the correlation between t_1 and t_3 is of a higher order of smallness than that between t_2 and t_3 ($t_1 < t_2 < t_3$); and, as $t_3 - t_2 \to 0$, the state at t_3 depends only on the state at t_2 and is "almost" independent of the state at $t_1 (t_1 < t_2)$.

Now let us calculate the correlation functions given by equation (37). We have merely to feed expression (39) into equation (37). If we assume a to be large, we shall get just the simple result that the densities at $t_1, t_2, \ldots, t_n$ ($t_1 < t_2 < \ldots < t_n$) are independent, provided that $t_i - t_{i-1} \gg 1/a$. But in any process of integration with respect to the t_i's, as, for example, in the use of Theorem I, it is fallacious to assume complete independence; for, as $t_i \to t_{i-1}$, a correlation exists which contributes a correction term of the order of $1/a$ when a is very large.

The approximation which assumes that a is large is mathematically equivalent to replacing $e^{-at'}$ by $1/a\delta(t')$—where δ is the Dirac δ-function—in any integration with respect to t' over any domain $0 \leq t' \leq t$ for which $t \gg 1/a$, since

$$\int_0^t e^{-at'} dt' = \frac{1}{a}(1 - e^{-at}) = \frac{1}{a} \quad \text{if} \quad t \gg \frac{1}{a}. \tag{42}$$

The contribution to this integral comes from a very small range $0 < t' < \gamma$, where γ is of order $1/a$. Thus, so long as $t \gg 1/a$, we can replace $e^{-at'}$ by $a^{-1}\delta(t')$; and hence in the integration with respect to t' we write (39) as

$$\Pi(\rho' \mid \rho; t' - t) = \psi(\rho')\left[1 - \frac{1}{a}\delta(t' - t)\right] + \frac{1}{a}\delta(\rho' - \rho)\,\delta(t' - t). \tag{43}$$

Using this, we shall calculate

$$M(t) = \int_0^t \rho(t')\, dt'. \tag{44}$$

Neglecting terms of the order of $(1/a)^2$, we obtain

$$\begin{aligned} \epsilon\{M^n(t)\} = \int_0^t dt_1 \int_0^t dt_2 \ldots \int_0^t dt_n \int_{\rho_n} d\rho_n \int_{\rho_{n-1}} d\rho_{n-1} \ldots \int_{\rho_1} d\rho_1\, \rho_1 \rho_2 \ldots \rho_n \\ \times \psi(\rho_1)\psi(\rho_2)\ldots\psi(\rho_n)\left\{1 + \frac{1}{a}\left[-\sum_{i=1}^{n}\delta(t_i - t_{i-1}) + \sum_{i=1}^{n}\frac{1}{\psi(\rho_i)}\right.\right. \\ \left.\left. \times \delta(\rho_i - \rho_{i-1})\,\delta(t_i - t_{i-1})\right]\right\} + O\left(\frac{1}{a^2}\right). \end{aligned} \tag{45}$$

This yields

$$\begin{aligned} \epsilon\{M^n(t)\} &= [\epsilon\{M(t)\}]^n + \frac{1}{a}\, n(n-1)\,[\epsilon\{M(t)\}]^{n-1}\epsilon\{\rho\} \cdot \frac{\epsilon\{\rho^2\} - [\epsilon\{\rho\}]^2}{[\epsilon\{\rho\}]^2} \\ &= [\epsilon\{M(t)\}]^n + a^2\tau_0 n(n-1)\,[\epsilon\{M(t)\}]^{n-1}, \end{aligned} \tag{46}$$

where $\epsilon\{M(t)\} = \epsilon\{\rho\}t$,

$$a^2 = \frac{\epsilon\{\rho^2\} - [\epsilon\{\rho\}]^2}{[\epsilon\{\rho\}]^2},$$

and

$$\tau_0 = \frac{\epsilon\{\rho\}}{a} = \gamma_0 \epsilon\{\rho\} \qquad \left(\gamma_0 = \frac{1}{a}\right).$$

We note, in particular, that

$$\epsilon\{M^2(t)\} - [\epsilon\{M(t)\}]^2 = 2a^2\tau_0\epsilon\{M(t)\} = 2a^2\tau_0\epsilon\{\rho\}t, \tag{47}$$

and hence the mean-square deviation of $M(l)$ is proportional to l if $l \gg 1/a$, i.e., the stochastic variables $M(l_1)$ *and* $M(l_2)$ *are independent* if the domains l_1 and l_2 have no common points.

We can immediately calculate the moments of the stochastic variable $e^{-M(l)}$ which will prove useful in the consideration of the astrophysical problem. The nth moment of $e^{-M(l)}$ is given by

$$\epsilon\{e^{-nM(l)}\} = \epsilon\left\{1 - nM(l) + \frac{n^2}{2!}[M(l)]^2 - \ldots\right\}. \tag{48}$$

Substituting the values of $\epsilon\{M^r(l)\}$ from equation (46), we obtain

$$\epsilon\{e^{-nM(l)}\} = e^{-n\epsilon[M(l)]}\{1 + n^2a^2\tau_0\epsilon[M(l)]\}. \tag{49}$$

V. APPLICATION TO THE ASTROPHYSICAL PROBLEM

In a series of papers[11] on the theory of fluctuations in brightness of the Milky Way, Chandrasekhar and Münch examined certain basic problems in stellar statistics arising from the irregular distribution of interstellar matter. In these papers it was assumed that interstellar matter occurs in the form of discrete clouds, that these clouds are characterized by a certain average optical thickness τ_*, and that they occur with an average frequency λ per unit distance. In a later paper, Chandrasekhar and Münch suggested that it might be worth while to inquire whether the observed fluctuations in the brightness of the Milky Way could also be interpreted in terms of continuous, but fluctuating (albeit a wildly fluctuating), density distribution.

We assume, as in the case of discrete clouds, (1) that the observer is at the origin $l = 0$; (2) that all along l there is a continuous, but fluctuating, distribution of interstellar matter *in a stationary* state; and (3) that from $l = 0$ to l the stars are uniformly distributed and give a deterministic contribution of radiation of intensity from the element of length between $l = \tau$ and $l = \tau + d\tau$. Our object is to find the probability distribution of the intensity of radiation as observed at the origin, when l is finite and in the special case when l tends to infinity. Chandrasekhar and Münch have derived only the first and second moments, but, using Theorem I, we shall deduce all the moments of the distribution.

If we let κ denote the absorption coefficient and let ρ denote the density of interstellar matter, then $M(l) = \kappa\int_0^l \rho d\tau$ is the "optical thickness" of matter corresponding to the distance l. Without loss of generality, κ can be put equal to $1/\epsilon\{\rho\}$ by suitably choosing the unit of l. This means that radiation of unit intensity, on passing through matter of extension l, is cut down to an intensity $e^{-M(l)}$, where

$$M(l) = \int_0^l \rho' d\tau, \qquad \rho' = \frac{\rho}{\epsilon\{\rho\}}.$$

Note that

$$\epsilon\{M(l)\} = l \qquad \text{and} \qquad a^2 = \frac{\epsilon\{\rho'^2\} - [\epsilon\{\rho'\}]^2}{[\epsilon\{\rho'\}]^2} = \frac{\epsilon\{\rho^2\} - [\epsilon\{\rho\}]^2}{[\epsilon\{\rho\}]^2}.$$

Now consider what happens to the radiation between 0 and l before it reaches the observer at $l = 0$. We shall set $\beta = 1$; this can be done without loss of generality by simply choosing the unit of intensity in a suitable manner. The amount of radiation emanating from $d\tau$ traverses a distance τ or an optical path $M(\tau)$ before reaching the observer and is cut down to $e^{-M(\tau)}d\tau$. Thus with each point τ we can associate a stochastic variable $Y(\tau) = e^{-M(\tau)}$; and what we want are the moments of the stochastic variable,

$$I(l) = \int_0^l Y(\tau)\, d\tau, \tag{50}$$

[11] *Ap. J.*, **112**, 380, 393, 1950; **114**, 110, 1951.

representing the intensity of radiation reaching the observer. All the integral moments of I can be calculated if we know the correlation function $\epsilon\{Y(t_1)Y(t_2)\ldots Y(t_n)\}$. If the probability that the optical length of matter of extension t lies between M and $M+dM$, is $\Pi(M,t)dM$, we get

$$\epsilon\{Y(t_1)Y(t_2)\ldots Y(t_n)\} = \int_0^\infty\int_0^\infty\ldots\int_0^\infty e^{-M_1}e^{-(M_1+M_2)}\ldots e^{-(M_1+M_2+\ldots+M_n)} \times\Pi(M_1,t_1)\Pi(M_2,t_2-t_1)\ldots\Pi(M_n,t_n-t_{n-1})\,dM_1dM_2\ldots dM_n. \tag{51}$$

This equation is obtained by arguing that the joint probability that the optical length corresponding to the interval 0 to t_1 lies between μ_1 and $\mu_1+d\mu_1$; the optical thickness corresponding to the interval 0 to t_2 lies between μ_2 and $\mu_2+d\mu_2\ldots$; and the optical thickness corresponding to the interval 0 to t_n lies between μ_n and $\mu_n+d\mu_n$ is

$$\Pi(\mu_1,t_1)\Pi(\mu_2-\mu_1,t_2-t_1)\ldots\Pi(\mu_n-\mu_{n-1},t_n-t_{n-1})\,d\mu_1d\mu_2\ldots d\mu_n. \tag{52}$$

We next apply the transformation

$$\mu_1=M_1,\qquad \mu_2-\mu_1=M_2,\ldots,\qquad \mu_n-\mu_{n-1}=M_n.$$

Since the Jacobian of this transformation is 1, we get equation (51), which can be written as

$$\epsilon\{Y(t_1)\,Y(t_2)\ldots Y(t_n)\} = \int_0^\infty\int_0^\infty\ldots\int_0^\infty e^{-[nM_1+(n-1)M_2+\ldots+M_n]} \times\Pi(M_1,t_1)\Pi(M_2,t_2-t_1)\ldots\Pi(M_n,t_n-t_{n-1})\,dM_1dM_2\ldots dM_n. \tag{53}$$

We note that

$$\int_0^\infty e^{-rM}\Pi(M,t)\,dM=\epsilon\{e^{-rM(t)}\}=e^{-r\epsilon[M(t)]}\{1+\gamma^2a^2\tau_0\epsilon[M(t)]\} =e^{-\gamma t}\{1+r^2a^2\tau_0 t\}. \tag{54}$$

Substituting this in equation (51) and neglecting terms of the order of τ_0^2, we obtain

$$\epsilon\{Y(t_1)\,Y(t_2)\ldots Y(t_n)\} = e^{-[nt_1+(n-1)(t_2-t_1)+\ldots+(t_n-t_{n-1})]} \times[1+\{n^2t_1+(n-1)^2(t_2-t_1)+\ldots+(t_n-t_{n-1})\}a^2\tau_0]\quad(t_1<t_2<\ldots<t_n). \tag{55}$$

Note that $\epsilon\{Y(t_1)Y(t_2)\ldots Y(t_n)\}$ exists even if $t_1,t_2,\ldots,t_n$ are not ordered. Since, by definition, it is a symmetrical function, we can always order them. Thus, without loss of generality, we can assume that $t_1,t_2,\ldots,t_n$ are ordered, but we must remember in computing $\int_0^t Y(\tau)d\tau$ that we integrate $\epsilon\{Y(t_1)Y(t_2)\ldots Y(t_n)\}$ with respect to t_1, t_2, $\ldots$, t_n, over the whole domain t. Therefore, we write

$$\epsilon\{I^n(t)\}-\int_0^t\int_0^t\ldots\int_0^t\epsilon\{Y(t_1)\,Y(t_2)\ldots Y(t_n)\}\,dt_1dt_2\ldots dt_n =n!\int_0^t dt_1\int_{t_1}^t dt_2\ldots\int_{t_{n-1}}^t dt_n\epsilon\{Y(t_1)\,Y(t_2)\ldots Y(t_n)\} \qquad (t_1<t_2<\ldots<t_n). \tag{56}$$

A case of particular astrophysical interest is that in which t tends to infinity.[12] In such a case

$$\epsilon\{I^n(\infty)\}=\epsilon\{I^n\}=\left[1+\frac{n(n+1)}{2}a^2\tau_0\right]+O(\tau_0^2) \tag{57}$$

[12] The author hopes to extend the results to finite t in a later note to this journal.

$$\epsilon\{I\} = [1 + a^2\tau_0] + O(\tau_0^2). \tag{58}$$

Hence

$$\frac{\epsilon\{I^n\}}{[\epsilon\{I\}]^n} = 1 + \frac{n(n-1)}{2} a^2\tau_0. \tag{59}$$

In particular, when $n = 2$,

$$\frac{\epsilon\{I^2\}}{[\epsilon\{I\}]^2} = 1 + a^2\tau_0, \tag{60}$$

which is a result obtained by Chandrasekhar and Münch.

VI. COMPARISON WITH THE DISCRETE CASE

We shall now compare the picture of a fluctuating density field with the original concept of discrete clouds. If between 0 and t, n clouds occur with a probability $e^{-\lambda t}(\lambda t)^n/n!$ and if the optical thickness of each cloud is τ_*, then the total optical thickness due to those clouds which fall between 0 and t is a stochastic variable, $M(t) = N(t)\tau_*$, $N(t)$ being the stochastic variable representing the number of clouds between 0 and t. Now it is a well-known property of the Poisson distribution that

$$\epsilon\{N^n(t)\} = \sum_{s=1}^{n} C_s^n [\epsilon\{N(t)\}]^s, \tag{61}$$

where the C_s^n's are coefficients defined earlier. Using this relation, we note immediately that

$$\epsilon\{M(t)\} = \tau_* \lambda t \tag{62}$$

and

$$\epsilon\{M^n(t)\} = \tau_*^n \sum_{s=1}^{n} C_s^n (\lambda t)^s. \tag{63}$$

We shall assume that τ_* is so small that τ_*^2 and higher powers can be neglected and that λt so large that $\tau_* \lambda t$ is of order unity. Then, using the values of C_n^n and C_{n-1}^n from equation (8), we find that

$$\epsilon\{M^n(t)\} = [\epsilon\{M(t)\}]^n + \frac{n(n-1)}{2} \cdot \tau_* [\epsilon\{M(t)\}]^{n-1}. \tag{64}$$

Compare equation (64) with equation (46). Note that $\lambda\tau_*$ corresponds to $\kappa\epsilon\{\rho\}$. *We find we can always replace a fluctuating density field with critical length* $\epsilon\{\rho\}/a = \tau_0$ *by a discrete cloud system with a Poisson distribution where the optical thickness of each cloud is given by*

$$\tau_* = 2a^2\tau_0. \tag{65}$$

Chandrasekhar and Münch deduced this result from a comparison of the second moments in the continuous and discrete cases. We have shown that this result is consistent ever when we compare the higher moments.

If we assume that a single cloud cuts down radiation of intensity I to Iq, then

$$q = e^{-\tau_*}. \tag{66}$$

For general q (i.e., without any restrictive condition that τ_* is small), Chandrasekhar and Münch obtained the following expression for the total intensity I when $t \to \infty$ and λ is set equal to 1:

$$\epsilon\{I^n\} = \frac{n!}{(1-q)(1-q^2)\ldots(1-q^n)}. \tag{67}$$

Here λ can be set equal to 1 without loss of generality by suitably choosing a unit of t, only if λ is finite. For general λ we have,

$$\epsilon\{I^n\} = \frac{n!}{\lambda^n(1-q)(1-q^2)\ldots(1-q^n)}. \tag{68}$$

Now, if we assume $\tau_* \ll 1$, i.e., $q = 1 - \tau_* + 0(\tau_*^2)$ and $\lambda \gg 1$, then λ can be set equal to $1/\tau_*$ by suitably choosing the unit of t. Then

$$\epsilon\{I^n\} \to \left[1 + \frac{1}{2}\frac{n(n+1)}{2}\tau_*\right]\frac{1}{(\lambda\tau_*)^n} = 1 + \frac{1}{2}\frac{n(n+1)}{2}\tau_*, \tag{69}$$

$$\epsilon\{I\} \to [1 + \tfrac{1}{2}\tau_*]\frac{1}{\lambda\tau_*} = 1 + \tfrac{1}{2}\tau_*, \tag{70}$$

$$\frac{\epsilon\{I^n\}}{[\epsilon\{I\}]^n} \to 1 + \frac{n(n-1)}{2}\frac{\tau_*}{2}. \tag{71}$$

Replacing τ_* by $2a^2\tau_0$ in the above equations, we get equations (57), (58), (59).

I wish to express my thanks to Professor S. Chandrasekhar, who suggested this problem to me in a private communication, and to Professor M. S. Bartlett and Dr. Nelson Limber for their valuable criticisms and suggestions.

NOTES

RADIO EMISSION FROM THE ORION NEBULA AND OTHER SOURCES AT λ 9.4 CM

For a 2-week period beginning November 27, observations were undertaken for the first time with a 50-foot paraboloidal reflector and a microwave radiometer at a wave length of 9.4 cm (3200 Mc/sec). During this period the radio emission from discrete sources and the galactic background was detected and measured for the first time at a wave length shorter than 21 cm. At least two of the sources have not been detected before at radio wave lengths: the Great Nebula in Orion and the Omega Nebula in Sagittarius. It is the purpose here to give preliminary results. Revised values will be published later. Table 1 lists the results of the observations relating to these sources and to drift-curves across the galactic plane at three declinations near the galactic center.

The antenna beam widths were $27'.0 \pm 0'.5$ in the horizontal plane (E-plane) and $24'.0 \pm 0'.5$ in the vertical plane. The antenna gain over an isotropic radiator was 1.4×10^6 within 20 per cent. A change in the noise power input to the radiometer equivalent to 1° K could be detected with a 1-second time constant. The hourly drift in receiver gain was normally less than 1 per cent. The output was recorded continuously on a paper tape moving $\frac{3}{4}$ inch/minute (see Fig. 1).

The antenna temperature, T_A, was obtained from the radiometer output deflection, which was calibrated against a heated resistive load, and is accurate to about 2° K. The brightness temperature, T_B, was obtained by dividing T_A by the ratio of the flux incident upon the antenna to that collected at the focus and was equal to 0.6 ± 20 per cent. At this wave length the "brightness" or specific intensity equals $3.14 \times 10^{-25}\ T_B$ watt meter^{-2} steradian^{-1} (cycle/sec)$^{-1}$.

The energy flux density, S, at the earth from a "point-source" radiator is obtained from T_A and the antenna gain and is accurate to about 25 per cent for the more intense sources. In Table 1 it is expressed in units of 10^{-25} watt meter^{-2} (cycle/sec)$^{-1}$ and is twice that observed in one plane of polarization.

The positions of the discrete sources were measured several times on more than one day, and for those sources previously known[1] and identified optically[2] the positions agree within the observational uncertainties of 0.2 minutes in right ascension and 5′ in declination.

The new sources Nos. 4 and 6 agree well in position with the "Omega" Nebula in Sagittarius NGC 6618, M17, and the Great Nebula in Orion NGC 1976, M42, respectively.[3]

The duration of the drift-curves at half-deflection was measured for the possible effect of broadening by a finite source size. The Orion Nebula drift-curves showed significant broadening after correcting for declination, i.e., from 108 seconds for a point source to 123 seconds for Orion; 140 seconds was observed for the moon. This places the diameter of an equivalent circular source at about 15′ and thus gives for Orion an apparent blackbody temperature of 100° K. On the assumption that the electron temperature in the

[1] B. Y. Mills, *Australian J. Sci. Res. A*, **5**, 456, 1952; and F. G. Smith, *Nature*, **168**, 555, 1951; **170**, 1065, 1952.

[2] W. Baade and R. Minkowski, *Ap. J.* (in press).

[3] See, e.g., J. C. Duncan, *A.S.P. Leaflet*, No. 240, March, 1949.

nebula is $10^{4°}$ K, the average opacity at 3200 Mc/sec over this region is then 0.01. Following J. L. Greenstein and R. Minkowski[4] on the assumption of thermal emission from the Orion Nebula, this opacity gives an emission measure, EM ($= N_e^2 l_{pse}$) of 2.6×10^6, which is closer to 10^6, the average for the nebula, than is 8×10^6, the value in its center. If the source were spherical in shape and at a distance of 400 parsecs, this value for EM

TABLE 1

SOURCES OBSERVED AT 9.4 CM

No.	Constellation	T_A (° K)	T_B (° K)	S*	R.A. (1950)	Declination (1950)	Optical Object
1	Cassiopeia	53±2	.....	150	$23^h 21^m.3$	58° 32′	Unusual gaseous nebulosity†
2	Taurus	28	.....	80	5 31.4	21 54	"Crab" Nebula, NGC 1952, M1.†
3	Cygnus	25	.....	70	19 57.8	40 34.5	Colliding galaxies†
4	Sagittarius	24	.....	68	18 17.9	−16 14	"Omega" Nebula, NGC 6618, M17; bright galactic nebula‡
5	Sagittarius	17	.....	48	17 42.5	−29 01	Not identified—radio source superimposed upon No. 9§
6	Orion	16	.....	45	05 33.0	−05 27	Great Nebula in Orion, NGC 1976, M42‡
7	Centaurus	7	.....	20	13 22.1	−42 50	Possibly colliding galaxies,† NGC 5128
8	Virgo	5	.....	14	12 28.2	12 37.5	Unusual galaxy with projecting "jet," NGC 4486, M87†
9	Sagittarius	6	10±4	.....	17 42.5±2	−29 1	Galactic background under source No. 5§
10	Sagittarius	3	5	(8.5)	17 59.0±0.5	−23 6	May be "Trifid" Nebula, NGC 6514, M20‡, or galactic plane
11	Sagittarius	2.5	4	(7)	18 01.0±2	−24 36	May be "Lagoon" Nebula, NGC 6523, M8‡, or galactic plane

* Flux density, S, is in units of 10^{-23} watt meter^{-2} (cycles/sec)$^{-1}$ for two polarizations and is accurate to about 25 per cent.

† Previously identified; optical position used in estimating our observational uncertainties in position.

‡ Bright irregular hydrogen-alpha emission nebula. We are indebted to Dr. Bart J. Bok for showing us a catalogue of hydrogen emission nebulae prior to publication.

§ Region of several hydrogen emission nebulae; also see S. Sharpless, *Ap. J.*, 118, 362, 1953.

indicates an average electron density within 7′.5 of the source center of 400 cm^{-3}. These results are also consistent with the failure to detect the Orion Nebula at λ 140 cm by J. E. Baldwin[5] at the Cavendish Laboratory, from which he concluded that the electron density falls to less than 400 cm^{-3} at an angular distance of 5′ from the center. Therefore, the results of the present measurements on the Orion source are in agreement with the hypothesis of thermal emission from the Orion Nebula, a very dense *H* II region, and thus lend support to the assumption of thermal emission by free-free transitions from other

[4] *Ap. J.*, **118**, 1, 1953; and J. L. Greenstein, *Ap. J.*, **104**, 114, 1946.

[5] *Observatory*, **73**, 155, 1953.

H II regions, perhaps those in the plane of the Galaxy[6] and in the constellation of Cygnus.[7]

Emission from sources Nos. 9 and 5 was recorded on the same drift-curves at $-29°$ declination and have about the same right ascension. No. 5 has about three times the deflection of No. 9 and has an extent in both declination and right ascension consistent with a discrete source. It was first detected at λ 25 cm by Piddington and Minnett.[8] Emission from No. 9 caused a gradual rise and fall in deflection noticeable for 10–12 minutes in right ascension, and the time of its maximum was within 2 minutes of source No. 5. Therefore, No. 9 is an extended source in the plane of the Galaxy, and its average

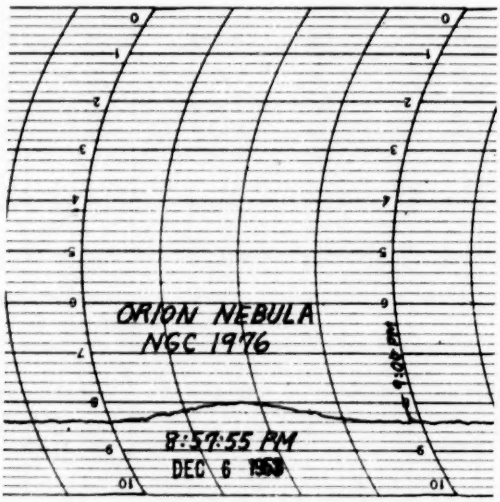

FIG. 1.—This photograph shows the record of the radiometer output deflection as the Orion Nebula, NGC 1976, drifted through the antenna beam on December 6, 1953. The time of maximum deflection was 8:57:55 P.M., E.S.T. Time increases toward the right 1 minute between vertical curves.

brightness temperature is $10° \pm 4°$ K at 9.4 cm wave length. Its angular extent is at least 2° in galactic latitude.

The time of maximum deflection for source No. 10 differed by less than 30 seconds from the right ascension of the "Trifid" Nebula,[3] in Sagittarius NGC 6514, M20, and the declinations also agree within the observational uncertainty. The duration and shape of the drift-curves are consistent with a discrete source; but when a drift-curve (source No. 11) was made 1°.5 below No. 10 to confirm this, a small deflection was again obtained, but with its maximum occurring about 2 minutes later in right ascension. The "Lagoon" Nebula,[3] NGC 6523, M8, would be 1.2 minutes later than the "Trifid" and was just within the antenna beam in declination. On the other hand, these two drift-curves and the greater and broader deflection obtained from source No. 9 are all consistent with emission from the galactic plane as given by Piddington and Minnett[8] at 25-cm wave

[6] P. A. G. Scheuer and M. Ryle, *M.N.*, **113**, 3, 1953.

[7] R. Hanbury Brown and C. Hazard, *M.N.*, **113**, 123, 1953; and J. H. Piddington and H. C. Minnett, *Australian J. Sci. Res. A*, **5**, 17, 1952.

[8] *Australian J. Sci. Res. A*, **4**, 459, 1951.

length. But the evidence is inadequate and further measurements in this region are needed.

We are grateful to Mr. J. Edwin Sees, Naval Research Laboratory, for preparing the antenna control system. We are indebted to Drs. John P. Hagen, Naval Research Laboratory, and F. Graham Smith, Cavendish Laboratory, for interest in these observations.

F. T. HADDOCK
C. H. MAYER
R. M. SLOANAKER

NAVAL RESEARCH LABORATORY
WASHINGTON, D.C.
December 23, 1953

Hα-EMISSION STARS ASSOCIATED WITH A DARK LANE IN LUPUS

Objective-prism photographs taken at the Lamont-Hussey Observatory with the Mount Wilson 10-inch camera reveal a group of six *Hα*-emission stars which lie within the dark lane, Barnard 228.[1] These stars are listed in Table 1.

TABLE 1

STAR	1875		m_{red}	INT.	REMARKS
	R.A.	Decl.			
CD−33°10685	$15^h37^m16^s$	−33° 53′.6	10.5	2–1	
LH*α* 450-5	15 37 21	−33 54.7	14.0	0–1	Doubtful
LH*α* 450-6	15 38 45	−34 6.9	12.0	1–3	
LH*α* 450-8	15 39 48	−35 5.2	13.0	0+–1	*Hα* broad
LH*α* 450-7	15 40 04	−34 52.7	11.5	1–3	
CD−35°10525	15 41 07	−35 15.9	10.0	3–3	*Hα* broad

The positions in Table 1 are measured with reference to the position of CD stars. The apparent magnitudes are eye estimates from a spectrum plate and are accurate to about ±0.5 mag. The first number recorded in the column headed "Int." gives the relative strength of the continuous spectrum on an arbitrary scale ranging from 0 to 5 (0 = continuum not visible), while the second number gives the intensity of *Hα* relative to the continuum on a similar scale.

The physical connection of this group with the dark lane is indicated by the fact that the total area of the lane is about 2 square degrees, whereas, in a surrounding area of about 170 square degrees, there occur only nine additional emission-line stars. Of these nine, one is the previously recognized T Tauri variable, RU Lupi,[2] which lies in a neighboring absorption patch some 3° southeast of the new group.

This new group of six stars bears a striking similarity to the R CorA group,[2,3] which, as seen on our plates, contains a total of five stars having *Hα* emission, including the variables S, R, DG, and VV CorA.

None of the stars in Table 1 are at present known to be variable, and no known irregu-

[1] *A Photographic Atlas of Selected Regions of the Milky Way* (1927), p. 18.

[2] Joy, *Ap. J.*, **102**, 168, 1945.

[3] Holopoff, *Astr. J. U.S.S.R.*, **27**, 233 1950.

lar variables lie in the vicinity of the dark lane. However, the presence of emission-line stars indicates that an investigation may reveal the presence of nebular variables in this region.

KARL G. HENIZE

OBSERVATORY OF THE UNIVERSITY OF MICHIGAN
October 28, 1953

RECENT CHANGES IN THE SPECTRA OF FOUR Be STARS

As an auxiliary program at the Perkins Observatory, spectra of some of the brighter Be stars are taken once each observing season, in order to detect some of the rather rapid spectral variations of which these stars are capable. The following four stars have exhibited such variations in the past year: *o* Andromedae, 66 Ophiuchi, 48 Librae, and Pleione. All spectrograms described below were taken with the two-prism spectrograph attached to the 69-inch telescope, with a dispersion of 28 A/mm at $H\gamma$.

1. *o* ANDROMEDAE[1]

The B6.5 star, *o* Andromedae, has passed through a shell stage several times since 1890.[2] In August, 1951, the spectrum was again that of a shell-type star: sharp and deep Balmer absorption cores plus a metallic absorption spectrum consisting largely of lines of *Fe* II. About one year later the writer received a communication from Miss Anne Underhill, of the Dominion Astrophysical Observatory, stating that the metallic shell spectrum of *o* Andromedae was no longer visible on Victoria plates. This was confirmed on a Perkins plate taken on September 6, 1952. The most recent Perkins spectrogram was obtained on July 3, 1953, and reveals no change since the 1952 observation. The most significant change in the blue-violet spectrum of *o* Andromedae since the shell stage of 1951 is the complete disappearance of the metallic absorption spectrum, as has been mentioned above. The sharp Balmer cores persist essentially unchanged, indicating the continued existence of a thin shell at least. The lines from the underlying star, including the hydrogen Balmer wings, are also present in about the same strength as in the earlier shell stage.

The only change in the red portion of the spectrum is the disappearance of emission at $H\alpha$. In 1951 the sharp absorption core at $H\alpha$ was flanked by weak, but easily visible, emission components, while a I-N plate of September 8, 1953, shows the absorption core as before, but no trace of emission. The metastable *O* I 7774 continues very strong in absorption.

Radial velocities of the *o* Andromedae shell during the period of the Perkins observations are given in Table 1. In view of the relatively low dispersion employed, as well as the small number of plates and measurable lines per plate, no attempt is made to interpret the radial velocities. Table 1 is included only because it may be of some interest in future investigations of this star.

2. 66 OPHIUCHI[3] (MWC 278)

66 Ophiuchi is a B2 main-sequence star, according to W. W. Morgan (private correspondence). Emission was discovered by H. F. Balmer,[4] who reported that on spectrograms taken in 1921 and 1922 $H\beta$ was a broad, weak absorption line with superposed double emission components of intensity somewhat less than that of the adjacent con-

[1] $\alpha(1900) = 22^h57^m3$; $\delta(1900) = +41°47'$; $m_v = 3.63$.

[2] *Ap. J.*, **115**, 573, 1952.

[3] $\alpha(1900) = 17^h55^m3$; $\delta(1900) = +4°22'$; $m_v = 4.81$.

[4] *Pub. A.S.P.*, **38**, 248, 1926.

tinuous spectrum, while $H\gamma$ was a fairly weak, narrow absorption line. His plates of 1924, however, showed no trace of emission at $H\beta$. By 1934 the shell had evidently returned, as a Mount Wilson spectrogram showed $H\alpha$ to be a very strong wide, bright line with a relatively weak, dark core.[5] It was gone again in 1937: a Perkins blue-violet plate shows the Balmer lines to be very broad absorption features with no trace of emission. In 1942 Swings and Struve reported $H\beta$ as nearly continuous, with $H\gamma$ weak in absorption.[6] Bright $H\alpha$ was extremely weak in 1947 on a Mount Wilson spectrogram,[7] and Miczaika reported the absence of emission lines in the blue-violet in 1948.[8] The shell was thus absent or very thin by that time.

A Perkins blue-violet spectrogram was obtained on May 10, 1953, and reveals the presence of a shell once more. Again $H\beta$ shows double emission of about the same

TABLE 1

RADIAL VELOCITIES OF *o* ANDROMEDAE, 1949–1953

PLATE	EMULSION	QUALITY	DATE	RADIAL VELOCITY (KM/SEC)			
				H Cores	No. of Lines per Plate	*Fe* II	No. of Lines per Plate
4999–5001	103-O	f	1949 Dec. 30	−20.2	2	−12.9	2
5615	103-O	g	1950 Aug. 12	+ 0.8	2	+ 8.5	2
6752	Process	g	1951 Aug. 29	−10.5	2	− 5.0	9
7663–7664	IIa-O	g	1952 Sept. 6	−12.5	3	.....	.....
8408	IIa-O	g	1953 July 3	−10.1	4	.....	.....

strength as the adjacent continuous spectrum, while the central absorption component is relatively sharp but not so deep as in *o* Andromedae and similar shell-type stars. Now $H\gamma$ and $H\delta$ are broad absorption lines with relatively narrow absorption cores. A I-N plate taken June 9, 1953, shows $H\alpha$ to be a fairly strong emission line with broad absorption wings. There is no trace of the infrared *O* I lines, and the Paschen series is rather washed out.

The binary character of 66 Ophiuchi was announced by Struve;[9] he observed a doubling of the lines, as have subsequent observers. The helium lines are very broad on the recent Perkins plate, and it is uncertain whether there was doubling at that phase. The line broadening corresponds to a rotational velocity of about 275 km/sec, but the axial rotation of the individual components may well be less than this if the lines are actually double on the Perkins plate.

3. 48 LIBRAE[10] (MWC 239)

The spectrum of the shell star 48 Librae has been studied in some detail at the Yerkes and McDonald Observatories and at the Mount Wilson Observatory. Most recently, P. W. Merrill[11] described the cyclical nature of the changes in the spectrum occurring between 1944 and 1952. A Perkins spectrogram of this star, taken on June 4, 1953, shows some changes which agree well with the periodicities described by Merrill.

[5] Merrill and Burwell, *Ap. J.*, **98**, 153, 1943.

[6] *Ap. J.*, **97**, 194, 1943.

[7] Merrill and Burwell, *Ap. J.*, **110**, 387, 1949.

[8] *A.N.*, **277**, 32, 1949.

[9] *Ap. J.*, **62**, 434, 1925.

[10] $\alpha(1900) = 15^h52^m6$; $\delta(1900) = -13°59'$; $m_v = 4.68$.

[11] *Ap. J.*, **117**, 7, 1953.

a) The radial velocity of the shell as measured from 14 *Fe* II lines was −31.2 km/sec, and from two hydrogen absorption cores ($H\gamma$ and $H\delta$) it was −25.2 km/sec. When these values are plotted with Merrill's velocity-curves for $H\delta$ and the *Fe* II lines from 1938 to 1952, they fit his curves quite well and indicate that the radial velocity of the shell was still decreasing in June, 1953.

b) The metallic-line spectrum was somewhat weaker in June, 1953, than it was on a Perkins plate taken in June, 1952.[12] Merrill states that "the intensities increased decidedly from 1950 to 1952. The indications are that the maximum intensity occurs on the falling branch of the velocity-curve." This conclusion is supported by the Perkins observations. The Balmer cores also appear to have weakened between 1952 and 1953 on the Perkins plates.

c) The red emission component of $H\beta$ was stronger than the violet component in June, 1953, while the opposite was true on Perkins plates of June, 1950, and June, 1952. This supports Merrill's conclusion that the V/R-curve for $H\beta$ "resembles the velocity-curve in shape and phase."

A I-N plate of June 9, 1953, shows little or no change from a similar plate taken on June 6, 1950; in particular, $H\alpha$ continues as a strong emission line and *O* I 7774 as a strong absorption line.

4. PLEIONE[13] (MWC 75)

The interesting shell star Pleione has been the subject of a number of investigations, climaxed by the recent study of P. W. Merrill,[14] who discussed the shell episode beginning in 1939 and ending at the present time. Perkins spectrograms of Pleione taken December 1, 1951, and February 1, 1954, indicate that the shell spectrum has weakened still further in the few years since Merrill's study.

The Balmer absorption cores are considerably weaker on the 1954 plate than on the 1951 plate: at $H\beta$, for example, the central absorption is now only about as deep as the absorption from the underlying star flanking the emission edges, whereas the 1951 plate showed it to be much deeper. The dark metallic shell lines, already weak in 1951, are now barely visible as a network of very faint lines, principally in the region between $H\gamma$ and $H\beta$.

Emission in the photographic region is confined to $H\beta$ and a few lines of *Fe* II between $H\gamma$ and $H\beta$. It is difficult to tell whether any change in the strength of the *Fe* II emission has occurred between 1951 and 1954. The double emission at $H\beta$ is decidedly stronger on the more recent plate, however. Further, the asymmetry in the sense that the longward emission component is the stronger, which was observed by Merrill in 1951, is also present on the Perkins 1951 plate and is much more pronounced on the 1954 plate.

ARNE SLETTEBAK

PERKINS OBSERVATORY
September 1953

[12] However, in a recent investigation ("The Spectrum of 48 Librae," *Pub. Dom. Ap. Obs. Victoria*, Vol. 9, No. 12; in press), Miss Underhill states: "In 1953 the general strength of the shell absorption lines was about the same as in 1950 and 1952." As a check on his visual estimate, the writer measured equivalent widths of a few shell absorption lines on the 1952 and 1953 plates. These confirmed the visual estimate: on the Perkins plates, the shell absorption spectrum is about 25 per cent stronger in 1952 than in 1953. I am indebted to Miss Underhill for sending me a copy of her paper in advance of publication.

[13] α (1900) = 3^h43^m2; δ (1900) = $+23°50'$; m_v = 5.18.

[14] *Ap. J.*, **115**, 145, 1952.

STELLAR WAVE LENGTHS OF *Eu* II AS AFFECTED BY HYPERFINE STRUCTURE

In analyzing the measurements of some 50 spectrograms (4.5 A/mm) of the peculiar star HD 188041 (F0p) for magnetic field intensity and for velocity, it was found that *Eu* II gave a velocity differing rather consistently by −2.4 km/sec from the mean of the other elements. The number of lines of all elements measured on each plate averaged about 50, and the probable error of the velocity per plate was usually about ±0.15 km/sec. From two to ten lines of *Eu* II were usually measured. The laboratory wave lengths had been adopted from the *Revised Multiplet Table*.[1]

The probable source of the discrepancy was found in consulting the original laboratory investigations of A. S. King[2] for *Eu* II. King pointed out that many of the lines of *Eu* II are broadened by hyperfine structure (hfs), and that, in particular, the prominent lines

TABLE 1

EFFECTIVE WAVE LENGTHS FOR *Eu* II

λ_{eff}	λ_{RMT}	λ_{sat}	No. Plates
3930.46	3930.50	0.42	3
3971.92	3971.98	1.89	5
4017.54	4017.58	Doublet	9
4085.32	4085.38	5.04	3
4129.712	4129.73	9.64	20
4151.60	4151.52	1.64	2
4204.989	4205.05	4.91	26
4355.10	4355.09	None	4
4383.12	4383.17	Bl?	1
4435.60	4435.58	5.46 bl ?	9
4522.62	4522.59	2.46 2.91	4

from λ 3819 to λ 4522, which themselves are complex, have sharp satellites about 0.1 A to the violet; the effect of this is to move the effective wave length about 0.02 A shortward of that of the strong component. Since in most astrophysical spectra the hfs components are unresolved due to broadening by Doppler and Zeeman effects if not by the instrumental profile, the mean wave length of the components must be employed rather than that of the strongest component as listed in the *RMT*. As mentioned by H. Abt[3] the effective wave length for the hfs blend in absorption will depend to some extent upon the degree of saturation.

In the laboratory, King found hfs for the rare earths *Tb* (65), *Ho* (67), *La* (57), and *Pr* (59), as well as for *Eu* (63), and he pointed out that only the rare-earth elements of odd atomic number show an observed hfs. Consistent with this is the fact that the few lines of *Gd* II (64) and *Ce* II (58) measured in HD 188041 do not show discrepant velocities.

The effective wave lengths for the lines of *Eu* II measured in HD 188041 have been computed to bring the velocities into accord with those derived from other elements. They are listed in the first column of Table 1 where the second column gives the wave length of the principal component from the *RMT* and the third column lists the wave length of the hfs satellite from King's paper. The last column gives the number of plates

[1] C. E. Moore, *A Multiplet Table of Astrophysical Interest* (Contr. Princeton U. Obs., No. 20, 1945).

[2] *Ap. J.*, **72**, 22, 1930; **89**, 380, 1939.

[3] *Ap. J.*, **115**, 199, 1952.

on which the corrected wave length depends. Hfs appears to account satisfactorily for the wave length discrepancies, except for λ 4435, where the difference may be due to a blend.

I am indebted to Miss Sylvia Burd for computational assistance and to her as well as to Mrs. A. J. Deutsch and Mr. J. R. Novotny for measurement of the plates.

HORACE W. BABCOCK

MOUNT WILSON AND PALOMAR OBSERVATORIES
CARNEGIE INSTITUTE OF WASHINGTON
CALIFORNIA INSTITUTE OF TECHNOLOGY
October 17, 1953

ON THE EFFECT OF ELECTRON SCREENING ON THERMONUCLEAR ENERGY GENERATION*

A recent paper of G. Keller[1] draws attention on the effect of electron screening on thermonuclear energy generation. This problem was treated by me in 1947,[2] but Keller has overlooked my publication.

The results of G. Keller are not essentially different from those I obtained five years ago. Nevertheless, it seems worth while to stress the following points:

1. Keller explains the change in energy generation rate by the change in height of the potential barrier. It seems more real to consider the change in transparency of the potential barrier as due to a change in thickness rather than to a change in height. As is well known, the most important term in the transparency of the potential barrier is the exponential

$$G = \exp\left[-2 \frac{\sqrt{(2m)}}{\hbar} \int_{r_1}^{r_2} \sqrt{(U-E)}\, dr \right].$$

It is quite obvious that a change in U and in $r_2 - r_1$ changes G. But in case of a coulomb potential screened by electrons, the approximate value of the exponential is

$$G = \exp\left[-2 \frac{\sqrt{(2m)}}{\hbar} \frac{\pi}{2} \sqrt{(Z_1 Z_2 e^2 r_E)} \right],$$

where r_E is the classical distance of approach.

In the case of a nucleus screened by a cloud of electrons, r_E is smaller than in the case of a bare nucleus. Consequently, the change in height of the potential barrier seems to be of little importance in determining changes in the transparency of the potential barrier.

2. In all cases (degenerate or nondegenerate gas of electrons) the average kinetic energy of electrons is much higher than the average binding energy of the electrons in the atom. Consequently, a good approximation is to suppose that the screening is produced by a negative fluid of uniform density. That approximation is not very good in the case of small density of the electron gas, especially if the electron gas is degenerate. In such a case, the constant $\pi/2$ which occurs in G should be multiplied by a factor α slightly smaller than 1 (in between 0.82 and 1). The factor exact can be obtained only by better methods of approximation, such as the method of the self-consistent fields used by Keller.

3. General expressions for the change in nuclear reaction rate have been given.[2] Here

* [Dr. Keller expresses his sincere regret that when he wrote his paper he was unaware of Dr. Schatzman's earlier contribution.—EDITOR.]

[1] *Ap. J.*, **118**, 142, 1953.

[2] *J. de phys. et le radium*, **9**, 46, 1948; *Contr. Inst. d'ap. de Paris*, No. 22.

we shall consider, for comparison with Keller's expression, only the case of comparatively small densities.

The change in nuclear reaction rate is given by a factor T:

$$T \cong \exp\left(\frac{\tau x}{2^{5/3}}\right), \tag{1}$$

where

$$\tau = 3\left(\frac{2\pi^4 \bar{A} H e^4 Z_1^2 Z_2^2}{h^2 kT}\right)^{1/3} \tag{2}$$

and

$$x = \left(\frac{8h^2 e^2}{3\pi^3 \bar{A} k^2 H^2} \frac{Z_2 \rho}{\mu T^2}\right)^{1/3}, \tag{3}$$

where Z_2, the proton charge, has to be set equal to 1.

The exponential term can be written as follows:

$$\frac{\tau x}{2^{5/3}} = 3^{2/3} 2^{-1/3} \pi^{1/3} e^2 Z_1^{2/3} Z_2 \left(\frac{\rho}{\mu H}\right)^{1/3} (kT)^{-1}. \tag{4}$$

When the factor α is taken into account, equation (1) is changed into

$$T \cong \exp\left[\frac{\tau x}{2^{5/3}} - \tau\left(\alpha^{-1/3} - 1\right)\right], \tag{5}$$

which shows that the value (1) is too great.

Numerically, in the case of the reaction of protons with N^{14},

$$\frac{\tau x}{2^{5/3}} = 1.24 \times 10^6 \left(\frac{\rho}{\mu}\right)^{1/3} T^{-1}. \tag{6}$$

Case I of Keller, with $\rho = 122$, $T = 11.6 \times 10^6$, and $\mu = 0.615$ gives $T = \exp(0.625) = 1.87$ (Keller's value, $T = 1.54$); case II of Keller, with $\rho = 443$, $T = 8.13 \times 10^6$, and $\mu = 0.615$ gives $T = \exp(1.368) = 3.92$ (Keller's value, $T = 3.3$)—thus in agreement.

4. It should be noticed that in a recent publication it was pointed out[3] that the change in nuclear reaction rate may be important in determining the sensitivity to temperature and density variations in a pulsating star.

EVRY SCHATZMAN

INSTITUT D'ASTROPHYSIQUE DE PARIS
PARIS, FRANCE
October 2, 1953; revised November 9, 1953

[3] E. Schatzman, *Ann. d'ap.*, **16**, 162, 1953.

THE DISPERSION IN ORIENTATION OF INTERSTELLAR POLARIZERS

It has been pointed out by Davis[1] and by Chandrasekhar and Fermi[2] that magnetohydrodynamics gives a connection between the strength of a general galactic magnetic field, the density of the gas and dust, the velocity of turbulent motion, and the average angular deviation of the magnetic field from a uniform direction. Theories have been sug-

[1] *Phys. Rev.*, **81**, 890, 1951.
[2] *Ap. J.*, **118**, 113, 1953.

gested by Davis and Greenstein[3] and by Spitzer and Tukey[4] that attribute the polarization of starlight to the action of a magnetic field on the dust clouds through which the light passes, the direction of the plane of polarization being determined by the direction of the field. Accordingly, calculations have been made of the root-mean-square deviation of the angle of polarization from data given by Hiltner.[5] The regions chosen were small enough that the result would not be confused by large-scale structure of the magnetic field. They were also chosen for a general uniformity of polarization angle and a high enough density of measured stars to conform to the small region requirement and still be statistically significant. No attempt is made in the present brief note to do more than make exploratory calculations in four interesting regions. The results are shown in Table 1.

TABLE 1

AVERAGE DEVIATION OF PLANES OF POLARIZATION AND AVERAGE RATIO OF POLARIZATION TO COLOR EXCESS

Group	Location	No. of Stars	$[\theta']_{av}$	σ (Radians)	$[\delta/(E_1+0.05)]_{av}$	No. of Stars with E_1 Listed
1.....	$\left\{\begin{matrix}68°<l<78°\\-6°<b<2°\end{matrix}\right\}$	76	82°.6	0.15	6.1	12
2.....	$\left\{\begin{matrix}89°.9<l<107°\\-6°<b<6°\end{matrix}\right\}$	242	90.8	.13	13.3	78
3.....	$\left\{\begin{matrix}100°<l<106°\\-6°<b<0°\end{matrix}\right\}$	103	92.9	.086	13.8	40
4.....	$\left\{\begin{matrix}l\approx 108°\\b\approx 2°\end{matrix}\right\}$	21	80.1	0.12	9.6	15

The approximate location of the groups of stars is given in terms of the galactic co-ordinates l and b shown in the second column, all stars listed by Hiltner in the region being included in the group. Group 4 consists of the 15 stars used by Hiltner in his Figure 13 plus 6 other stars at approximately the same location for which E_1 is not given. Group 3 forms a part of group 2. The various groups are easily located in Hiltner's Figures 8, *b*, 9, *b*, and 10, *a*. The third column gives the total number of stars in the group, and the last column the number for which values of E_1 are listed. The fourth column gives the mean over the entire group of θ', the position angle of the plane of vibration referred to the galactic co-ordinate system. The fifth column gives σ, the root-mean-square deviation of θ' from its mean value. In the sixth column is given the average of the polarization in per cent δ, divided by the color excess, E_1, for the stars of the group for which a color excess is given. A zero-point correction of 0.05 was added to E_1, and the items are weighted proportionally to $E_1 + 0.05$, since an error in the observed value of E_1 produces more effect on $\delta/(E_1 + 0.05)$ if E_1 is small.

The principal conclusion to be drawn from these calculations is that the value $a = 0.2$ radians for the mean angular deviation used by Chandrasekhar and Fermi[2] may be somewhat large. In the most favorable region σ is somewhat less than 0.1 radians, and in the general region of 100° galactic longitude σ is about 0.13 radians. If Chandrasekhar

[3] *Ap. J.*, **114**, 206, 1951.

[4] *Ap. J.*, **114**, 187, 1951.

[5] *Ap. J.*, **114**, 241, 1951.

and Fermi had used $\alpha = 0.1$ radians, they would have found that the magnetic field was 1.4×10^{-5} gauss. It is also of some interest to note the relationship between σ and $[\delta/(E_1 + 0.05)]_{av}$ in the different regions. With the exception of group 2, they are roughly inversely proportional, as would be expected if the polarization, δ, was caused by a magnetic field. The apparently anomalous behavior of group 2 could be explained by noting that the polarization angles show a bending with increasing galactic longitude through the large region. This may be seen in Hiltner's Figure 9, *b*. This produces the large value of σ and the change in $[\theta']_{av}$ from group 2 to group 3, but any subregion of group 2 (such as group 3) would allow smaller values of σ.

It is impossible at the present time to relate the magnetic field strength, the polarization, and the color excess in any very accurate way. Not enough is known about the structure of the magnetic field or the variation in density and velocity of the interstellar medium. And also, as has been suggested by various authors, including Hall and Mikesell[6] and Hiltner, there is no very good relation between the polarization and the color excess, because the particles causing both may not be the same and also because the starlight generally has passed through several clouds. The color excess is not affected by different particle alignments in different clouds, but the resultant polarization would be.

I should like to extend particular thanks to Dr. Leverett Davis, Jr., for suggesting the problem and for continued help in the analysis. I should also like to thank Dr. J. L. Greenstein for many helpful discussions.

GEORGE STRANAHAN*

CALIFORNIA INSTITUTE OF TECHNOLOGY
November 24, 1953

[6] J. S. Hall and A. H. Mikesell, *Pub. U.S. Naval Obs.*, Vol. 17, Part I, 1950.

* Now at Carnegie Institute of Technology.

ERRATUM

In *Ap. J.*, **116**, 21, 1952, on page 25, line 5, *for* "In *Cr* I" *read* "In *V* I." The designations in Table 6 are correct.

ABSTRACTS OF ASTROPHYSICAL JOURNAL SUPPLEMENT SERIES

Supplement No. 2, Volume I, pages 39–62, March, 1954.

SPECTROSCOPIC OBSERVATIONS OF MIRA CETI, 1934–1952

ALFRED H. JOY
MOUNT WILSON AND PALOMAR OBSERVATORIES
CARNEGIE INSTITUTION OF WASHINGTON
CALIFORNIA INSTITUTE OF TECHNOLOGY

A detailed study of 88 spectrograms of Mira Ceti obtained with high-dispersion spectrographs leads to many more definite conclusions with regard to the activities taking place within the atmosphere of the star than were previously possible.

The radial velocities deduced from 70 selected absorption lines, representing 16 cycles of the star's variation, indicate fluctuations from cycle to cycle in amounts comparable with the range within a single cycle. Maximum velocity of recession usually occurs shortly after maximum light in Mira Ceti and probably in several other long period variable stars observed by P. W. Merrill. The maximum velocity of a given cycle varied between +57.2 and +68.3 km/sec in Mira. Usually greater positive velocities occur at maxima of greatest brightness. Since these observations do not cover the phases of minimum light, conclusions with regard to the pulsation of the star as a whole are not possible.

Different elements yield slightly different velocities. Residuals from the mean for some elements are more than 0.5 km/sec. For *Sc*, *Fe*, and *Ni* the differences are definitely positive, but for *V*, *Cr*, and *Co* negative residuals prevail. The displacements of the *Fe* lines are correlated with the excitation potential. Certain lines of *K*, *V*, *Fe*, and *Mn* have unexplained residuals which necessitated their omission from the mean velocities.

The intensity of the numerous emission lines varies in different cycles, and the incidence of lines of different elements and multiplets is peculiar. Certain lines are greatly strengthened by fluorescent effects. The motion of the strata producing the bright lines is outward in the star with respect to the reversing layer, but the relative differences decrease with phase from maximum to minimum light. The bright-line velocities are correlated with excitation potential.

The *Fe* II emission is present throughout most of the cycle and sharp [*Fe* II] lines occur near minimum light in some cycles. With few exceptions, the bright lines are satisfactorily identified.

Variation in the relative intensity of the spectrum of the visual companion indicates that the light of this hot star may vary in a period of about 12-14 years.

Supplement No. 3, Volume I, pages 63–90, March, 1954.

AN ANALYSIS OF W VIRGINIS*

HELMUT A. ABT†
MOUNT WILSON AND PALOMAR OBSERVATORIES
CARNEGIE INSTITUTION OF WASHINGTON
CALIFORNIA INSTITUTE OF TECHNOLOGY
Received August 13, 1953

A study has been made of the 17-day population II cepheid, W Virginis, from high-dispersion spectra obtained by Sanford and Abt and from photoelectric colors and magnitudes obtained by Whitford and Code, Eggen, and Gordon and Kron. As was first found by Sanford, the absorption lines are double near maximum light and the curve of radial velocity is discontinuous. If the systematic velocity of the star is the same as the mean velocity of the absorption lines, then there exist simultaneously two absorbing layers, one of them rising while the other is falling inward. These layers must collide at about the time of maximum light. The total displacement of these layers is 35×10^6 km, or nearly three times the corresponding displacement of classical cepheids of the same period. The hydrogen emission lines are formed in the lower layer when it is first seen to rise.

The light- and color-curves were used to obtain relative radii. A comparison of these relative changes in radius with the displacements in kilometers obtained from an integration of the curve of radial velocity gives a maximum radius that is smaller than the total displacement of the absorbing-gas layers. The method fails probably because the photosphere where the continuous spectrum is primarily formed and the layers where the lines are formed have different motions. It is suggested that the photosphere oscillates between radii of about 18 and 40×10^6 km and that at each expansion a shell is thrown off which rises to at least 75×10^6 km. The shells rise and fall in about twice the pulsation period of the photosphere.

Curves of growth for 17 of the plates were constructed. *Fe* I excitation temperatures for two layers, seen simultaneously, differ by 700°–1000°. Ionization temperatures calculated from the degree of ionization of *Fe* I and the continuous opacity agree with the effective temperatures from the colors and with the *Mg* II excitation temperatures. The abundances of *Ba* and *Ca*, relative to *Fe*, are normal, but the *Sr* and *Sc* abundances are small by factors of 5 and 3, respectively.

From the computed densities in the layers and from the result that the layers are transparent during half the period, it is concluded that their thicknesses are of the order of 10^{-2} of their separations. Since no material has been detected in the regions between layers, these regions must have less than 10^{-4} of the densities in the layers.

In a possible model of a shock wave traveling through an extended atmosphere, the compressed region behind the shock front might represent the observed layers where the lines are formed. However, serious difficulties to such a model are: first, that the maximum compression by a shock wave in an adiabatic gas is only a factor of 4; and, second, that the large observed velocities of flow of material (about Mach 5) should produce temperatures of about 100,000° in the compressed regions, whereas we observe temperatures of less than 8000°.

The principal difficulty encountered by the model of thin shells being thrown off by the photosphere involves the collision of these shells. The shells appear to pass through one another, despite the result that the mean free path in the shells is of the order of a few centimeters. It may be that the shells are not uniform but consist of many cloudlike condensations. An understanding of the situation may have to await the solution of the general problem of the collision of transparent gas clouds at supersonic velocities.

* This project was completed in partial fulfilment of the requirements for a doctoral thesis at the California Institute of Technology.

† Now at the Yerkes Observatory, Williams Bay, Wisconsin.

ANNOUNCEMENTS

THE NATIONAL GEOGRAPHIC SOCIETY–PALOMAR OBSERVATORY SKY ATLAS

In 1949 the National Geographic Society and the Palomar Observatory entered into an agreement providing for photographing the whole sky observable from Palomar Mountain with the 48-inch Schmidt telescope. An atlas of the sky is being prepared from the plates of this National Geographic Society–Palomar Observatory sky survey. This survey covers the sky north of declination $-27°$ on 879 pairs of plates obtained with the 48-inch Schmidt telescope. Each plate of 14×14-inch size covers an area of 7°×7°; plate centers are separated by 6°, so that adjacent plates overlap by $\frac{1}{2}$°.

Each field is photographed in two colors in immediate succession. The blue exposures are obtained on the Eastman 103*a*–O emulsion, the red exposures on the Eastman 103*a*–E emulsion combined with a red Plexiglas filter which has 50 per cent transmission at a wave length of 6200 A. Both exposures reach the limit of the instrument; the photographic limit is 20.3 mag. The scale is 67".1 per millimeter.

The atlas will consist of negative photographic copies on double-weight paper, 14×14 inches in size. The limiting magnitude of the plates is maintained on the paper prints; but even the use of fine-grain photographic materials for the reproduction results in a slightly reduced resolution on the paper prints compared to the original.

Since the atlas will be made available at a price which covers only the cost of production and handling of the prints, it will not be possible to state a fixed price in advance.[1] Estimates based on present labor rates and costs of photographic paper and chemicals suggest a price of $2,000 per set of 1,758 prints (879 blue exposures and 879 red exposures), if 50 copies of the sky atlas are ordered, and of $1,600 per copy or set of 1,758 prints, if 100 copies are ordered. It is planned to distribute the atlas in three or four sections, to be delivered and paid for at delivery in approximately yearly intervals, the first section probably early in 1955.

Orders will be accepted until October 1, 1954. Before the printing of each section is started, a final estimate of the expected price will be made available, and cancellations of orders will be accepted if the estimated price is higher than $2,000 per copy. The actual price can be established only after the printing of a section is finished; cancellations cannot be accepted if the actual price exceeds the estimated price.

Only one printing of the atlas is being planned, and only the number of copies will be prepared for which orders have been received by October 1, 1954. After this date, no additional orders can be accepted. Orders should be addressed to: Mount Wilson and Palomar Observatories, 1201 East California Street, Pasadena, California.

LIÉGE SYMPOSIA

The volumes of proceedings of the 1951 symposium on "L'Étude optique de l'atmosphere terrestre," the 1952 symposium on "La Physique des comètes," and the 1953 symposium on "Les Processus nucléaires dans les astres" may be acquired by writing to the Société Royale des Sciences de Liége, University of Liége, Belgium, c/o Prof. R. H. J. Germay.

[1] The plates and other supplies used in this survey and the salaries of the personnel required are provided by the National Geographic Society, while the observing time with the 48-inch telescope necessary to take the negatives for the survey is provided by the Palomar Observatory. According to present estimates, approximately 8 years (1949–1956) of observing time will be required to obtain the negatives.

FREE

for joining now . . .

EITHER OF THESE TWO IMPORTANT BOOKS

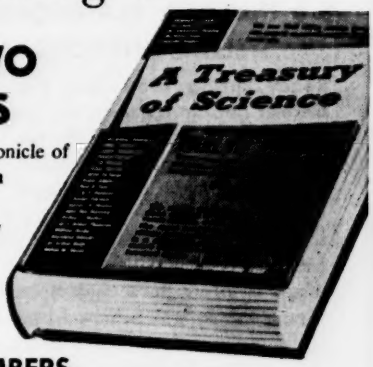

THE ICKES DIARY, a monumental and revealing chronicle of the Roosevelt era—the inside story of power in a nation going through a period of great change—or **A TREASURY OF SCIENCE**—more than 700 pages by the world's outstanding scientists, edited by Harlow Shapley—either of these books can be yours for joining the Book Find Club now.

The Best in Literature . . . AT SUBSTANTIAL SAVINGS TO MEMBERS

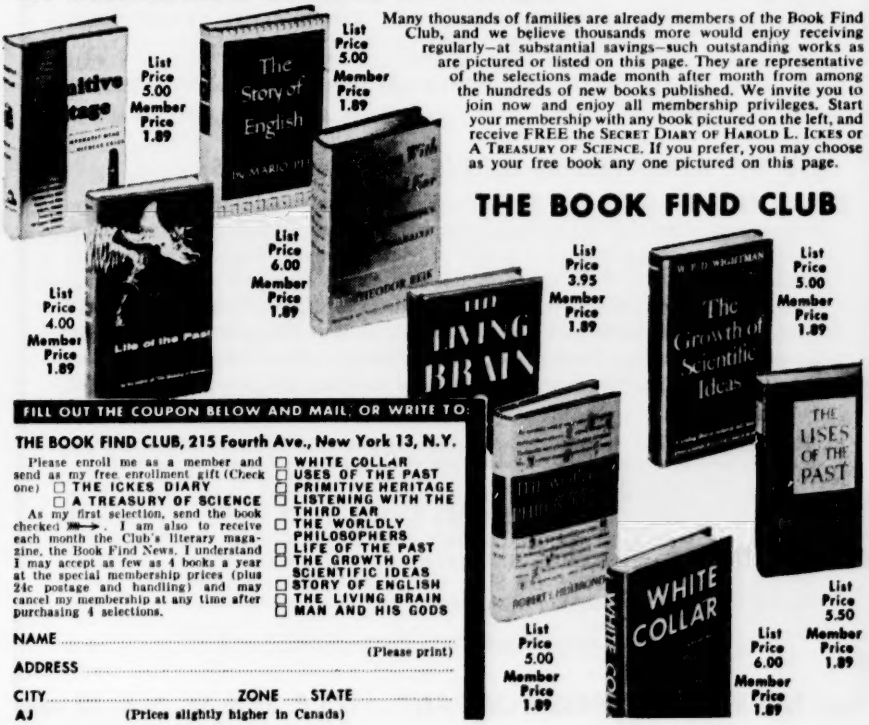
List Price 5.00 Member Price 1.89
The Story of English
List Price 5.00 Member Price 1.89
List Price 6.00 Member Price 1.89
List Price 4.00 Member Price 1.89
Life of the Past
THE LIVING BRAIN
List Price 3.95 Member Price 1.89
The Growth of Scientific Ideas
List Price 5.00 Member Price 1.89
THE USES OF THE PAST
List Price 5.50 Member Price 1.89
WHITE COLLAR
List Price 6.00 Member Price 1.89
List Price 5.00 Member Price 1.89

Many thousands of families are already members of the Book Find Club, and we believe thousands more would enjoy receiving regularly—at substantial savings—such outstanding works as are pictured or listed on this page. They are representative of the selections made month after month from among the hundreds of new books published. We invite you to join now and enjoy all membership privileges. Start your membership with any book pictured on the left, and receive FREE the SECRET DIARY OF HAROLD L. ICKES or A TREASURY OF SCIENCE. If you prefer, you may choose as your free book any one pictured on this page.

THE BOOK FIND CLUB

FILL OUT THE COUPON BELOW AND MAIL, OR WRITE TO:

THE BOOK FIND CLUB, 215 Fourth Ave., New York 13, N.Y.

Please enroll me as a member and send as my free enrollment gift (Check one) ☐ **THE ICKES DIARY** ☐ **A TREASURY OF SCIENCE**

As my first selection, send the book checked ➡. I am also to receive each month the Club's literary magazine, the Book Find News. I understand I may accept as few as 4 books a year at the special membership prices (plus 24c postage and handling) and may cancel my membership at any time after purchasing 4 selections.

- ☐ WHITE COLLAR
- ☐ USES OF THE PAST
- ☐ PRIMITIVE HERITAGE
- ☐ LISTENING WITH THE THIRD EAR
- ☐ THE WORLDLY PHILOSOPHERS
- ☐ LIFE OF THE PAST
- ☐ THE GROWTH OF SCIENTIFIC IDEAS
- ☐ STORY OF ENGLISH
- ☐ THE LIVING BRAIN
- ☐ MAN AND HIS GODS

NAME .....

(Please print)

ADDRESS .....

CITY ..... ZONE ..... STATE .....

AJ (Prices slightly higher in Canada)

IMPORTANT COMPANION VOLUMES IN

ASTROPHYSICS

LAWRENCE H. ALLER

Associate Professor of Astronomy, University of Michigan

▶▶ NUCLEAR TRANSFORMATIONS, STELLAR INTERIORS, AND NEBULAE

Ready Spring 1954—This pioneering work offers a comprehensive study of thermal nuclear reactions, the interiors of stars, pulsating variable stars, and the interstellar medium. It covers not only the fundamentals necessary for an understanding of this specialized branch of astrophysics, but also the major modern developments in the field. Emphasis is placed on methods and procedures for obtaining results, rather than on a simple presentation of the current status of the science. The book treats of the properties of matter at high temperatures, stellar energy generation, internal constitution of stars, stellar evolution and the origin of the elements, novae and supernovae, gaseous nebulae, with particular attention given to discoveries achieved by the new technique of radio astronomy. The work is illustrated with numerous diagrams and photographs, many reproduced here for the first time. *52 illustrations, 10 tables, 344 pages.* **$12**

CONTENTS: STELLAR INTERIORS AND NUCLEAR TRANSFORMATIONS—MODEL STARS—THE CEPHEIDS AND LONG PERIOD VARIABLES—STARS WITH EXTENDED ENVELOPES, NOVAE, AND SUPERNOVAE—THE PLANETARY NEBULAE—THE INTERSTELLAR MEDIUM

▶▶ THE ATMOSPHERES OF THE SUN AND STARS

Now Available—Thorough coverage of present-day knowledge concerning the atmospheres of the sun and stars and solar-terrestrial relationships. Provides a short introduction to astronomy and a review of relevant physics. Treats all major astrophysical principles—atomic structure and spectra, gas laws and velocity distribution, ionization, excitation, etc.—and applies them to the radiation of the sun and stars, to their continuous and dark-line spectra, to solar phenomena, and to solar-terrestrial relationships. Each principle is applied to a definite numerical problem concerned with the interpretation of stars and nebulae. *116 illustrations, 44 tables, 412 pages.* **$12**

"Hard to overemphasize the importance of this book . . . presents the subject of stellar atmospheres as it is known and accepted today."—**Publications of the Astronomical Society of the Pacific**

CONTENTS: SURVEY OF BASIC DATA—ATOMIC AND MOLECULAR SPECTRA—GAS LAWS AND EQUATIONS OF STATE, TURBULENCE—EXCITATION, IONIZATION, AND DISSOCIATION—EMISSION AND ABSORPTION OF RADIATION—RADIATION OF STARS—CONTINUOUS SPECTRA OF SUN AND STARS—THE FRAUNHOFER SPECTRUM—SOLAR PHENOMENA

Order through your bookstore or from:

THE RONALD PRESS COMPANY • 15 E. 26th St., N.Y. 10

THE SUN

The Solar System

VOLUME I

***Edited by* GERARD P. KUIPER**

The Sun, the first of four volumes intended to collect and systematize all significant information on the sun, the planets, the satellites, the comets, and the smaller bodies of the solar system, is written by twenty-three solar physicists from six different countries. It is designed with a dual purpose. On the one hand, it is an invaluable reference handbook for the specialist. On the other hand, it is intelligible to anyone versed in the physical sciences.

The Sun covers the divisions of solar physics comprehensively: the solar interior and energy production, the photosphere and the Fraunhofer spectrum; the chromosphere and the solar electrodynamics; and the many modern techniques of solar observation. All are discussed in detail. The book contains, in addition, many new illustrations and over one thousand references to the literature.

New models are given for the solar interior, based on integrations using the latest information on nuclear cross-sections. The photosphere models are critically reviewed, and a new compromise solution is proposed. Similarly, a very recent model for sunspots is reviewed. For both the chromosphere and the corona the temperature and density data are critically examined. An extensive treatment of solar radio astronomy adds significantly to the optical studies of solar phenomena treated in other chapters.

A special feature of *The Sun* is its two tables of solar observatories and their equipment, accessories, and programs. Other features include the latest results on the magnetic field and the solar component of cosmic rays, recent additions to instrumental techniques, and a record, as complete as possible, of the far-ultraviolet solar spectrum photographed on rocket flights.

Many illustrations, 784 pages, $12.50

THE UNIVERSITY OF CHICAGO PRESS

Announcing

MEASUREMENTS OF DOUBLE STARS, III

By GEORGE VAN BIESBROECK

PUBLICATIONS OF THE YERKES OBSERVATORY, VOLUME VII, PART VI

"This work lists measurements of the position angles and separations of about 2,500 close double stars, mostly in the years 1935 to 1951, with the 40-inch Yerkes refractor and the 82-inch McDonald reflector. New orbits are given for 19 binary systems, and new dynamical parallaxes are published for many slow-moving pairs."—*Sky and Telescope*

244 pages, paper, $10.00

THE UNIVERSITY OF CHICAGO PRESS

5750 ELLIS AVENUE CHICAGO 37, ILLINOIS

THE OBSERVATORY

FOUNDED 1877

* * *

A Magazine presenting current developments in Astronomy by means of Articles, Correspondence, Notes on discoveries and Reviews of important astronomical books. The papers read at the Meetings (Astronomical & Geophysical) of the Royal Astronomical Society and the discussions which follow are also fully reported.

* * *

Annual subscription for 6 issues, post free, £1 (U.S.A. and Canada, $3.00) should be sent to

The Editors, ROYAL GREENWICH OBSERVATORY

Herstmonceux Castle, Hailsham, Sussex, England

ANNOUNCING

THE ASTROPHYSICAL JOURNAL SUPPLEMENT SERIES

These *Supplements* are intended to provide a medium for the publication of extensive investigations, such as wave-length lists of stars of special interest, photometric data, results of numerical integrations pertaining to stellar interiors, model stellar atmosphere calculations, and theoretical investigations not immediately related to astronomical problems.

Supplement No. 1

"Chromospheric Structure of the K-type Component of Zeta Aurigae." O. C. Wilson and Helmut A. Abt.

Spectrograms of 10 A/mm dispersion taken during the 1947–48 eclipse have been measured for line intensities and for radial velocities, and the results are compared with those obtained previously for the 1939–40 eclipse.

(Price, $1.25)

Supplement No. 2

"Spectroscopic Observations of Mira Ceti, 1934–1952." Alfred H. Joy.

This is a detailed discussion of two decades of observations of this interesting star. The results of Coudé spectrograms with dispersions up to 2.3 A/mm permits a more critical study of the spectroscopic behavior of Mira Ceti than was possible with lower dispersions.

(Ready April, 1954. Price $1.25)

Supplement No. 3

"An Analysis of W Virginis." Helmut A. Abt.

This is a study of the population II Cepheid, W Virginis, from high dispersion spectra obtained by Sanford and Abt and from photoelectric colors and magnitudes obtained by Whitford and Code, Eggen, and Gordon and Kron.

(Ready April, 1954. Price, $1.25)

An abstract of each supplement will be published in THE ASTROPHYSICAL JOURNAL. The Supplements will appear irregularly, and may be purchased separately or by subscription. Each volume of Supplements will consist of approximately 500 pages.

Subscriptions

$8.00 per volume

Canada, $8.75. Foreign, $9.50.

To members of the American Astronomical Society, $6.00 per volume.

Orders now accepted.

THE UNIVERSITY OF CHICAGO PRESS

5750 ELLIS AVENUE CHICAGO 37, ILLINOIS

from McGraw-Hill

ASTROPHYSICS: A Topical Symposium

by A. J. HYNEK

Professor of Astronomy and Assistant Dean of the Graduate School, The Ohio State University, and Director of the McMillin Observatory, The Ohio State University.

"The volume should be required reading for all graduate students in astronomy and astrophysics, and all workers in the field will find a great deal of value in its pages."—DEAN B. McLAUGHLIN, *University of Michigan*, in *AMERICAN JOURNAL OF PHYSICS*

"The volume promises to become a classic in the field, and one can only become envious of all astronomers who belong to the family of Yerkes scientists, since a school boasting a group of people like the contributors to this book must necessarily produce a never-ending line of outstanding astrophysicists."—D. TER HARR, *University of St. Andrews*, Scotland, in *SCIENCE*

McGraw-Hill Astronomical Series

674 pages

6 × 9

145 illus.

$12.00

A symposium of papers treating "essentially all the active fields" of astrophysics. The fifteen contributors are leaders and authorities in their respective fields. The volume commemorates the Fiftieth Anniversary of the Yerkes Observatory and reviews the progress in astrophysics during the half-century since the founding of the observatory. The book combines many of the features of a textbook, a handbook, a historical study, and a technical treatise.

McGraw-Hill Book Company, Inc.

Send for a copy on approval

330 West 42nd Street New York 36, N.Y.